Biorefining of Spruce Wood for Nanocellulose and Reducing Sugars Production: Exploring Greener Alternatives

by

Pawan Kumar

Submitted in partial fulfilment of the requirements
for the degree of Doctor of Philosophy

at

Dalhousie University
Halifax, Nova Scotia
December 2023

TABLE OF CONTENT

LIST OF TABLES

LIST OF FIGURES

ABSTRACT

Lignocellulosic biomass, available in the form of agriculture and forest residues is an abundant renewable source of energy and products. Cellulose nanocrystals and fermentable reducing sugars are amongst the major bioproducts derived from woody biomass. Herein, the thesis explores developing non-conventional approaches of extraction cellulose nanocrystals (CNCs) and fermentable reducing sugars from Spruce wood.

First, acetosolv pulping-alkaline hydrogen peroxide bleaching of spruce wood were employed to produce bleached wood pulp (BWP) for the derivation of CNCs. Treatment of BWP using sulfuric acid at concentration of 65.0 wt.% and 62.0 wt.% led to CNCs yield of 8.0±3.2 wt.% of dry wood and 25.1±0.7 wt.%, respectively. The ultrasonic treatment of acid hydrolyzed pulp at 80.0 % amplitude for 5.0 min resulted in obtaining good quality CNCs with high aspect ratios (length/width) up to 48.1 and crystallinity index of 80.8±1.7%.

For fermentable reducing sugars production, different pretreatments of spruce wood were explored to improve the enzymatic digestibility of spruce wood. Acetosolv pulping-alkaline peroxide bleaching was the most effective pretreatment method, leading to total reducing sugar (TRS) yield of ~95.0 wt.% of total hydrolysable sugars (THS) in 144.0 hours of enzymatic hydrolysis process. Additionally, the impact of enzyme pretreatment on enzymatic hydrolysis yield was further investigated. It was found that prolonged $scCO_2$ pretreatment (16.0 MPa, 46.0 °C, 24.0 h) of enzyme cocktail decreased sugars yield in the subsequent enzymatic hydrolysis from 44.6±1.3 wt.% (untreated enzyme) to 6.3±1.1 wt.% (pretreated enzyme) at 24.0 h of enzymatic hydrolysis of BWP.

The optimized enzyme cocktail was immobilized into silica oxide aerogel by sol-gel synthesis followed by $scCO_2$ drying. The cocktail aerogel at 144.0 mg enzyme/g aerogel retained a residual yield of >50.0 % after fourth cycle of reuse compared to first cycle under atmospheric pressure. The activity was decreased due to leaching of enzyme and reduction in surface area and porous volume of aerogel enzyme over the cycles. TRS yield by the cocktail aerogel was <10.0 wt.% in second cycle of reuse under $scCO_2$ due to enzyme leaching from aerogel to hydrolysate showing unfavorable conditions for cocktail aerogel in high pressure system.

LIST OF ABBREVIATIONS USED

LC	Lignocellulose
SCF	Supercritical fluid
TGA	Thermogravimetric analysis
DSC	Differential scanning calorimetry
XRD	X-ray diffraction
CrI	Crystallinity index
S-IR	Solid state infrared spectroscopy
FTIR	Fourier Transform Infrared Spectroscopy
ssNMR	^{13}C solid state NMR
UV-Vis	Ultraviolet–visible spectroscopy
SEM	Scanning electron microscope
TEM	Transmission electron microscope
AFM	Atomic force microscopy
HPLC-RID	high-performance liquid chromatography refractive index detector
DLS	Dynamic light scattering
CHF	Coconut husk fiber
BSKP	Bleached softwood kraft pulp
MCC	Microcrystalline cellulose
CMC	Carboxymethyl cellulose
TEMPO	2,2,6,6-tetramethylpiperidine-1-oxyl
CNCs or NCC	Cellulose nanocrystals or Nanocrystalline cellulose
CNF	Cellulose nanofiber
DMAc	N,N-dimethylacetamide
DMSO	Dimethyl sulfoxide
TBAF	tetrabutylammonium fluoride
NMMO	N-methyl morpholine-N-oxide
GPC	Gel permeation chromatography
ILs	Ionic liquids
HTC	Hydrothermal treated cellulose
THS	Total hydrolyzable sugars
MFC	Micro fluidized cellulose
TRS	Total reducing sugar
CBH	Cellobiose from nonreducing
CLEA	Crosslinking of enzyme aggregates
MOF	Metal-organic framework
BET	Brunauer-Emmett-Teller
BJH	Barrett-Joyner-Halenda

ACKNOWLEDGEMENT

I would like to take this opportunity to express my deepest gratitude to all those who have contributed to the completion of this doctoral thesis. First and foremost, I am immensely thankful to my supervisor, Dr. Azadeh Kermanshahi-pour, and Co-supervisor, Dr. Satinder Kaur Brar, for their continuous support, guidance, and mentorship throughout this journey. Their expertise, patience, and encouragement have contributed significantly to shaping this research and helping me reach my true potential. I am truly fortunate to have had such an outstanding supervisor.

I would also like to extend my appreciation to the members of my supervisory committee, Dr. Chunbao Charles Xu and Dr. Sophia Quan He, for their valuable, timely advice, feedback, insights, and constructive criticism. Their expertise and guidance have significantly enriched the quality of this thesis.

I acknowledge the analytical and instrumental support from Sara Evans, Sarah Martell, Dr. Jan K. Rainey, Dr. Mita Dosag, Dr. Stanislav Sokolenko, Dr. Su-Ling Brooks at Dalhousie University, Dr. Ramon Filipe Beims from Western University, and Dr. Rahul Saini from York University. Also, I acknowledge Grace O'Conner, Dr. Kimberly Miller, Dr. Mahmoud Mirmehrabi, and Solid State Pharma Inc. (SSPI) team for the instrumental support and Industrial internship opportunity. I am grateful to the staff and faculty at the Department of Process Engineering and Applied Science, who have provided their administrative support, services, resources, and facilities and have played an essential role in facilitating the completion of the project. Furthermore, I thank my colleagues Aryan Samadi, Jianan Lin, Khashayar Bahri, Lauren MacEachern, and other fellow researchers within and outside of the university who have shared their knowledge experiences and made my intellectual journey joyful.

I am and will always be indebted to my parents and family for their unconditional love, encouragement, understanding, and patience throughout this long, challenging, and fruitful journey.

I sincerely hope that my research can make a positive impact in the area of research.

Thank you,
Pawan Kumar

CHAPTER 1 INTRODUCTION

1.1. Background

In the year 2020, the energy consumption from fossil resources (including coal, oil, and natural gas) amounted to 601.7 Terajoules out of a total consumption of 742.8 Terajoules, which led to the release of 31.4 Gigatons of CO_2 (99.3% of total CO_2 emissions) [1]. According to the International Energy Agency (IEA)'s projection, the world energy demand is forecast to increase by 24.0 % in 2040 [2]. Statistics published in the IEA report have shown that biofuels and waste-derived energy contributed to around 9.8% of the total energy supply in 2020 [1]. In 2019, lignocellulosic biorefinery produced more than 138 billion liters of bioethanol, 33.0 billion liters of biodiesel, and US $8.7 billion valued chemical bioproducts [3-6]. Lignocellulosic (LC) biomass is primarily available in feedstocks in biorefinery as an alternative to petroleum refineries using fossil resources as feedstocks.

Additionally, it has no serious competition with animal food resources like the first-generation feedstock of biofuels [7]. The lignocellulosic biorefinery concept involves the upgradation of woody and agricultural residues to energy and value-added bioproducts [8]. Implementing a biorefinery, in which multiple products are derived from renewable resources, offers significant potential for a circular system where waste production is minimized and the use of biomass is maximized, aiming at enhancing social and economic prosperity and environmental quality [9-12]. Developing a sustainable process with a high product yield remains a bottleneck in research and development. LC biomass is composed of anhydrous sugar polysaccharides (cellulose and hemicellulose) and aromatic polymer (lignin) as the

major components, and protein, extractives (lipophilic resins), and ash as minor components [13]. The composition of LC feedstock varies depending on the type of biomass due to their cell wall composition, as seen in Table 1-1[14]. It is worth mentioning that sum of the individual component of the LC biomass may not be 100 % of dry matter due to the variation and analytical errors in different methods [15-17].

Table 1-1. Fractional composition of major polymers and acetyl groups in various lignocellulosic feedstocks (wt.% of dry matter)

Feedstock#	Cellulose	Hemicellulose	Lignin	Acetyl group	Extractive content	Ash content	Others *	Ref.
Agricultural residues								
Sorghum stalk	40.5	22.7[a]	19.5	-	-	2.8	14.5	[16]
Wheat straw	38.5	24.9	17.7[b]	2.7	-	10.7	8.2	[18]
Wheat bran	34.2	22.1	24.3	-	11.5	0.5	7.4	[19]
Corn stover	30.0	26.1	11.0	-	28.0	4.9	-	[15]
Corn stover	40.6	24.7	4.2	-	-	-	22.8	[20]
Corn cob	36.8	26.3[a]	24.2	2.1	-	3.2	7.4	[21]
Sugarcane bagasse	40.5	28.5	21.6	4.8	4.2	3.7	-	[22]
Grasses								
Switchgrass	45.6	27.3	8.6	-	-	-	18.5	[23]
Mixed perennial grass	36.0	24.5	6.9	-	-	-	24.4	[20]
Elephant grass	34.6	24.3	15.7[b]	4.8	21.9	10.1	-	[17]
Woody feedstock materials								
Eucalyptus	41.4[c]	12.5[a]	29.8	-	-	-	12.1	[24]
Harwood chips	40.0[c]	17.0[a]	31.0	2.7	2.0	2.0	8.0	[25]
Aspen	44.0[c]	25.9	24.8	5.5	0.8	-	4.5	[26]
Mongolian oak	41.2[c]	23.5	26.4	-	0.5	0.5	7.9	[27]
Pine	41.3	22.1	31.6	-	1.7	0.6	2.7	[28]
Spruce	43.0	20.6	29.6	-	-	-	6.8	[29]
Poplar	46.1	34.7	19.1	-	-	-	0.1	[30]

* Determined by difference; The chemical composition of feedstock biomass is mentioned as per the reported studies. Acetyl group is part of hemicellulose. The sum of cellulose, hemicellulose, lignin, extractive, ash and other component may or may not be 100% due to the variation in the

analytical methods used in corresponding studies; [a] determined as xylan; [b] determined as Klason lignin; [c] determined as glucan.

Each biopolymer comprises one or more basic structural units (Figure 1-1). Cellulose is a carbohydrate polymer that constitutes 40.0-48.0 wt.% dry weight of woody biomass [30] [24] [27]. Cellulose is composed of a repeating unit of cellobiose in the form of crystalline and amorphous subregions. Cellobiose is a dimer of anhydrous glucose with reducing and non-reducing ends. The amorphous region is unorganized, whereas the crystalline region is a well-organized glucan microfibril stacked structure. Hemicellulose constitutes 12.0-34.0 wt.% dry weight of woody biomass [30] [24] [27]. It is composed of pentose (C5) and hexose (C6) anhydrous sugars polymers that include xylose, arabinose, mannose, galactose sugars, and some organic acids (i.e., acetic acid, galactoglucoronic acid). Lignin is an aromatic biopolymer composed of three aromatic units: *p*-coumaryl alcohol or *p*-hydroxyphenyl unit (P), coniferyl alcohol or guaiacyl unit (G), and sinapyl alcohol or sinapyl unit (S) [31]. These three aromatic units form lignin and are found in varying contents in grass, softwood, and hardwoods. Softwood contains 27.0-33.0 % lignin with guaiacyl (G) as the dominant unit, hardwood contains 20.0-26.0 % lignin mainly composed of guaiacyl (G) and syringyl (S) units, and herbaceous plants that contain a lower amount of lignin 13.0-19.0 % with all three monolignol units (Figure 1-1) [32]. These biopolymers are the source of a wide spectrum of bioproducts that can be produced by chemical, biological, physical- and thermochemical methods. Therefore, the biorefinery concept is a contemporary solution to meet these future needs of useful chemicals, polymers, and energy and to reduce the dependency on finite fossil resources [33].

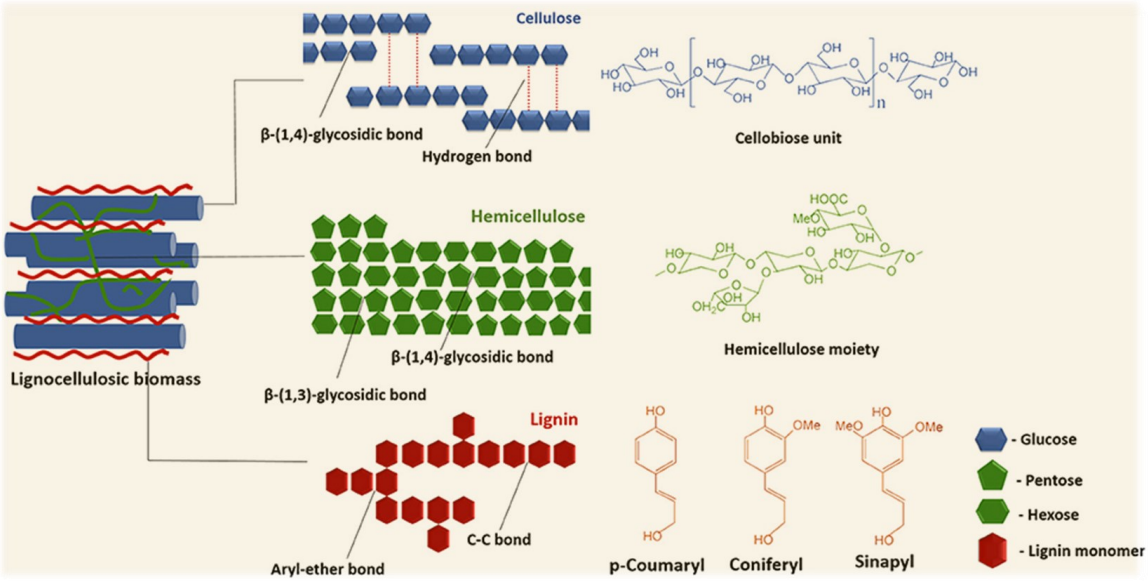

Figure 1-1. Structural units of lignocellulosic biomass - cellulose, hemicellulose, and lignin [34]

Plentiful lignocellulosic biomass material is available worldwide in the form of forests, crops, and grass. Geographically, the Russian Federation, Brazil, and Canada have significant forest lands in square kilometers, as shown in Figure 1-2 [35]. The global production of forest residues amounted to approximately 1.2 billion tons in 2018. These residues include by-products from wood processing, such as sawdust, plywood waste, and shavings [36].

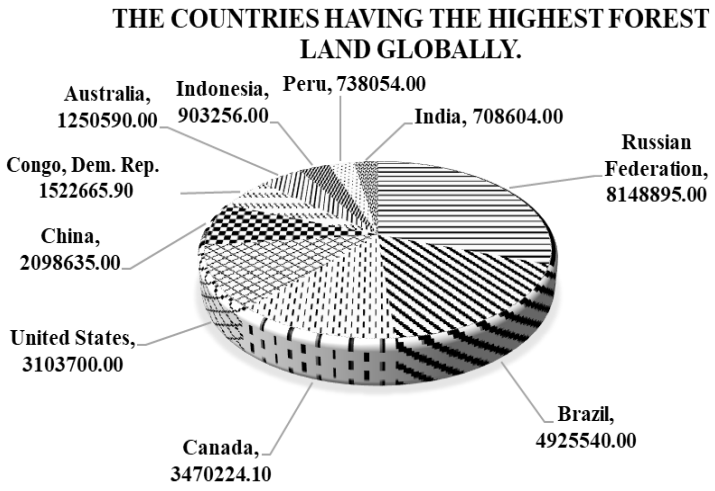

Figure 1-2. The countries with the highest forest land globally parks and gardens are excluded (World data bank, 2019) [35, 37].

The carbohydrate polysaccharides in the LC biomass contribute more than 60.0-80.0 wt.% of the composition and, therefore, the most utilized fraction. The major intermediate bioproducts derived from cellulose are nanocellulose in the form of cellulose nanocrystals (CNCs), cellulose nanofibers (CNF), and fermentable reducing sugars. These intermediate bioproducts are further converted to different platform commodities such as biosensors, membranes, biodegradable polymer additives, drug delivery ingredients, functionalized hydrogels, and xylitol, sorbitol, polylactic acid, bioethanol, biobutanol [10, 38-44]. The "Global Nanocellulose Fiber Market Report" published in 2020 by Research Insights predicted that the global Nanocellulose market will experience an annual growth rate of 18.8 % from 2018 to 2025 and is expected to reach $2.7 billion by 2025 [36]. CNC is one of the three major types of nanocellulose (nanocrystals, nanofibers, spherical nanocellulose) derived from either plant or bacterial cell-walls. Each type of nanocellulose has a different preparation method, characteristic features, and specific application [45-49]. In the lignocellulosic materials, these nanocellulose fibers stack to form microcrystalline fibers, and these microcrystalline fibers are complex with hemicellulose and lignin to form as rigid, complex structure in plant's cell walls to provide rigidity to lignocellulosic biomass [50-52]. The cellulose is structured in a very organized hierarchy from nanoscale fibers to microscales Figure 1-3.

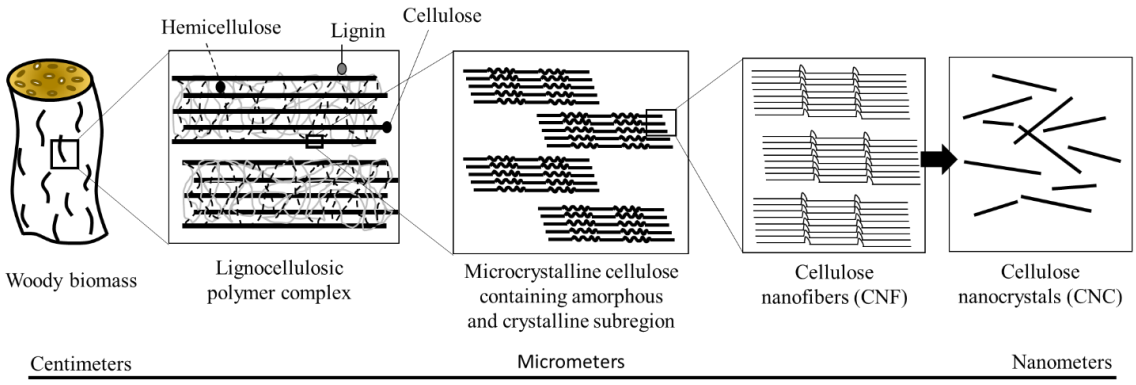

Figure 1-3. Schematic representation of cellulose and nanocellulose structures in the wood.

In the CNCs production process, cellulose is extracted from the biomass, then the amorphous cellulose is hydrolyzed, and finally, the individual nanocrystals are disintegrated by mechanical dispersion [46, 53-58]. The cellulose is extracted from LC biomass by harsh chemicals (i.e., chlorite and sulfite- NaOCl, $NaClO_2$, Na_2SO_3, Na_2SO_4), which results in pure and white-colored cellulose pulp. However, this process generates wastewater contaminated with lignin and chlorinated toxic compounds, also known as adsorbable organic halides (AOX) [59]. Organosolv pulping are an alternative method to fractionate the cellulose pulp from LC biomass with a potential of reusability of solvents and recovery of solubilized lignin [60-63]. Further, CNCs are extracted by acid hydrolysis or 2,2,6,6-tetramethylpiperidine-1-oxyl (TEMPO) oxidation methods [54, 58, 64-68]. Acid hydrolysis is a well-established method used in commercially producing CNCs [69]. After hydrolysis of the amorphous cellulose, the crystalline cellulose remains in the form of clumps of nanocrystals, further disintegrating by mechanical dispersion. Due to significant water consumption and wastewater generation by intense chemical methods, some emerging methods include dilute acid hydrolysis, sub- and supercritical water treatment, and enzymatic hydrolysis [70-72]. However, these methods are still

under development and limited to lab scales. The qualitative properties (surface area and aspect ratio, surface functional groups, zeta potential, hydrophilicity, and others) and yield (wt.% of cellulose or wt.% of initial feedstock) determine the application of CNCs. Method of extraction and process parameters (i.e., temperature, reaction time, acid concentration, mechanical power) influence CNC yield and properties of CNCs and, therefore, are important to investigate and optimize.

On the other hand, fermentable reducing sugars from renewable sources are feedstock for biofuels and bioenergy production (i.e., bioethanol and biobutanol) [44, 60, 73-75]. The LC biomass is the source of second-generation (2G) bioethanol, which relies on converting polysaccharide constituent of biomass to fermentable sugars followed by microbial fermentation to produce ethanol. The primary bottleneck in the LC biorefinery is the large-scale fermentable sugars extraction. Extracting monomeric sugars (C5 & C6) from the LC biomass, irrespective of the type of biomass, requires pretreatment to disrupt the structure by deconstructing the bonding of lignin with hemicellulose [44, 76-77]. The pretreatment process enhances the enzymatic digestibility of pretreated solids due to the destruction of a complex network of lignin-hemicellulose and crystalline cellulose; therefore, enzyme accessibility to carbohydrate polymers increases [78-79]. Typically, conventional strategies for biomass pretreatment involve the use of single-stage alkali solutions (such as NaOH, KOH, NH_3, and Na_2CO_3), inorganic acids (primarily H_2SO_4, H_3PO_4, HCl, and HNO_3), or water-based techniques (such as hot water, hydrothermal, sub-critical water, and steam explosion) [80-89]. Due to the severity of

pretreatment processes, the degradation of sugars and lignin occurs, which reduces yield and results in the formation of chemicals (i.e., furfuraldehyde, 5-hydroxymethyl furfural, levulinic acid) that inhibit the fermentation process [90]. Such processes lead to the generation of significant wastewater that makes the process environmentally unsustainable. As an alternative to intense chemical treatment methods, emerging technologies are being developed using ionic liquids, microwave-assisted methods, supercritical fluid treatments, ultrasound, and organosolv treatment. These methods generate less wastewater than the abovementioned methods, enable solvent recycling, and enhance the process's sustainability and economic viability [91-96].

1.2. Knowledge gap

Significant work has been done in the field of nanocellulose and sugar production from lignocellulosic biomass. However, most of the work is based on conventional methods that use chemical-intensive treatment, resulting in significant water consumption that raises environmental concerns. Therefore, emerging technologies for deriving products from biomass should be explored. The specific knowledge gaps which were the focus of this thesis include:

1. The majority of the processes developed for nanocellulose preparation rely on the extraction of cellulose from LC wood biomass by conventional chemical treatment such as kraft pulping and sodium chlorite bleaching [97-103]. Such processes face the challenge of wastewater containing reactive chemicals. Organosolv pulping, such as acetosolv pulping and ethanosolv pulping, has been a cleaner approach to fractionate LC biomass into sulfur-

free lignin, hemicellulose, and cellulose [57, 104-105]. However, most of the studies have been conducted on agricultural feedstocks, and a very limited studies explored woody biomass, specifically spruce wood with higher cellulose contents. To the best of our knowledge, the acetosolv pulping and alkaline hydrogen peroxide treatments have not been explored for nanocellulose production from spruce wood. CNCs production from the LC biomass is a multistep process that includes particle size reduction of wood biomass, delignification by pulping and bleaching, acid hydrolysis, and mechanical dispersion of the individual CNC. The type of biomass and process conditions influence the CNC's characteristics and yield. The effect of acid hydrolysis reaction conditions and type of mechanical dispersion methods on CNC properties and yield has only been studied to a limited extent and explored to a great extent in this thesis.

2. Use of supercritical fluids pretreatment of agricultural biomass prior to enzymatic hydrolysis for fermentable sugar production has been explored to a greater extent compared to woody biomass [15, 18, 106-110]. The obtained sugar yield varies depending on the type of biomass and process condition [111-112]. Ultrasound pretreatment is another emerging physicochemical pretreatment method that is less chemical-intensive compared to conventional methods. The efficacy of these pretreatment methods highly depends on the process conditions and biomass type, and therefore, it is worthwhile to further investigate under varying process conditions.

3. There are reports on the enhancement of enzyme activity under a high-pressure environment due to a molecular-level rearrangement in the enzymes' microenvironment (i.e., activation volume, reorientation of water molecule) [113]. Enzymatic hydrolysis in the presence of $scCO_2$ in one pot has been studied to hydrolyze microcrystalline cellulose for reducing sugar and nanocellulose production from microcrystalline cellulose (MCC) in just two different studies [50, 114]. However, there is a significant knowledge gap with respect to the enzymatic hydrolysis of spruce wood in the presence of $scCO_2$ and water.
4. The cost of enzymes is one of the bottlenecks in biomass conversion to fermentable sugars. Therefore, the recovery of the enzyme is an important consideration. Only a few studies evaluated the performance of immobilized cellulase under the supercritical CO_2 [115]. Additionally, the effect of enzyme load in immobilization (such as silica aerogel) on hydrolysis yield, morphology, and reusability have not been explored for cellulolytic enzymes.

1.3. Research Objectives

The thesis aims to produce cellulose nanocrystals with rod-shaped morphology and fermentable reducing sugar production from the spruce wood biomass with a greener approach. Therefore, the thesis explored less chemical-intensive and reusable solvents to address the above-discussed knowledge gap. The objectives are outlined as follows:

1. Developing an understanding of the influence of process parameters affecting the purity and morphology of the cellulose nanocrystals (CNCs)

derived from spruce wood using acetosolv pulping-alkaline hydrogen peroxide treatment.

2. Optimization of cellulolytic enzyme cocktail for enzymatic hydrolysis of pretreated spruce wood for fermentable reducing sugar production.
3. Investigation of the effect of various mild or less intense chemical pretreatment methods of spruce wood biomass on enzymatic digestibility by cellulolytic enzyme cocktail.
4. Immobilization of cellulolytic enzyme cocktail into silica oxide by entrapment for enzymatic hydrolysis carboxymethyl cellulose and spruce wood pulp. Understanding the effect of enzyme concentration in aerogel on its reusability and morphology and its use under supercritical CO_2.

1.4. Research scope

Among the variety of pretreatment methods, ultrasound, organosolv, and $scCO_2$ are emerging physicochemical pretreatment methods with the advantage of reduced wastewater generation or reusability of solvents [116-119]. The polysaccharides in the pretreated biomass are hydrolyzed to monomeric and oligomeric sugars by cellulolytic enzymes, which are among the expensive components of the process. Therefore, reducing the enzyme cost and enhancing the enzymatic hydrolysis rate are strategies to improve the process economics. The synergistic effect of enzymes increases the rate of hydrolysis by changing hydrolysis patterns [120-121]. This study explored a greener and sustainable process with less chemicals or reusable solvents for processing LC biomass, which could significantly eliminate the discharge of contaminated wastewater from

lignocellulosic biorefineries. This study focused on understanding the effect of process parameters on the yield of CNCs and fermentable sugar production using spruce wood biomass.

The production of nanocellulose crystals and fermentable reducing sugars under the proposed plan is schematically present in Figure 1-4. In this thesis, spruce wood was used as starting feedstock material for CNCs extraction. The process involved acetosolv pulping-alkaline hydrogen peroxide bleaching to extract purified microcrystalline cellulose followed by optimization of acid hydrolysis and mechanical disintegration of individual CNCs. The goal was to develop an understanding of the effect of process on yield and quality of CNCs.
In the context of fermentable sugar production from spruce wood, the effect of various pretreatment ($scCO_2$, alkali-assisted ultrasonic treatment, and acetosolv-alkaline hydrogen peroxide) on enzymatic hydrolysis yield was investigated. The enzyme cocktail consists of endoglucanase, exoglucanase, and β-glucosidase from cellulase, hemicellulase, β-glucanase, and pectinase from Viscozyme L enzyme complex. In addition, the enzyme cocktail prepared by response surface optimization for concentration, pH, and temperature was pretreated under $scCO_2$ to understand the effect of $scCO_2$ on enzyme activity and performance in the enzymatic hydrolysis of bleached wood pulp (BWP) (Figure 1-5).

Additionally, the enzyme cocktail was filtered to remove sugar and impurities and immobilized into the silica oxide aerogel by entrapment. The performance of the immobilized enzyme cocktail was evaluated for hydrolysis of the water-soluble form of derivatized cellulosic substrate, sodium carboxymethyl cellulose (CMC),

and water-insoluble BWP produced by acetosolv-alkaline peroxide pretreatment. Additionally, CMC was used to explore the potential of enzymatic hydrolysis under $scCO_2$ by an immobilized enzyme cocktail (Figure 1-6).

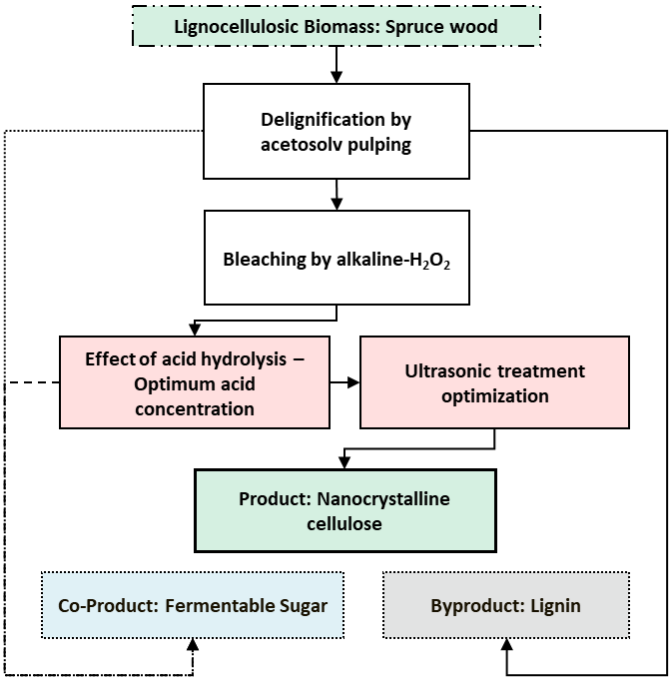

Figure 1-4. Production of nanocellulose crystals from Spruce wood acetosolv pulping -alkaline peroxide bleaching followed by acid hydrolysis

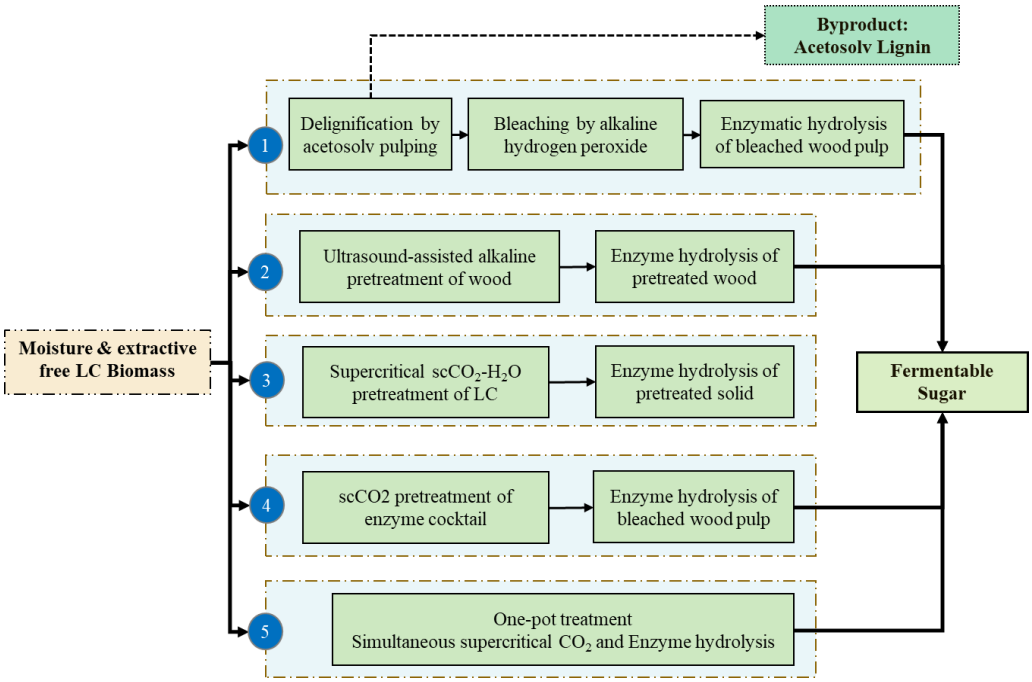

Figure 1-5. Production of fermentable sugars from Spruce by biomass an enzyme pretreatment followed by enzymatic hydrolysis

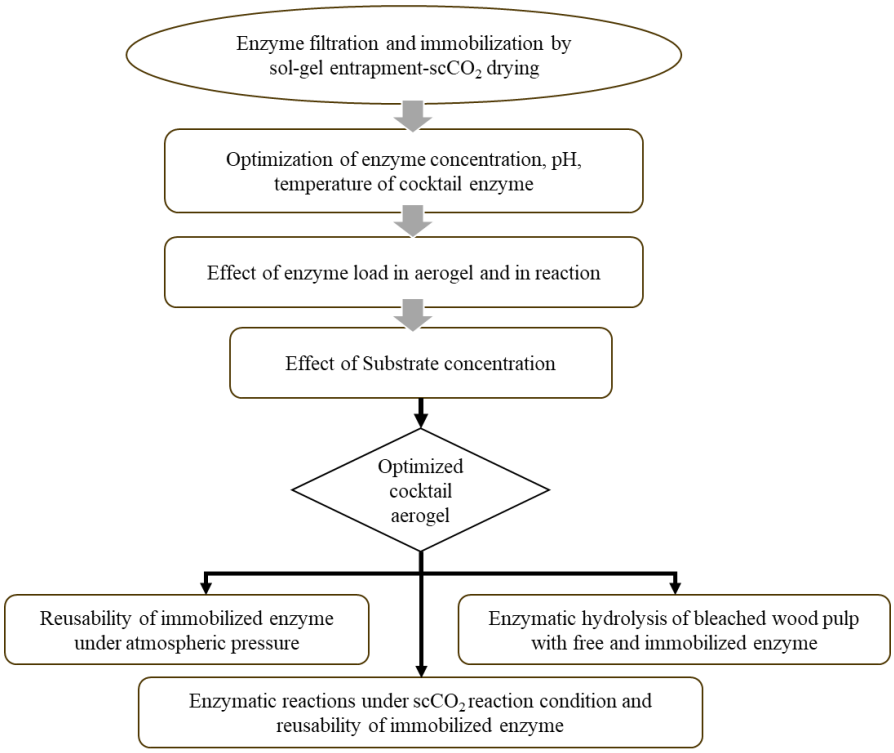

Figure 1-6. Production of fermentable sugars from pretreated Spruce wood by free and immobilized cocktail enzyme under atmospheric and supercritical CO_2

CHAPTER 2 LITERATURE REVIEW

This chapter provides a review of literature primarily focused on the production of nanocellulose and fermentable reducing sugars from lignocellulose cellulosic biomass. The production of nanocellulose, its characterization, application, and future perspective have been discussed in section 2.1. The supercritical CO_2 pretreatment of wood and agricultural biomass has been discussed in section 2.2. In section 2.3, the influence of high pressure and $scCO_2$ on free and immobilized cellulolytic enzymes has been critically analyzed.

2.1. Nanocellulose production, characterization, and application

2.1.1. Nanocellulose

Cellulose is well known for its outstanding physical and mechanical properties due to the hydroxyl group on its surface and strong hydrogen bonding network. Cellulose is mainly available in the form of microfibrils in the cell wall of the plants and bacterial cells [50-52]. The ordered structure on the fibrils with inter-chain hydrogen bonding leads to formation of crystalline region whereas disorder structure forms the amorphous region of the cellulose microfiber [122]. Due to the very ordered packing in the crystalline region, the hydrolysis of crystalline cellulose is difficult and takes substantially longer than the amorphous cellulose [121]. Therefore, a controlled digestion of cellulosic materials leads to formation of nanocrystalline cellulose (NCC) which has at least one dimension in nanometers. NCC is categorized into two major classes - cellulose nanocrystals (CNCs) and cellulose nanofibers (CNFs). CNCs could be in different morphological shape depending upon the feedstock and process parameters – spherical, spindle, or rod-shape [123-125]. CNCs have diameter of few nanometers and length below a

micrometer whereas CNFs have diameter of few nanometers and length up to several micrometers [122]. Another term bacterial nanocellulose (BNC) is used for the nanocellulose synthesized by microorganisms such as bacteria from genera *Agrobacterium, Aerobacter, Achromobacter, Azotobacter, Komagataeibacter* [126]. BNC is also gaining significant attention in the area of research [126-128]. Nanocellulose have gained interest owning their biodegradability, biocompatibility, lightweight-low density, and high surface area along with higher stiffness and strength than the Kevlar and cast irons [129-131].

Due to the attractive physicochemical characteristics' of nanocellulose, a Stockholm, Sweden based research and innovation institute 'Innventia' had announced the first pilot-scale plant operation in 2010 [132]. In 2012, CelluForce, Montreal, Canada based company celebrated world's first nanocrystalline cellulose (NCC) demonstration plant and ramped up its production capacity to 1,000 kg NCC per day. CelluForce used Kraft pulp in the acid hydrolysis process for the production of different types of NCCs [133]. In a market insight report (2018-2023), 'Fior Markets' estimated a global annual growth rate to be 18.8% for nanocellulose attaining a market size of US$1076.43 Million where Europe itself had 48% of total nanocellulose market volume around the world [134]. There are several commercial producers of nanocellulose in different types (i.e., Aqueous CNCs and CNFs or spray/freeze dried powders). In a recent report (2023-2028), 'IMARC group' expects that the nanocellulose companies will expand their product variants and the market will grow at global annual growth rate of 19.6% attaining a market size of US$ 1,476.9 Million by 2028. Currently operating companies in

nanocellulose industry and their establishment years are Borregaard AS (Norway, 1889), Cellucomp Ltd. (United Kingdom, 2005), CelluForce (Canada, 2010), FiberLean Technologies GmbH (Germany, 2008), GranBio Technologies (Brazil, 2011), Nippon Paper Industries Co. Ltd. (Japan, 1949), Stora Enso Oyj (Finland, 1998) [135].

2.1.2. Isolation of nanocellulose

Cellulose is the source polymer to produce nanocellulose which is available in the form of LC biomass pulp and microcrystalline cellulose (MCC). LC biomass is readily available and is the cheapest feedstock [35]. The production of nanocellulose from LC biomass is divided into two major stages. The first stage is dedicated to isolation microcrystalline cellulose pulp by pretreating the biomass. In the second stage, the isolated pulp is transformed to nanocellulose. In a conventional pulping process, the LC biomass is pretreated using reactive chemicals such as NaOCl, $NaClO_2$, Na_2SO_3, Na_2SO_4 to extract the cellulose pulp where non-cellulosic (hemicellulose and lignin) components are removed and remain unused. Kraft and sulfite pulping are the well-known and established conventional method of producing cellulose pulp at commercial scales specifically in paper and pulp industry [97-100]. However, these methods have concerns of high volume water consumption and wastewater generation contaminated with lignin and chlorinated toxic compounds [59]. In recent years, emerging methods are being studied to develop an integrated LC biorefinery which focuses on efficient utilization biomass components [136]. The emerging methods of LC biomass treatment includes reusable and advanced solvent such as organic solvent (methanol, ethanol), weak organic acids (formic acid, acetic acid), ionic liquid (ILs

- [BMIM]$MeSO_4$), deep eutectic solvents (DES – choline chloride with imidazole or oxalic acid) [61-62, 137-139]. Due to environmental concerns of conventional methods, non-conventional methods could be the alternative to develop a sustainable and environmentally friendly process of cellulose pulp and nanocellulose extraction from the LC biomass.

In the first stage, the process begins with the grinding of dry biomass to ~60.0 mesh sieve or lower size followed by removal of wax and extractive components by Soxhlet extraction [140-141]. The lignin and hemicellulose are removed by primary and secondary bleaching steps such as soaking in the alkaline pretreatment such as 3.0-6.0 wt.% potassium hydroxide (KOH) or 2.0-13.0 wt.% sodium hydroxide (NaOH), or calcium hydroxide ($Ca(OH)_2$), for 5.0-24.0 h at room temperature following high temperature ~80.0 °C for 2.0-3.0 h reaction [14, 57, 104]. These alkali pretreatments saponify the ester bonds of lignin and hemicellulose [52]. Chen et al., (2011) prepared chemically-purified cellulose pulp using poplar wood powder treated with acidified sodium chlorite at 75 °C to remove lignin followed by 3.0-6.0 wt.% KOH to leach the hemicellulose [141]. Whereas Heidarian et al., (2017) involved 1.0-3.0 M hydrochloric acid hydrolysis of aspen wood sawdust in between the primary and secondary bleaching stages in the process of producing cellulose nanofibers. The primary bleaching was carried out with 3.0 % (w/v) hydrogen peroxide (H_2O_2) and acetic acid (CH_3COOH) treatment to weaken the lignin – polysaccharides interactions. After acid hydrolysis treatment, secondary bleaching was carried out with 2.0 wt.% NaOH that leached out the soluble lignin, pectin and hemicellulose. This alkali step reduced the need of harsh of secondary bleaching

by acidified sodium chlorite [140]. Delignification and bleaching are the essential requirement in order to prepare purified cellulose pulp from LC biomass to produce nanocellulose with minimum non-cellulosic components and higher crystallinity and thermal properties [103, 140, 142].

In the second stage, bleached Kraft wood pulp is the most commonly used in nanocellulose production as it is easily available from the paper and pulp industries [46, 143-144]. The bleached pulp undergo acid hydrolysis, TEMPO oxidation, enzymatic hydrolysis, and/or mechanical disintegration that produces the individualized CNCs and CNFs [125, 145]. Acid hydrolysis is the well-established process in nanocellulose production. However, the physicochemical properties of the produced nanocellulose varies due to several factor over the sequential steps involved in the process [146]. The bleached pulp is hydrolyzed with acid at a very mild temperature ~45 °C to hydrolyze the amorphous subregion [147]. Strong acids such as sulfuric acid (H_2SO_4) and phosphoric acid (H_3PO_4) are used for the acid hydrolysis [52, 148-149]. For example, Camarero Espinosa et al. (2013) hydrolyzed Whatman filter paper with 6.2-10.7 M phosphoric acid at 50.0-100.0 °C under for 30.0-90.0 min. The morphology and size of the cellulose nanocrystals were varied based on the severity of the reaction and homogeneous CNCs were observed for the reaction at 100.0 °C for 90.0 min [150]. The sulfuric acid hydrolysis (62.0 wt.%, 44.0 °C, 90.0 min) of pinewood acetosolv pulp led to CNCs yield of 2.3 wt.% of the pulp with 67.8 % crystallinity [57]. Whereas sulfuric acid hydrolysis (58.0 wt%, 56.0 °C, 180.0 min) of bleached eucalyptus Kraft pulp resulted in 68.0 wt.% CNCs yield with 76.2 % crystallinity [54]. The yield, morphology, and properties of CNCs are

considerably dependent on the temperature and acid concentration as well as the process of cellulose pulp isolation from the biomass [150]. After hydrolyzing the amorphous cellulose, crystalline cellulose is treated with mechanical treatment to individualize the nanocrystals and nanofibers. Sonication, grinding, cryo-crushing, and high-pressure homogenization are commonly used methods. Mechanical treatment disperses the individual nanofibers homogeneously in the suspension [52, 57, 104, 140-141]. Further, nanocellulose is characterized for physicochemical properties such as crystallinity index, thermal degradation, surface functional groups, surface charge and aspect ratio for its end-use applications.

2.1.3. Nanocellulose characterization

Characterization of nanocellulose enables researchers to determine the physicochemical properties, quality improvement, and their potential applications. For the characterization, various parameters are analyzed using different equipment. Crystallinity index (CrI) is among the most important parameter for nanocellulose material. The nanocellulose are highly crystalline materials after removal of non-cellulosic and amorphous cellulose content from the pulp and microcrystalline cellulose [56, 151-152]. The crystallinity index is measured mainly by using an X-Ray diffraction pattern of the nanocellulose material. However, the calculation of crystallinity index is done by two methods – (1) Ratio of peak areas and (2) ratio of peak intensities of crystalline and amorphous regions [153-154]. The most used method for reporting the Crystallinity index of nanocellulose is based on the ratio of peak intensity also known as Segal method [153]. The measured crystallinity index has substantial differences based on the mentioned methods. For example, Thygesen et al., (2005) analyzed crystallinity index of different

cellulosic materials including Whatman filter paper, spruce, cotton linter cellulose, corn stover. The crystallinity index determined by peak intensity-height ratio method showed significantly higher results for all the materials. [154]. Therefore, it is very important to mention the method of crystallinity index analysis and its comparison with the literature.

Thermal stability of the nanocellulose is another important parameter which shows the thermal tolerance of the nanomaterials. Thermogravimetric analyzer (TGA), differential thermogravimetry (DTG), and differential scanning calorimetry (DSC) are used in a wide range of temperatures (30.0-550.0 °C) which shows the thermal decomposition of the nanocellulose materials [97, 155-157]. Infrared spectroscopy (IR) analysis shows the presence of various bonds and functional group. IR spectra confirms the structural changes (lignin and hemicellulose removal, sulfate group grafting on surface, exposure of more hydroxyl groups and hydrogen bonding) over the different chemical treatments of biomass and pulp in production of nanocellulose [129, 155].

Transmission electron microscopy (TEM), scanning electron microscopy (SEM), and atomic force microscopy (AFM) are the most common visual imaging equipment used in morphological analysis of nanocellulose [155-156, 158-159]. Such equipment uses a certain accelerating voltage and dyeing of the sample before visualization. In the preparation, samples are dispersed in the distilled water and diluted to 0.005-0.01 wt.% concentration of nanocellulose followed by ultrasonication for 1.0-2.0 minutes [143, 160]. The particle size and aspect ratio analysis are usually done by measuring the size of individual nanocrystals and

nanofibers from microscopy images where ImageJ is the most widely used software tool. The aspect ratio of the CNCs is the ratio of length to width. Higher aspect ratio enables it to have more functionalization capacity on its surface for various application [45, 161].

2.1.3. Nanocellulose applications and future perspectives

Production of nanocellulose from different feedstock source along with different chemical and mechanical treatments processes, has the potential to be tailored according to end applications [129]. Xu et al., (2019) studied the nanocellulose suspension rheology, colloidal phase behavior, and ordering of nanocrystals and pointed out that the morphology and dimensions of CNCs considerably vary based on the source and production process [162]. Nanocellulose has wide range of applications in different fields such as biomedical, composite material, adhesive, Pickering emulsions, nano paper and packaging materials [163-166]. For example, surface modified CNCs with amino-propyl-tri-ethoxy-silane (APTES) increased contact angle between the CNCs and urea-formaldehyde resin adhesive by 26.4 % [167]. In the evolution of nano-biomaterials, extensive research has been reported and others being continued employing nanocellulose in the field of biomedical (i.e., tissue repair, drug delivery, biosensing) due to its biocompatibility, biodegradability, no/low toxicity, high surface area-to-volume ratio, and mechanical characteristics, rheology, potential of functionalization and modification. Due to the nanoscale dimension, CNCs may enter cells, cause inflammatory response, oxidative stress [168-169]. However, such concerns could be addressed by functionalization of nanocellulose with specific groups of interest [129, 170]. For instance, Ntoutoume et al., (2016) synthesized a CNC/curcumin/cyclodextrin

complex where CNCs were functionalized by β-cyclodextrin (CD) and the synthesized complex exerted an antiproliferative effect on colorectal and prostatic cancer cells [171]. On the other hand, extensive research has been focused on the application of nanocellulose in contaminated water treatment and dye removal [165, 172-173]. Similarly, there have been numerous studies showing the growing potential of nanocellulose in the different. The variety of feedstock source availability and tailorability of nanocellulose, these is a wide scope for the development of cost-effective and environmentally sustainable method for nanocellulose production and further functionalization for different applications.

2.2. Conversion of lignocellulosic biomass to reducing sugars in high pressure and supercritical fluids: greener alternative for biorefining of renewables

Section 2.2 of this chapter has been published in Journal of Advanced Sustainable Systems:
Pawan Kumar, Azadeh Kermanshahi-pour, Satinder Kaur Brar, and Marianne Su-Ling Brooks. 2021. 'Conversion of Lignocellulosic Biomass to Reducing Sugars in High Pressure and Supercritical Fluids: Greener Alternative for Biorefining of Renewables', Advanced Sustainable Systems, 5: 2000275.

2.2.1. Abstract

Supercritical fluids offer great potential to be employed in lignocellulosic biomass (LCB) fractionation in biorefinery. Supercritical carbon dioxide and water are greener alternatives compared with conventional reagents (e.g., acid or base) and have been investigated for the pretreatment and hydrolysis of lignocellulosic biomass. This review is focused on examining the fundamentals that govern the function of supercritical fluids in pretreatment stage, as well as in the main hydrolysis reaction. Sub/Supercritical carbon dioxide is used in pretreatment and sub/supercritical water has been the solvent of choice in hydrolysis of LCB. Significant research has been gone into understanding the effect of process parameters such as temperature, pressure, co-solvent and use of external catalyst on the sugar yield in biorefining of the LCB in supercritical fluids. It is identified that processes with reduced environmental impact and energy consumption can significantly enhance biorefining of LCB at commercial scale. Enzymatic hydrolysis of LCB in supercritical carbon dioxide is a promising approach that can accommodate mild reaction condition. Developing an understanding on

performance of enzymes in high pressure systems and designing carriers for enzyme immobilization and further recycling will enable one pot pretreatment and hydrolysis and will be a milestone in processing renewable resources for deriving biofuel and value-added chemicals.

2.2.2. Introduction

Increased consumption of non-renewable resources for energy production and the release of carbon dioxide associated with the production and consumption of fossil fuel are amongst today's most pressing sustainability challenges. According to the International Energy Agency (IEA)'s projection, the world energy demand is forecast to increase by 24.0% in the year 2040 [2]. Implementing a biorefinery, in which multiple products are derived from renewable resources offers significant potential for a circular system where the production of waste is minimized, and the use of biomass is maximized aiming at enhancing social and economic prosperity, and environmental quality [9-12]. Additionally, in the circular economy, the waste and byproducts generated is used as feedstock for producing another product [174]. Lignocellulosic (LC) biomass mainly consists of three heterogenous biopolymers: - cellulose (16.0-56.0 %), hemicellulose (13.0-33.0 %), and lignin (4.0-55.0 %). The most common feedstock used in LC biorefinery includes softwood, hardwood, bagasse, stover, and straw [22, 175-177]. The world is rich in LC biomass with a wide distribution around the globe. For example, Russia, Brazil, and Canada have the highest forest land area, while China, India, and the United States are the primary producers of crops [178]. Despite the abundance of LC biomass, commercial LC biorefineries face significant sustainability challenges and they are not widely implemented. LC biorefineries require the feedstocks undergoing a pretreatment

process to remove or disrupt the recalcitrant lignin and hemicellulose network. Crystalline cellulose can also be partially converted to amorphous cellulose in the pretreated solids [116-117]. Conventional pretreatment methods are classified into biological (e.g., fungal and bacterial pretreatment), physical (e.g., milling, ultrasonic, microwave, mechanical extrusion); chemical (e.g., acid hydrolysis, alkaline hydrolysis, organosolv, oxidation delignification, ozonolysis), physicochemical pre-treatment (e.g., steam explosion, ammonia fiber explosion) methods [116-119]. Emerging technologies are developed based on the use of ionic liquids (ILs), deep eutectic solvents (DES), microwave-assisted methods, sub/supercritical fluids (SCFs), aiming at enhancing the recyclability of solvents/reagents of pretreatment processes [91-94, 96, 179-181]. These advanced solvents are recyclable and have high selectivity for removing non-cellulosic fractions of the LC biomass [40, 182]. DES are versatile for sustainable biorefinery applications and evaluated to be readily biodegradable [179, 183-186]. On the other hand, DES and ILs are expensive and some of them are toxic, requiring the use of ammonium salt, urea, and choline chloride [179, 183-186]. Processing of LCB in ILs and DES solvents requires solvent recovery as well as thorough washing of the pretreated solid for further hydrolysis reaction [187].

Sub and supercritical fluids (SCFs) have been used in pre-treatments since the last quarter of the 20th century [188-189]. It has gained attention in the past few years for use as reaction media and co-solvents in lignocellulosic biorefinery [10, 42, 177, 190-191]. SCFs are different from the high pressure or hot water and possess unique properties at critical points [192-194]. When the temperature and pressure of

a substance is above its critical temperature (T_c) and pressure (P_c), the properties of the fluid are between those of a gas and a liquid, with viscosity and diffusivity closer to those of gas and density closer to that of liquid [195-196]. As evident, when density is considered, SCF (200.0-900.0 kg/m^3) is more likely to behave as liquids (600.0-1200.0 kg/m^3), while its range of viscosity is closer to that of gas (SCF: 0.01-0.09 Pa.s; Gases: 0.01-0.03) [197]. Physicochemical properties of fluids can be changed significantly in response to small fluctuations in temperature and pressure, near the critical points that can result in favorable conditions such as enhanced dissolution of feedstock components, higher mass and heat transfer, and facile product separation [192, 198-202]. During the past few years, supercritical water (SCW, 22.1 MPa, 374.2 °C) has been gaining interest as a suitable reaction medium for biomass fractionation in a biorefinery [38]. $ScCO_2$ is also recognized for processing of woody biomass in recent years because of its role as an autocatalyst in the presence of water in modern biorefineries [203].

Water and CO_2 are considered as environmentally benign solvents due to their non-toxic nature and particularly in the case of CO_2, due to its lower critical temperature and pressure ($scCO_2$, 31.0 °C, 7.4 MPa) [190]. Deploying sub and supercritical CO_2 or water in processing LCB eliminates need for the use of acid and alkaline solution for hydrolysis, which are commonly employed pretreatment technologies and addresses the concerns related to large amount of high strength wastewater and the need for waste neutralization. Incorporation of enzymes into the SCF-based technologies will likely enhance sustainability, considering renewability and recyclability of enzymes and require milder rection conditions.

Therefore, supercritical fluid-based technologies are considered as potential greener alternatives compared to conventional methods. However, the knowledge gap towards enhancing the sustainability of such systems should be identified and thus the goal of this review paper is to provide an overview of the current state of research and development on the application of SCFs in processing LCB for sugar production (Figure 2-1) as well as identifying the knowledge gap and path forward toward innovating more sustainable approaches.

The fundamental phenomena governing the function of sub/supercritical carbon dioxide and water in pretreatment and hydrolysis of LCB are discussed (Section 2). Pretreatment of biomass in high-pressure and subcritical fluid (section 3) and supercritical carbon dioxide (section 4) followed by either acid or enzymatic hydrolysis are reviewed. Current advancement on the application of sub/supercritical water and carbon dioxide as the sole hydrolysis reaction media is investigated (section 5). The influence of the system parameters and reaction conditions (T, P, co-catalyst, feedstock particle size, etc.) on sugar yield (sugar released per amount of biomass and sugar released per amount of hydrolysable sugars) are critically analyzed (section 3,4,5). The performance of the enzymes under high pressure and potential for integration of $scCO_2$ and enzyme in one pot system (section 6) is examined. Moreover, the commercial status of the current technologies has been investigated (section 7).

Several review articles have been published in the area of bioenergy and bioproducts derived from LCB [10, 38-43]. Some works have particularly focused on the use of advanced solvents and supercritical fluids for processing different types

of biomass such as plant, lignin, and seaweeds for derivation of bioproducts, whereas others have paid attention to SCF application on liquefaction, gasification and pyrolysis with catalysts for LC biomass valorization [10, 42-43, 204-206]. In this review we particularly focused on processing agricultural and woody biomass in sub/supercritical fluids for derivation of sugars and made a significant effort in collecting and processing the data related to the pretreatment sugar yield as well as the overall yield (e.g., combined pretreatment and enzymatic hydrolysis) for comparing the performance of various sub/supercritical fluid-based systems. Another important aspect of our work, which has been overlooked in prior critical reviews is examining the potential of one $scCO_2$ pretreatment and enzymatic hydrolysis in one pot with respect to the reaction mechanisms and recent advancement in the field.

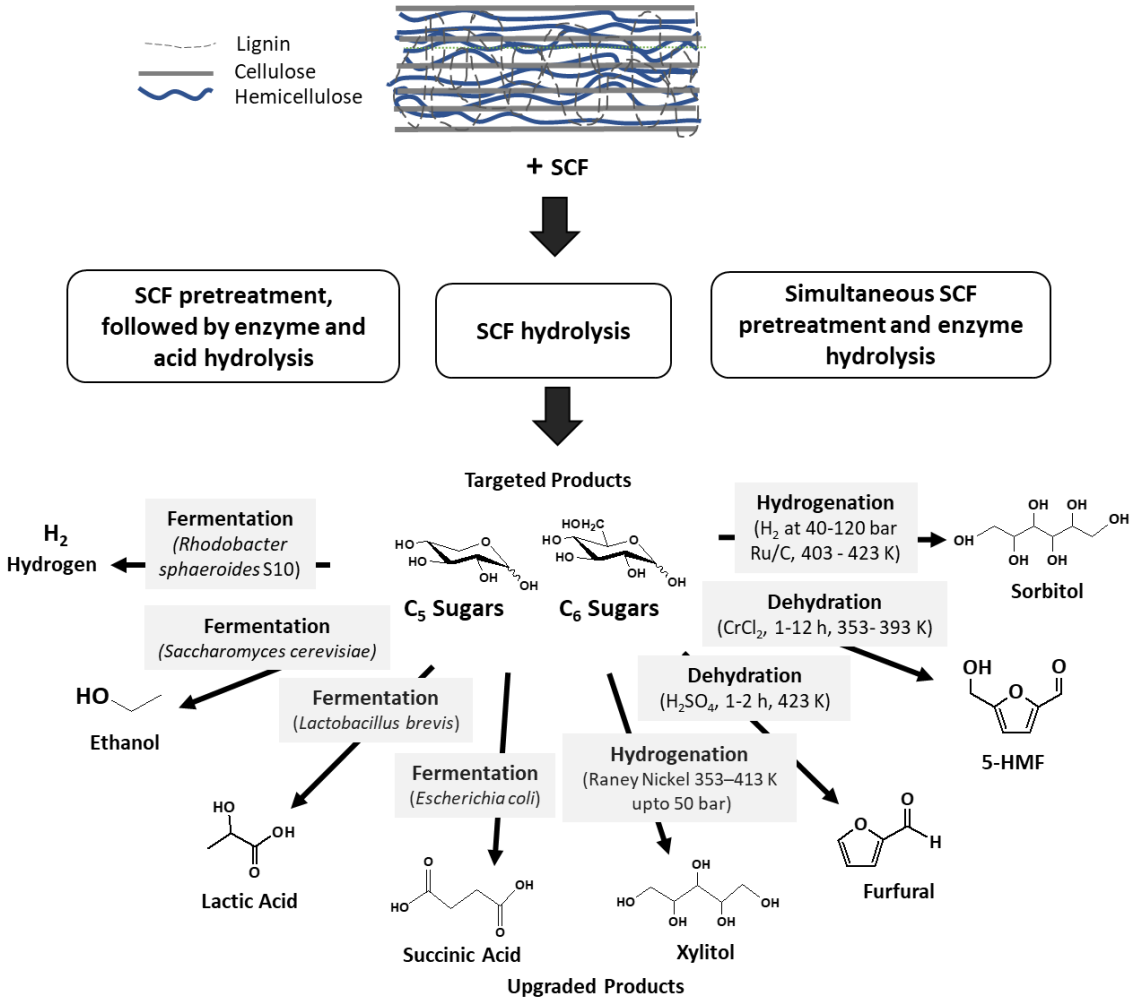

Figure 2-1 Application of supercritical fluids in lignocellulosic biorefinery to derive reducing sugars as intermediates to further produce platform chemicals.

2.2.3. Fundamentals of sub/supercritical carbon dioxide pretreatment and sub/supercritical water hydrolysis of lignocellulosic biomass

Different types of alkaline solutions, mineral acids, ionic liquids, and organic acids, are applied in the conventional pretreatment of lignocellulosic biomass for bioproduct production, including sugars [207-209]. Strong acids are widely applied on a commercial scale to pretreat or hydrolyze LC biomass [116, 210-211]. Technical and environmental challenges associated with the conventional pretreatment methods, including sugar degradation, equipment corrosion, high water consumption, and generation of the large volume of waste, limit their sustainability [76, 212]. The use of

sub and supercritical CO_2 in the presence of H_2O as co-solvent eliminates the need for the use of acid and alkaline solution and addresses the concern related to waste neutralization. The major role of sub/supercritical carbon dioxide in the pretreatment of lignocellulosic biomass is hemicellulose fraction hydrolysis and disruption of recalcitrant and crystalline structure [18, 213]. The hydrolysis process is catalyzed by the *in-situ* formation of carbonic acid due to the high pressure of sub/supercritical CO_2, as shown in Equation (1) and (2).

$$CO_2 + 2H_2O \leftrightarrow HCO_3^- + H_3O^+ \quad (1)$$

$$HCO_3^- + H_2O \leftrightarrow CO_3^{2-} + H_3O^+ \quad (2)$$

As can be seen in the above equilibrium reaction, the formed carbonic acid (H_2CO_3) is unstable in the reaction and CO_2 is released once the pressure reduced to atmospheric pressure [18, 214]. The solubility of CO_2 in water increases with increasing the pressure (i.e., solubility increases from 0.5 % to 2.0 % molar fraction of CO_2 in water when pressure is increased from 2.5 MPa to 30.0 MPa, at 85.0 °C), whereas increasing the temperature reduces the amount of dissolved CO_2 (i.e., 3.2 % to 2.25 % molar fraction of CO_2 in water when temperature increased from 15.0 °C to 85.0 °C, at 30.0 MPa) [215].

The presence of acetyl groups (CH_3CO) in LC biomass such as sugarcane bagasse and aspen wood facilitates hydrolysis by the release of acetic acid due to hydrolysis of hemicellulose [25, 176, 216]. This weak acid is strong enough to catalyze the hydrolysis of hemicellulose, whereas the cellulose fraction mainly remains intact [176-177]. Temperature and pressure of the high-pressure fluid, pH of the solution, and reaction time are the most influential parameters that drive the hydrolysis in high pressure CO_2–H_2O systems. At high pressure systems, as

pressure increases, the solubility of CO_2 in water increases to an optimum, resulting in pH reduction and promoting hydrolysis [217-218]. Increasing the temperature results in a decrease in the solubility of CO_2 in water, which is not favorable for hydrolysis. However, temperature influences hydrolysis reaction, as demonstrated in Equation (3) and therefore, must be optimized to increase the rate, while minimizing sugar degradation [217-218]. The combined effect of reaction time and temperature is termed the severity factor. The severity factor of the reaction R_o is defined in Equation (3):

$$\log R_o = \log \left[\sum_{i=1}^{n} t_i . \exp\left(\frac{T_i - T_o}{\varpi}\right)\right] \quad (3)$$

$$\varpi = \frac{T_f . R}{E_a} \quad (4)$$

Where t_i is the retention time, T_i is pretreatment temperature; T_o is the base temperature (100.0 °C), and *i* & *n* is denoted for *i*th pretreatment stage in total *n* number of stages. The empirical parameter ϖ with a value of 14.75, depends on the average temperature of the experiment (T_f), Gas constant (R), and activation energy (E_a) [25, 219-220]. The combined severity factor, which considers the collective effect of temperature, reaction time, and pH on CO_2-H_2O driven reactions, is expressed by Equation (5) [220].

$$Combined\ Severity = \log R_o - pH \quad (5)$$

Walsum (2001) studied the xylan hydrolysis using sub and supercritical CO_2 in the presence of water as co-solvent, that is governed by the carbonic acid formation.[220] Based on their study in varying partial pressure of CO_2 (0-13.7 MPa), reaction time (0.5–28.5 min) and temperature (170.0-230.0 °C), theoretical pH dependency was expressed in terms of temperature (T) and partial pressure of CO_2 (P_{CO2}) in Equation (6).

$$pH = \left[8 \times \left(\frac{T}{1000}\right)^2\right] + \left[2.09 \times \left(\frac{T}{1000}\right)\right] - [0.216 \times ln(P_{CO2})] + 3.92 \quad (6)$$

It is difficult to measure the exact pH during the reaction. Therefore, it could be predicted using Equation (6) with dependencies on the temperature and partial pressure. Morais, et al, (2014) calculated the pH using Equation (6) and compared it with the final measured pH of hydrolysate produced as the result of supercritical carbon dioxide pretreatment of agricultural biomass under varying severity conditions. Their measured pH (3.5 – 4.0) was close to calculated pH (3.71 – 4.21) using Equation (6). This difference was attributed to the acetic acid released from acetyl groups [213].

Walsum (2001) reported the hydrolysis of xylan to xylose with yield up to 26.4 wt.% of total hydrolysable sugars (THS) at 190.0 °C, 5.5 MPa and 28.5 min of reaction time [220]. The optimal severity factor of the hydrolysis reaction corresponds to the highest sugar yield with minimum degradation products. The optimum range of temperature for hemicellulose hydrolysis during pretreatment, has been reported within 160.0-200.0 °C with pressure in the range of 5.0-6.0 MPa by various research groups [18, 22, 176]. A temperature of higher than ~200.0 °C with long reaction time may cause degradation of the hydrolyzed sugar, resulting in decrease in the overall yield. Therefore, the combined effect of temperature and pressure to retain the dissolved CO_2 in water, and its subsequent role in pH adjustment plays a crucial role in the high-pressure and sub/supercritical fluid system to release the hemicellulosic sugars [220].

It is hypothesized that the predominant mechanism in sub/supercritical CO_2-based systems is based on the penetration of CO_2 to biomass, which is enhanced

by the presence of water. When sudden depressurization is applied after completing the pretreatment, strong shear forces, along with significant thermal changes in sub/supercritical water, result in collapsing the structure of LC biomass (explosion effect) and subsequent increase in porosity and decrease in crystallinity [177, 221-222]. The secondary mechanism is attributed to the interaction of water and CO_2 and subsequent carbonic acid formation, resulting in mild hemicellulose hydrolysis [223]. Both of these mechanisms make cellulose and hemicellulose more exposed to the subsequent step of hydrolysis (acid or enzymatic hydrolysis), resulting in improved sugar yield [177, 221-223].

There are some reports, indicating an attempt to optimize the influential parameters such as temperature, pressure, water content and reaction time in order to achieve both hydrolysis and explosion effects [214, 223]. Higher severity factor can be achieved in supercritical fluid pretreatment compared to high pressure and subcritical-fluid based pretreatment. In most studies, sub-critical CO_2 treatment, water to solid ratio of higher than 1.0 is used as opposed to typically less than 1.0 water to biomass ratio in the case $scCO_2$ (Table 2-1, Table *2-2*, and Table *2-3*).

Water–solid ratio below one is commonly used in $scCO_2$-based pretreatment to understand the effect of pretreatment on the enzyme digestibility of the biomass [111, 214]. For instance, Srinivasan and Ju (2010) used a water-solid ratio of 0.65 for guayule biomass, and reported that there was no release of sugars during the $scCO_2$ pretreatment (200.0 °C, 27.5 MPa & 30.0 min) and the polysaccharides were only present in residual solid [223]. However, Morais et al., (2014) obtained

28.5 % of the THS released in the subcritical CO_2–based pretreatment (215.0 °C, 5.4 MPa & 38.9 min) of wheat straw, when water-solid ratio of 10.0 was used [213]. However, regardless of whether sub or supercritical CO_2 is employed, hydrolysis of hemicellulose and subsequent release of monomers and oligomers into the liquor results in increased porosity of the residual solid along with loosening the rigid structure of the biomass [25, 213]. Therefore, the LC biomass pretreated in sub/scCO_2, results in increased cellulosic fraction in comparison to other biopolymers and high sugar yields in pretreatment step [224].

There is potential for the formation of sugar degradation products (*e.g.,* 5-hydroxymethylfurfural (5-HMF), furfural, formic and acetic acids) in CO_2-H_2O pretreatment processes at a higher temperature and longer reaction time, which results in reduction in sugar yield [22, 25, 216]. Additionally, these degradation products are inhibitory in downstream enzymatic hydrolysis and reducing sugars fermentation. The potential for sugar degradation may be reduced either by reducing the severity of reaction or functionalization to form stable intermediates. The stabilization of the reactive intermediate using chemical functionalization has been recently reviewed by Luterbacher and co-workers [225]. Sugar degradation is catalyzed by the dissociated ions of water, resulting in conversion of glucose to fructose, and further decomposition to 5-HMF [226-227]. The fructose is formed by keto-tautomerization reaction of glucose and then these hexoses are further decomposed to 5-HMF, erythrose, glycolaldehyde, glyceraldehyde and other byproducts [226]. Decomposition rate of glucose increases with an increase in the temperature [228]. These degradation product formations by different pathways are

represented in Figure 2-2. The hydrolysis of cellulose to glucose and decomposition of glucose under supercritical water is significantly influenced by the presence of ions of water molecules. Glucose isomerization to fructose and its further dehydration to produce 5-HMF are highly dependent on ions concentration. The concentrations of H^+ ions as well as OH^- ions of water, decrease from 10^{-6} to 10^{-12} M, when temperature increases from 300.0 °C to 400.0 °C at pressure 23.0 MPa, favoring radical reaction over ionic reaction [227]. Decrease in ion concentration (increase in pOH/pH), results in minimizing glucose isomerization to fructose and further dehydration of fructose to 5-HMF (Figure *2-2*). At this condition, the retro-aldol condensation pathway, which results in glycolaldehyde production was enhanced instead of isomerization/dehydration pathway, which results in 5-HMF production [226]. Furfural, 5-HMF and acetic acids are detected degradation products of C5 and C6 sugar in both pretreatment and main hydrolysis in sub/supercritical water [107, 229].

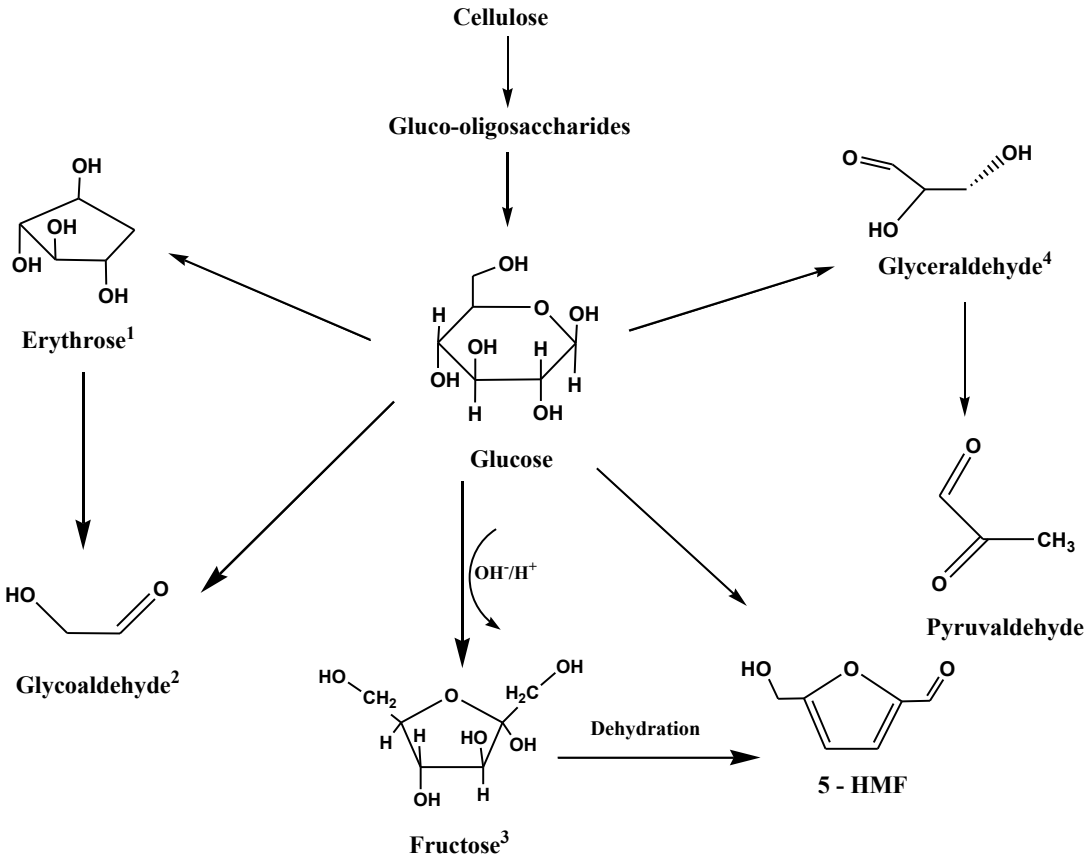

Figure 2-2. Conversion of cellulose to glucose, followed by the formation of degradation production where 1,2 - Retro – aldol condensation of glucose lead to the formation of erythrose and further to glycolaldehyde 3- Isomerization of glucose through keto tautomerization and conversion of glucose and fructose to 5-HMF; 4 - Glucose conversion to glyceraldehyde.

2.2.4. High pressure and subcritical fluids pretreatment of lignocellulosic biomass, followed by enzymatic hydrolysis

High pressure and subcritical fluids (CO_2 and water) are being applied for pretreatment of both agricultural and woody biomass. These pretreatments are carried out either at elevated temperature or the elevated pressure, but it does not meet the supercritical fluid conditions. The pretreatment step is often followed by enzymatic hydrolysis to complete the hydrolysis of polysaccharides. The yield unit reported in various studies vary in different units (i.e., simple percentage (%), mol.%, g/kg, wt.%). Therefore, overall yield of pretreatment and enzyme hydrolysis

is reported based on the two standard units: the weight of C_5 and C_6 sugars mono- and oligomers released per 100 g weight of the initial feedstock (IF) and weight of C_5 and C_6 sugars mono- and oligomers released per 100.0 g weight of THS (wt.%) ().[18] The two types of yield based on THS and IF (wt.%) can be calculated using the Equation (7) and (8):

$$Sugar\ Yield\ \ (wt.\%\ of\ Initial\ Feedstock) = \frac{Weight\ of\ obtained\ sugar}{Weight\ of\ initial\ biomass} \times 100 \quad (7)$$

$$Hydrolysable\ Sugar\ Yield\ \ (wt.\%\ of\ Initial\ Polysaccharide) = \frac{Weight\ of\ obtained\ sugar}{\frac{Weight\ of\ glucan\ in\ biomass}{0.9} + \frac{Weight\ of\ hemicellulosic\ polysaccharide\ in\ biomass}{0.88}} \times 100 \quad (8)$$

Where 0.90 (162.0/180.0) is the anhydrous correction factor for glucan, and 0.88 (132.0/150.0) is the anhydrous correction factor for xylan. These correction factors have been obtained from the ratio of molecular weight of glucose in glucan to the molecular weight of free glucose, and molecular weight of xylose in xylan to the molecular weight of free xylose, respectively [223]. Pretreatment yields, shown in Table 2-1 and Table *2-3* were calculated based on the major reported products (i.e., arabinose, xylose mannose, glucose, xylo-oligosaccharides, or cellu-oligosaccharide (also termed as gluco-oligosaccharide)) released during the pretreatment. The overall yield is calculated by summing the sugars produced in two steps (pretreatment & enzyme hydrolysis) and using the Equation (7) and (8). The denominator in Equation (8) represents the corresponding polymer of the released sugar in individual reactions.

Several studies on biomass pretreatment under high pressure and subcritical CO_2 and water have demonstrated yield of 11.2–28.5 % of THS, releasing glucose & xylose, and gluco-oligosaccharides (GluOS) & xylo-oligosaccharides (XOS) sugars during the pretreatment (Table 2-1). The total monomeric and oligomeric

C_5 and C_6 sugar yield of the overall process, including both pretreatment and enzyme hydrolysis, ranges 63.0–93.0 wt.% of THS (Table 2-1) [213, 216]. The pretreatment temperature was varied 170.0-220.0 °C under a pressure of 5.0-6.0 MPa, whereas longer reaction time up to 80.0-100.0 min was used at lower temperatures 170.0-180.0 °C [106, 224]. The residual solids after pretreatment, are further hydrolyzed by cellulases enzyme to produce reducing sugars [22, 176]. Feedstock slurry with water to solid ratio in the range of 5.0-10.0 was used for processing lignocellulosic biomass (Table 2-1). As discussed in the previous section, the presence of water helps CO_2 to penetrate the biomass to explode and disrupt the crystalline structure, resulting in improvement of enzyme accessibility in the subsequent stage.

The particle size of feedstock is another parameter that influences the reaction yield. Subcritical CO_2-H_2O pretreatment of sugarcane bagasse with particle size less than 1.0 mm, followed by enzymatic hydrolysis led to 93.0 wt.% of THS [224]. It was found that particle size smaller than 1.0 mm has high surface area and a significant influence on penetration of reaction media into the polysaccharides during the pretreatment of LC biomass but going beyond 0.4 mm was not giving any further improvement in sugar yield [110, 230].

The presence of acetic acid as a co-catalyst influence hemicellulose hydrolysis during the pretreatment. It reduces the pH of the reaction and catalyzes the reaction. Li et al., (2020) studied the effect of acetic acid (0–0.5 mol/L) as a co-catalyst to hydrolyze the hemicellulosic fraction of the wheat straw under high-pressure CO_2–H_2O (180.0 °C, 5.0 MPa). The hydrolysis yields were increased from

48.1 wt.% to 63.5 wt.% of xylan to xylose and XOS and 21.1 wt.% to 24.3 wt.% of THS in the presence of 0.3 mol/L acetic acid [176]. Morais et al. (2014) reported that a decrease in pH due to the presence of acetyl group in hemicellulose and dissociated carbonic acid under severe reaction conditions, might increase the degradation of the released sugar in the hydrolysate [213].

Some studies focused on reducing sugar degradation using multi-stage pretreatment system [23, 25]. For example, a single stage subcritical water pretreatment (200.0 °C, 20.0 min) of hardwood followed by enzyme hydrolysis was carried out. The hydrolyzed xylan based sugar recovery was maximum than 70.0 % at expense of more than 15.0 % sugar degradation.[25] The overall sugar yield of 63.7 wt.% of the THS was obtained in single staged pretreatment followed by enzyme hydrolysis. On the other hand, in three stage subcritical water pretreatments at 180.0 °C, 20.0 min (stage I), 200.0- 220.0 °C, 5.0-10.0 min (stage II) & 210.0-230.0 °C, 7.5-15.0 min (stage III), followed by enzymatic hydrolysis, an optimum overall yield of 81.0 wt.% of THS was obtained. The three-stage pretreatment allowed to recover the hydrolyzed pentoses sugars in three different stages of the pretreatment. This enables the researchers to prevent sugar degradation and improve the yield of the overall sugar production. The multi-stage pretreatment yielded 28.78 wt. % of THS with recovery of 92.0-95.0 wt.% of solubilized xylose in during pretreatment with reduced degradation from 15.0 % (in single stage) to 3.0 % (in multi stage) of THS of solubilized pentoses [25].

The high pressure and subcritical fluids (CO_2 and H_2O) offer relatively mild pretreatment conditions (160.0-230.0 °C, 5.0-6.0 MPa) (Table 2-1) and improve

the enzymatic yield of sugars in comparison to conventional pretreatment methods. The high pressure and subcritical pretreatment reaction are carried out in high-pressure reactors. Most of the reactors used are made of stainless steel with a high wall thickness of 0.5 inches to prevent corrosion, and some coupled with turbines to provide *in-situ* mixing of biomass [18, 229]. Majority of subcritical CO_2-H_2O pretreatment processes are performed in lab-scale batch reactors of varying reactor volume 30.0 mL to 1000.0 mL with the headspace at least 25.0 % [25, 224].

Table 2-1. High pressure and subcritical pretreatment before enzymatic hydrolysis of agricultural and lignocellulosic biomass as feedstock.

Feedstock	Pretreatment step reaction conditions [a]						Enzyme hydrolysis reaction conditions					Overall yield (wt.%) [b]		Ref.- Note
	SCF/ Co-solvent/ liquid solid ratio	T (°C)	P (MPa)	t (min)	Reactor Configuration/ Volume (mL)/mode	Pretreatment major products/ yield % (THS) * [a]	T (°C)	t (h)	Reactor Type/ Volume (mL)/ AR (rpm)	Enzyme	Sugar Product	g/100 g Initial feedstock (IF)	g / 100 g Total hydro-lysable sugar (THS)	
Agricultural Biomass														
Elephant grass	CO_2/ H_2O/ 10	220	5	-	High pressure stirred reactor/ 160/ Batch	Xylose & XOS/ 13.27	50	72	Falcon tube/15/ 150	Three types of Accellerase ®	Glucose	36.1 *	63.4*	[216] c, d)
Sugarcane bagasse	CO_2/ H_2O/ 6.67	180	5	100	Stirred tank reactor/ 1000/Batch	-	50	72	Flask/50 0/ 150	Cellulase	Glucose	38.5	93.0	[224] c)
Sugarcane bagasse	CO_2/ H_2O/ 10	220	5	-	High pressure stirred reactor/ 160/Batch	Xylose & XOS/ 18.0	50	72	Falcon tube/15/ 150	Three types of Accellerase ®	Glucose	47.3 *	69.6*	[216] c, d)
Wheat straw	CO_2/ H_2O/ 10	215	5.4	38.9	—	GluOS, XOS & Xylose/ 28.5	—	96	—/ —/ —	Cellulase (Celluclast) and β-glucosidase (Novozyme-188)	Glucose	55.3*	84.7	[213] e)
Sugarcane bagasse	CO_2/ H_2O/ 10	190	5	-	High pressure vessel/ 250/Batch	XOS & Xylose/ 16.32	50	-	- /10/ 200	Cellulase (Cellic CTec3) and hemicellulase (Cellic HTec3)	Glucose & xylose	57.0*	73.9	[22] f)
Woody Biomass														
Harwood chips (Mascoma Corporation)	H_2O/—/ 5.67	180, 210, 230	-	20,5,7.5	Stainless steel Batch/33.7	Xylose/ 24.5	50	72	-	Cellulase (Cellic Ctec)	Xylose galactose & Glucose	50.9	81	[25] g)

Eucalyptus	CO_2/H_2O/ 10	170	5	80	Stainless steel Batch/1000	XOS & xylose/ 11.3	50	60	Flask/50 0/150	Commercial cellulase	Glucose	50.6	84.1*	[106]

* Author calculated yield for comparing yield with consistent units using Equation (7) and (8).

a) The pretreatment major product yield is calculated based on the reported monomers and oligomers released from corresponding polysaccharide using Equation (8).

b) Overall reducing sugar yield obtained in the combination of pretreatment and enzymatic reaction.

c) A reaction carried out at 5.0 MPa initial pressure of CO_2. Stirring speed at 200.0 rpm is used. Carbon dioxide was applied in its subcritical condition.

d) Zero reaction holding time at isothermal temperature at 220.0 °C isothermal reaction temperature, the reactor was cooled down to room temperature by quenching with cold water once the temperature reached to set point.

e) The sugar yield was calculated for xylan to xylose. The overall sugar yield and minimum furfural concentration were obtained at 215.0 °C and 5.4 MPa.

f) Reaction carried out at 5.0 MPa initial pressure of CO_2 with zero reaction holding time at isothermal temperature at 190.0 °C isothermal reaction temperature, where 6.85 MPa was the corresponding pressure at 190.0 °C.

g) The temperature and reaction time correspond to three stages of pretreatments.

2.2.5. Supercritical carbon dioxide pretreatment of lignocellulosic biomass prior to acid/enzymatic hydrolysis

Supercritical carbon dioxide pretreatment prior to acid and enzymatic hydrolysis has been applied to process both woody and agricultural biomass and to determine the effect of pretreatment on overall sugar yield. Temperature (70.0-210.0 °C), pressure (12.4-27.5 MPa), and water/biomass ratio (0.5-4.0) varied during pretreatment to optimize the overall sugar yield [15, 20, 23, 221, 223, 229]. As discussed in the previous section, acid or enzymatic hydrolysis is required after pretreatment to hydrolyze cellulose into glucose. Enzymatic hydrolysis offers a greener alternative compared to acid or alkaline hydrolysis because it is conducted in aqueous solvent under mild reaction condition and does not produce harmful byproducts or generate large amount of waste streams. Additionally, enzymes are renewables and can be recycled for multiple use when immobilized on suitable support material [231-233]. Acid hydrolysis, which typically has a faster reaction rate compared to enzymatic hydrolysis, is also used after LC pretreatment (Table 2-2) [221]. The overall sugar yields of the acid hydrolysis of supercritical fluid pretreated biomass were varied in the range of 44.4 – 50.7 wt.% of THS. Liu et al., (2014) used dilute sulfuric acid at 1.0 wt.% to hydrolyze $scCO_2$–H_2O pretreated corncob, corn stalk and rice straw (100.0 °C, 15.0 MPa, 30.0 min). The yield of acid hydrolysis of pretreated biomass was comparable to the enzyme hydrolysis yield. However, acid hydrolysis was completed within 3.0 mins at 160.0 °C as opposed to enzymatic hydrolysis, which was often completed at 24 – 72 h (Table 2-2 and Table 2-3).

Table 2-2. Application of supercritical carbon dioxide in pretreatment prior to acid hydrolysis of agricultural biomass for sugar production.

Feedstock	Pretreatment Reaction conditions					Acid hydrolysis reaction conditions				Reaction Yield (wt.%) [a]		
	SCF/ Co-solvent /liquid solid ratio	T (°C)	P (MPa)	t (min)	Mode of process/ Volume (mL)	T (°C)/ P (MPa)	Acid concentration	t (s)	Product	g/ 100 g Initial feedstock (IF)	g / 100 g hydrolyzable sugar (THS) polysaccharides	Ref.- Note
Corncob	CO_2/H_2O /1	100	15	30	Batch/ 30	160/ 0.1	1 wt.% H_2SO_4	1800	Reducing sugars	39.6	45.8 *	[221] [b]
Cornstalk	CO_2/H_2O /1	100	15	30	Batch/ 30	160/ 0.1	1 wt.% H_2SO_4	1800	Reducing sugars	27.4	44.4 *	[221] [b]
Rice straw	CO_2/H_2O /1	100	15	30	Batch/ 30	160/ 0.1	1 wt.% H_2SO_4	1800	Reducing sugars	36.6	50.7 *	[221] [b]

* The yields are calculated by the authors for comparing yield with consistent units Equation (7) and (8).

[a] The reducing sugar yield is presented for the overall two-step process.

[b] 1.5 g water was added to 1.5 g biomass to gain 50.0 % moisture content, resulting in the liquid - solid ratio of 1. The acid hydrolysis was conducted in an oil bath.

Enzymatic hydrolysis of the $scCO_2$ pretreated biomass is more widely explored compared to acid hydrolysis (Table 2-3). Enzymatic hydrolysis of sc-CO_2 pretreatment showed up to 3-4 fold increase in sugar yield compared to the case of non-pretreated biomass, although a long pretreatment time of 12.0-60.0 h may be necessary in some cases where lower temperature ranges (50.0-80.0 °C) are used [15]. The improved sugar yield was attributed to the presence water with $scCO_2$ at higher pressure of 17.5-25.0 MPa for 24.0 h, which easily penetrates into the biomass, causing swelling and explosion effects [15].

Luterbacher et al., (2010 and 2012) used $scCO_2$-H_2O to investigate the effect of a two-stage pretreatment process on enzyme digestibility of pretreated biomass [20, 23]. The two-stage pretreatment involved a hydrolysis process conducted at a higher temperature and shorter reaction time (210.0 °C, 1.0 min for switchgrass, and 210 °C, 16.0 min for hardwood) followed by a lower temperature and longer reaction time (160 .0°C, 60.0 min) maintained under backpressure of heated reactor at 20.0±1.0 MPa. The results indicated that highly amorphous hemicellulose was hydrolyzed at a faster rate in the first stage than the residual hemicellulose hydrolyzed in the second stage [23]. The overall sugar yields of 55.0 wt.% and 65.0 wt.% of THS were obtained for switchgrass and hardwood, respectively [23]. Also, the continuous stirring in large reactor (1.0 L) prevented the formation of hot spots and allowed to use large particles (up to 9.5 mm), whereas particles less than 1.0 mm had shown reduced yield lower by 10.0 wt.% of THS compared particle size 1.0-9.5 mm in large volume reactor [23] The formation of hotspots due to high temperature leads to polysaccharide hydrolysis at a faster

rate and further sugar degradation, which is not desirable [23]. The stirring of the biomass during the reaction favors the hydrolysis of hemicellulose and reduces the degradation of sugars by providing uniform temperature in the reactor [22-23].

Solid loading of biomass is another important parameter that influences the reaction performance [23]. High solid loading requires strong mixing to avoid the hot spot formation, leading to higher power consumption. Using the $scCO_2$ can enhance the mass transfer rate and subsequently reduce power consumption due to mixing [20, 23]. Given that the applied CO_2 can be recovered and reused for further reactions, high pressure and SCFs pretreatment and hydrolysis offer the benefits of negligible cost of reaction solvents and easy recovery of the solvent and products [107, 234].

Table 2-3. Supercritical carbon dioxide pretreatment prior to enzymatic hydrolysis of agricultural and lignocellulosic biomass as feedstock.

Feedstock	Pretreatment conditions						Enzyme hydrolysis conditions					Reaction yield (wt.%) [a, b]		
	SCF/ Co-solvent/ liquid solid ratio	T (°C)	P (MPa)	t (min)	Reactor Configuration / Volume (mL)	Pretreatment major products/ yield % (THS) [a]	T (°C)	t (h)	Reactor Type/ Volume (mL)/ AR (rpm)	Enzyme	Sugar Products	g/ 100 g Initial feedstock	g / 100 g hydrolyzable sugar polysaccharides	Ref.- Note
Agricultural biomass														
Switchgrass	CO_2/ H_2O/1.5–4	170	20	60	Batch reactor/ —	Hemicellulosic sugars / 7.3	50	72	—/ —/ —	Cellulase, xylanase, β-glucosidase	Glucose	28.33 *	81	[20]
Switchgrass	CO_2/ H_2O/1.5	210 and 160	20	16 and 60	Stirred reactor/ 1000	-	50	72	—/—/—.	Cellulase, xylanase, cellobiase, β-glucosidase	C5 and C6 sugars	31.1 *	55	[23] c)
Switchgrass	CO_2/ H_2O/0.75	150	24	60	Batch reactor/ 94.7	-	47	24	Conical tube/ 50/ —	Cellulase and β-glucosidase	Glucose	14	42.0 *	[214] d)
Big bluestem	CO_2/ H_2O/1.5–4	170	20	60	Batch reactor/ —	Hemicellulosic sugars / 4.2	50	72	—/ —/ —	Cellulase, xylanase, β-glucosidase	Glucose	27.6 *	66	[20]
Mixed perennial grass	CO_2/ H_2O/1.5–4	170	20	60	Batch reactor/ —	Hemicellulosic sugars / 4.0	50	72	—/ —/ —	Cellulase, xylanase, β-glucosidase	Glucose	27.2 *	68	[20]

Sugarcane bagasse	CO_2/ H_2O/0.8	187	15.6	40	Stainless steel reactor/50	-	50	72	—/ —/ —	Cellulase (CTec-2)	Glucose	-	97.8	[111] e)
Corn stover	CO_2/ H_2O/0.75	150	24	60	Batch reactor/ 94.7	-	47	24	Conical tube/ 50/ —	Cellulase and β-glucosidase	Glucose	30	66.5 *	[214] f).
Corn stover	CO_2/ H_2O/1.5–4	160	20	60	Batch reactor/ —	Hemicellulosic sugars / 4.4	50	72	—/ —/ —	Cellulase, xylanase, β-glucosidase	Glucose	38.3 *	85	[20]
Corn stalk	CO_2/ H_2O/0.5	170	20	150	Batch reactor / 30	-	50	72	Conical flask/ 100/ 100	Cellulase	C5 and C6 Reducing sugars	24.3 *	46.4	[221] g)
Corn stalk	CO_2/ H_2O/0.5	170	20	150	Batch reactor / 30	-	50	72	Conical flask/ 100/ 100	Cellulase	C5 and C6 Reducing sugars	16.4 *	30.0	[221] h)
Corn cob	CO_2/ H_2O/0.5	170	20	30	Batch reactor / 30	-	50	72	Conical flask/ 100/ 100	Cellulase	C5 and C6 Reducing sugars	58.5 *	87.0	[221] i)
Corn cob	CO_2/ H_2O/0.5	170	20	30	Batch reactor / 30	-	50	72	Conical flask/ 100/ 100	Cellulase	C5 and C6 Reducing sugars	41.7 *	62.0	[221]
Guayule	CO_2/ H_2O/2	180	12.4	30	High-pressure vessel/ 250	-	50	48	Flask/ 250/ 250.	Cellulase, β-glucosidase, xylanase	C5 and C6 Reducing sugars	42.0 *	82.8	[229]
Guayule	CO_2/ H_2O/0.6	200	27.5	30	Batch reactor / 500	-	50	72	Conical flask/ 125/ 200	Cellulase, β-glucosidase, xylanase	C5 and C6 Reducing sugars	32.8 *	86	[223]

Sorghum stalk	CO_2/ H_2O/3	60	30	360	Batch tubular reactor/ 30	-	50	48	Conical flask/ 50/ 100	Cellulase	C5 & C6 reducing sugars	45.5	64.2 *	[235] j, k)
Corn stover	CO_2/H_2O /3	70	22.5	2880	Stainless steel /80	-	50	48	Conical flask/ 100/ 100	Cellulase (endoglucanase and β-glucosidase)	C5 and C6 Reducing sugars	39.2	62.2	[15]
Wood Biomass														
Mixed hardwood	CO_2/ H_2O/1.5	210 and 160	20	16 and 60	Stirred reactor/ 1000	-	50	72	—/—/—	Cellulase, xylanase, cellobiase, β-glucosidase	C5 and C6 sugars	41.25 *	65	[23] c)
Mixed Hardwood	CO_2/ H_2O/1.5 –4	170	20	60	Batch reactor/ —	Hemicellulosic sugars / 8.6	50	72	—/ —/ —	Cellulase, xylanase, β-glucosidase	Glucose	34.7 *	73	[20]
Aspen	CO_2/ H_2O/0.73	165	21.4	30	High-pressure vessel/ —	-	50	72	—/ —/ 100	Cellulase	Reducing sugar	63.3 *	84.7	[112] l)
Southern yellow pine	CO_2/ H_2O/0.73	165	21.4	30	High-pressure vessel/ —	-	50	72	—/ —/ 100	Cellulase	Reducing sugar	—	27.3	[112]

* Author calculated yield for comparing yield with consistent units Equation (7) and (8).

a) The pretreatment major product yield is calculated based on the major monomer and oligomer released from a polysaccharide Equation (8).

b) The reducing sugar yield is presented for the overall pretreatment and hydrolysis stages.

c) Two-stage pretreatment method (I shorter time high temperature + II longer time low temperature).

[d] Switchgrass composition (cellulose 45.6 %, hemicellulose 27.3 % & lignin 8.6 %) was obtained from reference in order to calculate the yield (THS) [23].

[e] The pretreatment was done in two subsequent steps by $scCO_2$, followed by hydrogen peroxide prior to enzyme hydrolysis.

[f] The corn stover composition (cellulose 40.6 %, hemicellulose 33.6 % & lignin 4.2%) was obtained from reference in order to calculate the yield (THS) [20].

[g] Treated also by ultrasound at 20 kHz, 600 W, 80 ℃ for 8 h. The composition of corncob (cellulose 35 %, hemicellulose 25 % & lignin 23%) was obtained from reference in order to calculate the yield (THS) [21].

[h] The corn stalk composition (cellulose 30.9 %, xylan 15.7%, arabinan 2.25 % & lignin 23.5 %) was obtained from reference in order to calculate the yield (THS) [236].

[i] Treated also by ultrasound at 20 kHz, 600 W, 80 ℃ for 6 h. The composition of corncob (cellulose 35 %, hemicellulose 25 % & lignin 23%) was obtained from reference in order to calculate the yield (THS) [21].

[j] Biomass composition (glucan 40.5%, xylan 22.7% & lignin 19.5%) of sorghum stalk information was obtained from reference in order to calculate the yield (THS) [16].

[k] Supercritical carbon dioxide pretreatment was combined with ultrasonic treatment at 50 ℃ for 5 h. The ultrasonic treatment (0.2 g biomass in 10 mL buffer, at 50 °C, 5 h, 100 W, 40 kHz) was performed prior to $scCO_2$ treatment.

[l] The aspen composition (glucan 44 %, xylan 19 %, mannan 2.4 % & lignin 24.8%) was obtained from reference in order to calculate the yield (THS) [26].

In an integrated innovative approach, $scCO_2$ with water as co-solvent, pretreatment of sugarcane bagasse was sequenced with ultrasound and alkaline hydrogen peroxide treatments, individually in separate processes. The pretreated biomass was further hydrolyzed with enzyme to produce sugars. $ScCO_2$ pretreatment followed by enzymatic hydrolysis (control) resulted in 61.3 wt.% of THS for glucose. The combined process of $scCO_2$–alkaline hydrogen peroxide pretreatment and $scCO_2$–ultrasound pretreatment processes coupled with enzyme hydrolysis resulted in overall yield of 97.8 wt.% and 65.8 wt.% of THS for glucose, respectively [111]. Yin et al., (2014) used the ultrasound treatment prior to $scCO_2$ pretreatment reported an improved C5 & C6 reducing sugar yields from 62.0 wt.% (control) to 87.0 wt.% THS of corncob [221]. The ultrasound energy wave loosens the cellulose fiber bundles and exposes more surface area that improves the enzyme digestibility. Whereas alkaline hydrogen peroxide helps in the delignification of the feedstocks [111]. Therefore, a combination of these techniques to supercritical technology has shown improved yield of reducing sugars.

In these experiments conducted to study the effect of $scCO_2$ pretreatment on the performance of enzymatic hydrolysis of pretreated biomass, the pretreatment step has been carried out in high pressure-batch reactors at lab scales and the enzyme hydrolysis reaction were carried out in shaking flasks with agitation speed of 100.0-250.0 rpm (Table 2-4) [221, 229]. Mixing is necessary in enzymatic hydrolysis to provide a homogeneous mixture and for an increased contact of biocatalyst and its substrate. The reaction time of enzymatic hydrolysis was reported in the range of 24.0-72.0 hours to ensure the completion of the enzymatic reaction [214, 224, 235].

2.2.6. Sub/supercritical fluid for hydrolysis of woody and agricultural lignocellulosic biomass for sugar production

In addition to the applications in pretreatment, SCFs have also been used as a sole reaction medium for the one-step hydrolysis of woody and agricultural biomass. Pressure, temperature, and reaction time have been studied extensively to maximize hydrolysis yield and minimize sugar degradation products. As shown in (Table 2-4), high yields were obtained upon using SCFs for a single stage for sugar production from a variety of feedstocks such as microcrystalline cellulose (>95.0 wt.% of THS), agricultural biomass, (73.0 wt.% of THS) and hardwood mixed biomass, (71.2 wt.%, of THS) [19, 227, 234]. Supercritical CO_2 and H_2O have been applied as hydrolysis reaction media without any involvement of enzyme. Variety of LC biomass have been treated at different pressure (1.0-34.1 MPa), temperature (40.0-400.0 °C), and reaction time (0.02–1500.0 s) with the reported sugar yield ranging from 43.2 to 95.0 wt.% of THS (Table 2-4) [177, 227-228, 237].

Hydrolysis of the polysaccharides in the bamboo by compressed hydrothermal treatment (170.0-180.0 °C, 1 MPa, 25.0 min of hydrolysis reaction) was carried out to produce C5 and C6 reducing sugars. The hydrolysis yield was improved from 25.5 to 42.2 wt.% of THS with an increase in the temperature from 170.0 to 180.0 °C. Further increase in temperature led to a reduction in the total reducing sugars (TRS) yield, to less than 18.0 wt.% of THS at 220.0 °C due to the sugar decomposition to degradation products [228]. Additionally, at 180.0 °C, the overall xylose and arabinose yields were notably higher than yields of glucose and fructose. This shows that hemicellulose is hydrolyzed faster than cellulose in compressed hydrothermal treatment [228].

Sasaki et al., (2000) reported that cellulose hydrolysis rate was higher than the glucose and cellobiose decomposition rates, when it was treated at a temperature above 350.0 °C with supercritical water (SCW). They reported >99.0 % conversion of cellulose at 400.0 °C temperature and 25.0 MPa with a yield of 57.1 wt.% of THS including 14.5 wt.% of gluco-oligomers and 42.6 wt.% of monomers (glucose & fructose) within 0.15 s of reaction time [238]. Kazachkin et al., (2015) reported 49.2 wt.% of THS for the monomeric sugars from hardwood within 1 sec of reaction time using subcritical water at 370.0 °C, 23.1–24.1 MPa [177].

Table 2-4. Application of Sub/Supercritical fluids as sole reaction media in single-step biomass hydrolysis for sugar production using woody and agricultural lignocellulosic biomass as a feedstock.

Feedstock	Sub/supercritical hydrolysis reaction conditions						Reaction Yield [a]		Ref-Note
	SCF/ Co-solvent /liquid solid ratio	T (°C)	P (MPa)	Time (s)	Reactor Configuration/ Volume (mL)/ Mode of Process	Product	g /100 g of Initial Feedstock	g /100 g of Hydrolyzable Sugar polysaccharide	
Agricultural biomass									
Sugarcane bagasse	CO_2/H_2O/ 0.65	40	10	120	High pressure vessel/ —/ Batch	Glucose	28.7	53.8*	[237] b)
Wheat straw	CO_2/ H_2O/10	200	6	—	Batch stirred tank reactor / 600/ Batch	XOS	12.9	70.6	[18] c)
Wheat straw	CO_2/H_2O/10	200	6	—	Batch stirred tank reactor / 600/ Batch	Xylose, Arabinose mono- and oligomers	15.2 *	60.5 *	[18] c)
Corn stover	CO_2/C_2H_5OH–H_2O/3	285	7.5 to 8	180	Batch tubular reactor/1.2/ Batch	Xylose	—	51.7	[234] d)
Cellulose	H_2O/—/12.3	400	25	0.02	Series of tubular reactor/0.12 to 8/ Continuous	glucose, and fructose	—	>95.0	[227] e)
Sugar beet pulp	H_2O/—/—	390	25	0.11	Ultra-fast reactor/ —/ Continuous	C5 and C6 sugars	27.14 *	66.4	[239]
Wheat bran	H_2O/—/0.082	400	25	0.19	Micro-reactor (pilot scale)/ 0.05 to 8/ Continuous	C5 and C6 sugars	42.3 *	73.0	[19] f)
Woody biomass									
Bamboo	H_2O/—/20	180	1	1500	Stainless steel vessel/ 500/ Batch	C5 and C6 sugars	42.2	59.0*	[228] b)
Mongolian oak	H_2O/—/50	380	23	<1	Pilot scale reactor/—/ Continuous	C5 and C6 sugars	35.3	49.8	[27] g)

Hardwood (Mix of Oak & Birch flour)	CO_2/H_2O (l) & CO_2/C_4H_9OH (II)/—/10	250	10	60	Two-stage pilot plant reactor/ —/ Continuous	Xylose monomers and oligomers	17.3 *	89.4*	[234] h)
Hardwood	H_2O/—/25	364 - 383	23.1 – 34.1	1	—/ 3.6/ Continuous	Glucose, xylose, mannose	30.9 *	44.6*	[177]
Softwood	H_2O/—/25	364 - 383	23.1 – 34.1	1	—/ —/ Continuous	Glucose, xylose, arabinose, mannose, galactose	27.9 *	43.4*	[177]

* Author calculated yield for comparing yield with consistent units Equation (7) and (8).

a) The reducing sugar yield is presented for overall sugar production.

b) The reducing sugars were estimated by the DNS method to measure reducing sugars. However, the calculation is made based on glucose.

c) The reported results correspond to the condition in which high sugar with minimum amounts of furfural as an inhibitory material was obtained.

d) The solid biomass (1 g) was mixed in water-ethanol (1:1) mixture (3 g), and xylose was solubilized with lignin and remaining retained as cellulose in solid.

e) The 7.5 % cellulose suspension along with heated water was fed to make final concentration of cellulose in the reactor at 1.5 w/w %.

f) No additional water other than moisture content was used in the process.

g) 0.01 – 0.1 % (w/w) H_2SO_4 was used to catalyze the hydrolysis reaction, and 0.1 % concentration of sulfuric acid was found to be optimum.

h) THS yield corresponds to only xylan-based sugars in two stage hydrolysis.

$scCO_2$ with water and alcohol as co-solvents were used in the one-step hydrolysis of both agricultural and woody biomass [234]. Kilambi et al., (2012) reported supercritical alcohol assisted fractionation of lignin, hemicellulose, and cellulose from the biomass. They used corn stover and mixed hardwood of oak & birch as their feedstocks and obtained 51.7 wt.% and 89.4 wt.% of THS of xylose and XOS sugars from solubilized biomass, respectively [234]. The hardwood mixture was hydrolyzed at pilot scale with processing capacity of 100 kg dry biomass a day in two stage process, where in first stage, $scCO_2$ with water as co-solvent, and in second stage, $scCO_2$ with butanol as co-solvent were used. The application of supercritical CO_2 (250 °C, 10 MPa, 1 min) with subcritical water and supercritical ethanol (1:1, vol) as co-solvent in the hardwood biomass fractionation, hydrolyzed the hemicellulose along with dissolving lignin (>90%), while cellulose was retained in solid. A yield of 51.7 wt.% of THS based on xylose, was obtained in this process [234].

Completing hydrolysis reaction in sub/supercritical water requires high-pressure reactor. Reactor corrosion due to a high concentration of water dissociated ions at high temperatures can be regarded as a notable concern of sub/supercritical water technologies. However, it could be controlled by employing corrosion resistant materials such as stainless steel and liners in the reactors [240]. SCW hydrolysis requires more severe reaction conditions compared to those of $scCO_2$-H_2O. However, this system offers a fast hydrolysis process that can be completed in a few seconds and have been evaluated in different reaction modes, including batch, semi-continuous, and continuous mode [18, 227, 234].

Although there are significant compositional differences in the type of LC biomass (wood, agricultural plant, grass), the effect of pretreatment condition also varied in different studies listed studies in Tables (2-1 to 2-5), and therefore, the sugar yield range are similar for the different biomass. However, the high temperatures lead to partial hydrolysis of the hemicellulose fraction in presence of water. Since agricultural plant and grass LC biomasses have higher hemicellulose and other non-cellulosic component (i.e., extractives, ash, protein), the enzymatic digestibility could significantly improve in comparison to woody biomass. It would be beneficial if the different types of LC biomass would be pretreated with same or closely related instrument under similar reaction parameter.

2.2.7. Enzyme-assisted supercritical CO_2 for hydrolysis of lignocellulosic biomass

There have been interests in developing an understanding on the effect of high pressure on enzymes' activity and stability. Although the main application of high pressure is enzyme activation, there are several reports on enhanced enzyme activity under high pressure systems [113, 241-242].

The effect of pressure on the function of enzymes is influenced by factors such as temperature, pH, salt and substrate concentrations [241, 243]. The increase in temperature and pressure increases the enzyme's kinetic parameters– turn over number and effective substrate concentration, whereas the enzyme efficiency of turning substrate to product remains near constant [241]. The elevated pressure strengthens the hydrogen bonds and limits the hydrophobic interactions [244]. Salts molecules might pair up with the hydration layer of enzyme that can change the activation volume due to disorganization of water molecule. Therefore, salts can

enhance or reduce the enzyme activity by affecting the pressure stability of enzyme [243].

Eyring and Magee (1942) developed mathematical models to explain the effect of high pressure on reaction rate based on the molecular level changes in the enzyme and reaction conditions, as expressed in Equation (9) [245].

$$\left(\frac{\partial \ln k}{\partial P}\right)_T = -\frac{\Delta V^{\neq}}{RT} \quad (9)$$

Where k is the specific reaction rate constant, P is pressure, $\Delta V^{\neq}$ is activation volume, R is gas constant, and T is the absolute temperature of the reaction. The activation volume could be negative, positive, or neutral depending upon reaction conditions and changes in structural conformation of the enzyme [246-247].

The effect of high pressure by lowering the activation volume of the transition state complex favours the enzyme activity [241, 245]. If the active enzyme conformation is stable at high pressure, an increase in the enzymatic reaction rate may be observed in response to an increase in pressure [243]. Activity and stability of enzyme under high pressure condition depends on several parameters such as enzyme structural conformation, inter– and intramolecular hydrogen bonds, the arrangement of the secondary and tertiary structure, presence of aqueous layer around the enzyme active site, hydroxyl groups, charged groups, and presence of organic solvents, and depending on the reaction conditions, increasing pressure can enhance or inhibit enzyme activity and increase or decrease enzyme stability [50, 113, 243, 248-250].

For example, Eisenmenger & Reyes-De-Corcuera (2009) have reviewed 25 enzymes that include peroxidases, dehydrogenases, amylases, *β*-glucosidase, mainly lipases, which have been studied for activity under high-pressure condition

[113]. It was shown that higher pressure (1.0-500.0 MPa) results in enhancing enzyme stability and activity to a certain extent [113]. For instance, high pressure of 470 MPa atm increased the enzyme activity of *α*–chymotrypsin (*α*–CT) to 6.5 folds in aqueous solution and decelerated the thermal inactivation at high temperature (up to 55.0 °C). The enhanced enzyme activity was claimed due to the changes in the hydration layer of the active site and conformational rearrangement [250]. For cellulase enzyme, up to 26.0 % increase in the enzyme activity was reported for enzymatic reaction under pressure of 50.0-100.0 MPa at 50.0 °C and pH of 5.0 [251]. The effect of high pressure on the interaction of water and charged molecules of the enzyme is explained by Mozhaev et al., (1996), where high pressure causes a decrease in the activation volume due to the reduced hydrophobic and electrostatic bonds of the enzyme. The water molecules in the hydration layer of the charged groups, become oriented in an ordered manner that leads to a reduction in the activation volume [250]. In a recent study, the enzyme activity of free enzymes (*α*–CT and horseradish peroxidase) were compared with immobilized enzymes on different interfaces (positively and negatively charged, polar and nonpolar) materials under high pressure reaction conditions. Immobilized enzymes with positive activation volume change were found to be deactivated, while enzymes with negative activation volume change showed enhanced enzyme activities as a result of increase in pressure [252].

In sub/supercritical fluid conditions, CO_2 can interact with the hydration layer surrounding the surface functional groups of the enzyme [50, 249]. The possibility of stripping off the water molecules from the hydration layer of enzyme's active site

by nonpolar $scCO_2$, is less compared with polar solvents, given that CO_2 is less soluble in water compared to polar solvents [253]. This hydration layer is stripped off or desorbed when polar solvents such as methanol, *n*-propanol, *n*-butanol are present in the reaction media. Gorman and Dordick (1992) reported that the presence of methanol in enzymatic reaction media desorbed 38.0 % of the water from the enzyme, while the non-polar solvent such as toluene and hexane desorbed only 10% [253]. This is due to the fact that non-polar (hydrophobic) solvents are immiscible in water and keep the enzyme's native structure unopened [254].

The maximum activity of lipase under supercritical CO_2 was found to be at 15.0 MPa, 35.0–50.0 °C [249]. The high temperatures (>65.0 °C or the higher than optimum temperature) led to thermal deactivation of the enzyme by breakage of the non-covalent bonds in the enzyme [255-257]. The lipase activity was enhanced by increasing the pressure to 15.0 MPa and exposure duration to 2.5 h, whereas increasing the pressure beyond 15.0 MPa or the exposure duration above 2.5 h reduced the enzyme activity [249] It was hypothesized that below the threshold pressure value, $scCO_2$ interacts with tryptophan and tyrosine residues present in enzyme, leading to conformational changes and more accessibility of active site of enzymes to substrate [258]. Above the threshold value, the free enzyme activity decreases, which is attributed to the strong chemical interaction of CO_2 with tryptophan and tyrosine with irreversible changes [249]. Loss of hydration layer of the enzyme's microenvironment is caused by the presence of $scCO_2$. Li et al., (2020) investigated the cellulose structure and enzymatic conformational changes

in the presence of $scCO_2$ (8.2 MPa, 50.0 °C). On the effect of $scCO_2$ on cellulose, an increase in the content of free hydroxyl groups in the cellulose was observed, resulting in decrease of cellulose crystallinity and increase in the enzyme's accessibility to cellulose [50]. The helical structure content of cellulase decreased due to the destroyed intracellular hydrogen bond structure of cellulase, resulting in a decrease in the stability of the enzyme [50, 249].

There are scarce studies conducted for the LC material hydrolyzing enzymes (cellulases and hemicellulases) under a high-pressure environment. For example, Paljevac et al., (2007) used one pot treatment method for the hydrolysis of carboxymethyl cellulose by an immobilized enzyme in a supercritical CO_2–H_2O system **(**Table 2-5**)** [114]. There are advantages of employing simultaneous $scCO_2$–H_2O based pretreatment and enzymatic hydrolysis in one-pot such as conducting hydrolysis under mild reaction conditions, one step sugar production, and reduced processing costs. The major advantage of the supercritical CO_2 driven pretreatment method is the lower critical point (31°C, 7.4 MPa), which can accommodate the enzymatic hydrolysis at the same reaction condition used for pretreatment instead of using a two-step treatment. The temperature range of enzymatic hydrolysis reaction typically lies between 40 – 55 °C. There has been on-going effort to develop enzymes with stability at high temperatures. For example, particular cellulosic enzyme has been derived from *Caldicellulosiruptor bescii* that has thermal stability up to 73 °C for hydrolysis of crystalline cellulose to reducing sugar [259].

Table 2-5. Simultaneous pretreatment and enzyme hydrolysis in one pot under $scCO_2$

Feedstock	SCF /co-solvent/ liquid-solid ratio	T (ºC)	P (MPa)	t (min)	Reactor/ volume/ rpm	Enzyme	Product	Yield		Ref
								g/100 g of initial biomass	g/ 100 g hydrolyzable sugar polysaccharides	
Carboxy - methyl cellulose	CO_2/H_2O/1. 67	40	10	300	Autoclave/ —/500	Cellulase (Celluzyme 0.7T) immobilized on silica-gel	Glucose	73	73	[114]

Despite several advantages of the application of enzyme in high pressure systems, long-term stability and reusability hinders the industrial application of these natural biocatalysts. Extensive efforts have gone to overcome the drawbacks of the enzyme applications by immobilizing the enzyme on various support materials to recycle enzymes for their repeated application [232, 260-262]. However, development of the immobilization support materials to be used in high pressure and SCFs based technologies is still largely unexplored.

2.2.8. Commercial status: application of sub/supercritical fluids in lignocellulosic biorefinery

In the LC biorefinery, a broad spectrum of bioproducts can be produced from the sugars derived from the cellulose and hemicellulose fraction of the biomass via chemical and biochemical pathways. Glucose followed by xylose and mannose sugars offer high potential for transformation to bioproducts of commercial interest due to their abundance in biomass [263-265]. For example, glucose is converted to a range of intermediates or final products such as 5–HMF, isosorbide, polylactic acid, and valeric acid via catalytic hydrogenation, dehydrogenation, dehydration, and oxidation in the presence of acid or metal-supported catalysts such as Ru/C, Cu-Ru/C, $SnCl_2$, Amberlyst-15 at 90-240 °C [263-264, 266-267]. Ethanol, lactic acid, succinic acid and adipic acid are produced via biochemical pathways through fermentation [268-270]. These value–added bioproducts are platform chemicals for various industries with a variety of applications, ranging from organic solvents to liquid fuels.

Industrial interest is growing for the use of sub/supercritical fluid-based technologies due to the tunable properties of these solvents, which can be

deployed for the fractionation of biomass to produce a range of bioproducts within a biorefinery scheme by minimizing the waste. A recent study was conducted at Hanwha Chemical, Seoul, the Republic of Korea at pilot-scale (capacity 50 kg/day) to produce sugar and ethanol from *Quercus mongolica* using supercritical water in continuous mode.[27]

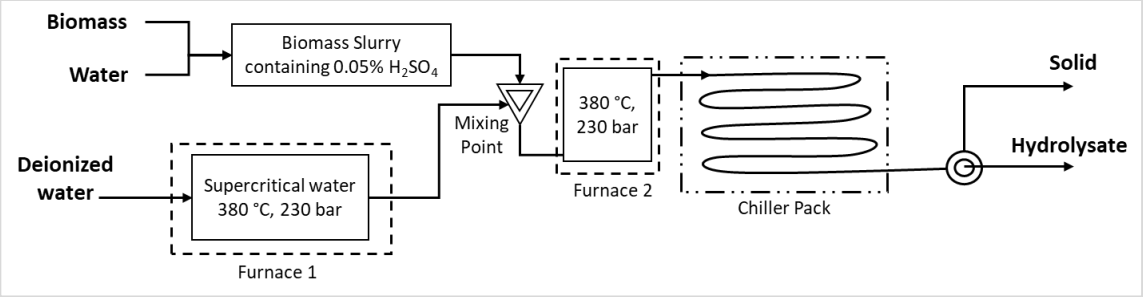

Figure 2-3. Pilot scale production of sugar from woody biomass for upgradation to ethanol using supercritical water.

As shown in Figure 2-3, the biomass slurry, containing 0.05% sulfuric acid as a catalyst is brought in contact with supercritical water for 1 sec reaction time at 380 °C and 23 MPa. After the reaction, the hydrolysate containing glucose and xylose and residual solid is cooled in a chiller. This process leads to the production of 27.3 kg of sugar monomers per 100 kg of biomass [27]. Renmatix Inc. has developed a commercial scale supercritical fluid-based technology, which applies supercritical water for producing C5 and C6 sugars. The continuous process produces multi tons of sugar per day in the Renmatix Inc. plant located in Kennesaw, Georgia.[271] In 2011, three tones of dry biomass, including hardwoods, softwoods, and agricultural residues (e.g., corn stover, palm residues, bagasse), and grasses (e.g., switchgrass, miscanthus) were converted into sugar by the supercritical technology, called Plantrose® process.[272] Among several patented

processes of high pressure and sub/supercritical fluid technology, one of the developed processes was patented in 2015 and has been elaborated here. The biomass is first chopped, ground, and mixed with water to make a slurry. The slurry goes through a pretreatment reactor operated with hot compressed water with 5% of $scCO_2$ (240 °C, 10 MPa, 1 min) to hydrolyze the hemicellulose to xylose and XOS sugars. Hydrolysate is separated from residual biomass and is further hydrolyzed in the presence of hot compressed water and 0.2 % sulfuric acid as catalysts. In the next step, the pretreated solid is mixed with water to make a slurry, which is further heated to reach supercritical water condition (367 °C, 22.5 MPa, 1 sec) to hydrolyze the cellulose fraction into glucose and glucose oligosaccharide (GluOS) sugar. The aqueous glucose and GluOS are separated from lignin and undergo further hydrolysis to produce glucose using 0.2 % sulfuric acid-catalyzed subcritical water (240.0 °C, 10.0 MPa, 1.0 sec) hydrolysis reaction (Figure 2-4) [191]. To our best knowledge, Renmatix Inc. is the only industry producing sugar from lignocellulosic biomass using supercritical water technology at commercial scale [273-274]. Recently, Renmatix Inc. secured $14.0 million in support to increase the annual production capacity of cellulosic sugars to one million tons with supercritical fluid technology [275].

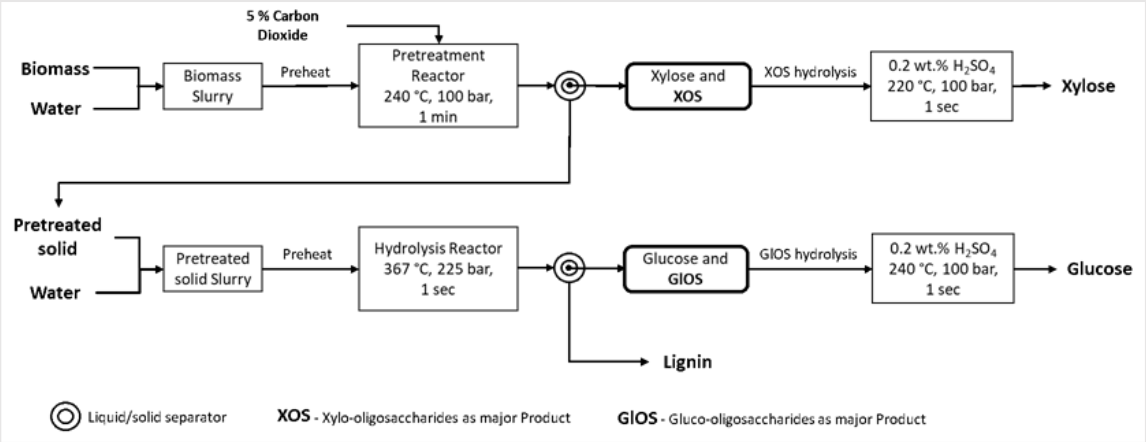

Figure 2-4. Pilot scale C5 and C6 production process using supercritical fluid technology developed by Renmatix Inc.

2.2.9. Summary and outlook

Supercritical fluid-based technologies have been explored for biorefining of renewable resources, leading to success in commercialization in some cases such as supercritical water-based systems. The use of supercritical fluids can overcome the environmental burden of the conventional LC biomass processing by enhancing recyclability and reducing water consumption and waste stream generation. The application of sub/supercritical carbon dioxide and water has been reviewed in both pretreatment and hydrolysis reaction for reducing sugar production from LC biomass. In the pretreatment process, sub/scCO_2-water were the common media employed, resulting in reducing cellulose crystallinity and partial hemicellulose hydrolysis. Pretreatment of LC biomass using sub/scCO_2 is often followed by enzymatic hydrolysis to convert the remaining polysaccharides into reducing sugars. Multistage pretreatment such as ultrasound, or alkaline hydrogen peroxide pretreatment sequenced with SCFs pretreatment have shown improved sugar yields when combined with enzyme hydrolysis. The small particle size in the range of 0.4-1 mm has shown improved

yield in stirred reactor where the high solid loading up to 40 wt.% can be used with two staged $scCO_2$-H_2O pretreatments followed by enzyme hydrolysis. Among the several studies, the use of sub/supercritical CO2-H2O pretreatment of LC biomass including wood and agricultural biomass have shown similar

The cost of enzymes and slow enzymatic reaction rate (e.g., reaction time of 24-72 hours) challenge the industrial application of enzymes in the energy sector. These challenges can be overcome by research into enzyme immobilization, improving enzymes recyclability and stability. Supercritical water is being used as the main reaction media in LC biomass for hydrolysis, eliminating the need for the pretreatment stage and enzymatic hydrolysis in the overall process and their associated cost. Hydrolysis in supercritical water is completed within a very short period (e.g., fraction of a second or a few seconds). However, this fast reaction is achieved at the expense of high temperature (e.g., critical temperature of 374 °C), and degradation of sugars to furfurals and organic acids to some extent. Safety feature consideration and the use of corrosion-resistant materials in design and construction of supercritical water-based reactors contribute to their complexity.

An important step towards enhancing the sustainability of LCB valorization systems is the use of supercritical carbon dioxide and enzymes in one pot system, which enables conducting the hydrolysis reaction under milder condition. There are some reports on enhanced stability of enzymes' structure and their activity at high pressure, highlighting that exploring one pot supercritical carbon dioxide pretreatment and enzymatic hydrolysis is a very worthwhile effort. However, there

is only a very limited number of studies available on the hydrolysis of cellulose and hemicellulose by free and immobilized enzymes under high pressure and supercritical fluid reactions. Developing an understanding the parameters that influence the stability and activity of hydrolytic enzymes under high pressure, development of thermophilic enzymes to improve hydrolysis rate, designing materials as enzyme carriers, and enzyme immobilization methods to enhance the enzyme reusability can significantly enhance the environmental benefits and process economics and pave the route towards commercialization.

2.2.10. Acknowledgment

The financial support of NSERC-Strategic and Nova Scotia Innovation Hub is acknowledged. Pawan Kumar is thankful for the NSERC-CREATE ASPIRE scholarship.

2.3. Influence of elevated pressure and pressurized fluids on microenvironment and activity of enzymes

This chapter has been published in Journal of Advance Biotechnology:
Pawan Kumar, Azadeh Kermanshahi-pour, Satinder K. Brar, Quan Sophia He, and Jan K. Rainey. 2023. 'Influence of elevated pressure and pressurized fluids on microenvironment and activity of enzymes', Biotechnology Advances: 108219.

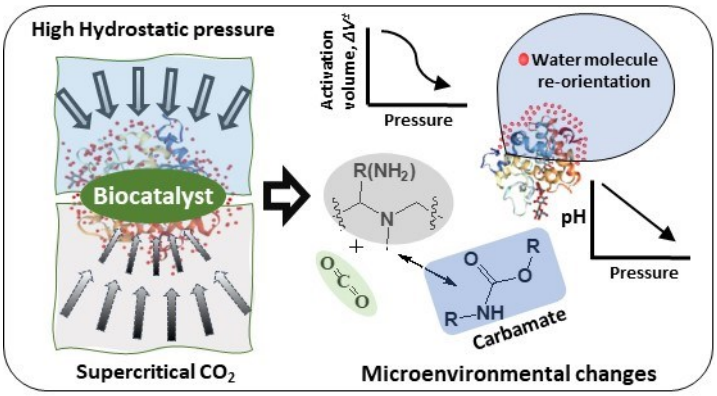

2.3.1. Abstract

Enzymes have great potential in bioprocess engineering due to their green and mild reaction conditions. However, there are challenges to their application, such as enzyme extraction and purification costs, enzyme recovery, and long reaction time. Enzymatic reaction rate enhancement and enzyme immobilization have the potential to overcome some of these challenges. Application of high pressure (e.g., hydrostatic pressure, supercritical carbon dioxide) has been shown to increase the activity of some enzymes, such as lipases and cellulases. Under high pressure, enzymes undergo multiple alterations simultaneously. High pressure reduces the bond lengths of molecules of reaction components and causes a reduction in the

activation volume of enzyme-substrate complex. Supercritical CO_2 interacts with enzyme molecules, catalyzes structural changes, and removes some water molecules from the enzyme's hydration layer. Interaction of $scCO_2$ with the enzyme also leads to an overall change in secondary structure content. In the extreme, such changes may lead to enzyme denaturation, but enzyme activation and stabilization have also been observed. Immobilization of enzymes onto silica and zeolite-based supports has been shown to further stabilize the enzyme and provide resistance towards perturbation under subjection to high pressure and $scCO_2$.

2.3.2. Highlights

- Enzymatic reaction under high pressure alters enzyme structure at molecular level
- Hydration layer at active site and enzyme surface is essential for enzyme activity
- Immobilization protects enzymes from high pressure and enhances activity/stability
- Each enzyme may behave differently due to its unique enzyme structure and source

2.3.3. Keywords

Enzyme activity; cellulase; enzyme activation; pretreatment; high pressure; supercritical CO_2.

2.3.4. Introduction

Enzymes play vital roles in the bioprocessing of biomass in a green and sustainable approach. However, due to challenges, such as the recalcitrant structure of lignocellulosic (LC) biomass, the high cost of enzyme and its recovery, and slower reaction rates, biocatalysts have been underutilized compared to chemical catalysts. Most LC biomasses require a pretreatment process to remove or disrupt the recalcitrant lignin and hemicellulose network to facilitate the enzymatic digestibility by enzymes to hydrolyze the polysaccharides constituent to monomeric sugars. In order to enhance reaction rate and enzyme recovery, several studies have evaluated enzymatic reactions under high pressure or supercritical CO_2 ($scCO_2$) using free or immobilized enzymes [276-283]. High pressure has been investigated as a physicochemical factor in enzymatic reactions since the early 1900s [284]. However, exploring this parameter for enhancing the enzyme activity has been started since the late 1980s [243, 246-247, 257, 279, 282, 285-291]. The influence of high hydrostatic pressure (HHP) and $scCO_2$ on enzymes, particularly molecular level changes, are investigated [241, 247-248, 251, 285, 289, 292]. Importantly, HHP and $scCO_2$ do not contribute to chemical waste generation. The density of the $scCO_2$ is controlled by its temperature and pressure, providing a range of solvent characteristics with gas-like mass transfer and liquid-like solvating capability [282]. The attractive physicochemical properties and low critical temperature and pressure of CO_2 (31.0 °C and 7.3 MPa, respectively) make $scCO_2$ a greener solvent than other supercritical fluids [196, 293]. It is also worth mentioning that HHP differs from a pressurized or $scCO_2$ high-pressure environment. HHP creates a high pressure inside the reactor due to hydraulic pressure and may alter

the enzyme structure, dielectric constant of reaction media, and the activation volume of the enzyme-substrate complex [289, 294-295]. On the other hand, $scCO_2$ systems are pressurized by CO_2. In addition, CO_2 forms carbonic acid in presence of water (or moisture) which decreases the pH of the medium. Further the $scCO_2$ interacts with amine group of lysine and histidine amino acids of enzyme molecule and forms carbamate bond [296-297]. CO_2 is released when the reaction vessel is depressurized to atmospheric pressure conditions, and carbamate is reverted to amine groups as well as carbonic acid to water.

High pressure has been used for the pretreatment of enzymes before enzymatic reactions at atmospheric pressure as well as for one-pot enzymatic reactions where the substrate and enzyme are placed under high pressure during the reaction [115, 282-283, 298-299]. For example, Senyay-Oncel and Yesil-Celiktas (2013) pretreated the immobilized α-amylase on sodium zeolite support under $scCO_2$ (24.0 MPa, 41.0 °C, 4.0 g/min CO_2 flow and 2.5 h) that increased the enzyme activity by 67.7% [299] whereas Zheng and Tsao (1996) hydrolyzed avicel cellulose by cellulase enzyme under $scCO_2$ (13.6 MPa, 46.0 °C, 24.0 h) that produced 75.0 wt.% glucose sugars yield [282]. Studies of enzyme treatment by high-pressure or $scCO_2$ systems have shown that enzyme activity and stability may be either positively or negatively altered compared to atmospheric conditions [44, 113, 241]. High pressure simultaneously affects several parameters of the enzymatic reaction, such as the enzyme's molecular structure and hydration layer. In addition, there have been studies evaluating the effect of pressure on free and immobilized enzymes. Enzyme immobilization allows the enzyme to be reused, reduces the

overall cost, and protects the enzyme under high pressure and in $scCO_2$ systems [300] [301].

Similarly, cellulases and hemicellulase are a group of enzymes used in the paper and pulp, ethanol, detergent, and textile industries [302-303]. However, there are limited studies to understand the effect of high-pressure systems on enzyme molecular structure and activity. The application of enzymes is growing in various industries, such as α- & β-amylase and β-glucanase in the brewing industry and lipase in the oil and dairy industry [304-307]. Despite their high degree of utilization, even cellulases are not well explored under the high pressure and $scCO_2$ reaction conditions.

In this review, the role of high pressure and $scCO_2$ on enzyme activity with respect to molecular-level changes such as the primary, secondary, and tertiary structure of the enzyme, the activation volume of the enzyme-substrate complex, and the water content and arrangement in the hydration layer of the active site and at the protein surface have been critically analyzed. In addition, the role of immobilization methods and available support matrices that could be used in the enzymatic reaction under high pressure have been reviewed. Among the various enzymes, lipase enzyme has been widely studied for the molecular level reaction mechanisms such as activation volume change of the intermediate compounds and CO_2 interaction with amino acids of protein under high pressure. Therefore, this study has reviewed the different enzymes, including lipases and cellulases in free and immobilization forms, and their performance under high-pressure reaction systems.

2.3.5. Enzymatic reactions in high-pressure systems

The effect of high pressure on the enzyme activity and stability is influenced by several parameters such as reaction solvent, substrate concentration, temperature, and pH [241]. Under high pressure, the conformation of enzymes is changed by modulation of interactions with solvent, electrostatic charge interactions, van der Waals forces, and hydrogen bonds. Several studies have found that high pressure (1.0-500.0 MPa) leads to increased enzyme activity and stability compared to atmospheric reaction conditions [113]. For example, the enzyme activity of α-chymotrypsin (α-CT) was increased by 6.5-fold in an aqueous reaction under high pressure (20.0 °C, 470.0 MPa of HHP) with reduced thermal denaturation (up to 55.0 °C) compared to atmospheric reaction conditions (0.1 MPa, 20.0 °C) [289]. The active conformation of an enzyme may be stabilized at high pressure due to enzyme-substrate binding that protects the enzyme from denaturation and due to the reduction in the activation volume (the volume of enzyme-substrate complex or enzyme volume in active state) that leads to increased activity [285, 289]. However, all substrates may not protect a given enzyme (α-CT) from denaturation under high pressure, as observed for α-chymotrypsin. α-Chymotrypsin was stabilized by N-succinyl-L- phenylalanine-p-nitroanilide substrate with increased activity but poorly stabilized by another substrate (p-nitrophenyl acetate) [289]. Mozhaev et al. (1996) explained that HHP reduces an enzyme's hydrophobic and electrostatic bonds and systematically reorients the hydration layer's water molecules around charged groups. These changes cause a reduction in the activation volume that may enhance the reaction rate [289]. Another study investigated ginsenoside saponin extraction from ginseng roots by

cellulase and β-amylase enzymes at HHP of 100.0 MPa, 50.0 °C, and pH 5.0, where the reaction yields were increased by 26.0 % and 19.0 %, respectively, in comparison to atmospheric pressure conditions. Here, the increased yield was attributed to the effect of high pressure on the solubility of the ginsenoside from ginseng roots. However, no analyses were performed on the enzyme's molecular structure [251]. In recent studies, $scCO_2$ was used to pretreat the cellulase enzyme to enhance its activity [280, 283, 300]. Hojnik Podrepšek et al. (2019) reported a 47% increase in enzyme activity of free cellulase with cellulose after $scCO_2$ (10.0 MPa, 40.0 °C, 3.0 h) pretreatment of enzyme [280].

Although the effect of high pressure on an enzyme's structure in correlation with enzyme activity is not apparent, some studies suggest various effects on the enzyme caused by applying a high-pressure system. The effects can be divided into subcategories, as discussed in the following subsections, to develop an understanding of the effect of the high-pressure system on the enzyme.

2.3.5.1. Effect on activation volume of enzyme-substrate complex

The activation volume of the enzyme-substrate (transition) complex is influenced by structural changes in the active site and the reorientation of water molecules around the enzyme, reduction in bond lengths, and modulation of bond angles. Eyring and Magee developed mathematical models that relate the dependence of the activation volume of the substrate-enzyme complex to the reaction rate constant under HHP, as expressed in Equation (9) [245]:

$$\left(\frac{\partial \ln k}{\partial P}\right)_T = -\frac{\Delta V^{\neq}}{RT} \quad (9)$$

where k is the reaction rate constant at pressure P, and temperature T, the change in activation volume of enzyme-substrate complex due to pressure is $\Delta V^{\neq}$, and R

is the gas constant. The activation volume varies with both the pressure and the temperature at which the reaction is carried out, and this change can be negative, positive, or zero [245-247]. The activation volume is a kinetic property of the enzyme-substrate transition state, which may be estimated using experimental data through linear regression of the relationship between reaction rate constant (ln k) and pressure (P) [247, 308]. Changes in activation volume are mainly caused by electrostriction (a tendency of ordering the water molecule) of charged groups, packing defects or unfolding of polypeptides, and solvation of exposed surfaces [291]. The rate constant should increase based on Equation (9) as the activation volume decreases upon an increase in pressure. However, several parameters associated with an enzymatic structure and denaturation (i.e., hydration layer, pH, the temperature of enzyme) influence enzyme activity simultaneously. For example, Melgosa et al. (2017) reported decreased activation volume and increased reaction rate of lipase-catalyzed ethanolysis of fish oil. In contrast, Marszałek et al. (2019) used $scCO_2$ and HHP to inactivate the horseradish peroxidase (POD) and polyphenol oxidase (PPO) enzymes. The authors observed a decrease in the activation volumes of POD and PPO enzymes, as shown in Table *2-6*, as well as a substantial reduction (>80%) in the enzyme activity by the high pressure of HHP and $scCO_2$ [308].

Table 2-6. Changes in activation volumes of enzyme-catalyzed reactions due to high pressure and $scCO_2$ treatment

Enzyme	Change in activation volume * ($\Delta V^{\neq}$) mL/mol	Effect on enzymatic reaction	Ref.
Immobilized lipase from *Rhizomucor miehei*	-47.7 to -158.0 under $scCO_2$ (9.0-30.0 MPa, 50.0-80.0 °C)	Increased reaction rate	[276]
Horseradish peroxidase from *Amoracia rusticana* roots (EC 1.11.1.7)	-4.8 to –9.8 under HHP (200.0-600.0 MPa, 5.0-45.0 °C)	Enzyme inactivation	[308]
	−20.5 to −25.6 under $scCO_2$ (10.0-60.0 MPa, 5.0-45.0 °C)		
Polyphenol oxidase from *Agaricus bisporus* (PPOs) (EC 11.14.18.1)	−2.5 to −4.0 under HHP (200.0-600.0 MPa, 5.0-45.0 °C)	Enzyme inactivation	[308]
	−34.0 to −44.7 under $scCO_2$ (10.0-60.0 MPa, 35.0-65.0 °C)		
Cellulase from *Aspergillus niger*	6.17 under HHP (0.1-200.0 MPa, 30.0 °C) in buffer solution	Decreasing activity	[309]
	-6.3 under HHP (200.0-400.0 MPa, 30.0 °C) in buffer solution,	Increasing activity	
	1.68 under HHP (500.0-675.0 MPa 30.0 °C) in buffer solution	Decreasing activity	
	1.58 under HHP (200.0-600.0 MPa, 30.0 °C) in 10.0 % [Bmim]Cl solution	Increasing activity	
α-chymotrypsin from bovine pancreas	-2.2±0.1 in pure Tris-HCl buffer under	k_{cat} increases by about 15.0-20.0 %	[310]
	-3.1±0.5 in 1M trimethylamine-N-oxide (TMAO)	k_{cat} increases by about 20.0-25.0 %	
	-4.1±0.8 in 2.0 M urea		
	-0.9±0.4 in 1.0 M TMAO	k_{cat} increases by about 35.0 %	
	under HHP (0.1-200.0 MPa, 20.0 °C)	No Significant effect	

*Activation volumes were estimated from linear regression of ln *k* versus *P* using the Eyring equation (Equation 9).

2.3.5.2. Effect on protein structure

The effect of high pressure on the structure of enzymes may be analyzed at primary (1°), secondary (2°), and tertiary (3°) levels. For example, de Souza Melchiors et al. (2017) treated the enzyme lysozyme with different pressurized gases or fluids ($scCO_2$ and liquified petroleum gas (LPG), and 1,1,1,2-tetrafluoromethane (R134a)) at a range of pressures (10.0-20.0 MPa), ionic strengths (0.0-50.0 mM), and depressurization rates (0.1-0.5 MPa/min). The activity of treated enzymes was compared with untreated enzyme activity and correlated to changes in the structures at primary (1°), secondary (2°), and tertiary (3°) levels [311]. The primary structure was investigated using matrix-assisted laser desorption ionization-time of flight coupled with mass spectrometry (MALDI-TOF-MS) and sodium dodecyl sulphate-polyacrylamide gel electrophoresis (SDS-PAGE) [311-312]. No protein degradation or chemical modification in the $scCO_2$ pretreated enzymes (i.e. lysozyme, Lipases) has been observed in several studies based on their molecular weight analyses [258, 311-312]. Similar results for the primary structure were observed for lipases by Liu et al. (2012) and Liu, Chen, and Wang (2013) [258, 312]. Secondary structure has typically been investigated using circular dichroism (CD) spectropolarimetry [311-312]. Far-ultraviolet (far-UV) CD spectra are influenced by protein secondary structure as a linear combination at a given wavelength of contributions from α-helix, β-sheet, b-turn, disordered, and other structural elements. Based on the results of de Souza Melchiors et al. (2017) shown in Table 2-7, a decrease in the α-helix and an increase in β-sheet content was observed for lysozyme, which had increased enzyme activities compared to the untreated enzyme. The changes in the secondary structure introduced by

treatment with different pressurized fluids were attributed to promoted substrate access to the active site of the enzyme and, therefore, enhancement in the enzyme activity [311]. Li et al. (2020) found a similar result for cellulase enzyme where the proportion of α-helix was reduced and while β-sheet and b-turn content increased, consistent with loss of H-bonds in α-helical regions concomitant with new H-bond formation in β-sheets and b-turns [50]. In contrast, Liu et al. (2012) observed significantly increased enzyme activity, from 100.0 % to 188.0 %, in the treated lipase, which had increased α-helical and decreased β-sheet content after the $scCO_2$ treatment of the enzyme lipase compared to the untreated enzyme. After $scCO_2$ treatment, the activity in all conditions increased by 1.6-1.9-fold [258].

Table 2-7. Elements of the secondary structure of enzymes before and after treatment in a pressurized system, including *scCO₂*

Treatment	α-Helix (%)	β-Sheet (%)	Residual Activity (%)[1]	Ref.
Egg-white lysozyme				[311]
Control (untreated enzyme)	34.2 ± 2.2	14.2 ± 1.6	101.3 ± 1.3	
Treated with LPG (15.0 MPa, 40.0 °C, 2.0 h)	27.2 ± 0.0	22.1 ± 0.1	131.9 ± 0.3	
Treated with $scCO_2$ (15.0 MPa, 40.0 °C, 2.0 h)	31.1 ± 0.0	16.6 ± 0.0	119.1 ± 3.4	
Treated with R134a (15.0 MPa, 40.0 °C, 2.0 h)	26.3 ± 0.0	18.8 ± 0.0	132.5 ± 0.5	
Cellulase				[50]
Control (untreated enzyme)	13.0 ± 0.3	45 ± 0.2	100.0 ± 5.0	
Treated with $scCO_2$ (8.2 MPa, 50°C, 3.0 h)	3.1 ± 0.5	48.8 ± 0.2	96.0 ± 5.0	
Lipase (*Candida rugosa* Lip7)				[258]
Control (untreated enzyme)	13.4	30.6	100.0	
6.0 MPa CO_2, 35.0 °C, 0.5 h	13.6	21.6	161.0 ± 4.1	
10.0 MPa CO_2, 40.0 °C, 0.5 h	21.5	30.0	188.0 ± 2.1	
10.0 MPa CO_2, 40.0 °C, 2.5 h	13.5	29.5	176.0 ± 1.1	

*Activity is defined as the ratio of activity remaining after treatment to initial activity without treatment.

Fluorescence spectroscopy has been employed to evaluate tertiary structural perturbation by monitoring intrinsic tryptophan fluorescence. Namely, both the intensity and position of the emission maximum for tryptophan are sensitive to the local environment around the side chain of this amino acid, with changes in tertiary structuring, thus also potentially modulating the observed tryptophan fluorescence [313]. Using this experimental strategy, the intrinsic tryptophan fluorescence intensity increased for $scCO_2$ pretreated lysozyme, implying a change in tertiary structuring and a concomitant increase in residual enzyme activity [311]. In contrast, the intrinsic tryptophan fluorescence intensity decreased for $scCO_2$ pretreated *Candida antarctica* lipase B (CALB) in conjunction with increased residual enzyme activity [312]. $scCO_2$-treated cellulase also had a reduced tryptophan fluorescence intensity compared to the untreated enzyme. However, in this instance, enzyme activity did not significantly change [50]. Also, Li et al. (2020) studied cellulose hydrolysis by placing cellulase and cellulose substrate in an autoclave reactor and conducting the hydrolysis reaction under $scCO_2$ (8.2 MPa, 50.0 °C, 24.0 h) (also known as one-pot method). The hydrolysis reaction happened at a faster rate, and the sugar yield was approximately double as compared to atmospheric reaction conditions over a 24.0 h period. Converse to this, pretreated cellulase under $scCO_2$ (8.2 MPa, 50.0 °C, 180.0 min) produced a similar sugar yield compared to the atmospheric reaction with untreated enzyme upon hydrolysis of cellulose [50]. Finally, in another study, although tryptophan fluorescence of $scCO_2$-treated hydrolases suggested no enzymatic conformational change, there was a slight reduction in the stability of the enzyme [257].

Related to both far-UV CD spectroscopy and fluorescence spectroscopy but typically somewhat less sensitive in terms of response to conformational or environmental change, UV absorption spectroscopy is another method that has been applied to compare enzymes before and after treatment with $scCO_2$ [50]. Namely, absorption by backbone peptide bonds (i.e., in the far-UV) and aromatic sidechains (i.e., in the near-UV) may be influenced by enzyme conformational change through changes to secondary structuring and through modulation of the local environment upon tertiary structure change. In a study on cellulase, for example, a decrease in absorbance in the near-UV was attributed to a tertiary structural change that led to aromatic sidechain exposure to solvent [50]. In general, UV absorption spectroscopy would be expected to provide a correlated response to changes observed by CD and/or fluorescence spectroscopy. Still, it would be less straightforwardly interpretable in its own right.

In summary, the studies reviewed herein have shown a lack of primary structure perturbation due to high pressure. However, under high-pressure reaction conditions, the hydrogen bonds in the enzyme could be expected to get shortened and thus strengthened. Electrostriction of the water molecules of hydration layer could also decrease the molar volume, with the water molecules being compressed and the inter-atomic electrostatic forces weakening due to the increased distance between atoms [288]. Such physicochemical changes may promote conformational rearrangements in the secondary and tertiary structure of the enzyme [50, 258, 311-312].

2.3.5.3. Effect on hydration layer of enzyme

The hydration layer is bound to the enzyme's active site and polar surfaces, an essential part of catalytically active enzymes. The formation of the hydration layer is thermodynamically favored in polar and charged regions. Still, it should be noted that not all surfaces of the enzyme necessarily need to be covered by the hydration layer. Namely, this may be localized to the enzyme's polar surface at a minimum [314]. The hydration layer of enzymes holds significant importance, especially for enzymes employed in hydrophobic substrate reactions within organic solvent-based reaction media. Among these processes, the esterification reaction catalyzed by lipase (a hydrophilic enzyme) has been extensively studied under high pressure and $scCO_2$ conditions [315-316]. The nature of the solvent (polar or nonpolar), pressure, and temperature of the system affect the water content in the hydration layer. Under the high pressure environment with $scCO_2$ and other solvent, the water molecules of hydration layer (partially or completely) may interact with the solvents molecules depending on their water solubilizing power, and therefore, water may leave the enzyme molecule during the depressurization of reactor [253, 314, 317]. The water solubility in CO_2 varies from 0.25 % to 3.0 % mole fraction for increase in pressure and temperature from 10.0 MPa, 0 °C to 40.0 MPa, 100.0 °C [318-319]. The ability of stripping off the bound water of an enzyme by non-polar $scCO_2$ is lower than the polar solvents such as methanol, *n*-propanol, and acetone. For example, Gorman and Dordick (1992) found that methanol removed 38.0% of the water from an enzyme hydration layer. In contrast, nonpolar organic solvents (hexane and toluene) removed only 10.0 % water from the enzyme [253]. Up to this point, there is a scarcity of evidence confirming the restoration of enzyme

activity upon rehydration following exposure to $scCO_2$. The presence of organic solvent in an enzymatic reaction mainly affects the hydration layer of the enzyme [320-321]. Supercritical carbon dioxide acts as a nonpolar organic solvent that forms unstable carbonic acid (Equations (1 and 2)) in aqueous conditions [322]. However, CO_2 has very low solubility in water, which further varies with the temperature and pressure of the system. For example, CO_2 solubility in water increased from 0.5 to 2.0 % mole fraction when the pressure increased from 25.0 to 30.0 MPa at 85.0 °C. In contrast, the solubility of CO_2 in water decreased from 3.2 % to 2.25 % mole fraction in water when the temperature increased from 15.0 °C to 85.0 °C at 30.0 MPa pressure [323].

$$CO_2 + 2H_2O \leftrightarrow HCO_3^- + H_3O^+ \quad (1)$$

$$HCO_3^- + H_2O \leftrightarrow CO_3^{2-} + H_3O^+ \quad (2)$$

Hobbs & Thomas (2007) proposed the hypothesis that lysine residues on an enzyme surface will form carbonate with CO_2 and destabilize the enzyme, leading to inactivation. On the other hand, some researchers suggest that carbamate formation is useful in bio-catalysis [296-297]. Using molecular dynamics simulation to evaluate post-translational modifications (PTMs), Monhemi & Housaindokht (2016) compared acetylation, carboxylation, and phosphorylation of lysine side chain to analyze the relative stability of a lipase enzyme in $scCO_2$ because these modifications convert the positive charge (of lysine) to negative charge on the enzyme surface [324]. Acetylation and phosphorylation were not found to modulate stability. In contrast, carboxylation seemed to improve the enzyme stability significantly in $scCO_2$ because the carboxylate's net negative charge on the enzyme's surface restricts the CO_2 interaction from forming carbamate. The

formation of an excess hydrogen bond or negative charge on an enzyme surface has the potential to perturb enzyme structure, leading to its destabilization and inactivation in $scCO_2$ [324].

2.3.5.4. Effect of temperature and pH

An enzyme's activity under high pressure depends on local changes in the enzyme's microenvironment governed by pressure and temperature. In the liquid phase equilibrium of the H_2O-CO_2 biphasic system, the solubility of CO_2 increases with an increase in pressure and decreases with an increase in temperature. Therefore, the pH of the aqueous medium changes in response to the amount of solubilized CO_2 in water [322, 325]. Changes in pH due to $scCO_2$ lead to changes in the microenvironment of the enzyme and, therefore, the activity and product yield [292].

There was no change in the optimum pH of cellulase after $scCO_2$ pretreatment of this enzyme. However, the optimum temperature for pretreated cellulase increased slightly (54.0 °C vs. 50.0 °C) compared to untreated cellulase [283]. Muratov, Seo, & Kim (2005) found that three cellulases from different species (*Trichoderma viride, Trichoderma reesei, and Aspergillus niger*) released 20.0-26.0 % more reducing sugars from cotton fibres under $scCO_2$ (10.0-16.0 MPa, 50.0 °C, pH 5.0 of 0.1 M acetate buffer) in a one-pot hydrolysis reaction than the atmospheric reaction condition with untreated enzymes at 100 rpm shaking conditions in 48.0 h reaction time. However, no observation was made for the pH of the enzymatic reaction under the $scCO_2$ [326]. Under $scCO_2$, the pH of enzymatic reaction in aqueous media will be lower than the optimum pH of the enzyme at

reaction at atmospheric conditions and therefore, analyzing the effect pH of one-pot reactions would bring more insights.

2.3.5.5. Effect of pressurization-depressurization of reactor

It is challenging to observe the exact effect of high pressure of HHP or $scCO_2$ in different stages – pressurization, holding time, and depressurization during the pretreatment of the enzyme. The pressurization step does not affect enzyme structure or performance because there is a slow mass transfer between CO_2 and the reaction mixture [327-328]. During the pretreatment holding time, $scCO_2$ interacts with the enzyme, which may form carbamate bonds. Finally, dissolved $scCO_2$ gets released from the reaction medium during the depressurization of the reactor. The release of CO_2 is critical because it can strip off the enzyme's essential hydration layer and alter the enzyme's conformation [327]. The release of $scCO_2$ could thus cause partial structural unfolding. Here, S-S bonds play a critical role in preventing the unfolding of enzyme structure, and the enzymes with S-S bridge should preferably be used in $scCO_2$ solvents. For example, Kasche et al. (1988) studied a-chymotrypsin and trypsin (monomeric enzymes) with an S-S bridge and penicillin amidase (oligomeric enzyme) without an S-S bridge under dry and humid $scCO_2$. The enzymes with the S-S bridge were partially denatured less than those without the S-S bridge. The partial denaturation might have been caused due to the depressurization step. Kasche et al. (1988) further reported that depressurization rates between 1.0-2.0 MPa min^{-1} showed a negligible degree of inactivation of enzyme in dry $scCO_2$ compared to humid (moisture content 3.0 % w/v) $scCO_2$ [286]. Kamat et al. (1992) and Zheng & Tsao (1996) found that the loss of cellulase

activity could be prevented by releasing pressure more gradually than 1.0-2.0 MPa min^{-1} [282, 287].

The denaturation of a protein depends more on the number of depressurization steps than the time of exposure to $scCO_2$. Aucoin & Legge (2001) investigated the effect of applying multiple pressurization-depressurization cycles (1, 3, & 5) of the reactor along with holding time (4.0, 8.0, & 12.0 h) and depressurization rate (0.43–0.45 MPa min^{-1}, 0.86–0.89 MPa min^{-1}, & 8.6–8.9 MPa min^{-1}) on the lipase enzyme Lipozyme. The 5-time pressurization-depressurization over 12.0 h exposure time using the lowest depressurization rate (0.43-0.45 MPa min^{-1}) showed the highest activity for the immobilized enzyme [329]. Conversely, another study showed slightly decreased enzyme activity of immobilized lipase when the number of pressurization-depressurization cycles was increased from 1.0 to 3.0 using 3.0 h incubation time under $scCO_2$ (10.0-25.0 MPa, 50.0 °C). Also, a longer exposure time (3.0-6.0 h) was shown to reduce the enzyme activity [249]. A high depressurization rate leads to the formation of cracks and rough surfaces in the case of immobilized enzymes, which could increase the porosity and the mass transfer of substrate and CO_2 to the enzyme, enhancing enzyme activity [249, 283]. However, there would be a risk of loss of enzymes from the cracks over time, leading to a loss of the ability to reuse of enzymes. Therefore, a slow depressurization rate has been proposed to be positive in most studies of free and immobilized enzymes under high pressure and $scCO_2$.

2.3.5.6. Influence of external parameters

The high-pressure treatment of the enzymes under HHP or $scCO_2$ has various effects at the molecular level. However, external parameters such as instrumental

configurations and enzyme amino acid sequences can be categorized as external parameters. Various studies have used differently designed equipment and enzymes sourced from different microorganisms with distinct amino acid sequences.

2.3.5.6.1. Effect of instrumental configuration

Various types of reactor models and configurations have been used in the literature, with different pressurization methods, sample-holding compartments, and instrument configurations. In HHP, the MV2 chamber (Unipress, Poland) has been used to achieve pressure ranges up to 900.0 MPa with quick pressurization. HHP equipment with a sample cell of 2.0 mL volume in a stainless steel jacket was used to treat the enzyme α-chymotrypsin to characterize the effect of high pressure. Specifically, the reaction mixture in a 2.0 mL quartz cuvette closed with a flexible membrane was subjected to 470.0 MPa pressure for up to a 0.67 h min treatment at 20.0-65.0 °C. The activity of α-chymotrypsin was observed to be stimulated more than 80.0 % of atmospheric activity by high pressure 0.1-350.0 MPa, and decelerated by a further increase in pressure 350.0-450.0 MPa [289]. In another study, separately, 3.0 mL of polyphenol oxidase (PPO) and horseradish peroxidase (POD) enzyme solutions were pressurized 200.0-900.0 MPa within 80.0-90.0 s and depressurized in 2.0-4.0 s, which are very high pressurization and depressurization rates. This configuration was used to inactivate the enzymes by high-pressure treatment. In this instance, the high-pressure treatment was observed to lead to the residual enzyme activity of 20.0 % at 900.0 MPa and 25.0 °C with a 10.0 min holding time. This significant activity reduction was attributed to

the change in the enzyme's molecular structure that changed the activation volume [308].

Compared to HHP, $scCO_2$ treatment systems use lower pressure, typically around 10.0-25.0 MPa, and a slower depressurization rate. $scCO_2$ interacts with enzyme molecules and alters the enzyme structure, activation volume, and hydration layer. Reaction vessel volumes vary substantially in different studies. For example, a Speed, SFE 4 (Applied Separations, USA) system with a 50 mL volume vessel was used in $scCO_2$ treatment (10.0-65.0 MPa for 10.0-30.0 min at 35.0-65.0 °C) of 5.0 mL volumes of PPO and POD enzyme solutions, separately. The reactor was pressurized at 60.0 MPa/min and depressurized at 5.0 min (~12.0 MPa/min). The enzyme activities were reduced from 100.0 % to 12.0 % at 65.0 MPa at 45.0-50.0 °C in 10.0-30.0 min [308]. A $scCO_2$ system with a series of high-pressure cells was used to treat free enzyme solution and liquid-free immobilized enzyme using a 3.0-10.0 mL internal reactor volume. The reactor was placed in a thermostatic water bath at 35.0-75.0 °C and pressurized to 10.0-25.0 MPa in 0.5 min for a holding time of 1.0-6.0 h. Increased activity has been observed in most experimental conditions (i.e., 10.0-15.0 MPa, 35.0-50.0 °C, 1.0-3.0 h) except with long exposure to very high pressure (i.e., 25.0 MPa, 50.0 °C and 3.0 h) that led to decreased residual activities. The authors claimed that the $scCO_2$ reaction conditions are critical parameters affecting enzyme activity [249]. Another parameter that may affect the enzymatic reaction could be the flow rate of $scCO_2$ during a dynamic reaction where the reaction is pressurized by $scCO_2$. Senyay-Oncel and Yesil-Celiktas observed that increasing the CO_2 flow rate could reduce the mass

transfer resistance, but it was not mentioned that the reaction was carried out in static or dynamic conditions [283]. The increased flow rate may also remove unwanted water from the reaction environment to reach optimum enzyme activity [330]. Namely, the configuration of high-pressure systems, such as the reactor's internal volume, pressurization, depressurization rate, and static or dynamic flow of CO_2 (in the case of $scCO_2$ based reactor system), may influence the reaction conditions and, therefore, the enzyme.

2.3.5.6.2. Effect of enzyme amino acid sequence

The amino acid sequences of individual enzymes are enzyme-specific and species-dependent, with a corresponding potential to change secondary, tertiary, and quaternary structuring as well as stability and response to environmental factors. Therefore, the properties of the same enzyme, i.e., cellulase (EC3.2.1.4) from different microorganisms, show differences in reaction conditions. An enzyme treated with high pressure using HHP or $scCO_2$ may behave differently with an increase or decrease in enzyme activity. For example, the cellulases produced by different microorganisms exhibit different 3D structure, ligand and water arrangements. These enzymes also have different molecular weight, number of amino acid residues and peptide chains [331-334]. Based on the amino acid sequences and the corresponding 3D structure of the active site of an enzyme, high pressure and $scCO_2$ alter the enzymatic reactions, which could enhance the accessibility of substrate to the active site and activation of the enzyme. In contrast, deformation could obstruct substrate-enzyme interactions, leading to inactivation [276, 308, 324].

There has been substantial research using different enzymes from different sources under high pressure, either by HHP or $scCO_2$. The results of these studies show both positive and negative effects on enzyme activity, even in situations where similarities had been observed in the enzyme structure or microenvironment. After high-pressure treatment, an enzyme may form a specific stable state with increased or decreased enzyme activity. Therefore, each potential enzyme might need to be investigated for its behavior under high pressure. Possible changes include the rearrangement of enzyme secondary and tertiary structure, inter- and intramolecular hydrogen bonds, the aqueous layer around the enzyme active site, hydroxyl groups, charged and polar groups, and the presence of organic solvents [50, 248-249]. Apart from these effects, the solubility of the substrate and co-solvent in a compressed/pressurized medium, viscosity, and mass transfer also significantly affect enzyme activity in high-pressure systems [243, 249, 317].

There is also a rich history of nuclear magnetic resonance (NMR) spectroscopy studies of enzymes under high-pressure conditions. This class of study provides the potential to elucidate atomic-level detail about the effects of pressure upon a macromolecule in real-time [335-336] with most modern studies relying upon a commercially available apparatus using a hydrostatic pump connected through pressure-safe tubing to a specialized NMR cell that allows solution-state samples to be subjected in a dynamic and controllable manner to pressures of up to 300.0 MPa [337]. Kitahara et al. (2000) showed clear pressure dependence of E. coli dihydrofolate reductase confirmation [338]. This enzyme is in

a conformational equilibrium between occluded and open forms. Over pressures of 3.0-200.0 MPa, and pressure-dependent increase in the population of the open form is observed, in turn, linked to a large negative $\Delta V^{\neq}$ which is proposed to arise both from compression of cavities within the protein and due to a concomitant increase in hydration. Because the open form is critical for cofactor binding and, thus, enzyme activity, the ability to observe this pressure-dependent increase in the open conformation and characterization of this state of the enzyme provides key thermodynamic and conformational detail and demonstrates the potential for elevated pressure to modulate an enzyme's conformational ensemble in a functionally critical manner. Thus, high-pressure NMR spectroscopy has enormous potential to provide insight into enzyme conformational changes and dynamic processes induced by pressure. Importantly, this allows these changes to be evaluated in real time as a function of pressure.

2.3.6. Enzyme immobilization

Immobilization of enzymes has shown a substantial potential to protect enzymes from harsh reaction conditions such as high pressure or alcoholic media components [115, 280, 283]. Therefore, it is worth looking at the methods of immobilization and the available support matrices that can be potentially used in a high-pressure system.

2.3.6.1. Methods of immobilization

Immobilization is the handiest approach in promoting the recovery and reusability of enzymes in bioprocess engineering. It further enhances stability and prevents adverse impacts of reaction conditions such as autolysis, denaturation by heat, or organic solvents [301, 339]. Enzymes are immobilized to various support materials

using different methods, including support binding, adsorption, entrapment, encapsulation, and cross-linking (Figure 2-5).

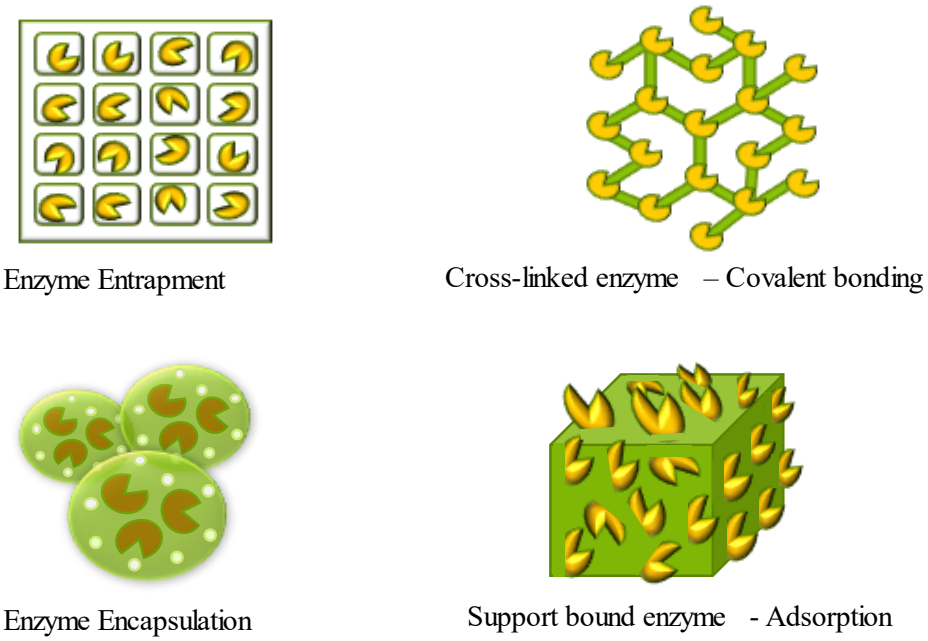

Figure 2-5. Illustration of different types of enzyme immobilization techniques

The entrapment and encapsulation methods are similar, with the minor difference that additional cross-linking agents are applied to covalently attach the encapsulated enzyme [340-341]. The enzyme is entrapped in a polymeric gel material based on the molecular size of the enzyme and the pore size of the matrix support material in case of enzyme entrapment. In comparison, the enzyme is encapsulated in a mesoporous semipermeable membrane (i.e., zeolitic membranes) of support material in the enzyme encapsulation method to trap the enzyme molecules with covalent bonds. For example, the enzyme β-galactosidase encapsulated in the hybrid carrier alginate-gelatin-calcium phosphate (AGCaP) has shown good mechanical stability and minimal enzyme inactivation by physical immobilization and results in a material that prevents the leakage of the enzyme

[342]. Silica-based sol-gel has been utilized as a well-known entrapment method of immobilization that leads to form silica-based aero- and xerogels [343-344]. However, the entrapment method has the disadvantage of diffusional limitation and is better for only small-sized substrates of enzymes.

Support binding may occur due to physical or chemical interactions (van der Waals, physisorption and/or hydrophobic interactions) or through covalent linking of amino, phenolic rings, sulfhydryl, and hydroxyl groups of an enzyme to reactive functional groups (i.e., silanol, epoxy) of the support matrix [345-346]. Physically adsorbed enzymes tend to have weak interactions that keep the enzyme immobilized onto the support. In contrast, ionic and covalent bonded immobilized enzymes show insignificant disintegration or leaching out from the support during the reaction [301, 339, 345, 347]. For example, the enzyme lipase was immobilized on a silica-based mesoporous support matrix by applying adsorption and covalent bonding techniques. Firstly, lipase was immobilized on succinated hyperbranched polyethyleneimine (PEI, MW = 60,000.0) grafted mesoporous silicate materials (MCM-41) termed MCM-41@PEI by physical adsorption. Then cross-linking agent glutaraldehyde was used for covalent immobilization to cross-link between lipase and amino groups on the surface of MCM-41@PEI (Figure 2-6) [345]. Covalently binding methods have the advantage of minimal enzyme leakage over other methods but the prone to loss of enzyme active site due to chemical interactions of enzyme with support matrix.

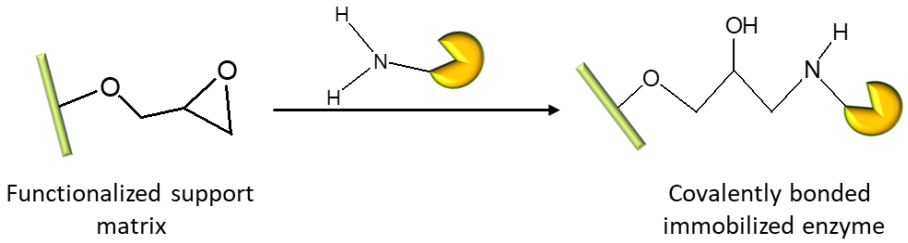

Figure 2-6. Schematic representation of enzyme immobilization by covalent bonding on the functionalized support matrix.

Metal-organic frameworks (MOFs) are emerging supports for the entrapment technique of enzyme immobilization (Figure 2-7) [348-349]. MOFs are a crystalline network of organic and inorganic materials with tunable porosity like zeolites. In MOFs, *p*-block elements, alkaline earth metals, and actinides are typically used in combination with multidentate organic linkers such as amines, nitrates, carboxylates, phosphate, and sulfonates to form different frameworks. The primary advantage of MOFs is the flexibility with which they can be tailored with respect to porosity, large surface area, high thermal and mechanical stability, and magnetic and optical properties [348].

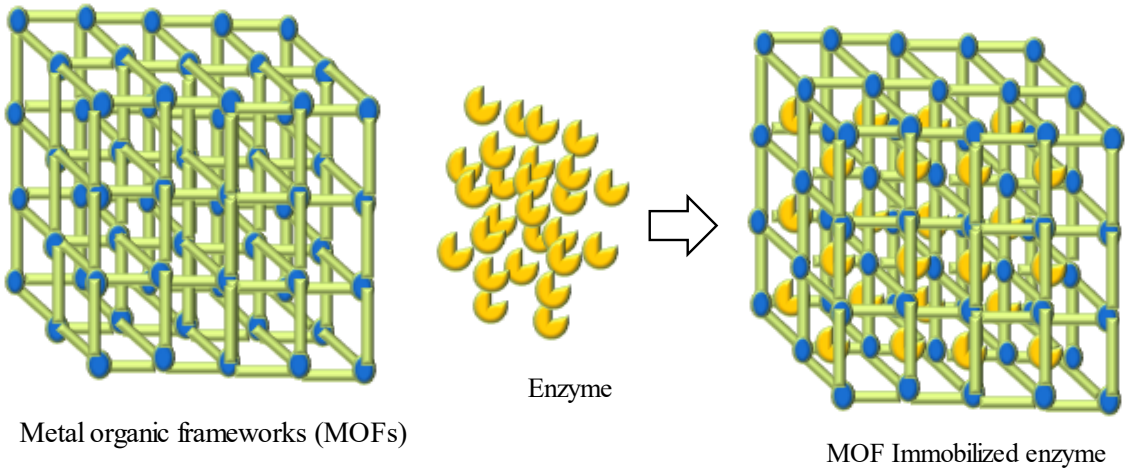

Figure 2-7. Illustration of enzyme immobilization in metal-organic frameworks

Cross-linking of enzymes using a bifunctional reagent is a carrier-less covalent immobilization technique. This technique requires fewer steps to prepare

an immobilized enzyme without using carriers, making it economically attractive [339]. Carrier-free immobilized enzymes, such as cross-linked enzyme aggregates (CLEAs) and cross-linked enzyme crystals (CLECs), offer low production cost, high stability, and concentrated enzyme activity [339]. Preparing CLEAs involves the precipitation of the water-soluble protein by adding a salt that does not denature the protein (Figure 2-8). Subsequently, the addition of cross-linking agents makes the enzyme permanently insoluble as an aggregate [342, 350]. The appropriate selection of the precipitant can improve the activity of cross-linking immobilized enzymes before aggregation. For example, polyethylene glycol precipitated cellulase-derived CLEA exhibited 40.0 % of the initial activity of immobilized enzyme after the fourth reuse cycle. In contrast, *tert*-butyl alcohol deactivated the enzyme during precipitation, and ammonium sulphate precipitated CLEA showed only 10.0 % residual activity after the first cycle [350].

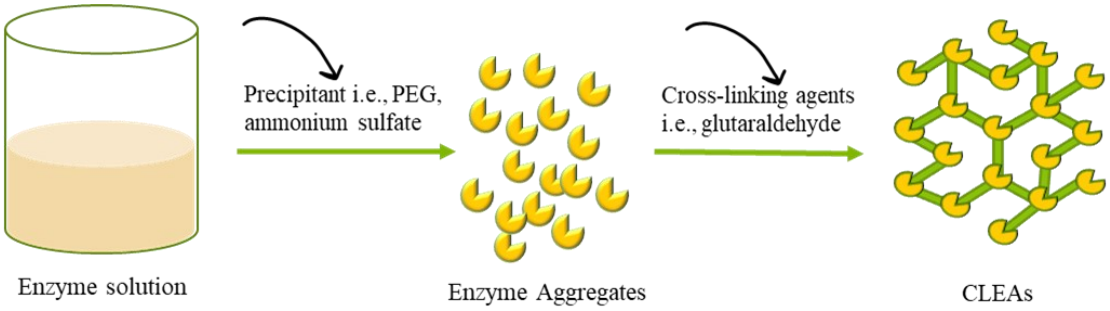

Figure 2-8. Illustration of Cross-linking immobilization

2.3.6.2. Type of support materials

The immobilization support material can be a natural biopolymer, synthetic organic polymer, composite metal support, or hybrid support [339-340, 348]. Selecting a suitable material is essential for higher enzyme stability and increased activity [351]. For example, the affinity of the functional groups of the support for those of the

enzyme should be high enough for covalent bonding to prevent the enzyme from leaching into the reaction solution, or the entrapment gel matrix should be thin and strong enough to contain the enzyme without mass transfer issue. The active site should also be exposed to the reaction solution in adsorption-based immobilization to reduce diffusional limitations [351-352]. Alftrén and Hobley used non-porous silica-coated superparamagnetic particles to immobilize a mixture of cellulase enzymes. They reported 80.0 % of the initial activity of the immobilized enzyme, and 66.0 % of the free enzyme's initial activity was retained after the second reuse cycle [353]. On the other hand, nanotechnology is being increasingly applied in immobilization applications. Nanomaterials provide several desired characteristics, such as an increased surface area to volume ratio, high enzyme loading, easy functionalization, high mechanical stability, and reduced diffusional resistance [354]. The MOFs-based method also introduced above uses magnetic metal nanoparticles, which provides several benefits: increased enzyme loading, inhibitor tolerance, increased stability and catalytic efficiency, and easy recovery for reusability [355].

Various support materials have been used, including recently developed techniques for immobilizing enzymes (Table 2-8). From the industrial application perspective, problems associated with the recovery of immobilized enzymes by filtration and centrifugation techniques may cause decreased activity due to the internal mass transfer limitation. Centrifugation or filtration techniques can result in the compression and squeezing of immobilized enzymes, particularly those that are cross-linked or entrapped. This compression can lead to a reduction in pore

size, which in turn limits the internal mass transfer of the substrate during subsequent cycles of enzyme reuse [356]. The application of magnetic nanoparticles (MNPs) has been proposed as the most suitable immobilization method because of their easy recovery, stability and reusability [357]. A functionalized magnetic core is mostly used to immobilize the enzymes on to the surface by making covalent bonding between functional group of support and the enzymes [355, 358].

Table 2-8. Immobilization of cellulase enzymes on different support materials and their reaction conditions for converting cellulose to glucose under atmospheric pressure.

Immobilization technique	Support materials	Enzyme	Substrate	Reaction conditions	Reusability	Ref.
Covalent bonding	1 µm non-porous silica-coated super-paramagnetic particles	CellicCTec2 Cellulase	Wheat straw Carboxymethyl cellulose (CMC)	6.0 FPU/g, pH 4.8, 50.0 ºC, 72.0 h	Retention of 80.0 % of activity in 2nd cycle	[353]
Covalent cross-linking	40 nm magnetic nanoparticles	Recombinant Cellulase from *T. reesei*	hemp hurd biomass, CMC	20.0 CMCase unit, pH 4.0, 60.0 ºC, 0.5 h	30.0 % of the initial activity was retained after 10th cycle on CMC substrate	[359]
Covalent cross-linking	Salt-precipitated cellulase cross-linked to glutaraldehyde-based CLEA	Novozymes Cellulase	hydroxyethyl cellulose (HEC)	16.0 U/g, pH 5.0, 37.0 ºC, 24.0 h	40.0 % of the initial activity retained after 4th cycle	[350]
Covalent cross-linking	Carrageenan polymeric gel coated with cationic polymer	Cellulase	CMC	pH 5.0, 50.0 ºC, 0.5 h	60.0 % relative active remained after the 7th cycle. Immobilized enzyme had a broader range of temperatures.	[360]
Covalent cross-linking	Magnetic UIO-66-NH_2 based MOF composite support	Commercial Cellulase	CMC	25.0 U/g, pH 5.0, 50.0 ºC, 48.0 h	Increased tolerance to inhibitor compounds, i.e., formic acid, vanillin	[355]
Adsorption	100 nm silica particles enzymogel support	Cellulase β-Glucosidase	Cellulose, Cellobiose	10.0 FPU/g, pH 4.8, 50.0 ºC, 72.0 h 10.0 CBU/g, pH 4.8, 50.0 ºC, 6.0 h	~96.0 % of activity retained after hydrolysis	[358]

Adsorption	Silica-coated magnetic nanoparticles	CEL Cellulase from Sigma-Aldrich	*p*-nitrophenol-cellobiose (*p*-NPC)	16.0 U/g, pH 5.0, 37.0 ºC, 24.0 h	75.0 % recovery without leaching of enzyme	[361]
Adsorption	Commercial activated carbon powder	Cellulase from *Aspergillus niger*	Methylcellulose powder (Tylose MH1000)	pH 4.8, 30.0 °C, 1.0 h	70.0 % of the initial activity was maintained till the 5th cycle of reuse.	[362]

2.3.7. Free and immobilized enzymes under high pressure and in sub/supercritical fluids

Immobilized enzymes are a key target for several industrial applications due to their recoverability, improved activity, stability, and resistance to environmental variation. It should be noted that the residual activity of immobilized enzymes, compared to free enzyme activity, may increase or decrease, provided the type and source of the enzyme, the nature of the support material, and the reaction conditions. Considering the solubility of the substrate in the reaction media is crucial when studying the effects of high pressure and $scCO_2$ in enzymatic reactions. The solubility of the of the substrate and $scCO_2$ in reaction aqueous or non-aqueous media could be increased by adding cosolvent as modifier which will increase the mass transfer and therefore, the reaction rate [363-365].

Melgosa et al. (2015) studied four commercial lipases treated with $scCO_2$ in free and immobilized forms. The free recombinant lipases (from *R. miehei* and *C. antarctica*) enzymes under mild conditions of pretreatment improved the enzyme activity (around 112.0-135.0 % residual activity) due to confirmational change in the tertiary structure, whereas activity decreased for immobilized enzymes in all conditions of $scCO_2$ pretreatment with a range of 80.0-99.5 % residual activities [249]. In contrast, Nyari et al. (2018) used $scCO_2$ (12.0 MPa, 37.0 °C, 1.0 h) for the activation of lipase from *Candida antarctica*, immobilized in polyurethane and

additionally used the activated immobilized enzyme in esterification reaction. The activated lipase had 315.0 % residual activity and 113% conversion yield compared to untreated enzyme. The authors inferred that the polyurethane support prevents the $scCO_2$ to form the carbamate with the immobilized lipase [366].

Badgujar and Bhanage (2015) investigated the enzyme activity of immobilized lipase entrapped in a biocompatible support matrix developed from polyvinyl alcohol and chitosan (PVA/CHI). The immobilized enzyme had 42.0 % higher activity than the free enzyme without $scCO_2$ treatment. In addition, the immobilized lipase had a 94.0 ± 1.5% yield. Whereas the free enzyme had only 23.0 % yield when the reaction was conducted to synthesize the laurate compounds by free and immobilized lipase under $scCO_2$ (8.8 MPa, 46.0 °C, 3.5 h). The activity was decreased when the free enzyme was exposed to $scCO_2$, and after the 5^{th} cycle of reuse of free enzyme, a total 65.0 % reduction in the yield was observed, which might be due to continuous exposure to an alcoholic substrate, high-pressure and washing during the recovery of immobilized enzyme [300].

A silica-based sol-gel immobilized cellulase has been used for carboxymethyl cellulose (CMC) hydrolysis at atmospheric and supercritical conditions of CO_2 (10.0 MPa, 40.0 °C, 5.0 h). The activity of pre-incubated (10.0 MPa, 40.0 °C, 24.0 h) immobilized cellulase on a Tetramethoxysilane (TMOS) support was increased to 461.0 % of the free enzyme activity at atmospheric pressure, and the reusability significantly improved with 15 consecutive cycles for the hydrolysis reaction at atmospheric pressure and up to 20 cycles under $scCO_2$. It was postulated that the increased activity over 20 cycles observed under $scCO_2$ might be due to an

increase in the pore size of the immobilized support upon application of high pressure [115]. Senyay-Oncel and Yesil-Celiktas (2015) characterized zeolite (NaY) supported immobilized cellulase enzyme activity and reusability after $scCO_2$ pretreatment (18.0 MPa, 54.0 °C, 2.0 h). The enzyme activity of the $scCO_2$-treated immobilized cellulase was enhanced to 148.0 % of the untreated immobilized cellulase activity. After reusing the $scCO_2$-treated immobilized enzyme for four cycles in enzymatic reaction at atmospheric pressure, the activity was decreased to <60.0 % of the initial activity. The activity was interestingly regenerated by $scCO_2$ treatment (18.0 MPa, 54.0 °C, 10.0 min), regaining 85.0 % of the initial activity with activity decreased <55.0 % after 3-4 cycles of reuse. 65.0 % of the initial activity was retained after 10 cycles of reuse of $scCO_2$-treated immobilized enzyme, with three cycles of regeneration of enzyme activity by scCO2 treatment included. The activity could not be revived significantly after the 10^{th} cycle, with less than 50.0 % residual activity at that point [283]. The immobilized cellulase prepared by cross-linking of the aggregates (CLEAs) was exposed to $scCO_2$ (10.0 and 20.0 MPa, at 40.0 and 50.0 °C for 1.0 to 24.0 h) to investigate their stability. The residual activity of the enzyme demonstrated a consistent decrease in from 100.0% (untreated) to approximately 85.0% at 10.0 MPa, 40.0 °C, 24.0 h, and 63.0 % at 20.0 MPa, 40 .0°C, 24.0 h of incubation. However, intriguingly, the residual activity surpassed 100.0% (untreated), reaching 143.0%, when the enzyme was exposed to 10.0 MPa at 50.0 °C for an incubation up to 3.0 hours. High pressure and long exposer (4.0-24.0 h) decreased the residual activity of CLEAs enzyme to up to 65.0 %. The free cellulase substantially benefited from the $scCO_2$ treatment and the residual

activity were reached to 147.0 % for 10.0 MPa, and 138.0 % for 20.0 MPa for 3.0 h incubation time at 40.0 °C [280]. The increase in the activity of free cellulase could be attributed to changes in the conformation changes in the enzyme and the presence of lysine residues on the surface. These surface lysine amino acids are involved in the cross-linking reaction of CLEAs formation which would not have interacted with CO_2 in case of immobilized enzyme. The CLEAs enzymes were found to be advantageous for their stability under the $scCO_2$ reactions and reusability applications [280].

The utilization of scanning electron microscopy (SEM) analysis on immobilized enzymes subjected to high pressure and $scCO_2$ treatment facilitates the identification of physical and morphological changes. Melgosa et al. (2015) used external agitation for mixing and still observed the cracks on the surface of immobilized lipase from *Rhizomucor miehei* on Duolite A568 (a macro-porous hydrophilic granular weak base anion exchange resin) and Lipozyme 435 from from *C. antarctica* expressed in *Aspergillus niger*, immobilized on Lewatit VP OC 1600 (a macro-porous hydrophobic resin presented in spherical beads) [249]. In contrast, Santos et al. (2016) did not find any wear and tear on the $scCO_2$ (20.0 MPa, 40.0 °C, 6.0 h) treated immobilized lipase from *Candida antarctica* (Lipozyme 435) on a macro-porous anionic resin [278]. Under high pressure and $scCO_2$, the immobilized enzyme exerts mechanical stress due to stirring if internal agitation such as magnetic stirring or impeller is used, and may cause additional morphological deformation [367]. SEM analysis showed that the immobilization support was affected by minor hole and crack formation due to $scCO_2$ treatment.

The cracks may have allowed for increased mass transfer and exposed more enzymes to the substrate, however, the activity of treated enzyme firstly increased and then decreased below 65.0 % after 2-3 cycles of reuse [283]. Oliveira et al. (2006) found that the roughness of surface of immobilized lipase enzyme (Novozym 435) was increased after $scCO_2$ treatment, and the activity was decreased. In comparison, the same immobilized lipase was treated with compressed *n*-butane and there was no impact on the surface of immobilized lipase, and the activity was increased as well [368].

Enzymatic reactions conducted under high pressure or $scCO_2$ have been summarized in Table 2-9, including the reaction conditions and the reactor instruments used. The free enzyme activity has been compared with the high-pressure-treated free enzyme, with the immobilized enzyme under atmospheric and high pressure, wherever possible. Studies on cellulase enzymes have shown similar or increased activity after exposure to high pressure, relating to the molecular-level comparison of enzymes under high pressure analyzed in section 2.

Table 2-9. Comparison of untreated and treated enzyme activity under $scCO_2$ or high pressure in the free and immobilized state.

Enzyme	Reaction conditions (T/P/t/pH/Substrate/CO_2 flow)	Analyses	Reactor arrangements	$scCO_2$ treated enzyme activity	Ref.
		Cellulase enzyme			
Free cellulase (Cellusoft conc. L) from Novozymes [#]	40.0 °C, 10.0 MPa, 3.0 h, -, cellulose	DNS method for sugar; Bradford method for protein; FTIR for immobilization	120.0 mL batch reactor; No mixing	147.0 %	[280] *
Immobilized CLEA cellulase	40.0 °C, 10.0 MPa, 3.0 h, -, cellulose			143.0 %	[280]
Cellulase from *Trichoderma viride* [#]	50.0 °C, 12.0 MPa, 48.0 h, cotton cellulose	Glucose oxidase-peroxidase method for sugar	250 mL SS316 reactor vessel; magnetic bar mixing 100 rpm	120.0 %	[326] a
Commercial cellulase powder from *Trichoderma longibrachiatum* [#]	54.0 °C, 18.0 MPa, 2.0 h, Phosphate buffer pH 4.8, cellulose	DNS method for sugar; NMR; SEM	SFE 100, Thar Instruments, Inc., UK, 2006; dynamic mode (100 mL); No mixing	148.0 %	[283] b
NaY zeolite immobilized cellulase				156.0 %	[283] c
Crude cellulase from fungus *H. insolens* (Celluzyme 0.7T) [#]	35.0 °C, 10.0 MPa, 24.0 h, 4.8, cellulose	DNS method for sugar; Folin-Lowry assay for protein	500 rpm mixing; BSTR reactor detail NA;	101.7%	[115]
TMOS Immobilized cellulase from fungus *H. insolens* (Celluzyme 0.7T) [#]	35.0 °C, 10.0 MPa, 24.0 h, 4.8, phosphate-citrate buffer, cellulose,			461.0 %	[115]
		Other enzymes than cellulases			
Lysozyme from egg-white	40.0 °C, 15.0 MPa, 2.0 h, cell wall of *Micrococcus lysodeikticus*	Primary structure by MALDI-TOF-MS; 2° structure by CD spectra; 3° structure by fluorescence spectroscopy	Customized system; syringe pump; SS reactor with 28 mL volume	141.0 %	[311] d
Powdered α-amylase from *Aspergillus oryzea*	41.0 °C, 24.0 MPa, 4.0 g/min CO_2 flow, 2.5 h	DNS method for sugar; NMR; SEM	SFE 100, Thar Instruments, Inc., UK, 2006; dynamic mode (100.0 mL); No mixing	167.7 %	[298] e

Free lipase (from *Burkholderia cepacia*)	46.0 °C, 8.8 MPa, 3.5 ml/min CO_2 flow, 3.5 h	GC-MS, SEM, TGA,	NA	91.0-93.0 %	[300] f
PVA/CHI immobilized lipase (from *Burkholderia cepacia*)	46.0 °C, 8.8 MPa, 3.5 ml/min CO_2 flow, 3.5 h	GC-MS, SEM, TGA,	NA	98.2-98.7 %	[300] f

Enzyme is not available commercially – either discontinued or information not available.

* Cellulase in buffer solution was treated in $scCO_2$ in a batch reactor.

a The cotton fibers were hydrolyzed under $scCO_2$ condition for 48.0 h and increased productivity to 1.2 times.

b The $scCO_2$ treatment was done at a flow rate of 2.0-14.0 g/min, and 10.0 g/min was optimum.

c Repeated treatment of $scCO_2$ was done when the activity of reused enzyme reached below the untreated enzyme until the maximum activity decreased below the untreated enzyme activity.

d The depressurization rate was optimized at 3.0 MPa/min. Enzyme solution loaded in the reactor and pressurized with fluid CO_2, LPG

e 500 mg enzyme powder was placed in the sample cartridge of 100.0 mL reactor vessel SFE 100 system from Thar instrument, Inc. UK.

f The influence of $scCO_2$ incubation at different temperatures, pressure, and time were recorded and compared with untreated enzyme activity of free and polyvinyl alcohol-chitin (PVA/CHI) immobilized lipase. The product yield under $scCO_2$ by free and immobilized enzymes was 23.0 % and 94.0±1.5 %.

2.3.8. Conclusion and Future perspectives

Enzymes are biocatalysts and are sensitive to variation in reaction conditions such as temperature, pH, and substrate. Pressure is another factor that can affect an enzyme's performance significantly. Several studies have explored enzymatic reactions under high pressure created by high hydrostatic pressure or supercritical CO_2. Upon exposure to the pressurized pretreatment/reaction, enzymes have been shown to undergo molecular level changes (i.e., electrostriction, reduced bond length, hydrogen bonds), which leads to a change in the activation volume of the enzyme-substrate transition complex and, therefore, the activity. Notably, no consistent trend was observed in the correlation of molecular changes to enzyme activity for different enzymes from different sources.

Nevertheless, there is clear potential for altering enzymatic activity using high pressure. In addition, the immobilization of enzymes has been shown to have the potential to protect enzymes from harsh reaction conditions and has positive effects on enzymatic activity under pressure. For some enzymes, such as oxidase and peroxidase, the pressure-induced activation volume reduction causes enzyme activation, whereas lipases and cellulase have shown increased enzyme activities. CO_2 influences the performance of enzymes under $scCO_2$ in equilibrium with the aqueous medium by reducing the instantaneous pH and forming carbamate bonds. Though CO_2 reverts to gas and disappears from the reaction medium, it can catalyze changes in the enzyme's secondary structural composition and tertiary/quaternary structural arrangement and in water molecules present in the microenvironment of active sites. The immobilization of enzymes provides more stability and protects the enzyme at molecular levels from harsh reaction

conditions. After $scCO_2$ pretreatment, cellulases have mainly shown increased enzyme activity, enhancing up to 156.0 % compared to untreated cellulase at atmospheric reaction conditions. Various immobilization support materials have been synthesized from natural and synthetic materials. However, only a few have been studied under pressurized or $scCO_2$ systems with an immobilized enzyme. Silica-based sol-gel from tetra-methoxy-silane (TMOS) has shown strong stability for the cellulase enzyme under $scCO_2$ with more than 20 cycles of reuse with 461.0 % residual activity.

The majority of studies on enzymes under high pressure and $scCO_2$ conditions have focused on lipases, with some research conducted on cellulases. There is wide scope for further exploration of the effects of high pressure and $scCO_2$ on enzymes, as well as their substrates and reaction components, which can influence the performance of enzymes. To gain a broader understanding, it would be beneficial to consider the maximum achievable yield of both treated and untreated enzymes in both free and immobilized conditions. Additionally, investigating the impact of such systems on the nature of immobilization support materials (e.g., hydrophilic, hydrophobic, synthetic, or natural) with a consistent set of enzymes would aid in selecting appropriate support materials for use in high pressure and $scCO_2$ systems. The loss of lipase activity caused by water depletion from the hydration layer presents a significant challenge, which can be mitigated by immobilizing the enzyme onto a suitable support material. Future research could explore the possibility of restoring activity by rehydrating the enzymes in subsequent cycles.

Each enzyme has a unique molecular structure and active site that may be related, non-trivially, back to its amino acid sequence. Therefore, for a given enzyme, characterization of catalysis under high pressure or $scCO_2$ is required to determine the effects of high pressure and to allow for optimization of conditions. From this perspective, in order to understand the trends or patterns of enzyme activity as a function of high pressure in correlation to the corresponding molecular changes, it would be worth exploring different enzymes from different sources with a similar pressurized system to eliminate dissimilarities in instrumental configurations and operating conditions. Although – to the best of our knowledge – not yet been performed, in situ evaluation of the effects of $scCO_2$ upon enzymes by high pressure-NMR spectroscopy may also be fruitful given the long history of evaluating chemical catalysts in $scCO_2$ by NMR spectroscopy.

2.3.9. Declaration

The authors declare no competing financial interest

2.3.10. Acknowledgments

The research was financially supported by an NSERC-Strategic grant [506346-2017-STPGP] and Nova Scotia Innovation Hub awarded to Dr. Satinder Kaur Brar and Dr. Azadeh Kermanshahi-pour. Pawan Kumar acknowledges scholarship support from NSERC-CREATE-ASPIRE.

CHAPTER 3 NANOCRYSTALLINE CELLULOSE DERIVED FROM SPRUCE WOOD: INFLUENCE OF PROCESS PARAMETERS

This chapter has been published in Journal of Biological macromolecules:
Pawan Kumar, Kimberly Miller, Azadeh Kermanshahi-pour, Satinder Kaur Brar, Ramon Filipe Beims, and Chunbao Charles Xu. 2022. 'Nanocrystalline cellulose derived from spruce wood: Influence of process parameters', International Journal of Biological Macromolecules, 221: 426-34.

3.1. Abstract

Developing processes that rely on the use of less hazardous and toxic reagents for the production of cellulose nanocrystals (CNCs) are of significant interest. This study employed acetosolv pulping followed by alkaline peroxide bleaching, eliminating highly reactive chemicals such as Na-chlorites and Na-sulfite for microcrystalline cellulose (MCC) extraction from spruce wood. A yield of 41.53±0.68 wt.% of dry wood was obtained as bleached wood pulp with a crystallinity index of 85.0 %. MCC was hydrolyzed with 59-65 wt.% H_2SO_4 followed by ultrasonic treatment to produce CNC. Further optimization of ultrasonic treatment and acid hydrolysis resulted in CNCs with high aspect ratios (length/width) up to 48.0 and yields from 8.03±3.17 wt.% to 25.06±0.74 wt.% of the original wood biomass. Mechanical treatment of the acid hydrolyzed suspensions, aimed at improving CNC dispersion and particle morphology, showed no effect on crystallinity index based on the statistical analysis. The extracted CNC showed high crystallinity index of 80.8±1.7 %, aspect ratio up to 48, low residual hemicellulose (<2.0 %) and lignin (<0.66 %) content, and high-char content of 26.7 wt.% from thermal degradation.

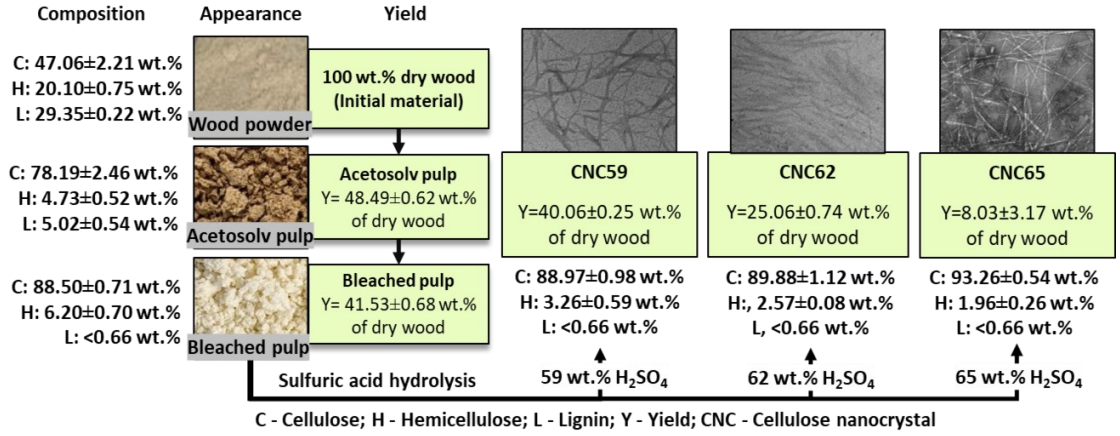

3.2. Keywords: Nanocellulose, Nanocrystals, Acetosolv pulping, Alkaline peroxide bleaching, Acid hydrolysis, Lignocellulosic biomass.

3.3. Highlights

- S and Cl free pulping and bleaching processes were used for cellulose extraction.
- Pure cellulose nanocrystals from spruce were obtained in high yield.
- High aspect ratio of up to 48 and crystallinity index of 80.8±1.7 % were achieved.
- Ultrasonic treatment showed no negative impact on the crystallinity index of CNCs.

3.4. Introduction

Nanocrystalline cellulose (NCCs), also known as cellulose nanocrystals (CNCs), consist of whisker-shaped or rod-like nanoparticles with high surface areas and particle sizes varying from 2.0-20.0 nm diameter and 100.0-500.0 nm length. CNCs can be extracted from lignocellulosic (LC) and bacterial biomass by hydrolyzing the β-1,4-glycosidic bond present at amorphous regions of cellulose [122]. CNCs are an important additive of reinforced and composite materials with biodegradability, biological compatibility, and a potential candidate for remediation of wastewater [369-372]. The hydroxyl groups form inter- and intramolecular hydrogen bonds within cellulose chains that maintain a significant, cohesive force to hold

nanocellulose chains together. It makes the composite or reinforced materials mechanically stronger, thermally stable, lightweight, and enhances biodegradability [373-374]. Increased surface area and aspect ratio (length/diameter) of CNCs allow further functionalization of nanocellulose for adsorption of hazardous pollutants in water [371, 375].

Currently, commercial MCC production processes involve highly reactive chemical treatments such as pulping and bleaching of wood with chlorite and sulfite (i.e., NaOCl, Na_2SO_4), which results in high purity and white-colored MCC [97-100]. In recent studies, there have been some development less intensive treatment of lignocellulosic biomass using organic solvent in the presence of acid catalysts. Extraction of CNCs is dominantly carried out by acid hydrolysis of MCC pulp using 58.0–64.0 wt.% sulfuric acid at 35.0–65.0 °C under atmospheric pressure [68, 376-379]. This process results in hydrolysis of the amorphous substructure, and the crystalline cellulose remains intact primarily in the form of micro-clumps of hundreds and thousands of CNC particles with sulphate groups grafted over the surface. Therefore, mechanical treatment such as ultrasonic treatment, high-pressure homogenization, microfluidization is required following the sulfuric acid hydrolysis to individualize the small chains in the form of needle-like nanocrystals [57, 380-381].

Production of high-quality MCC and CNCs extraction requires a better understanding of the influential process parameters on yield and properties of the final product. The yield of MCC and CNC and their properties (i.e., chemical purity, degree of polymerization, crystallinity index, thermal properties) could vary with the

type of biomass species and extraction process conditions [70]. Pinewood pulp hydrolyzed in sulfuric acid (62.0 wt.%, 44.0 °C, 1.5 h) led to CNC yield of 2.3 wt.% of the pulp with 67.8 % crystallinity [57]. In contrast, hydrolysis of bleached eucalyptus Kraft pulp in sulfuric acid hydrolysis (58.0 wt.%, 56.0 °C, 3 h min) resulted in 68.0 wt.% CNC yield with 76.2 % crystallinity [54].

The mechanical treatment is applied at different intensities or pressures (i.e., ultrasonic probe treatment, high-pressure homogenization, micro fluidization) to disintegrate the individual nanocellulose crystals [57, 380-381]. In particular ultrasonic dispersion of CNC, varying range of intensity has been used, such as amplitudes of 25.0–85.0 % for a few minutes to as long as 30 min in multiple studies [30, 152, 380, 382-383].

To the best of our knowledge, the collective effect of sulfuric acid concentration, the intensity of the mechanical treatment on CNC yield, and its properties (i.e., crystallinity index, particle morphology) is not well explored. Additionally, obtaining CNC with high yields and desirable properties (i.e., high surface area, high crystallinity) under mild process conditions is challenging in the current practices. In this study, acetic acid pulping and alkaline peroxide bleaching were used to extract MCC from Spruce wood to reduce the environmental footprint of the pulping and bleaching processes. Further, MCC was hydrolyzed using sulfuric acid followed by mechanical treatment to extract CNC. The lignin was also recovered and characterized for molecular size and purity. Our goal was to develop an understanding of the effect of sulfuric acid and ultrasonic treatment on yield, morphological properties, thermal stability, and crystallinity of CNC-derived spruce.

3.5. Materials and Methods

3.5.1. Materials

Spruce wood chips were grinded using a coffee grinder (Hamilton Beach, Canada) to a particle size range of 63.0–180.0 μm, sieved with stacked ASTM mesh screens #80/230 and used as starting material. Analytical grade glacial acetic acid, hydrogen peroxide 30.0 wt.%, hydrochloric acid 37.0 wt.% were purchased from VWR chemicals BDH (Canada), and sodium hydroxide pellets, calcium hydroxide powder, and toluene were purchased from Sigma-Aldrich (Canada), The sulfuric acid 95.0-98.0 wt.% used in the experiments was purchased from EMD (USA).

3.5.2. Moisture, ash, and extractive content analysis

The moisture content of the wood powder was determined by drying at 105.0 °C in an oven (Across International) under active vacuum (~-30.0 in Hg) for four hours or until the weight stabilized (no change >0.1 mg). Ash content was determined by ashing the moisture-free wood powder in the muffle furnace at 575.0±25.0 °C for 24.0±2.0 h.

The lipids extractives of the wood powder were removed by Soxhlet extraction with water and then a toluene-ethanol (2:1, v/v) mixture. Each extraction was carried out over six hours with six reflux cycles per hour. The extractive content was measured as the mass recovered in the solvents during Soxhlet extraction and reported as the wt.% of the dried wood used.

3.5.3. Cellulose extraction from wood

Cellulose pulp was isolated from extractive and moisture-free wood powder using acetosolv pulping followed by an alkaline hydrogen peroxide bleaching reaction, as described in Ditzel et al. (2017) [57]. The wood powder was heated isothermally

for 3.0 h with 92.9 wt.% acetic acid in the presence of a hydrochloric acid catalyst (0.3 wt.%) at 115.0±2.0 °C using 10.0 mL/g of solid. The reaction was carried out in a flat bottom boiling flask under a reflux setup with 400-450 rpm magnetic stirring. Acetosolv pulp was filtered using 11.0 µm filter paper and washed with 92.5 wt.% acetic acid and water until pH of ~7.0 was reached. Acetosolv filtrates were collected for lignin recovery, and the pulp was dried at 55.0 °C under active vacuum for 24.0 h.

The dried acetosolv pulp was then treated with 4.0 wt.% sodium hydroxide and 13.5 wt.% hydrogen peroxide in a solid-liquid ratio of 1:40 (g/mL) by suspending 1.0 g of solid in 20.0 mL of sodium hydroxide solution and adding 20.0 mL of hydrogen peroxide solution, dropwise. Following the addition of hydrogen peroxide, the slurry was held isothermally, with stirring (350.0-400.0 rpm), for 2.0 h at 50.0±2.0 °C. The bleached pulp was filtered and washed with water until a pH 7.0 was reached. The pulp was dried in oven at 55.0 °C under active vacuum for 24.0 h.

3.5.4. Lignin recovery

The lignin was recovered from acetosolv filtrate by adapting the method described by Nascimento et al. (2014). The filtrate black liquor collected from acetosolv pulping was concentrated to one-tenth volume by removing acetic acid using rotary evaporator. The concentrated black liquor was quenched with 10-fold distilled water and treated at 75.0±5.0 °C with magnetic stirring of 300.0-350.0 rpm for 0.5 h. A further 10-fold volume of water was added at room temperature to the solution before holding stagnant for 24.0 h for the lignin to precipitate and settle. Precipitated lignin was filtered and washed with distilled water until a pH of ~7.0

before drying at 55.0 °C for 24.0 h under an active vacuum. The obtained lignin was characterized by infrared spectroscopy (IR) and gel permeation chromatography (GPC).

3.5.5. Acid hydrolysis

The oven-dried bleached pulp was used in sulfuric acid hydrolysis reactions in three different concentrations 59.0 wt.%, 62.0 wt.%, and 65.0 wt.% in pulp to acid ratio of 1:10 (g/g) for 1.5 h isothermally at 44.0 °C with continuous magnetic stirring at 600.0-650.0 rpm. The reaction was quenched by adding a 5-fold volume of cold distilled water, and the hydrolyzed pulp solid was separated by centrifugation at 9500.0 rpm or 13,117.0 g-force (Eppendorf 5804/FA-45-6-30 rotor) for 5.0 min. The initial supernatant was collected as acid hydrolysate to analyze the released sugar for mass balance. The remaining solids were washed (2-3 cycles) with distilled water until the supernatant started to become turbid. The washed pulp was dialyzed using a semi-permeable membrane (cutoff weight 14.0 kDa) for 2-4 days until a pH of 7.0.

3.5.6. Mechanical treatment

The dialyzed pulp suspensions were diluted to 1.0 wt.% in water prior to mechanical treatments. Firstly, three methods of mechanical treatment were applied on 62.0 wt.% sulfuric acid hydrolyzed pulp treated sample, magnetic stirring (1000.0 rpm, 15.0 min), sonication bath (Branson m1800, 15.0 min), or an ultrasonic probe (Sonics ultrasonic processor, VCX750, 13.0 mm probe diameter, 80.0 % amplitude for 5.0 min). Then ultrasonic probe treatment was further investigated for optimization of the amplitude (30.0-80.0 %) and treatment time (5.0-15.0 min) for the acid hydrolyzed pulp at 62.0 wt.% sulfuric acid concentration.

The ultrasonic probe treatment was performed using an ice bath to dissipate the generated heat and maintain the ambient temperature. The crystallinity index was considered the response factor and was statistically analyzed with three center points.

3.5.7. Freeze drying

The aqueous suspensions obtained after ultrasonic treatment were dried for 72.0 h by a freeze dryer (FreeZone 2.5 L, Labconco) at -50.0 °C. Prior to freeze-drying, the suspension was frozen in a 20.0 mL vial using liquid nitrogen.

3.5.8. Solid characterization

3.5.8.1. Yield and chemical composition analysis

The yield of the bleached wood pulp and CNC were calculated based on the weight of dry wood used as starting material. For the chemical composition analysis, 300.0 mg of the wood produced pulp, and nanocellulose samples were individually hydrolyzed in a two-step acid hydrolysis. The resulting hydrolysates were analyzed using the NREL method for cellulose, hemicellulose, and lignin content [384]. Samples (300.0 mg) were first treated in 3.0 mL of 72.0 wt.% sulfuric acid at 30.0±2.0 °C for 1.0 h using a 120.0 mL pressure tube (Ace Glass) with a water bath. Following treatment, the acid concentration was diluted to 4 wt.% in a pressure tube, then closed and hydrolyzed in an autoclave at 121.0 °C, 15.0 psi for 1.0 h. The acid hydrolysate was filtered over a glass filter and analyzed by the HPLC-RID method (described in supporting information) after neutralizing to pH 5.0-6.0 using calcium hydroxide. The solids on the filter were dried under an active vacuum at 55.0 °C for 24.0 h before measuring the acid-insoluble lignin content.

3.5.8.2. Particle morphology analysis

The morphology of produced CNCs were analyzed using a scanning electron microscope (FE-SEM, Mira3 LMU, Tescan, Czech Republic), and using a transmission electron microscope (JEOL 1230 TEM) at 80.0 kV accelerating voltage. The particle's length and diameter were measured for 100 particles using digital image analyzing software (ImageJ) and the data plotted in Origin software for particle size distribution analysis.

3.5.8.3. Infrared (IR) spectroscopy analysis

The dried pulps and CNCs were analyzed as solids on the Smart iTX accessory with high-efficiency optic reflectors and diamond ATR crystal attenuator in the wavenumber range of 400.0 cm^{-1} to 4000.0 cm^{-1} at a 0.4 cm^{-1} resolution using by solid-state infrared spectroscopy using a Thermo Scientific Nicolet iS10 FTIR Spectrometer with a helium-neon laser.

3.5.8.4. Thermal stability

The thermal stabilities of the samples were analyzed using a Mettler Toledo TGA/DSC^{3+}-thermogravimetric analyzer (Mettler Toledo, Canada) by heating from 30.0 to 575.0 °C at a rate of 10.0 °C/min under nitrogen gas flow rate of 50.0 mL/min. Samples (5.0-10.0 mg) were weighed directly into a hermetic aluminum pan with a pinhole for analysis.

3.5.8.5. Crystallinity index

The X-ray diffraction spectra were collected using Bruker D8 Advance equipped with an LYNEYE detector in reflection mode. X-ray diffractograms were collected at the scan rate of 3 step/sec in a 2Θ range of 4-45° (wavelength = 1.54 Å) using

an X-ray tube setting of 40.0 kV and 15.0 mA. The crystallinity indices of samples were determined using Equation (11) as defined by Segal et al. (1959) [153]:

$$CrI\ (\%) = \frac{I_{200} - I_{am}}{I_{200}} \times 100 \quad (11)$$

Where I_{200} represents the peak intensity of crystalline phase containing crystalline and amorphous domains maximum intensity at 2Θ of 22-23° and I_{am} represents the peak intensity for the amorphous domain maximum intensity at 2Θ of ~18.5°.

3.5.8.6. Statistical analysis

The ultrasonic treatment for optimizing amplitude and time with respect to crystallinity index was performed using the center-point method considering the significance level of 95.0 % ($p < 0.05$).

3.6. Results and discussion

3.6.1. Chemical composition and yield

The chemical composition analysis of wood showed that total polysaccharide content was 67.17 wt.%. It was composed of 47.01 wt.% cellulose, 20.10 wt.% hemicellulose, and 29.35 wt.% lignin (Table 3-1).

Table 3-1. Chemical composition of spruce wood as starting material g/100 g original wood (starting material) (n=3).

Cellulose	Hemicellulose	Lignin	extractives	Ash	Moisture
47.06±2.21	20.10±0.75	29.35±0.22	3.90±0.28	0.20 ± 0.02	4.32±0.45

The acetosolv pulping reaction of the extractive and moisture-free wood sample resulted in a 48.49±0.62 wt.% yield compared to the original sample mass of dry wood. Most of the lignin and hemicellulose (91.7 % and 88.6 % of the initial content) were removed from the produced acetosolv pulp. Some of the solubilized lignin was deposited on the surface of the pulp. Therefore, the appearance was

dark brown, as shown in (Figure 3-1). The lignin in the acetosolv filtrate was recovered by precipitation in water at 75.0±5.0 °C, and the yield of the recovered lignin was 90.77 wt.% of the original lignin content in the wood sample with a purity of 83.15±2.14 % (analyzed by acid hydrolysis as described in the supplementary information (SI section 11)). The alkaline hydrogen peroxide bleaching treatment oxidized the residual lignin from the pulp. It resulted in a yield of 85.65±1.54 wt.% of used acetosolv pulp, representing 41.53±0.58 wt.% of the dry wood as the overall yield of microcrystalline cellulose pulp. The alkaline peroxide bleaching process oxidized the residual lignin from the pulp. The yield of overall bleached pulp is significantly improved compared to the 33.0 wt.% in [57] and 11.0 wt.% in [53] using a similar method but different biomass.

The nanocrystalline cellulose produced by acid hydrolysis at three sulfuric acid concentrations (59.0 wt.%, 62.0 wt.%, and 65.0 wt.%), followed by the ultrasonic treatment, were designated as CNC59, CNC62, and CNC65. The key effects of increasing the acid concentration were a significant reduction in yield, improved cellulose purity up to 93.25±0.54 wt.%, and an increased aspect ratio of CNC. The yield decreased from 40.06±0.25 wt.% to 25.06±0.74 wt.% and 8.03±3.17 wt.% of dry wood when the acid concentration was increased from 59.0 wt.% to 62.0 wt.% or 65.0 wt.%. The hemicellulose content in the CNCs decreased from 3.26±0.59 wt.% to 2.57±0.08 wt.% and 1.96±0.26 wt.% of the pulp. The CNC yield from 62.0 wt.% and 65.0 wt.% treated samples are significantly higher than 2.3 wt.% extracted from pinewood pulp (62.0 wt.% H_2SO_4, 44.0 °C, 1.5 h) as reported in Ditzel et al. work [57].

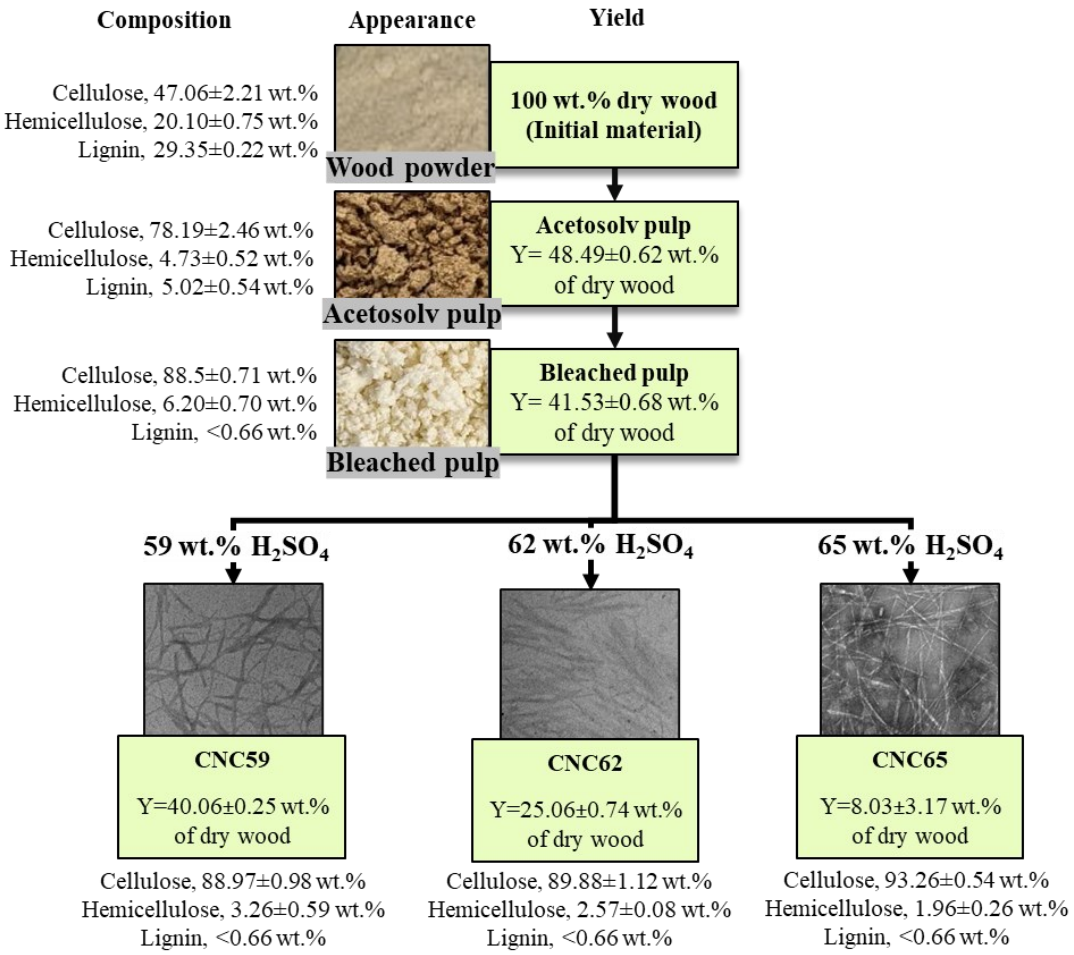

Figure 3-1. The appearance of the pulp and CNC samples, experimental yields, and the corresponding chemical composition of cellulose, hemicellulose, and lignin, where Y is yield and CNC is cellulose nanocrystals.

3.6.2. Solid characterization

3.6.2.1. Mechanical treatment for nanocellulose crystals dispersion

Acid hydrolyzed pulp (at 62.0 wt.%) was subjected to mechanical treatments of magnetic stirring (1000.0 rpm, 15.0 min), water bath sonication (15.0 min), and ultrasonic probe treatment (80.0 % amplitude, 5.0 min), intensity varying from very mild to very intense treatments. The particle morphology of the samples was analyzed using FE-SEM. Magnetic stirring had the least impact on the dispersion of the CNC particles, with most particles appearing as microparticles. The water

bath sonicator resulted in a mixture of nanoparticles and microparticles. In contrast, treatment with the ultrasonic probe treatment resulted in a dispersion of nanocellulose with no micron-sized particles observable by SEM (Figure 3-2). The ultrasonic probe treatment was found as an effective mechanical treatment to disperse the individual CNC, but it harmed CNC structure when used for more than 5 min (Figure S7-3). Amiralian et al. (2017) used an ultrasonic probe with an amplitude of 25.0 % and 500.0 W output energy for 20.0 min to disperse the CNC after acid hydrolysis (40.0 wt.% sulfuric acid, 45.0 °C, 3.0 h) of the bleached pulp, which produced a high aspect ratio of 144.0 and CrI of 76.0 % from spinifex grass [385]. Zhao et al. (2019) used high-pressure grinding at 1500.0 rpm in a Super Mass Collider for CNC preparation from rice straw and poplar, producing CNC with an aspect ratio of 16.0 and 13.4 and a CrI of 68.0 % and 72.9 %, respectively [386]. Mohd Ishak et al. (2020) used ultrasonic treatment at 60.0-90.0 % amplitude for 5.0-20.0 min for CNC preparation following the ionic liquid (BmimCl) hydrolysis of MCC, producing CNC with aspect a ratio of 9.0-17.0 with CrI of up to 73.0 % [382] The dispersion of particles and their morphology strongly relies on the extent of hydrolysis and the penetration of sulfuric acid molecules inside the cellulose chains [385].

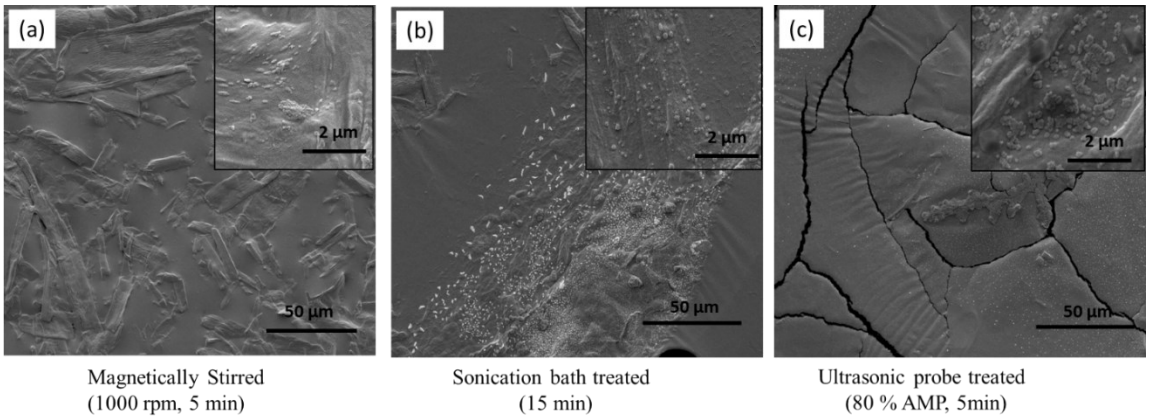

Figure 3-2. SEM images of (a) magnetic stirred at 1000.0 rpm for 5.0 min, (b) water bath sonicated for 15.0 min, and (c) ultrasonic probe treatment at 80.0 % amplitude for 5.0 min

Ultrasonic probe treatment was optimized for the amplitude and duration of the treatment and analyzed for particle morphology by TEM and crystallinity index of freeze-dried CNC. TEM analysis showed that the sample treated for 5.0 min at 30.0 % and 80.0 % amplitudes had a needle-like morphology, whereas the sample treated for more than 5.0 mins had destroyed the CNC morphology (Figure S7-3 and Figure S7-3). Much less dispersion of CNC was observed when 30.0 % amplitude was used, whereas a setting of 80.0 % amplitude for 5.0 min resulted in a homogeneous dispersion of CNC (Figure 3-3). Further, the acid hydrolyzed suspensions produced by acid hydrolysis at 59.0 wt.%, 62.0 wt.%, and 65.0 wt.% were treated with the ultrasonic probe at 30.0 % and 80.0 % for 5.0 min. The average size of 100 particles analyzed from the TEM image of each sample is listed in Table 3-2, and typical distribution plots are presented in Figure 3-3 and Table 3-2 show that the high concentration of 65.0 wt.% sulfuric acid has better penetration into MCC chains. Therefore, it had better dispersion of CNC and fine diameter of 4.95±1.1 nm, and a high aspect ratio of 48.0. However, more of the MCC was hydrolyzed with increased acid concentration. The extracted

nanocrystals were well dispersed by ultrasonic treatment at 30.0 % and 80.0 % of amplitudes in 5.0. min, possibly due to the charged surfaces impacted by the sulfate groups. In comparison, the 59.0 wt.% sulfuric acid-treated sample had a high yield (97.0 wt.% of bleached pulp) due to little penetration into the cellulose chains and insignificant hydrolysis. This result was confirmed with electron microscopic analysis (Figure S7-3).

Table 3-2. Particle size analysis CNCs produced by acid hydrolysis (59 wt.%, 62 wt.%, and 65 wt.% sulfuric acid concentrations) followed by ultrasonic treatment at 30 % and 80 % amplitudes for 5 mins (Average ± std. dev. of 100 particles)

Amplitude		**Sulfuric acid concentration (wt.%)**		
		59.0 %	**62.0 %**	**65.0 %**
30 %	Particle length (nm)	306.7±113	218.6±80.5	181.17±62.90
	Particle diameter (nm)	16.34±3.8	8.68±1.7	10.44±1.8
	Aspect ratio	18.77	25.18	17.35
80 %	Particle length (nm)	306.7±99.6	225.4±64.5	237.7±90.6
	Particle diameter (nm)	16.9±5.21	19.6±4.9	4.95±1.1
	Aspect ratio	18.14	11.48	48.06

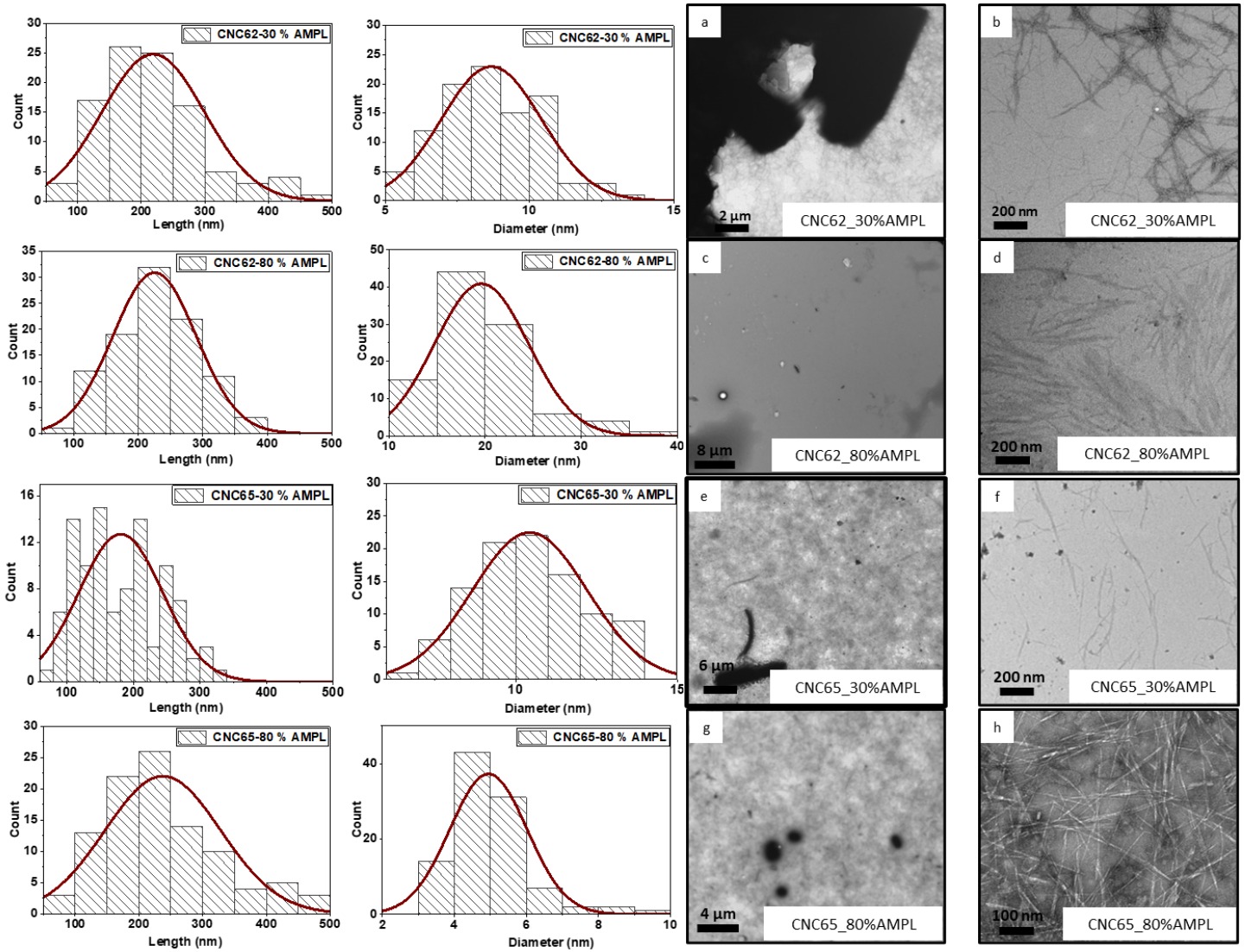

Figure 3-3. TEM Images of CNCs produced from acid hydrolyzed samples using 62.0 wt.% and 65.0 wt.% sulfuric acid followed by ultrasonic treatment where samples were treated with (a-b) 30.0 % amplitude, CNC62; (c-d) 80.0 % amplitude, CNC62; (e-f) 30.0 % amplitude, CNC65; and (g-h) at 80.0 % amplitude, CNC65

3.6.2.2. Infrared spectroscopic analysis

The presence of different functional groups was identified using IR absorption spectroscopy. The absorption bands of characteristic bonds and their functional groups have been interpreted based on the information available in the literature and briefly listed in Table S7-8.

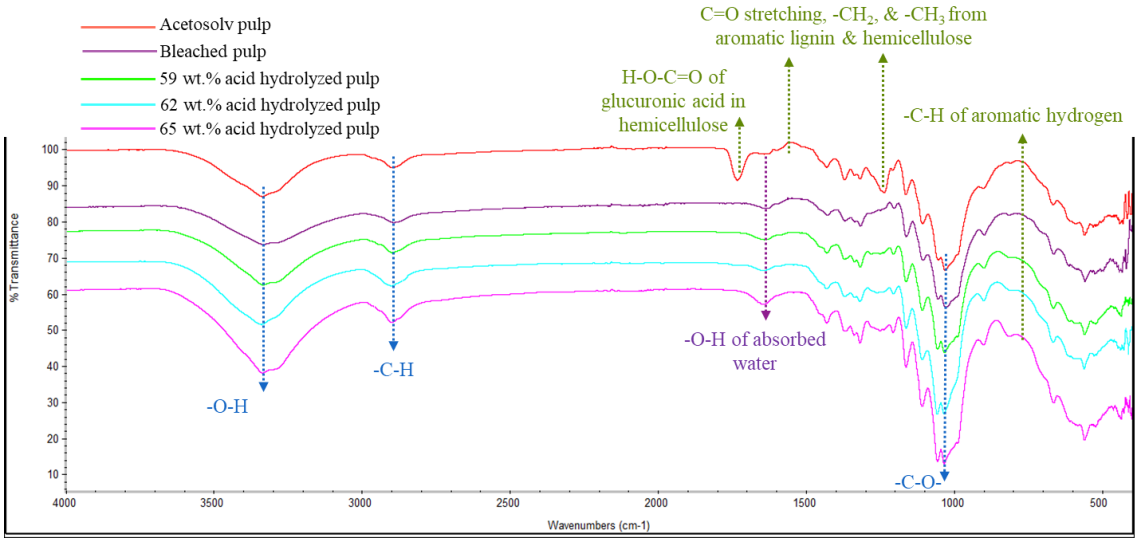

Figure 3-4. Comparison of solid-state IR spectra of wood pulp and CNCs from different chemical treatments.

During chemical treatment, acetosolv pulping removed most of the lignin and hemicellulose, and the residual lignin was removed during the bleaching process. These chemical changes can be observed in Figure 3-4 at 1457.0-1593.0. cm^{-1}, which corresponds to the C=C stretching vibration of lignin and hemicellulose, with the characteristic absorption band at 700.0-900.0 cm^{-1} for the aromatic $–CH_2$ as the chemical environment was significantly changed during bleaching. Increased intensities of bands corresponding to the hydrogen bonding environment of the O-H group (3330.0 cm^{-1}), the anti-symmetric C–H stretch (2890.0 cm^{-1}), and C–O–C stretch of the pyranose ring (1050.0 cm^{-1}) were observed in CNC samples as compared to acetosolv and bleached pulps [160, 387-388]. The reduced transmittance

between 800.0-900.0 cm^{-1} was more visible in CNC samples, specifically in CNC65, than bleached pulp due to the presence of S–OH among CNCs. The absorption band intensity for fiber absorbed water at 1640.0 cm^{-1} was significantly increased for the CNC samples due to the high hydrophilicity [155, 389]. A characteristic solid band at 1732.0 cm^{-1} in acetosolv was observed and correlated to the acetyl and ester groups of the hemicellulose or aromatic acid of the lignin. The presence of –C=O stretching, $–CH_2$, and $–CH_3$ aromatic deformations were observed with the lignin in the region of 1457.0–1593.0 cm^{-1} and mainly observed in acetosolv and bleached pulp samples [390].

3.6.2.3. Crystallinity index (CrI) analysis

The crystallinity index of the processed samples was determined by calculating the peak intensity height ratio using the method of Segal et al. (1959) [153]. The CrI of wood samples was determined to be 67.4±0.6 %, and the crystallinity of samples was increased to 85.1±1.2 % for bleached pulp as the non-cellulosic component was removed from the wood during the pulping and bleaching processes.

Some studies have indicated that ultrasonic treatment intensities reduce the CrI of the cellulose [158, 382]. The ultrasonic treatment was optimized to disperse the CNC by maintaining the crystalline structure, whisker-like morphology, and high aspect ratio while reducing energy spent over the ultrasonic shearing process. The results showed that the optimization model had a high p-value (0.19), showing the insignificant impact of ultrasonic treatment on CrI (Table S7-5). However, the whisker shape of the nanocrystals was destroyed at treatment times more than 5.0 min by the ultrasonic probe (Figure S7-4). The CrI of CNC decreased compared to the bleached pulp, possibly due to the freeze-drying and presence of moisture in

CNC samples (Figure 3-5). Pen et al. (2013) have observed reduced crystallinity of freeze-dried samples compared to spray dried due to the heat treatment during the spray drying that occurs at 50.0-100.0 °C [391].

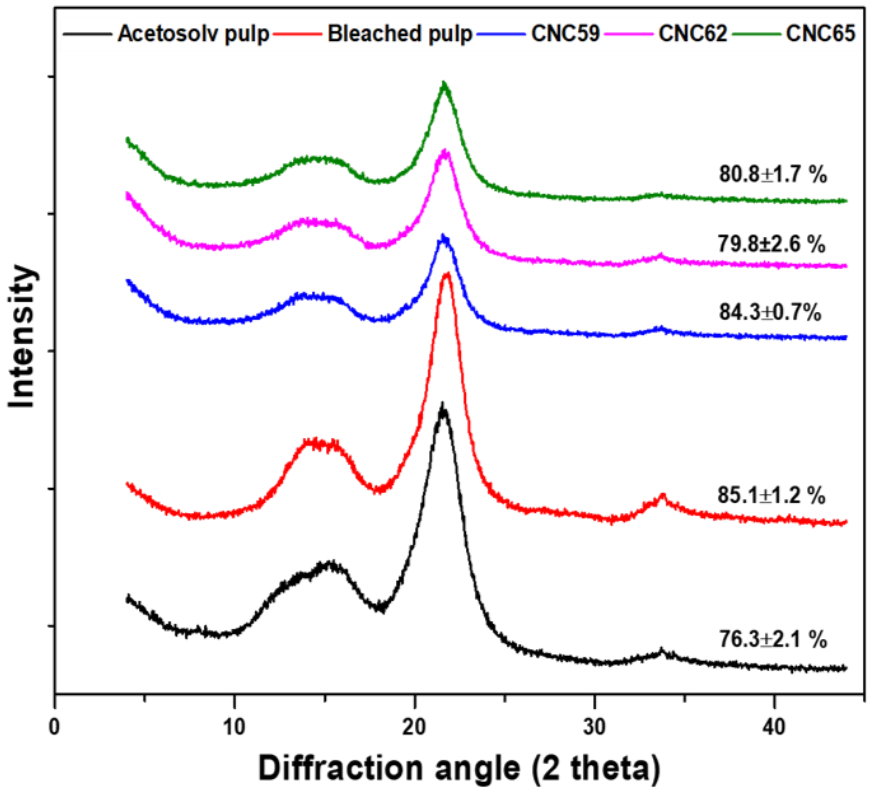

Figure 3-5. Diffraction patterns of acetosolv pulp, bleached pulps, and CNCs.

3.6.2.4. Thermal degradation analysis

The thermal degradation analysis was performed on the acetosolv pulp, bleached pulp, and CNC samples. Before performing thermal degradation analysis, the acetosolv pulp and bleached pulp samples were oven-dried at 55.0 °C for 24.0 h, and the CNC samples were freeze-dried over 2 days. The thermal degradation of the samples revealed a moisture content of 4.5-8.0 wt.%, indicating hydrophilicity of the nanocellulose due to the high surface area with hydroxyl and sulfate groups on the surface. The mass yield of the char produced at 575.0 °C was low for acetosolv pulp (11.8 wt.%) and bleached pulp (18.0 wt.%) and high for CNC59

(22.9 wt.%), and 26.3 wt.% and 26.7 wt.% for CNC62 and CNC65 due to increasing crystalline content. As shown in Figure 3-6, single-step degradation of acetosolv and bleached pulps was observed. In contrast, the thermal degradation of CNCs occurred over two steps due to the sulfate group grafted onto the surface during acid hydrolysis. Similar behavior was observed for bleached pulp and CNC samples reported in previous studies [392-393].

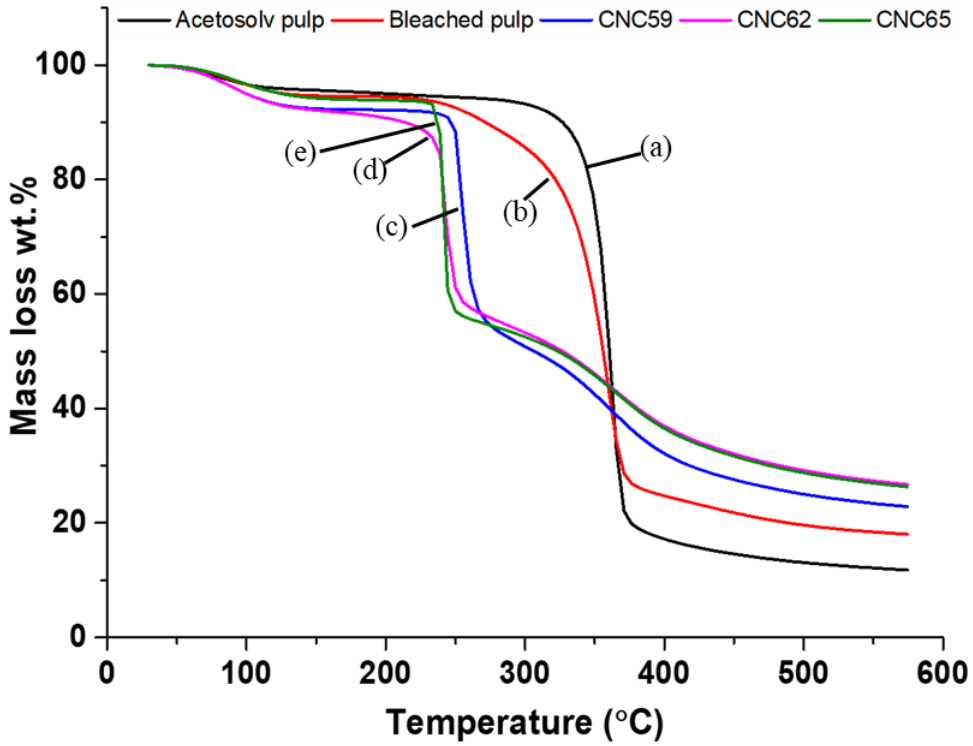

Figure 3-6. Thermal degradation profile of (a) acetosolv pulp, (b) bleached pulp, (c) CNC59, (d) CNC62, and (e) CNC65.

The degradation of CNCs occurred over two steps with a corresponding mass loss of 50.0-55.0 wt.%. The first mass loss occurred between 240.0-280.0 °C with a mass loss of 38-42 wt.%, and the second mass loss of 22.0-28.0 wt.% occurred at 280.0-575.0 °C during pyrolysis. The remaining 22.9-26.7 wt.% was leftover as char. The thermal stability of the nanocellulose could be further improved by

neutralizing the residual sulfate groups [394]. These sulfate groups increase the electrostatic repulsion force among the nanocellulose chains and disperse them in suspension solution. However, it harms the thermostability of the nanocellulose as the sulfates catalyze the thermal degradation reactions at high temperatures. However, this degradation could be minimized by neutralizing sulfate groups on NCC [394-395].

3.7. Conclusions

Spruce wood has a high cellulose content and could be used during high yield nanocrystalline cellulose production. The study resulted in a significantly high yield of 25.06±0.74 wt.% of dry wood using 62.0 % acid concentration. Further increasing concentration helped in improving the dispersion of CNC with a high aspect ratio of 48.0 at the expense of low yield of 8.03±3.17 wt.% of dry wood. Mechanical treatment of the acid hydrolyzed suspensions, aimed at improving dispersion and particle morphology, did not affect the crystallinity index based on the statistical analysis. The ultrasonic treatment with 80.0 % amplitude for 5.0 minutes provided sufficient nanocrystals dispersion. Using 65.0 wt.% sulfuric acid produced an aspect ratio of 48.0 with minimal impurity. It could be a potential candidate for functionalization in applications such as heavy metal remediation.

In contrast, applications such as the formulation of composite materials could benefit from the higher yield production of CNCs observed with 62.0 wt.% sulfuric acid. The selection of acid hydrolysis reaction conditions, mechanical treatment parameters, and therefore the yield would depend on the end-use of the produced CNC. The overall process replaced reactive chemicals by utilizing organosolv

pulping and chlorine-free bleaching processes. As a conventional method, the outcome of this study showed the influence of process parameters to improve the desired characteristics of CNC with a high yield. Still, it is strongly recommended to develop an alternative method of acid hydrolysis to further the overall goal of developing an environmentally friendly process with reduced wastewater effluents

3.8. Acknowledgment

Solid State Pharma Inc. Halifax, NS is acknowledged for technical support and providing access to the equipment and the internship opportunity. The author P.K. acknowledges Natural Sciences and Engineering Research Council of Canada (NSERC)-Strategic and NSERC Aspire-Create, and R.F.B acknowledges the Coordination for the Improvement of Higher Education Personnel (CAPES) (Process Number 88881.174355/2018-01) for providing the scholarships for their Ph.D. program. NSERC-Discovery is acknowledged for their support.

CHAPTER 4 ENZYMATIC DIGESTIBILITY OF LIGNOCELLULOSIC WOOD BIOMASS: EFFECT OF ENZYME TREATMENT IN SUPERCRITICAL CARBON DIOXIDE AND BIOMASS PRETREATMENT

The chapter is considered for the peer reviewed journal publication.

4.1. Abstract

Energy and resource intensive mechanical and chemical pretreatment along with the use of hazardous chemicals are major bottlenecks in widespread lignocellulosic biomass utilization. Herein, the study investigated different pretreatment methods on spruce wood namely supercritical CO_2 ($scCO_2$) pretreatment, ultrasound-assisted alkaline pretreatment, and acetosolv pulping-alkaline hydrogen peroxide bleaching, to enhance the enzymatic digestibility of wood using optimized enzyme cocktail. Also, the effect of $scCO_2$ pretreatment on enzyme cocktail was investigated after optimizing the concentration and temperature of cellulolytic enzymes. The impact of $scCO_2$ and ultrasound-assisted alkaline pretreatments of wood were insignificant for the enzymatic digestibility, and acetosolv pulping-alkaline hydrogen peroxide bleaching was the most effective pretreatment that showed the release of total reducing sugar yield (TRS) of ~95.0 wt.% of total hydrolyzable sugars (THS) in enzymatic hydrolysis. The optimized enzyme cocktail showed higher yield than individual enzymes with degree of synergism 1.34 among the enzymes, and $scCO_2$ pretreatment of cocktail for 0.5-1.0 h at 10.0-22.0 MPa and 38.0-54.0 °C had insignificant effect on the enzyme's primary and global secondary structure of cocktail and its activity.

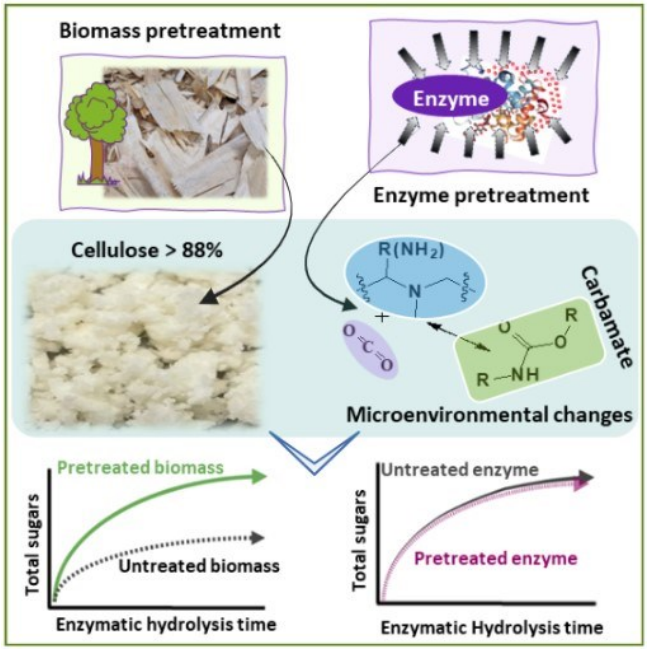

4.2. Keywords

Lignocellulosic biomass, biomass pretreatment, enzyme pretreatment, supercritical CO_2, cellulase, enzymatic hydrolysis, fermentable sugars.

4.3. Highlights

- Wood and enzyme pretreatment performed separately prior to enzymatic hydrolysis
- $scCO_2$ and alkali assisted-ultrasonic methods were ineffective for wood pretreatment
- Short exposure (0.5-1.0 h) of enzyme to $scCO_2$ does not affect the enzyme activity
- Sugar yield of ~95.0 wt.% was achieved in enzymatic hydrolysis by acetosolv pulping

4.4. Introduction

Lignocellulosic (LC) biomass is one of the most abundant sources for the production of commodity and value-added chemicals. However, the polymeric network of cellulose, hemicellulose and lignin is complex and resistant to conversion to monomeric components [94, 396]. Biomass must go through different pretreatment processes to disrupt the recalcitrant structure to enhance the saccharification of polysaccharides (cellulose & hemicellulose) to reducing sugars (cellobiose, glucose from cellulose, xylose, mannose, arabinose from hemicellulose) by enzymatic hydrolysis. Agricultural biomass has been studied more extensively compared to woody biomass. Conventional pretreatment including Kraft or sulfite pulping and chlorinated bleaching methods are effective in enhancing the enzymatic digestibility of biomass [397-400]. A performance evaluation based study showed that the combination of methods such as alkali-peroxide, mechanical and enzymatic treatment, is less energy intensive and generate lower amount of waste compared to conventional biomass pretreatment methods such as chemical soaking and thermochemical treatments [77, 401-402]. Although the use of chemicals is not eliminated in these methods, the amount of hazardous chemicals and therefore the environmental impact associated with hazardous waste management are reduced. Therefore, it is very worthwhile to explore such non-conventional method on wood biomass. Among the variety of such pretreatment methods available, ultrasound, organosolv, and supercritical CO_2 ($scCO_2$) pretreatment are emerging as physicochemical pretreatment methods with the advantage of reduced wastewater generation and potential for solvent recyclability [116-119]. Organosolv pulping using organic solvents and acids

such as ethanol, formic acid, and acetic acid in the presence of mineral acids (i.e., sulfuric acid, hydrochloric acid) to catalyze the breaking of the ether bonds of lignin and initiate solubilization. The process loosens the biomass structure exposing the polysaccharides [158, 403-404]. Ultrasound pretreatment in an alkaline aqueous medium produces hydroxyl radicals and results in high temperature and extreme shear force due to cavitation, which breaks linkages in the lignin and hemicellulose network [405-406]. In addition, an alkaline medium leads to a lower extent of sugar degradation compared with acid or thermal pretreatments [407]. The $scCO_2$ as a pretreatment solvent, has the advantage of high diffusivity and low viscosity, penetrating the moistened LC biomass solids and forming unstable carbonic acid, which catalyzes hemicellulose hydrolysis. Additionally, $scCO_2$ disrupts the polymeric network of biomass by an explosion effect upon rapid pressure release [214, 221].

The polysaccharides in the pretreated biomass are hydrolyzed to monomeric and oligomeric sugars by cellulolytic enzymes. Cellulase enzyme is a mixture of endoglucanase, exoglucanase, and β-glucanase enzymes, which are produced by a variety of microbial species. Reducing the enzyme loading and enhancing the enzymatic hydrolysis rate are the strategies to improve the process economics. The synergistic effect of enzymes increases the rate of hydrolysis by changing hydrolysis patterns [120]. For example, cellulose hydrolysis mechanisms of two enzymes (free cellulase cocktail named Ctec2 and cellulosomes or self-assemblies of macromolecular enzyme complex) were observed by transmission electron microscope. The free cellulase hydrolyzed from the edges of cellulose

fibers, whereas the cellulosome separated the cellulose microfibrils and increased the surface area. The avicel cellulose was completely hydrolyzed in 24 h using cocktail of enzymes whereas the free cellulase and cellulosome enzymes hydrolyzed ~70 % and ~100 %, respectively, of cellulose in 48 h when used separately [121]. Another emerging strategy for enhancing enzymatic hydrolysis rate or/and yield is the pretreatment of an enzyme under $scCO_2$. It has been reported in recent studies that enzymes exposed to $scCO_2$ have shown improved stability and activity in free and immobilized conditions [115, 280, 283, 298-299, 311].

This study explores a greener and more sustainable process with mild reaction conditions for processing LC biomass resources, which could significantly reduce the discharge of contaminated wastewater from lignocellulosic biorefineries. The goal of this study is to explore the use of $scCO_2$ as a greener and less chemical-based pretreatment method to understand its impact on the enzymatic digestibility of spruce wood. In the course of this study, we have specifically developed an understanding on the effect of the $scCO_2$ treatment of cellulose-degrading enzyme cocktails on enzyme activity and performance in hydrolysis of spruce wood. Therefore, the current work specifically investigated the effect of $scCO_2$ pretreatment, ultrasound-assisted alkaline pretreatment, and acetosolv pulping-alkaline peroxide pretreatment of spruce wood biomass on its enzymatic digestibility for total reducing sugar (TRS) production. Improved enzymatic activity has been reported for $scCO_2$-treated enzymes and is considered as an emerging method for enhancing enzyme activity [408]. Therefore, the effect of $scCO_2$ pretreatment of enzyme cocktail on enzymatic hydrolysis of pretreated

wood for the total reducing sugar (TRS) production was also investigated. Exploration of such pretreatment methods could substantially reduce the use of chemicals and wastewater generation that could help to approach a more sustainable process [409-410].

4.5. Materials and methods

4.5.1. Materials

Spruce wood chips were ground using a coffee grinder (Hamilton Beach, Canada) and screened to a particle size range of 0.5-1.0 mm with ASTM mesh screens #18.0/35.0. Extractives from the biomass were removed by a Soxhlet extraction apparatus using distilled water followed by a toluene-ethanol mixture (2.0:1.0, v/v) separately for 6 h each. The extractives-free biomasses were dried at 105.0 °C in an oven under an active vacuum. Liquid CO_2 (99.9% with eductor) was sourced from Praxair, Inc.

Cellulase (lyophilized powder of purified enzyme) from *Trichoderma reesei* ATCC 26921 (C8546-10KU) and cellulolytic enzyme complex Viscozyme L (solution containing xylanases, pectinases, β-glucanase enzymes along with high concentration glucose and xylose sugars) from *Aspergillus aculeatus* (V2010-50ML), and all chemicals were obtained from Sigma-Aldrich unless otherwise noted. Cellulase powder was dissolved in distilled water at 15.0 g/L. Sodium citrate buffer (1.0 M) was prepared by mixing citric acid monohydrate and sodium hydroxide, diluted to 10.0 mM, and pH was adjusted to 5.0 using sodium hydroxide [411]. 0.002 % (w/v) sodium azide was used as an antimicrobial agent [412]. Enzymes were used without further purification and enzymatic reactions were conducted at pH 5.0 of 10 mM concentration citrate buffer to facilitate hydrolytic activity of

enzymes. Cellulase and Viscozyme L were mixed at an optimum concentration determined by the response surface method (RSM) to prepare the enzyme cocktail to be used in the enzyme hydrolysis reaction (detailed in supplementary information section 2).

4.5.2. Analytical methods

The protein content of enzyme solutions was determined by colorimetric assay using Pierce™ bicinchoninic acid (BCA) reagents, (Thermo Scientific) using bovine serum albumin (BSA) for calibration curve development [413]. The reducing sugars were analyzed by high-performance liquid chromatography (HPLC) with a refractive index detector (RID) (Agilent 1260 infinity II) with water as mobile phase at 0.6 mL/min, Agilent Hi-plex H (300.0x7.7 mm, particles size 8.0 µm) at temperature 65.0 °C, and RID temperature at 55.0 °C.

4.5.3. Chemical composition of biomass

The total hydrolyzable sugars (THS) in the wood samples were determined by their compositions using national renewable energy laboratory (NREL) standard method for carbohydrate and lignin analysis before and after the pretreatments [384]. The biomass was dried in the oven at 105.0 °C for 6.0 h under an active vacuum to determine the moisture content. Further, 0.3 g of dry solid were treated with 3.0 mL of 72 wt.% sulfuric acids in a pressure tube for 1.0 h at 30.0 °C in a water bath. After 1.0 h, 83.0 mL water was added to the reaction tube to reach an acid concentration of 4.0 wt.%. The reaction mixture was autoclaved (Sterilmatic Market Forge) for 1.0 h at 121.0 °C and 0.1 MPa (15.0 psi). The solution was cooled to ambient temperature and filtered using an 11.0 µm glass filter to separate the insoluble lignin. The insoluble lignin on the glass filter was dried by oven at

105.0 °C for 6.0 h under an active vacuum. The filtrate was neutralized to pH 5.0-6.0 using calcium hydroxide, filtered using a 0.2 µm syringe filter and analyzed by HPLC-RID [403].

4.5.4. Pretreatment of lignocellulosic biomass

4.5.4.1. Supercritical CO_2 pretreatment

Spruce wood was pretreated with $scCO_2$ at different temperatures (100.0, 140.0, and 180.0 °C) and times (0.5, 1.0, 2.0, and 4.0 h) under pressure (15.0, 20.0, and 25.0 MPa) with a water to solid ratio of 2.0 mL/g (2.0 mL water with 1.0 g wood) in a 20.0 mL scintillation vial. Further, the effect of water solid ratio was investigated in the range of 1.0,2.0, 4.0, and 10.0 mL water per g wood. The scintillation vial containing water and biomass was placed in the 100 mL supercritical fluid reaction vessel and closed the reactor (Figure 4-1). The reactor vessel was pressurized with liquid CO_2 after preheating the reactor. The CO_2 inlet and outlet valve were closed, and the reaction was carried out in static conditions. After supercritical CO_2 pretreatment, the reactor was depressurized rapidly (3.0-4.0 MPa/min). The pretreated wood was dried and resuspended in 10 mL distilled water to determine the hydrolyzed sugars during the $scCO_2$ pretreatment. Before the enzymatic digestion, the pretreated wood was washed with distilled water followed by drying in an oven at 105.0 °C for 6.0 h under an active vacuum.

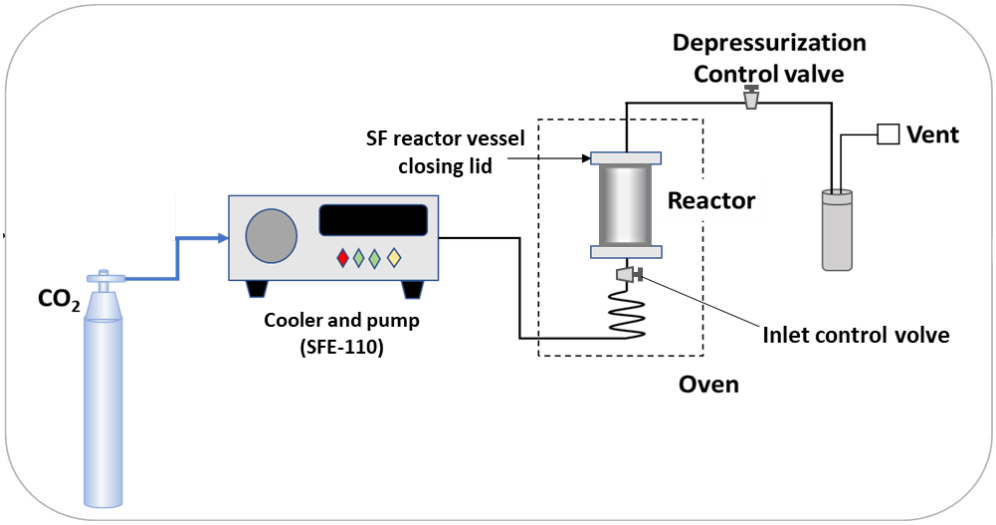

Figure 4-1. Schematic diagram of supercritical CO_2 reactor configuration

4.5.4.2. Ultrasound pretreatment

Spruce wood samples (2.0 g) were pretreated with an ultrasound probe (Sonics ultrasonic processor, VCX750, 13.0 mm probe diameter) at 90.0 % amplitude for 20.0 min in 40.0 mL of 2.0 % w/v NaOH solution without temperature control. To evaluate the effect of NaOH, 2 g wood was treated in 40.0 mL of 2.0 % w/v NaOH solution at 70.0 °C for 20.0 min at 125.0 rpm (revolutions per minute) without any ultrasound treatment as control. About 2.0 g wood was also treated with an ultrasonic probe at 90.0 % amplitude for 20.0 min in 40.0 mL water instead of 2.0 % w/v NaOH solution as the second control. After pretreatment, wood samples were adjusted to a neutral pH (6.5-7.0) by washing with distilled water.

4.5.4.3. Acetosolv pulping followed by alkaline-peroxide bleaching pretreatment

The extractive-free spruce 20.0 g was pretreated using 198.6 mL of 92.5 % w/w acetic acid in the presence of 1.4 mL hydrochloric acid catalyst (0.3 % w/w) for 3.0 h at 115.0±2.0 °C. The pulp obtained was bleached by 13.5 % w/w hydrogen peroxide in 4.0 % w/v sodium hydroxide solution for 2.5 h at 50.0 °C [403]. The pulp

from acetosolv pulping and bleaching was then adjusted to neutral pH (pH 6.5-7.0) by washing with distilled water and dried in the oven at 55.0 °C under active vacuum for 24.0 h as described in [403].

4.5.5. Supercritical CO_2 pretreatment of enzyme

The enzyme cocktail (cellulase 1.94 mg with cellulolytic complex enzymes 131.0 mg) in sodium citrate buffer was pretreated with supercritical CO_2 (8.0 mL enzyme cocktail in a 20.0 mL scintillation vial) in a 100.0 mL reactor vessel (Figure 4-1). The reactor was pressurized to set pressure with liquid CO_2 at set temperature, the effects of temperature (38.0-54.0 °C), pressure (10.0-22.0 MPa), and holding time (30.0-60.0 min) were examined. The reactor was depressurized at a slow rate of 0.3-0.4 MPa/min after the holding time. The enzyme cocktail was also pretreated for 24.0 and 48.0 h time at 46.0 °C, 16.0 MPa to investigate the effect of exposure of enzyme cocktail to $scCO_2$ for a longer time.

4.5.6. Enzymatic hydrolysis

Each of the untreated and pretreated wood were subjected to enzymatic hydrolysis in 25.0 mL Erlenmeyer flasks at 150.0 rpm in a Corning LSE Benchtop Shaking Incubator. Enzymatic hydrolysis reactions were performed at 2 % (w/v) substrate in 10 mL sodium citrate buffer (10.0 mM, pH 5.0) containing 0.002 % (w/v) sodium azide as an anti-microbial agent. The enzyme loads per g biomass for each enzyme separately as well as for the enzyme cocktail, and temperature were optimized at a range of concentrations (5.9-38.8 mg cellulase/g spruce wood and 44.4-625.4 mg Viscozyme L/g spruce wood) and temperatures (30.0-55.0 °C) by response surface method (RSM) (supplementary information). During enzymatic hydrolysis, samples were withdrawn from the reaction over time to investigate the

hydrolysis profile. Specifically, the yield of reducing sugars was determined using Equation (8) where total reducing sugar (TRS) is represented by the sum of the cellobiose, glucose, and xylose released in reaction. The residual activity of the enzyme after the $scCO_2$ pretreatment was calculated using Equation (10).

$$TRS\ yield\ (wt.\%\ of\ THS) = \frac{total\ released\ sugar\ (mg)}{\frac{cellulose\ in\ feedstock\ (mg)}{0.9} + \frac{hemicellulose\ (mg)}{0.88}} \times 100 \quad (8)$$

$$Residual\ activity\ (\%) = \frac{Sugar\ yield\ by\ pretreated\ enzyme}{Sugar\ yield\ by\ untreated\ enzyme} \times 100 \quad (10)$$

For comparison of the enzyme load, the enzyme activity was determined by filter paper hydrolysis at optimum temperature of enzyme. One filter paper activity unit (FPU) is defined by release of 1.0 μmol of reducing sugars per min per mg of enzyme in one hour reaction. The synergy between the two enzymes was evaluated following by Andersen et al., (2008) using Equation (12) where the enzymatic reactions with cellulase, cellulolytic enzyme complex, and the cocktail were conducted under their optimum conditions [414-415].

$$Degree\ of\ synergism = \frac{Extent\ of\ conversion_{Cellulase+cellulolytic\ enzyme\ complex}}{Extent\ of\ conversion_{Cellulase} + Extent\ of\ conversion_{cellulolytic\ enzyme\ complex}} \quad (12)$$

4.5.7. Structural characterization of enzyme

4.5.7.1. Primary structure analysis

The effect of $scCO_2$ on the primary structure enzymes was analyzed using SDS-PAGE (sodium dodecyl sulfate–polyacrylamide gel electrophoresis). The treated and untreated enzyme (cellulase, cellulolytic complex enzymes , and cocktail) protein samples were prepared by mixing equal volumes of 4.0 mg/mL protein sample and 2.5× SDS-PAGE reducing loading buffer and heated at 90.0 ˚C for 10.0 minutes. The samples and a molecular weight ladder (Precision Plus Protein Unstained Stained Standards, Bio-Rad Laboratories) were resolved by

electrophoresis using a 15.0 % sodium dodecyl-sulfate polyacrylamide gel (200.0 V for 50.0 minutes) and visualized by staining with Coomassie Brilliant Blue R-250.

4.5.7.2. Secondary structure analysis

Fourier transform infrared (FTIR) spectra were collected (32.0 scans, 4.0 cm^{-1} resolution, range of 4000.0 to 700.0 cm^{-1}) using a Nicolet iZ10 spectrometer (Thermo Fisher Scientific) equipped with a liquid nitrogen cooled mercury cadmium telluride (MCT) detector (Thermo Fisher Scientific) and a ConcentratorIR2 Multiple Refraction Attenuated Total Reflection (ATR) attachment with a Silicon ATR crystal (Harrick Scientific Products Inc.) at room temperature (22.5 ± 2.5 ˚C). 15.0 µL of each protein sample in 20.0 mM sodium citrate buffer at pH 5.0 were deposited on the ATR crystal immediately prior to data acquisition. Data collection and analysis were performed using Omnic version 9.11.745 (Thermo Fisher Scientific) with OriginPro version 10.0.0.154 used for visualization. Following baseline correction, the amide I region (1600.0-1700.0 cm^{-1}) was deconvoluted to evaluate protein secondary structure using Byler and Susi (1986) for wavelength attributions to secondary structure [416].

Circular dichroism (CD) spectra were acquired using an Olis DSM20 CD Spectrophotometer with integration time determined as a function of High Volts in Olis SpectralWorks Version 5.888.272. CD spectra were acquired at room temperature (22.5 ± 2.5 ˚C) from 270.0-180.0 nm with a 1.0 nm step size using quartz cuvettes of 0.01 mm path length (Hellma). Spectra were obtained by averaging three individual scans. The spectra of 20.0 mM sodium citrate blanks were measured before the samples and were subtracted from the 0.1 mg/mL protein sample CD spectra. Since the samples are mixtures of proteins and, hence,

molarity is not known, to directly compare from sample to sample each spectrum was normalized to its respective minimum in the far-UV regime [417]. The secondary structure was analyzed using two popular method FTIR and CD spectra to provide a qualitative difference between the results.

4.5.8. Statistical analysis

All the experiments were performed using at least independent duplicates. The Data was analyzed with one way-ANOVA at 95 % confidence level ($p<0.05$) for the statistical significance. A paired t-test ($P<0.05$) was used to analyze the significances of different pretreatment conditions of enzyme pretreatment on TRS yield. The statistical analyses were performed in Minitab® 21.4.

4.6. Results and discussion

4.6.1. Chemical composition of spruce wood and enzymes

The chemical composition of the untreated and pretreated spruce wood was analyzed using the NREL method and the compositions are shown in Table 1. The spruce wood polysaccharide content is 65.0-70.0 wt.% similar to reports in the literature [29, 418]. The $scCO_2$ treatment of the untreated wood did not have a significant influence on the chemical composition of the solids. The ultrasound-assisted alkaline pretreatment of the wood showed a reduction in total polysaccharide component from 67.0 wt.% to 54.0 wt.% whereas lignin content slightly increased from 29.0 to 32.0 wt.% because of polysaccharide decomposition (Table 4-1). The polysaccharide content was increased from 65.0-67.0% to 95.0-96.0% after acetosolv pulping followed by alkaline hydrogen peroxide bleaching treated wood, a process which removed most of the lignin. The wood pulp derived from acetosolv pulping followed by alkaline-peroxide bleaching

was also pretreated with $scCO_2$ and no significant change in the chemical composition was observed (data not shown).

Table 4-1. Chemical composition of untreated and pretreated spruce wood in wt.% (n=3)

Biomass Component	Untreated biomass	$scCO_2$ pretreatment (20.0 MPa, 180.0 °C, 1.0 h, 2.0 g/mL)	Ultrasound-assisted 2.0 wt.% NaOH pretreatment	Pulping-bleaching pretreatment
Cellulose	47.1 ± 2.2	39.7 ± 0.8	36.2 ± 0.7	88.5 ± 0.7
Hemicellulose	20.1 ± 0.8	19.3 ± 0.9	17.8 ± 0.7	6.2 ± 0.7
Lignin	29.4 ± 0.2	31.1 ± 0.6	29.4 ± 2.9	<0.7

Before enzymatic hydrolysis of the untreated and pretreated biomass, the commercial enzymes cellulase and Viscozyme L were used to prepare the enzyme cocktail and characterized for their sugar and protein content. Sugar and protein were analyzed by HPLC and BCA protein assay, respectively (Table 4-2). Since the cocktail is made up of a crude enzyme complex solution (Viscozyme L), the protein concentrations of cocktail are substantially high in comparison to cellulase from *T. reesei*. The prepared enzyme cocktail using the commercial enzymes was used without further filtration, and therefore, an initial sugar concentration of 15.2±0.4 g/L was present in the reaction mixture at the beginning of the reaction. However, there was no significant influence of initial sugars concentration on the activity and TRS yield (Figure S8-6).

Table 4-2. The commercial enzyme (as received) characterization for sugar and protein content (n=3)

Commercial enzyme	Sugar concentration	Protein concentration	Enzyme activity (FPU/g), temperature (°C), pH
Cellulase	None	1.2 ± 0.0 g dissolved protein/g enzyme powder	75.2±0.4, 46.3, 5.0
Cellulolytic complex enzymes (Viscozyme L)	289.7 ± 6.8 g/L	210.8 ± 8.4 g/L enzyme solution	23.0±3.3, 37.4, 5.0

4.6.2. Optimum concentration and temperature of individual enzymes in the cocktail mixture

Optimal enzyme concentration (cellulase 5.9-34.1 mg, cellulolytic complex enzymes 44.4-256.5 mg) and temperature (30.0-58.0 °C) were investigated using TRS yield (wt.% of total hydrolyzable sugars) as a response in RSM (Table S8-1 – Table S8-7). The TRS yields from wood by individual enzymes showed that cellulase has an optimum temperature of 46.3 °C and cellulolytic complex enzymes have 37.4 °C (Figure S8-1 and Figure S8-2) in sodium citrate buffer (10.0 mM, pH 5.0). The differences in the optimum temperature and activities of enzymes are highly dependent on the source microorganism growth and reaction conditions [419-421]. The optimum concentrations of these commercial enzymes in the enzyme cocktail were 9.7 mg cellulase and 598.4 mg cellulolytic complex enzymes per gram of untreated spruce wood substrate at 2.0 wt.% substrate concentration in 10.0 mL sodium citrate buffer (10.0 mM, pH 5.0) at 42.5 °C and 150.0 rpm. Under optimized condition for the enzyme cocktail, the untreated wood showed a maximum total reducing sugars (TRS) yield of 14.1±0.8 wt.% of total hydrolyzable sugar (THS) in 72.0 h at atmospheric pressure (Figure S8-4).

Under the same optimized reaction conditions of cocktail, the bleached wood pulp (BWP) showed a TRS yield of 74.9±0.8 wt.% of THS in 72.0 h. Therefore, BWP was used as a substrate for the enzyme cocktail to investigate the synergy between the two enzymes present in the cocktail. The BWP was hydrolyzed by individual enzymes at the same amount as is present in the enzyme cocktail and the reaction was carried out at their optimum temperatures for 96.0 h. In individual runs, cellulase released 44.9 wt.% TRS at 46.3 °C and cellulolytic complex

enzymes released 20.0 wt.% TRS at 37.4 °C whereas the TRS yield increased to 86.9±1.78 wt.% by the enzyme cocktail in 96.0 h at 42.5 °C. The synergism between enzymes was 1.3 showing the performance of the enzyme cocktail to be 34.0 % higher than individual component's performance (Figure 4-2). The Viscozyme L commercial enzyme was used as hemicellulase equivalent enzymes hydrolyzes arabinan and xylan from the hemicellulosic network [422-423]. Endoglucanase has also been found in Viscozyme L cellulolytic complex enzymes which hydrolyzes the glucan chains in cellulose from the interior and releases short chains of glucan [424]. The exposed chains of cellulose are easily accessible for exoglucanase and β-glucanase enzymes that release cellobiose and glucose monomers. Simultaneously, hemicellulase also acts on hemicellulose chains and releases hemicellulosic monomers (i.e., xylose, mannose). The presence of these enzymes in the enzyme cocktail released around ten times more xylose than the cellulase alone and synergism between enzymes led to higher TRS yield.

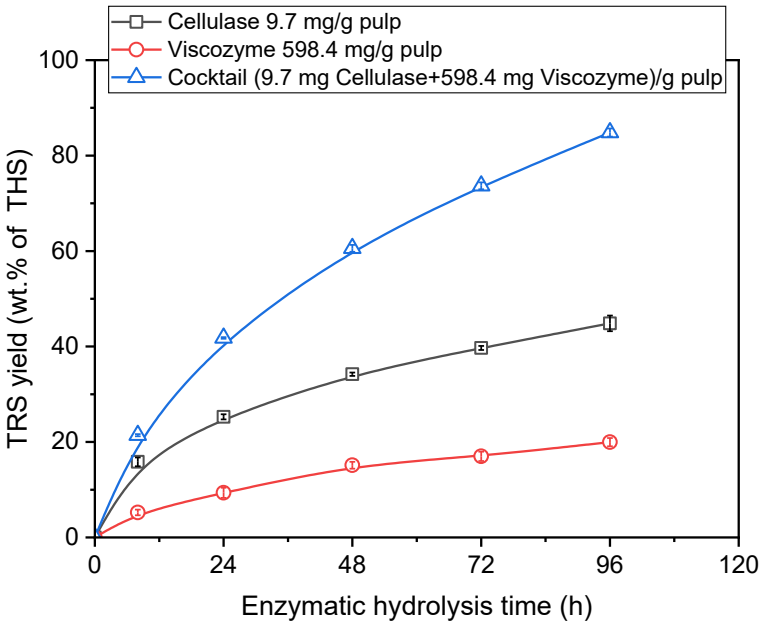

Figure 4-2. Synergistic effect between the cellulase and cellulolytic complex enzymes for TRS yield from bleached wood pulp over time (Cellulase 9.7 mg/g pulp, Viscozyme 598.4/g pulp separately as well as combined in cocktail) (n=2)

4.6.3. Effects of pretreatments on spruce wood

The pretreated wood was enzymatically digested with the enzyme cocktail under its optimized reaction condition (2.0 % solid, enzyme cocktail: Cellulase 9.7 mg/g pulp, Viscozyme 598.4/g pulp biomass, 42.5 °C) and compared with the TRS yield from untreated biomass.

4.6.3.1. Effect of supercritical CO_2 pretreatment on spruce wood

The effectiveness of the $scCO_2$ pretreatment on spruce wood was analyzed by enzymatic digestibility of pretreated solids using an enzyme cocktail under optimized conditions. The spruce wood was pretreated with 2.0 mL water per g wood (dry weight) under 20.0 MPa pressure at temperatures 100.0-180.0 °C for 0.5-4.0 h holding time. The total reducing sugar of 4.0 wt.% of THS at maximum were released at high temperature (180.0 °C) and 10.0 mL/g water-solid ratio whereas lower temperature (100.0-140.0 °C) did not show any detectable amount of sugar during the $scCO_2$ pretreatment. The temperatures below 180.0 °C were not able to disrupt the recalcitrant structure of wood and the TRS yield from pretreated wood was similar to untreated wood (Figure 4-3). The increase in the water-solid ratio from 1.0 mL/g to 10.0 mL/g in $scCO_2$ pretreatment at the respective temperature and pressure of 180.0 °C and 20.0 MPa, had shown slightly increased yield from 16.1±1.8 wt.% to 19.5±1.0 wt.% at 72.0 h in the subsequent stage of enzymatic hydrolysis for pretreatment. The effect of pretreatment was also done on agricultural biomass cornstalk to verify the instrumental setup. The enzymatic digestibility of $scCO_2$ pretreated cornstalk (20.0

MPa, 170.0 °C, 2.5 h) showed slightly improved TRS yield from 21.89±2.9 wt.% (untreated) to 29.3±2.6 wt.% of THS at hydrolysis time of 96.0 h at water-solid ratio of 0.5 mL/g whereas increasing the water-solid ratio to 4.0 or 10.0 mL/g did not enhance the enzymatic digestibility of pretreated cornstalk (Figure S8-5).

Under the same condition of pretreatment, Yin et al., (2014) observed an increase from 16.6 wt.% (untreated cornstalk) to 46.4 wt.% of THS for pretreated cornstalk in 72.0 h at water-solid ratio of 0.5 mL/g, however, effect of water to solid ratio was not investigated [221]. A few studies have reported that $scCO_2$ pretreatment enhanced enzymatic digestibility, showing 27.3-84.7 wt.% of THS yield from different wood biomass (i.e., aspen wood 84.7 % [112], Southern yellow pine 27.3% [112], mixed hardwood 73.0 % [20]). However, the reported yields vary significantly depending on the biomass type and pretreatment conditions. For example, aspen wood was pretreated with $scCO_2$ (21.4 MPa, 165.0 °C, 0.5 h) with a water to solid ratio of 0.7 mL/g leading to 84.7 wt.% of THS yield in enzymatic hydrolysis. Whereas only 27.3 wt.% of THS yield was obtained in the enzymatic hydrolysis of $scCO_2$ pretreated southern yellow pine under the same condition as the aspen wood [112]. The higher yield observed with hardwood biomass could be related to its distinct chemical composition as well as to the pretreatment conditions employed. The high temperature with $scCO_2$ conditions hydrolyzes the hemicellulose fraction and reduces the crystalline structure of biomass which improves the enzyme-carbohydrate interaction in the pretreated biomass [20, 112]. Another major reason could be the presence of higher lignin content which may form non-productive binding with enzyme and reduce enzyme-carbohydrates

interaction [425-426]. The lower lignin content in hardwood compared to softwood may lead to substantial differences in the enzymatic hydrolysis yield after the $scCO_2$ pretreatment. The collective effect of lignin content and hemicellulose hydrolysis during pretreatment could be attributed to the substantial difference in the yield softwood compared to yield from hardwood [20, 112]. However, woody biomass is generally under-explored as a LC biomass for $scCO_2$ pretreatment; therefore, further investigation with respect to a comparative study of softwood and hardwood biomass from different species would provide greater insight into the effect of wood type-dependent chemical composition on hydrolysis yield.

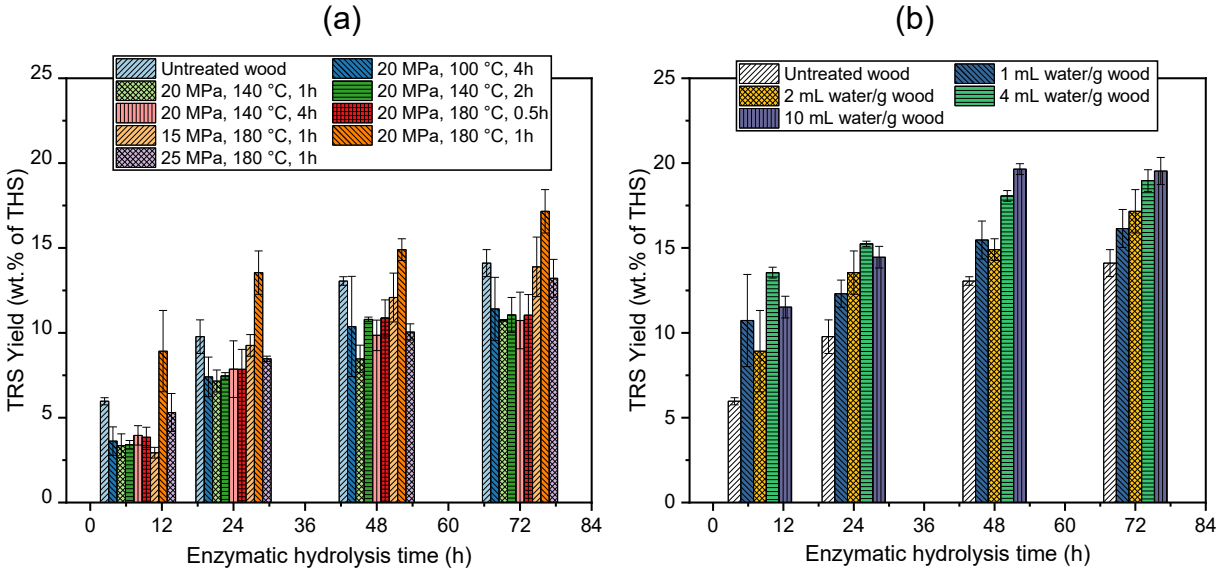

Figure 4-3. (a) Effect of $scCO_2$ pretreatment (Pressure, Temperature, holding time) keeping the water-solid ratio constant at 2.0 mL/g and (b) effect of water solid ratio at 180.0 °C, 20.0 MPa for 1.0 h $scCO_2$ pretreatment on spruce wood for TRS yield in enzymatic hydrolysis (n=2).

After sub and supercritical CO_2 pretreatment, agricultural biomass of various species had shown a TRS yield of 42.0-97.8 wt.% of THS upon enzymatic hydrolysis (i.e., sugarcane bagasse 97.8 % [111], switchgrass 42.0-80.0 % [20, 23, 214], corn stover 66.5-85.0 % [20, 214], Guayule 82.8-86.0 % [223, 229]). For example, Phan

& Tan (2014) used $scCO_2$ pretreatment of sugarcane bagasse (15.6 MPa, 187.0 °C, 0.67 h) followed by hydrogen peroxide treatment before enzymatic hydrolysis of the pretreated solid that yielded 97.8 wt.% of THS whereas untreated biomass had a yield of only 13.4 wt.% of THS [111]. Luterbacher et al. (2010) obtained a yield that increased from 53.0±2.0 wt.% (untreated corn stover) to 85.0 wt.% of THS yield in enzymatic hydrolysis of $scCO_2$ pretreated (20.0 MPa, 160.0 °C, 1.0 h) corn stover biomass without any additional pretreatment [20].

4.6.3.2. Effect of ultrasound-assisted alkaline pretreatment

Alkaline pretreatment at low alkali concentration (2.0 wt.% NaOH) at 70.0 °C for 20.0 min, ultrasound-assisted alkaline pretreatment, and ultrasound pretreatment without an alkaline solution were performed to investigate the effect of ultrasound treatment and alkaline pretreatment. Ultrasound pretreatment of wood in an aqueous solution of 2.0 % NaOH showed an increased yield (20.0±2.8 wt.% of THS) in enzymatic hydrolysis in comparison to the yield from untreated wood (14.1±0.8 wt.% of THS) in 72.0 h. Pretreatment with alkaline conditions and ultrasound pretreatment without alkaline conditions both led to slightly increased TRS yield in enzymatic hydrolysis in comparison to untreated wood (Figure 4-4). However, the increase in the TRS yields was statistically significant ($p=0.13$). The ultrasound treatment generates hydroxyl radicals from water, high temperature, and extreme shear force due to cavitation which helps in the deconstruction of the lignin and hemicellulose network [405-406]. However, a lower concentration of sodium hydroxide at low temperatures (rose to 70.0 °C by the 20.0 min ultrasound treatment, measured by thermocouple) and lower treatment duration (20.0 min) was not sufficient to facilitate enhanced enzymatic digestibility, with the spruce

wood polymeric structure remaining intact. The chemical composition of the spruce before and after the pretreatment was compared (Table 4-2) and it was found that the lignin content remained the same whereas the cellulose and hemicellulose contents were hydrolyzed partially during ultrasound-assisted alkaline pretreatment of wood. Similar compositional results (hemicellulase decreased from 20.8 to 13.9 %, and lignin remained at 28.3 to 27.6 %) were obtained for spruce wood after pretreatment with 7 wt.% sodium hydroxide at -15.0 to 100.0 °C for 2.0 h but cellulose content increased (from 43.0 to 50.6 %) in all the conditions without ultrasound treatment [427]. Increasing the concentration of sodium hydroxide and the treatment duration may help to enhance the enzymatic digestibility of pretreated wood, but it would lead to wastewater generation.

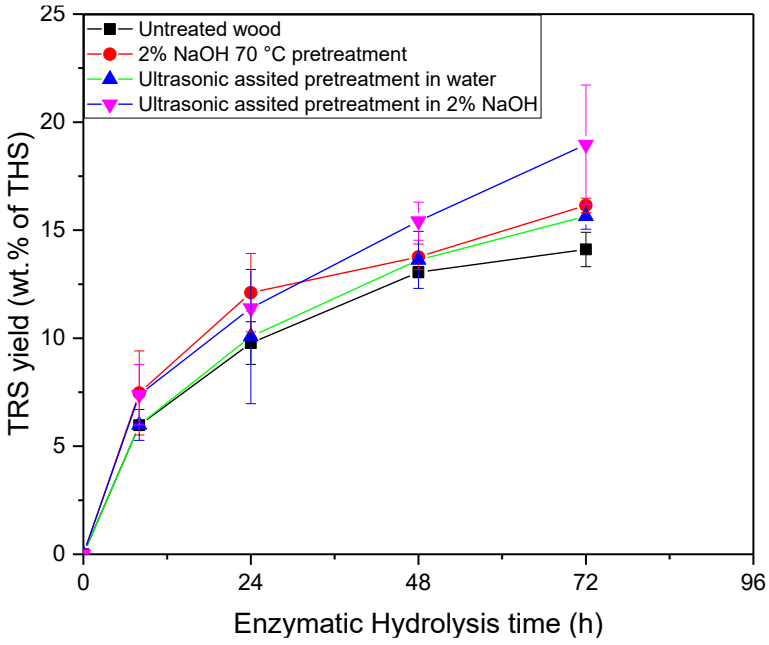

Figure 4-4. Effect of alkali and ultrasound-assisted pretreatments of wood for TRS yield in enzymatic hydrolysis (n=2)

4.6.3.3. Acetosolv pulping-alkaline peroxide bleaching pretreatment

The acetosolv pulping process hydrolyzed 19.4 % of the initial cellulose, 88.6 % of the initial hemicellulose, and 91.7 % of the initial lignin was removed during acetosolv pulping and >95.0 % overall delignification was achieved after bleaching of the acetosolv pulp in alkaline hydrogen peroxide solution. The pulping and bleaching process disrupts the lignin and hemicellulosic network and exposes the cellulose, allowing it to be more readily accessed by the enzymes [403]. The enzymatic hydrolysis of BWP by enzyme cocktail released a TRS yield of 74.9±0.8 wt.% of THS in 72.0 h and reached ~95.0 wt.% in 144.0 h. The acetosolv pulping-bleaching method produced high-purity pulp (lignin <0.7 wt.%) equivalent to a pure cellulosic substrate for enzymatic hydrolysis. However, the presence of 6.2±0.7 wt.% hemicellulose in the bleached pulp led to significant resistance for enzymatic hydrolysis by cellulase alone and the TRS yield was only 44.9 wt.% of THS in 96.0 h at 46.3 °C, whereas the TRS yield reached 88.9 wt.% in the presence of xylanase from the Viscozyme L in the cocktail enzyme (xylose yield increased to 10.0 folds) at 42.5 °C. Also, it is worth noting that the enzyme loading is substantially lower (0.15 FPU cellulase with 2.79 FPU cellulolytic complex enzymes) for bleached wood pulp in comparison to other organosolv pulping methods where a minimum of 15.0 FPU cellulase enzymes have been used to yield similar of sugar at similar rates [60, 428-429] (Table 4-3). The synergy between the two enzymes (cellulase and cellulolytic complex enzymes), as well as the optimization of enzyme amount per gram of substrate and the temperature led to achieving a lower enzyme loading requirement.

Table 4-3. Comparison of organosolv pulping pretreatment method and their enzymatic digestibility by different enzyme loads

Biomass	Organosolv pretreatment (solvent, catalyst, temperature, time)	De-lignification	Enzymatic hydrolysis (substrate concentration, enzyme U/g substrate)	TRS yield by enzymatic hydrolysis	Ref.
Eucalyptus wood	Propanol 70.0 % v/v, None, 220.0 °C, 2.0 h	73.9 %	5.0 % solid, 15.0 FPU Cellic@CTec2	79.4 % in 72.0 h	[428]
	Propanol 50.0 % v/v, None, 220.0 °C, 2.0 h	81.3 %		88.6 % in 72.0 h	
Norway spruce	Ethanol 63.0 % v/v, 0.05 M formic acid, 235.0 °C, 1.5 h	65.0 %	1.0 % cellulose, 30.0 FPU Celluclast 1.5 L with 32.0 pNPGU	100.0 % in 48.0 h	[60]
Eucommia ulmoides Oliver wood	Ethanol 50.0 % v/v, 1 % HCl, 180.0 °C, 0.5 h	70.4 %	5.0 % solid, 15.0 FPU cellulase	~88.0 % in 96.0 h	[429]
Spruce	Acetic acid 93.0 % v/v, 0.3 % HCl w/w, 115.0 °C, 3.0 h	>95.0%	2.0 % solid, 0.15 FPU cellulase with 2.79 FPU cellulolytic complex enzymes	86.9 % in 96.0 h	This study*

* Acetic acid pulping was followed by alkaline peroxide bleaching and net delignification was >95.0 %.

It has been found that enzyme works inefficiently in the presence of lignin due to adsorption of enzyme protein on lignin by hydrophobic, electrostatic, and hydrogen bonding interactions which block the enzyme-carbohydrate interaction [426, 430-431]. Several lignin-blockers have been shown to be effective in reducing this effect on enzymes, such as surfactants (i.e., TWEEN and poly ethyl glycol) and non-catalytic proteins (i.e., bovine serum albumin, soy protein) [432-434]. For example, Luo et al. (2019) used a soy protein for the hydrothermally pretreated wood biomass that blocked the attachment of enzyme to lignin and enhanced the enzymatic hydrolysis efficiency and TRS yield up to 200 % [433]. Biomass pretreated with $scCO_2$, and alkali-assisted ultrasonic pretreatment methods did not result in lignin and hemicellulose removal which resulted in inefficient enzyme-

carbohydrate interaction and no substantial improvement in TRS yield. In contrast, the acetosolv pulping-alkali peroxide method, which is capable of lignin removal, successfully achieved high yield at a very low load (3.0 FPU in total) of enzyme cocktail.

4.6.4. Effect of supercritical CO_2 pretreatment on enzyme cocktail

Under the strategy of exploring the effect of $scCO_2$ pretreatment of enzyme, the enzyme cocktail was treated under $scCO_2$ and characterized for enzyme activity and structural changes. SDS-PAGE analysis of untreated and $scCO_2$ pretreated enzyme cocktail solution showed that there was no breakage or agglomeration in the primary structure of the enzymes (Figure 4-5). Namely, the profile of resolved proteins observed for the untreated enzymes were present and maintained the same ratio of intensities in the pretreated enzyme solutions. All enzymes in the cocktail thus appear resilient at the primary structural level to high pressure for up to 24.0 h of static exposure of $scCO_2$ at 10.0-22.0 MPa and 38.0-54.0 °C (Figure 4-5). The individual enzyme mixtures were also resolved by SDS-PAGE, showing the expected presence of multiple constituents with different molecular weights in both the cellulase and cellulolytic complex enzyme mixtures.

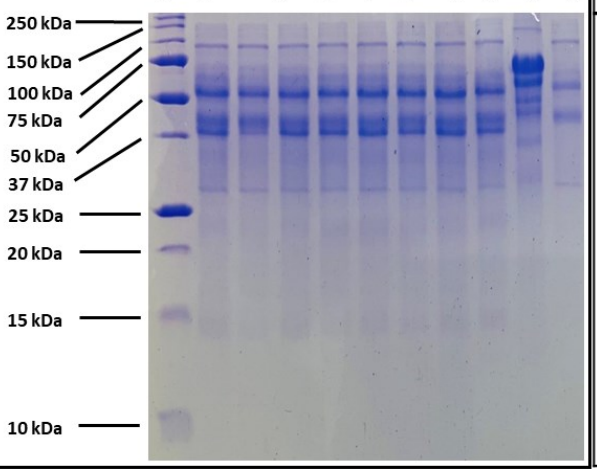

Sample name	Pretreatment conditions	TRS yield in 96 h (wt.% THS)
L	Ladder (marker protein)	-
C	No treatment/Control	94.76±2.2%
1	10 MPa,46 °C, 60 min	93.82±0.9%
2	16 MPa, 46 °C, 60 min	97.11±1.6%
3	22 MPa, 46 °C, 60 min	91.42±1.7%
4	16 MPa, 46 °C, 30 min	93.42±4.6%
5	16 MPa, 38 °C, 30 min	95.01±0.4%
6	16 MPa, 54 °C, 30 min	91.60±0.3%
7	16 MPa, 46 C, 24 h	6.26±1.1%
8	Cellulase	44.85%
9	Viscozyme	19.96%

Figure 4-5. Comparison of untreated and $scCO_2$ pretreated enzyme's primary structure analyzed by SDS-PAGE (n=2) where TRS yield is from enzymatic hydrolysis of BWP by untreated and pretreated enzyme cocktail in 96.0 h.

The enzyme cocktail pretreated for short time (0.5-1.0 h) under $scCO_2$ at 38.0-54.0 °C and 10.0-22.0 MPa, did not have any significant change in the enzyme activity in comparison to the untreated enzyme for hydrolyzing the bleached wood pulp (BWP). The TRS yield profile in enzymatic hydrolysis with $scCO_2$ pretreated enzyme has been shown along with untreated enzyme in Figure 4-6a. The protein secondary structure content of the untreated and treated enzyme cocktails was analyzed using both FTIR and CD spectroscopy (Figure 4-6b and 4-6c). In both cases, the global secondary structural composition is observed, reflecting the overall ensemble-averaged structuring of all the different enzymes (endoglucanase, exoglucanase, and β-glucosidase from cellulase, and xylanases, β-glucanase, pectinases, hemicellulases from Viscozyme L enzyme complex) present in the enzyme cocktail.

Spectral decomposition was carried out for the amide I band of FTIR spectra (Figure S8-7), allowing evaluation of protein structural composition for each

cocktail. In each case, a mixture of a-helical, b-strand/sheet content, turn, and disordered structuring is observed, with b-strand/sheet being the predominant structural component (Figure 4-6b). This is fully consistent with structural expectations for these typically b-sandwich or mixed b-sheet/a-helical enzymes. Based on ANOVA test, the observed differences in secondary structure content are insignificant ($p=0.27$). The secondary structure of untreated enzymes as well as the samples with the greatest and least TRS yield were also analyzed using CD spectroscopy. The virtually unchanged far-UV CD spectral lineshape regardless of condition clearly indicates that the treatments did not significantly alter the global secondary structure composition of the enzyme cocktail (Figure 4-6c). The single minimum band observed at approximately 216.0 nm is consistent with predominant b-strand/sheet composition in the cocktail [435], following the FTIR-based spectral decomposition.

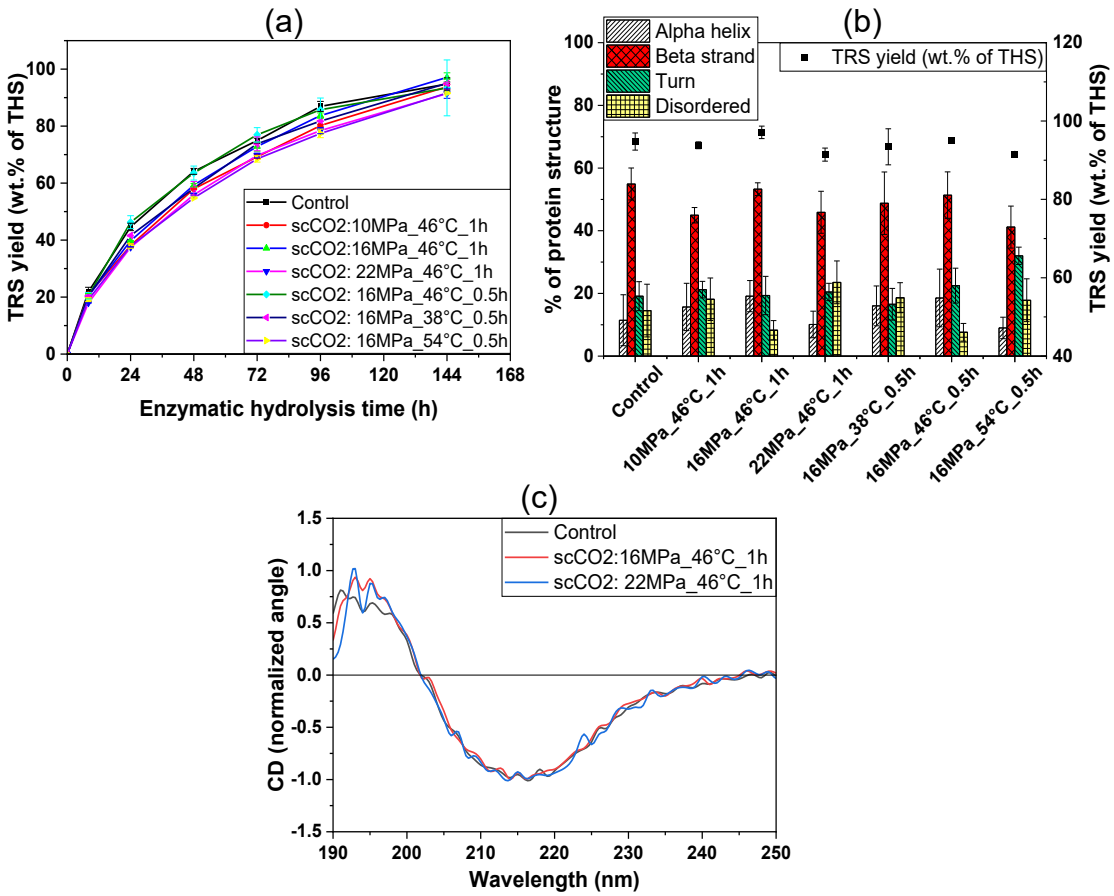

Figure 4-6. (a) Effect of $scCO_2$ pretreatment on TRS yield (n=2), (b) the enzyme's secondary structure analyzed by FTIR and corresponding TRS yield profile for BWP hydrolysis, and (c) secondary structure analyzed by CD specroscopy (n=3).

Although the enzyme cocktail is a mixture of proteins, changes in secondary structuring of individual enzyme components of the mixture upon $scCO_2$ treatment will be reflected in spectroscopically observable changes in the global secondary structure composition providing valuable information about cellulolytic enzyme treatment with high pressure and $scCO_2$ [50, 436-437]. Herein, FTIR and CD spectroscopy thus independently demonstrate that enzyme's global secondary structuring is not substantially perturbed by pretreatment. Considering the lack of protein truncation observed in SDS-PAGE and the lack of global secondary structural perturbation apparent by both FTIR and CD spectroscopy,

this is consistent with the tertiary structure of the enzymes in the cocktail also generally being insensitive to the pretreatment process given consistent hydrolytic activity It is worth mentioning that there might have been changes in the secondary and tertiary structures of individual enzymes, which cannot be observed in a cocktail or mixture of enzymes. Therefore, further separation of enzymes and treatment of individual enzymes will be beneficial to understand the effects on their secondary structures influenced by the $scCO_2$ and high pressure [438-439]. Conversely, the enzyme cocktail pretreated with long exposure to $scCO_2$ (16.0 MPa, 46.0 °C, 24.0 h) had a substantial reduction in yield from 44.6±1.3 wt.% (untreated enzyme) to 6.3±1.1 wt.% (pretreated enzyme) of THS at 24.0 h of enzymatic hydrolysis of BWP. Oliveira et al. (2006) and Melgosa et al. (2015) had also observed negative influence on enzyme activity of different lipase enzymes for the long exposure (3.0-6.0 h) at high pressures (25.0-28.0 MPa) of $scCO_2$ [249, 368]. The reason for this decreased hydrolytic activity could be the structural changes in the microenvironment of enzyme, its active sites, and the low pH due to carbonic acid formation by CO_2 under high pressure [330]. In contrast to this latter finding, Paljevac et al. (2007) exposed crude cellulase to $scCO_2$ (10.0 MPa, 35.0 °C, 24.0 h), and the activity remained at 101.7 % of the untreated enzyme [115]. The influence of exposure time on cross linked enzyme aggregates (CLEAs) of cellulase enzyme was investigated by Hojnik Podrepšek et al. (2019). They found that the short exposure at low pressure of $scCO_2$ (10.0 MPa, 40.0 °C, 1.0-3.0 h) treatment had enhanced residual activity (147%) whereas long exposure of 4.0 to 24.0 h had residual activity of <80.0 % [280]. The cellulase and lipase enzymes have

shown enhanced enzyme activities after $scCO_2$ pretreatment. Senyay-Oncel & Yesil-Celiktas investigated the effect of $scCO_2$ on cellulase enzyme under 12.0-24.0 MPa, 41.0-67.0 °C for 1.5-2.5 h of pretreatment time. The cellulase activity was increased from 6.25 U/mL (untreated) to 9.27 U/mL (148.3 % residual activity) after $scCO_2$ pretreatment at optimum condition (18.0 MPa, 54.0 °C, 2.0 h) and 10.0 g/min CO_2 flow rate whereas the activity was decreased to a residual activity of 4.61 U/mL at 12.0 MPa, 41.0 °C, 2.5 h and 4.0 g/min flow rate. The study showed that the enzymes have an active conformation at certain optimum condition of $scCO_2$ and apart from that the enzyme could be partially inactivated [283]. However, the effect of $scCO_2$ on the structure of enzyme for increased or decreased activity was not investigated [280, 283]. Since the enzymes are biomolecules and have different primary, secondary, and tertiary level structures, each enzyme may behave differently.

4.7. Conclusions

The focus in LC biorefinery is to explore alternative approaches to traditional chemical pretreatments of lignocellulosic biomass. This study aims to investigate the comparative effectiveness of greener alternatives in enhancing the enzymatic digestibility of spruce wood biomass. Supercritical CO_2, acetosolv pulping-alkaline peroxide bleaching, and ultrasound-assisted alkaline pretreatment methods were used to disrupt the resilience of spruce wood biomass structure to enhance the enzymatic digestibility for producing reducing sugars. The pretreated solids were hydrolyzed with an enzyme cocktail, a mixture of cellulolytic enzymes at optimized reaction conditions (i.e., enzyme concentration, temperature). The mixture of

enzymes (commercial cellulase from *Trichoderma reesei* ATCC 26921 (9.65 mg enzyme/g solid) and cellulolytic enzyme complex Viscozyme L from *Aspergillus sp.* (599.4 mg enzyme/g solid)) showed a TRS yield of ~95.0 % at 42.5 °C at pH 5.0 in citrate buffer in 144.0 h with degree of synergism of 1.34 between enzymes. Acetosolv pulping followed by alkaline peroxide bleaching was the most effective method among the three pretreatment methods examined in this study. The $scCO_2$ (20.0 MPa, 180.0 °C, 1.0 h) pretreatment of wood at high water-solid ratio of 4.0-10.0 mL/g slightly increased the TRS yield from 14.1±0.8 wt.% to 19.5±0.8 wt.% of THS. However, the improvement in enzymatic digestibility of spruce wood by $scCO_2$ was not substantial in comparison to acetosolv pulping method of pretreatment. Furthermore, when subjected to short-term pretreatment under supercritical carbon dioxide ($scCO_2$), the enzymes present in the enzyme cocktail exhibited no significant alterations in their primary and secondary structures. This outcome aligns with the observed preservation of enzyme activity during the pretreatment process. However, the activity declined to 25.0 % of untreated enzyme activity for prolonged exposure (24.0 h) under $scCO_2$. This study, along with the literature, indicates that enzymes derived from different sources exhibit varying levels of effects (positive, negative, or neutral) on enzyme activity after pretreatment under $scCO_2$. The outcomes of this study suggest that the acetosolv pulping-alkali peroxide bleaching method has promising yield from the spruce wood biomass and therefore the study could be extended to its application on various biomass and scaling up to large scale in order to explore industrial potential. Additionally, the use of acetosolv pulping method could be explored

under supercritical CO2 condition in order to investigate the potential effect. It is worth mentioning that scCO2 is a non-polar solvent and therefore, it may need to use a polar co-solvent to extract the solubilized component during the $scCO_2$ assisted-acetosolv pulping pretreatment under the safe operating condition (associated hazards: flammable solvent, high temperature). Further exploration of cellulolytic enzymes and biomass using greener pretreatment methods, as demonstrated in this study, could aid in achieving the goal of developing sustainable and environmentally friendly methods for utilizing abundantly available lignocellulosic biomass.

4.8. Declaration of Competing Interest

The authors declare that they have no known competing financial interests or personal relationships that could have appeared to influence the work reported in this paper.

4.9. Acknowledgments

The research was financially supported by a Natural Sciences and Engineering Research Council of Canada (NSERC) -Strategic grant [506346-2017-STPGP] and Nova Scotia Innovation Hub awarded to Dr. Satinder Kaur Brar and Dr. Azadeh Kermanshahi-pour and by an NSERC Discovery Grant [RGPIN/05907-2017] awarded to Dr. Jan K. Rainey. Pawan Kumar acknowledges scholarship support from NSERC-CREATE-ASPIRE and Sara Evans acknowledges scholarship support from the NSERC CREATE Training Program in BioActives (510963). Key infrastructure was provided through NSERC Research Tools and Instruments grants awarded to Dr. Jan K. Rainey.

Appendix A. Supplementary data

Supplementary information.docx

CHAPTER 5 EXPLORING THE USE OF SUPERCRITICAL CARBON DIOXIDE IN ENZYMATIC HYDROLYSIS OF CELLULOSIC SUBSTRATE

This chapter has been considered for journal publication.

5.1. Abstract

Enzymes are among the key components for production of fermentable sugars in lignocellulosic biorefineries. Herein, the enzymatic hydrolysis of cellulosic substrates was investigated with a prepared enzyme cocktail in free and immobilized form under atmospheric and supercritical CO_2 ($scCO_2$) conditions. The cocktail was immobilized into silica oxide aerogel at different enzyme loads (36.0 to 144.0 mg enzyme/g aerogel) using sol-gel entrapment method using $scCO_2$ drying. The free cocktail enzyme produced total reducing sugar (TRS) yield of 50.5±0.3 wt.% of total hydrolysable sugars (THS), whereas the cocktail aerogel showed a TRS yield of 36.0±3.8 wt.% in 72 h under atmospheric condition. The immobilized cocktail at 144.0 mg/g aerogel enzyme load retained a relative TRS yield of >50.0 % after fourth cycle of reuse. In contrast, relative yield of lower enzyme loads decreased by <50.0 % after third cycle compared to first cycle under atmospheric pressure. TRS yield by the cocktail aerogel was below 10.0 wt.% in second cycle of reuse due to enzyme leaching from aerogel to hydrolysate under $scCO_2$ showing unfavorable conditions for cocktail aerogel in high pressure system. Further, characterization of unused and reused cocktail aerogels showed decreased surface area and porous volume over the reuse cycles under atmospheric condition.

5.2. Highlights

- Cellulolytic enzyme cocktail formulation was optimized for enhanced activity.
- Enzyme immobilized into silica oxide aerogel by entrapment method for enzyme reuse.
- Enzymatic hydrolysis of water-soluble/insoluble cellulose conducted under $scCO_2$.
- Surface area and porous volumes of aerogel reduced over reuse cycles.

5.3. Keywords

Lignocellulosic biomass; Enzyme entrapment; enzyme immobilization; supercritical CO_2; enzyme aerogel; Fermentable sugars.

5.4. Introduction

Lignocellulosic (LC) biomass is an abundant resource and is available in the form of agricultural and forest residues. Cellulose and hemicellulose are major constituents of the LC biomass, which can further be hydrolyzed to monomeric (hexoses and pentoses) sugars as the platform chemicals to produce bioethanol and a variety of bioproducts [44, 440]. The biomass first undergoes mechanical, chemical, thermal, or supercritical fluid pretreatments to enhance the enzyme accessibility to polysaccharides [26, 43, 111, 441-442]. Then, the polysaccharides in pretreated biomass are hydrolyzed to fermentable monomeric sugars by the cellulase (endoglucanase, cellobiohydrolase, and β-glucosidases) and accessory enzymes (i.e., xylanases and lytic polysaccharide monooxygenase (LPMO)

Auxiliary Activities Family 9) [303, 420, 443-445]. The accessory enzyme helps the cellulase to hydrolyze the substrate faster in a synergistic manner.

Enzymes are generally among the most expensive components of biochemical reactions. The cost of enzymes is one of the bottlenecks in LC biorefineries. For example, cellulase is estimated to account for 25.0-30.0% of the operational cost in the second generation of biorefinery [446]. Additionally, the free-state enzymes in reaction solutions have limitations in their applicability for industrial applications. These limitations include instability in reaction mixtures, lack of reusability, and sometimes low tolerance to high temperatures, pH variations, salt concentrations, metal ions, and product contamination [447-448]. Immobilization techniques help to reduce these barriers and enhance the productivity of enzymatic processes. Adsorption, covalent bonding, cross-linking, encapsulation, and entrapment methods are commonly used for enzyme immobilization [340-341, 408]. Cross-linking and covalent immobilization firmly attach enzymes to the support materials. However, in this process, the enzyme's active site may get distorted and lost by the covalent formation and, therefore, shows reduced performance of enzymes [301, 339, 345, 347].

On the other hand, encapsulation and entrapment methods provide limited interaction of the support material and the enzyme's active site, and hence, the enzyme performance is preserved. However, encapsulation and entrapment methods face the issue of enzyme leakage over the reuse cycles, and productivity decreases over time [342]. The existing knowledge about the performance of immobilized cellulolytic enzymes under high pressure and supercritical CO_2

($scCO_2$) is very limited. For example, Senyay-Oncel and Yesil-Celiktas (2015) treated cellulase immobilized on to a sodium zeolite (NaY) support material under $scCO_2$ (18.0 MPa, 54.0 °C, 2.0 h) prior to using it for hydrolysis of cellulosic substrate. The enzymatic activity was increased to 148.0 % relative to the untreated immobilized enzyme, and a 60.0 % decrease in the residual activity of the immobilized enzyme after the fourth cycle was observed compared to the first cycle [283].

The enzyme aerogels are prepared by sol-gel synthesis followed by drying using different methods, namely simple evaporation, vacuum drying, and supercritical drying which leads to different extents of the aerogel/xerogel shrinkage. The shrinkage of the aerogel/xerogels depends on the capillary contraction stress. The $scCO_2$ drying limits the capillary contraction stress due to the fluid exchange; therefore, the meso- and macropores remain abundant [449]. The aerogels possess highly mesoporous structures and are known for their low density, high porosity, and surface area [450]. Such properties of the sol-gel entrapped enzyme immobilization method offer several advantages, including biocompatibility, structural uniformity and chemical stability, low processing temperature, and non-toxic and environment-friendly immobilization material [451].

This study investigated the immobilization of cellulolytic enzyme cocktail by entrapment method into an aerogel support matrix to explore (1) the impact of $scCO_2$ on enzyme activity, (2) the reusability of immobilized enzyme, and (3) the effect of enzyme loading on morphology and performance of immobilized enzyme under atmospheric and $scCO_2$ environment. Therefore, the enzyme cocktail has

been optimized for concentration, pH, and temperature, and immobilized into silica oxide using the sol-gel entrapment method. The immobilized enzyme was also used to compare the enzyme activity under atmospheric and $scCO_2$ conditions. It is hypothesized that the immobilization of the enzyme cocktail may enhance the enzyme stability and activity under the $scCO_2$ conditions and increase the hydrolysis rate of cellulosic substrates. Furthermore, the performance of free enzymes cocktail and cocktail aerogel was investigated for enzymatic hydrolysis of water-insoluble cellulosic substrate bleached wood pulp (BWP) to determine the applicability of aerogel enzyme on insoluble cellulose in comparison to soluble cellulose. The reusability of immobilized enzymes was investigated, and the surface morphology of immobilized enzymes was characterized to elucidate the effects of the reuse of immobilized enzymes. The outcome of this study will contribute to filling a crucial knowledge gap with respect to the application of aerogel-immobilized enzymes under different hydrolysis conditions and the cellulosic substrates.

5.5. Materials and methods

5.5.1. Substrate and chemicals

Cellulase (lyophilized powder) from *Trichoderma reesei* ATCC 26921 (C8546-10KU) and cellulolytic enzyme complex Viscozyme L (crude enzyme solution) from *Aspergillus sp.* (V2010-50ML), tetramethoxysilane (TMOS), ammonium hydroxide (338818-100ML, 28.0 % solution of NH_3), and carboxymethyl cellulose (CMC, 419273-100G) were purchased from Sigma-Aldrich, Canada. Spruce wood chips were used as starting material to prepare the bleached wood pulp (BWP) by method as described in Kumar et al. (2022) [440]. Cellulase enzyme powder was

dissolved in distilled water at 15.0 mg/mL concentration. The enzymatic reactions were conducted in sodium citrate buffer (10.0 mM) of pH in the range of 3.0-6.0 with sodium hydroxide in presence of 0.002 % (w/v) sodium azide as an antimicrobial agent [411-412].

5.5.2. Analytical method

The protein content of enzyme solutions was determined by colorimetric assay using Pierce™ bicinchoninic acid (BCA) reagents (Thermo Scientific, US) using bovine serum albumin (BSA) for calibration standard curve preparation [32]. The total reducing sugars (TRS) released in the enzymatic hydrolysis reaction were determined by the 3, 5-dinitrosalicylic acid (DNS) method of sugar estimation using glucose as standard sugar [452-453]. The TRS yield was calculated using the Equation (8). The total hydrolysable sugars (THS) in the substrate CMC and BWP were determined by the NREL method of acid hydrolysis for total carbohydrate content determination in biomass.

$$TRS\ yield\ (wt.\%\ of\ THS) = \frac{total\ released\ sugar\ (mg)}{\frac{cellulose\ in\ feedstock\ (mg)}{0.9} + \frac{hemicellulose\ (mg)}{0.88}} \times 100 \quad (8)$$

$$Residual\ yield\ or\ activity\ (\%) = \frac{Sugar\ yield\ by\ pretreated\ enzyme}{Sugar\ yield\ by\ untreated\ enzyme} \times 100 \quad (10)$$

The residual yield or activity (%) in Equation (10) was used to determine the effect of different reaction conditions on the TRS yield relative to the optimum yield at atmospheric pressure conditions.

5.5.3. Chemical composition analysis of biomass and pulp

The chemical composition of bleached wood pulp (BWP) derived from spruce and CMC was analyzed using the NREL standard method for cellulose and hemicellulose sugars with modification in sugar quantification by using the DNS

method instead of HPLC method to determine the total hydrolysable sugar content in cellulosic substrates [384].

5.5.4. Enzyme immobilization

5.5.4.1. Sol-gel synthesis

The silica precursor TMOS (4.0 g) was added to 16.0 g anhydrous ethanol and stirred with a magnetic stir bar for 15 minutes. The aqueous solution of the enzyme cocktail in 10.0 mM buffer was added to the TMOS-ethanol mixture to maintain a 1:10 mol ratio of TMOS to water (Appendix: Supplementary information). The enzyme load in silica-based supports has been reported in range of 10.0-200.0 mg enzyme/g aerogel [454-455]. This study used 36.0, 72.0, and 144.0 mg enzyme cocktail/g aerogel. A 0.091 mL of 28.0 wt.% of NH_3 solution was added after 1 min stirring of enzyme and TMOS solution at 1000.0 rpm until the alcogel was formed (3.0-4.0 min). The headspace was purged with nitrogen gas to remove air and closed the vial. The vial was left at room temperature (~21.0 °C) for 24.0 h and then moved to the refrigerator (4.0 °C) for 72.0 h [456].

5.5.4.2. Supercritical CO_2 drying of gel

The aged alcogel was transferred to the $scCO_2$ reactor (Supercritical Fluid Extractor SFT-110, USA) with a 100.0 mL vessel, and the alcogel was submerged in anhydrous ethanol to avoid the evaporation of solvent from alcogel. The vessel was preheated to 40.0 °C at CO_2 tank pressure (5.5 MPa) and pressurized by pumping liquid CO_2 into the reactor. Ethanol was replaced with CO_2 during the $scCO_2$ drying process over 4.0-5.0 h. At the end of drying, the reactor was depressurized at 0.3-0.4 MPa per min (10.0 MPa in ~0.5 h). The cocktail aerogel

was recovered and dried in a vacuum oven at 35.0 °C for 2.0 h under active vacuum. Assuming all the enzymes were entrapped into the aerogel, the enzyme content (mg protein per g aerogel) was determined by the weight of the aerogel after drying. The aerogel was stored at 4.0 °C for further use in enzymatic reaction.

5.5.5. Optimization of working parameters for free and immobilized enzyme

The pH, temperature and individual enzyme concentration of the free enzyme cocktail were determined by the response surface optimization model using a pH range (3.1-5.5), temperature range (31.8-54.2 °C), cellulase (0.9-4.3 g/L), and Cellulolytic enzyme complex Viscozyme L (13.5-61.5 g/L) as described in the supplementary information (Table S9-1). The pH and temperature optima of the cocktail aerogel was determined in a range of temperature (33.0-53.0 °C) and pH (3.0-5.5) for CMC hydrolysis in a 10.0 mM sodium citrate buffer for 2.0 h. The reaction was stopped by placing the vials in boiling water for 5.0 minutes. The TRS yield was determined by DNS assay.

The effect of free enzyme cocktail and cocktail aerogel concentration in the reaction was investigated using different concentrations of free enzyme (4.1-12.3 g/L) and aerogel (7.5-45.0 g/L or equivalent free enzyme of 1.0-6.2 g/L). Further, the effect of enzyme concentration in the aerogel was investigated by immobilizing the different amounts of enzyme cocktail 36.0-144.0 mg per g aerogel during preparation. The effect of substrate concentration in the reaction was investigated using different concentrations of CMC (7.5-30.0 g/L) at optimum reaction conditions of free and immobilized enzymes.

5.5.6. Fed-batch process

The potential of the fed-batch hydrolysis reaction with intermittent introduction of substrate was investigated to compare with the batch process to explore the potential for reusing the enzyme. The reaction started with a 10.0 mL reaction mixture in a 25.0 mL flask at CMC substrate concentration of 22.5 g/L and optimum pH and temperature of free (pH 3.3, 43.0 °C) and cocktail aerogel (pH 4.0, 48.0 °C) as determined by section 2.5. A 5.0 mL of CMC solution in the same buffer was subsequently added to the reaction after reaching plateau TRS concentration.

5.5.7. Enzymatic hydrolysis of bleached wood pulp

The bleached wood pulp (BWP) is a water-insoluble cellulosic substrate derived from spruce wood. The BWP was hydrolyzed by free enzyme cocktail and cocktail aerogel under the optimum reaction conditions od CMC by substituting the CMC with BWP substrate in the reaction.

5.5.8. Enzymatic hydrolysis under supercritical CO_2

The enzymatic hydrolysis of CMC was conducted at optimum temperature, pH, substrate, and enzyme concentration under $scCO_2$ in the same reactor used for aerogel preparation in section 2.4.2. The reaction was performed at different pressures (10.0-22.0 MPa) and temperature (42.0-54.0 °C) to understand the influence of $scCO_2$ on the enzymatic reaction and compare the free to immobilized enzyme activity under atmospheric and $scCO_2$ conditions. The effect of mixing on enzymatic hydrolysis was investigated in the SFT-110 reactor equipped with MagneDrive overhead stirrer-six-bladed turbine impeller.

5.5.9. Reusability and morphological characterization of immobilized enzyme

The enzymatic hydrolysis of the CMC substrate was conducted under the optimized reaction condition of the immobilized enzyme for 72.0 h reaction per cycle under the atmospheric condition and 4.0 h per cycle under the $scCO_2$ condition. The aerogel enzyme was recovered by vacuum filtration on a 0.2 µm membrane filter, washed with buffer, and dried in a vacuum oven for 2.0 h at 35.0 °C.

The morphology of the aerogel was analyzed with a scanning electron microscope (SEM, Zeiss Sigma 300 FESEM) and Brunauer-Emmett-Teller/Barrett-Joyner-Halenda (BET/BJH) nitrogen adsorption-desorption apparatus (Micromeritics 3FLEX, GA, USA). The aerogel samples (1) aerogel with no enzyme (control), (2) Aerogel with enzyme load of 36.0, 72.0, and 144.0 mg enzyme/g aerogels before use in the reaction, (3) aerogels after three cycles of use were analyzed to understand the effect of protein load and recycling/reusing of immobilized enzyme. The SEM samples were prepared with gold sputter coating of thickness 5.0 nm and analyzed at 5.0 kV accelerating voltage.

5.5.10. Statistical analysis

All the experiments were performed using at least independent duplicates. The Data was analyzed with one-way ANOVA (analysis of variance) at 95.0 % confidence level ($p<0.05$) for statistical significance. A t-test ($P<0.05$) was used to analyze the significance of TRS yield at different reaction conditions treated under supercritical CO_2. The statistical analyses were performed in Minitab® 21.4.

5.6. Results and Discussion

5.6.1. Chemical composition of cellulosic substrates

The total hydrolysable sugars (THS) in the cellulosic substrates CMC and BWP were analyzed by the NREL method of carbohydrate content analysis, which showed that the water-soluble cellulosic substrate CMC has 38.4±0.3 g total reducing sugars per 100.0 g dry weight. The bleached wood pulp (BWP, water-insoluble) derived from wood had 108.4±0.9 g total reducing sugars per 100.0 g dry weight of BWP, which is similar to pure microcrystalline cellulose (MCC) derived from cotton linters with 103.2±4.6 g TRS per 100.0 g dry weight of MCC (Table 5-1).

Table 5-1. Composition analysis of cellulosic substrate for total reducing sugars (n=3).

Cellulose substrates	**Total hydrolysable sugars (g THS/100 g substrate)**
Carboxymethyl cellulose (CMC)	38.4±0.3
Microcrystalline cellulose (MCC)	103.2±4.6
Bleached wood pulp (BWP)	108.4±0.9

The enzyme cocktail was prepared by adding two commercially available enzymes at optimized conditions after analyzing the total protein content in the enzyme (Appendix: supplement information). The Viscozyme enzyme is a crude mixture of several enzymes, including cellulase, hemicellulases, β-glucanase, and pectinase as well as reducing sugars; therefore, the total protein and sugar concentration in the enzyme (as received) were analyzed (Table 5-2). The high concentration of sugars and other impurities in the Viscozyme crude enzyme interfered with the polymerization reaction of the sol-gel immobilized process. Therefore, the Viscozyme enzyme was filtered using Spin-X® UF Concentrators (Corning) with a molecular cutoff weight of 10.0 kDa to remove the sugar before

enzyme cocktail preparation. The filtration process removed 91.0-95.0 wt.% of the sugars and 49.0 wt.% of the protein without significant loss of enzyme activity (Appendix: Supplementary information).

Table 5-2. Commercial enzyme (as received) characterization for sugar and protein content (n=3).

Commercial enzyme	Sugar concentration	Protein concentration	Enzyme activity (FPU/g), temperature (°C), pH
Cellulase	None	1.2 ± 0.0 g dissolved protein/g enzyme powder	75.2±0.4, 46.3, 5.0
Cellulolytic complex enzyme solution (Viscozyme L)	289.7±6.8 g/L enzyme solution	210.8 ± 8.4 g/L enzyme solution	23.0±3.3, 37.4, 5.0

5.6.2. Enzyme activity

5.6.2.1. Effect of pH and temperature

The pH and temperature optima of the free enzyme cocktail were determined by the response surface optimization model, which showed the optimum activity at pH 3.3 of 10.0 mM citrate buffer and 43.5 °C temperature (Appendix: Supplementary information). The optimized cellulase concentrations (2.7 g/L) and filtered Viscozyme L (38.2 g/L) in the enzyme cocktail was immobilized into aerogel. The pH and temperature optima of cocktail aerogel was determined by conducting enzymatic hydrolysis of CMC reaction with equivalent enzyme load as the free condition in a range of pH (3.0-5.0) and temperature (33.0-53.0 °C) at 150.0 rpm of agitation speed. The optimum activity of the cocktail was found to be at pH of 4.0 and 48.0 °C, slightly higher than the free enzyme condition (Figure 5-1).

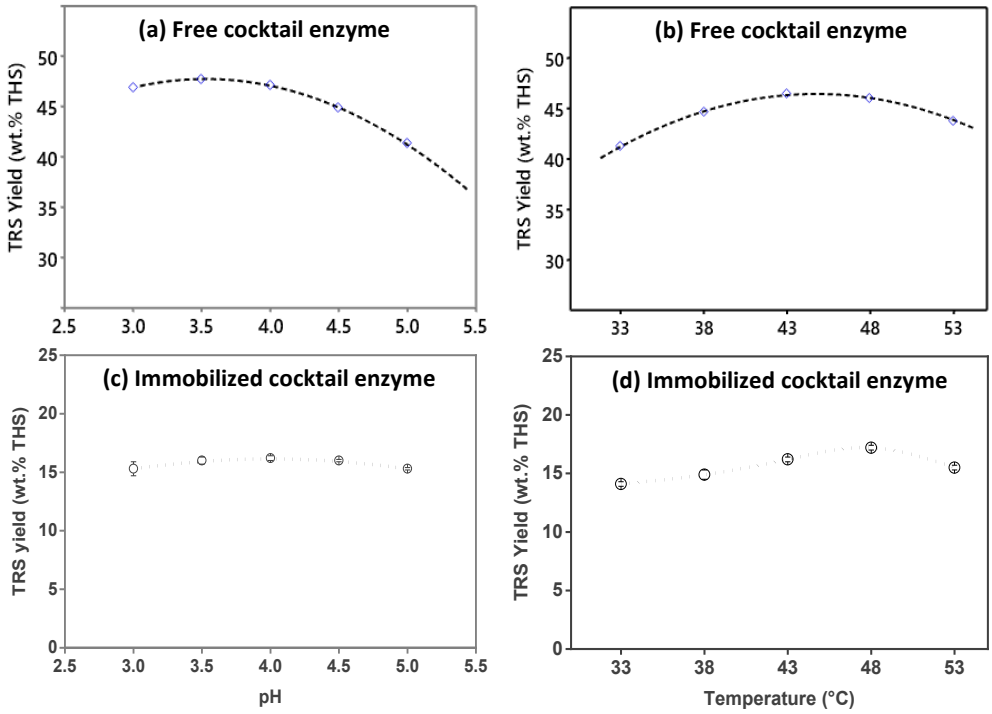

Figure 5-1. Identification of optimum pH and temperature at 4.1 g/L of free enzyme cocktail concentration (a & b) and at 29.6 g/L aerogel immobilized (equivalent 4.1 g/L free) enzyme cocktail concentration (c & d). Concentration of carboxymethyl cellulose substrate was maintained at 15.0 g/L. Reactions were done at 150 rpm for 2 h reaction time (n=3).

The optimum pH and temperature of the immobilized enzymes may vary from the free enzyme due to the protein's structural arrangement in support materials [115, 457-458]. For example, Celluclast 1.5 L (*Trichoderma reesei* CCN 03116) showed pH optimum at 4.8 and 5.0 for covalently bond immobilized and free enzyme, respectively [343]. Silica oxide immobilized Cellulase (fungus *Humicola insolens*) and free Cellulase showed optimum temperature at 40.0 °C and 30.0 °C, respectively. Optimum pH was the same for both conditions [115].

5.6.2.2. Effect of enzyme concentration

Figure *5-2*a shows that the enzyme load in aerogel linearly increased the TRS yield. However, the increase in TRS yield is economically insignificant for an increase in the amount of enzyme. The effect of enzyme load increase from 36.0

to 144.0 mg/g aerogel was investigated, which increased the TRS yield from 28.7±0.36 to 33.8±0.4 wt.% of THS at 72.0 h of enzymatic hydrolysis of CMC (Figure 5-2b and 5-2c).

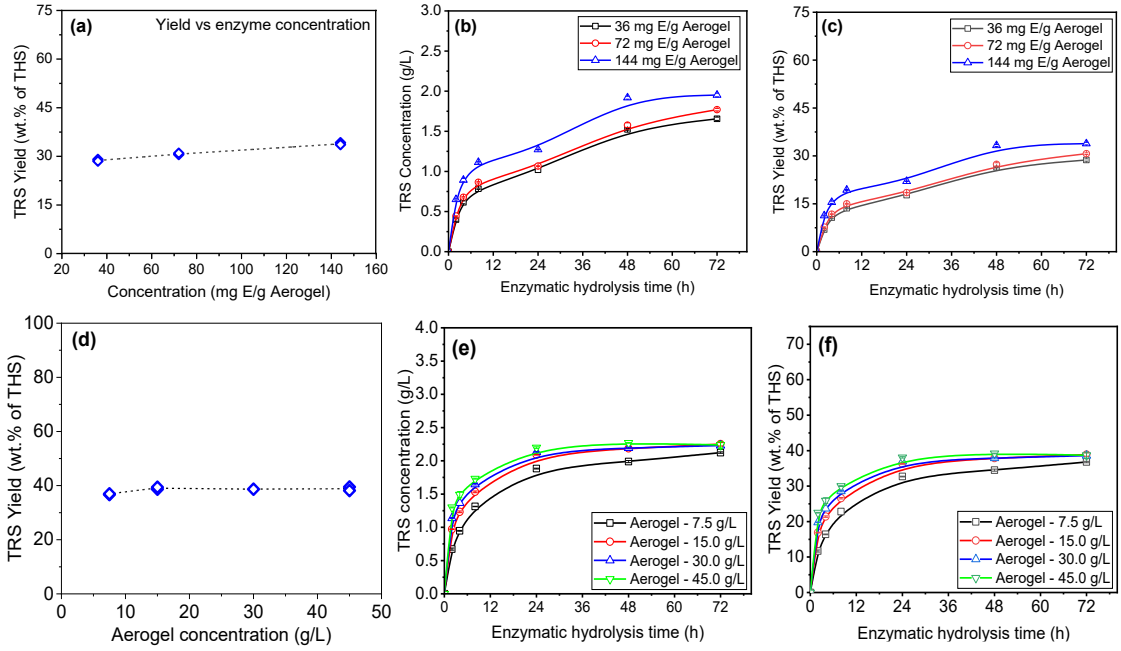

Figure 5-2. Enzymatic hydrolysis of CMC (15.0 g/L) with cocktail aerogel (15.0 g/L) where (a) Total reducing sugars (TRS) yield vs. enzyme concentration, (b) TRS concentration (c) TRS yield for varying enzyme concentration in aerogel; and (d) TRS yield vs. aerogel concentration in reaction, (e) TRS concentration and (f) TRS yield for varying aerogel concentration.

By fixing the enzyme cocktail load at 144.0 mg/g aerogel, the effect of aerogel concentration in the reaction was investigated using aerogel concentration range from 7.5 to 45.0 g/L (equivalent to 1.0 to 6.2 g/L of free enzyme concentration). Concentration of aerogel was increased from 7.5 to 15.0 g/L that led to an increase in TRS yield from 36.8±0.2 to 38.9±0.5 wt.% of THS. Further increasing the aerogel concentration from 15.0 to 45.0 g/L did not increase in the TRS yield (Figure 5-2e-f). The increase in the aerogel concentration led to an increase in the initial rate of hydrolysis, but all the aerogel concentrations reached the same yield at 72.0 h. These results suggest that a limited number of the active sites of entrapped

enzymes in the aerogel can hydrolyze the CMC substrate. Further increase in enzyme load into the aerogel or the aerogel concentration in the reaction may not be economically favorable. Therefore, 15.0 g/L aerogel (equivalent free enzyme 2.1 g/L) with an enzyme load of 144.0 mg/g aerogel was used in further investigations.

5.6.2.3. Effect of substrate concentration

The effect of substrate concentration in the reaction was investigated by using a range of substrate concentration (7.5-30.0 g/L) in the reaction and with 4.1 g/L of free enzyme cocktail or 15.0 g/L aerogel enzyme (equivalent to 2.1 g/L free enzyme). The result showed that increasing the substrate concentration from 7.5 to 30.0 g/L increased the TRS concentration from 1.5±0.1 g/L to 5.6±0.1 g/L (Figure *5-3*a) with no significant effect on corresponding TRS yield of 51.3±2.2 to 48.1±1.2 wt.% for the free enzyme cocktail (Figure *5-3*b). In the case of cocktail aerogel, TRS concentration increased from 0.9±0.0 g/L to 3.5±0.0 g/L (Figure *5-3*c) for the cocktail aerogel without any significant impact on the corresponding TRS yield (Figure 5-3d). An increase in the substrate concentration led to mass transfer limitation due to the increasing viscosity of the CMC solution. Therefore, the TRS yield slightly decreased at 30.0 g/L of CMC in reaction and further increased CMC concentration would not be beneficial under the investigated condition.

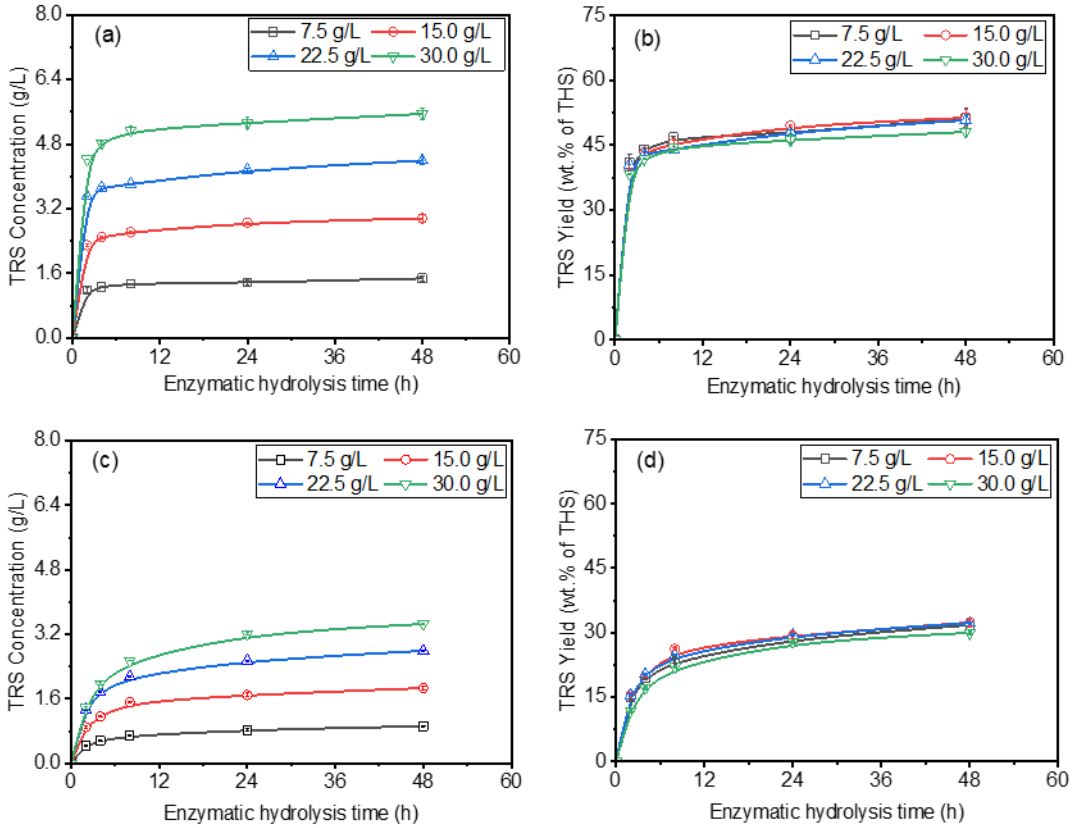

Figure 5-3. Enzymatic hydrolysis of carboxymethyl cellulose (7.5-30.0 g/L) with free (4.1 g/L) and cocktail aerogel I (15.0 g/L) where (a) Total reducing sugars (TRS) concentration & (b) TRS yield with free enzyme cocktail at pH 3.3 at 43.5 °C, and (c) TRS concentration & (d) TRS yield from cocktail aerogel at pH 4.0 and 48 °C (n=2).

Studies claim that the reduction in the hydrolysis rate is due to the β-glucosidase enzyme inhibition by the accumulation of glucose produced over time [459-460]. In contrast, Figure 5-3a and Figure 5-3c showed that the sugar concentration increased with the substrate concentration; however, the TRS yield profile did not show any substantial change (Figure 5-3b and Figure 5-3d). Further increase in substrate leads to the increased viscosity reaction solution due to the high viscosity of CMC at higher concentrations. It could lead to a decreased hydrolysis rate and TRS yield, which explains the reason that several studies used lower concentrations of CMC (2.5-10.0 g/L) in the enzymatic reaction [461-462].

These results further agree that depletion in the amorphous cellulose leaves the crystalline cellulose hydrolyzed at a slower rate than the amorphous cellulose [463].

5.6.3. Fed-batch process of CMC hydrolysis

The fed-batch processes are widely used to enhance the cumulative substrate conversion efficiency while maintaining the low viscosity in the reaction. Therefore, substrate and enzyme introduction in a fed-batch mode received attention [464-466]. In this study, the fed-batch process of enzymatic hydrolysis of CMC was started with 22.5 g/L CMC under optimized reaction conditions of free enzyme cocktail (pH 3.3, 43.0 °C) and cocktail aerogel (pH 4.0, 48.0 °C) in 10.0 mL reaction volume where all the enzyme was introduced prior to the start of reaction. CMC solution in buffer was subsequently fed at every 48 h when the hydrolysis rate decreased to plateau. The fed-batch strategy in Figure 5-4 showed that more than double the amount of the substrate was fed into the reaction compared to the batch strategy without any significant loss in the yield and the enzyme activity over the 144.0 h hydrolysis duration. The TRS yield remained in the range of 46.7-50.1 wt.% of THS for free enzyme cocktail and 32.3-34.7 wt.% for cocktail aerogel (Figure 5-4). Previous studies on the fed-batch process have reported positive, negative, or negligible effects on the yield compared to the batch process. A similar result was observed for hydrolysis of filter paper cellulose in fed-batch vs. batch operation using free cellulase. The glucose yield was 47.0-49.0 % in the fed-batch and 48.0 % in the batch operation [464]. The higher substrate loading in the batch operation could face several difficulties, including improper mixing and non-uniform enzyme availability of free and immobilized catalysts [467-468].

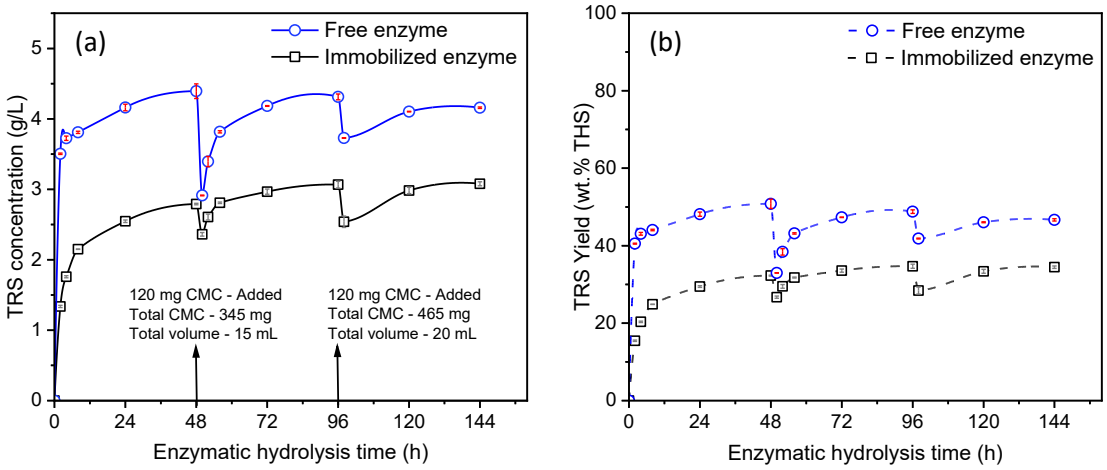

Figure 5-4. Enzymatic hydrolysis of carboxymethyl cellulose (22.5 g/L) with free (4.1 g/L) and cocktail aerogel (15.0 g/L) at their optimum pH and temperatures. (a) Total reducing sugars (TRS) concentration and (b) TRS yield in fed-batch process, reaction volume of 10 mL (n=2).

5.6.4. Comparison of enzymatic hydrolysis of CMC and BWP

The cellulosic substrates (22.5 g/L) CMC and BWP were hydrolyzed using free enzyme cocktail (enzyme conc. 4.2 g/L, pH 3.3, 43.0 °C) and cocktail aerogel (15.0 g/L, pH 4.0, 48.0 °C) under atmospheric pressure. A TRS yield of 61.1±0.3 wt.% of THS was achieved in the case of BWP hydrolysis with free enzyme cocktail, whereas only 14.8±0.1 wt.% TRS yield was obtained by cocktail aerogel in 72.0 h of hydrolysis (Figure 5-6). In comparison to the BWP substrate, a yield of 51.7±0.8 wt.% was achieved from CMC with free enzyme cocktail and 32.3±0.1 wt.% yield with the cocktail aerogel under the same reaction conditions as the BWP (Figure 5-7c-d). The substantial difference in the yields from BWP by free and immobilized enzymes could be attributed to the mass transfer limitation to the water-insoluble substrate, which might not have reached the entrapped enzyme cocktail into the porous aerogel compared to the water-soluble CMC. Due to the partial hydrolysis of BWP with aerogel, the separation of cocktail aerogel was not reusable with water-insoluble cellulosic substrate.

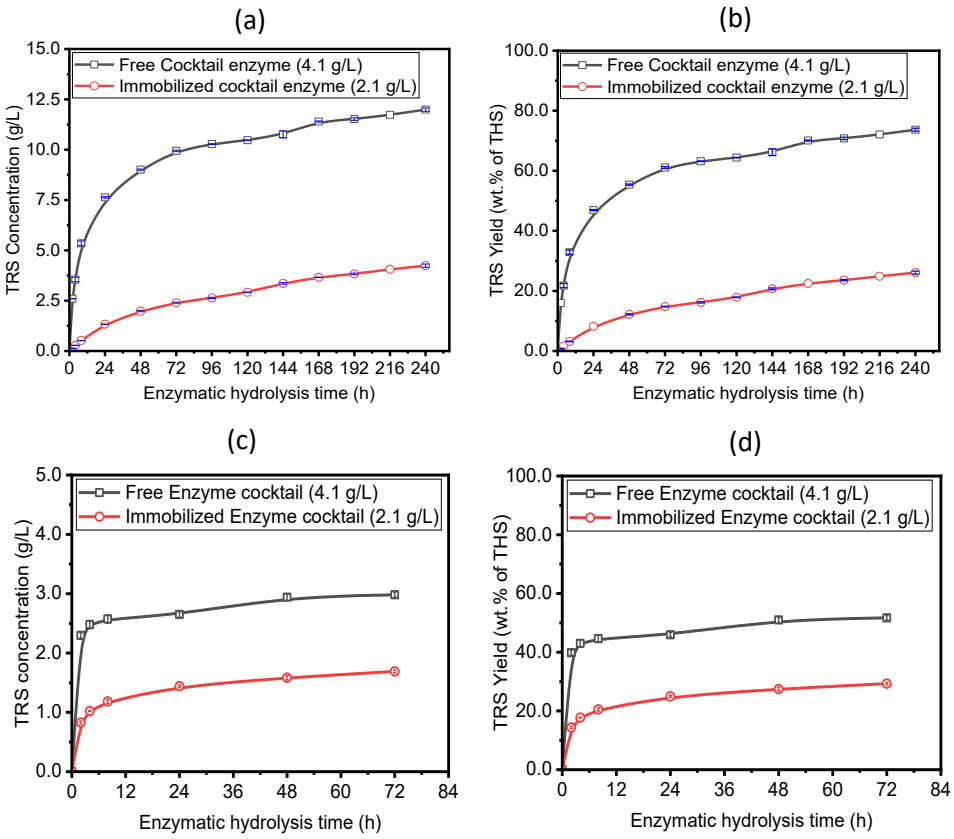

Figure 5-5. Enzymatic hydrolysis of cellulosic substrate (22.5 g/L) BWP (a & b) and carboxymethyl cellulose (c & d) with free enzyme cocktail (4.1 g/L) and cocktail aerogel (15.0 g/L) (n=3).

5.6.5. Enzymatic hydrolysis under supercritical CO_2

The enzymatic hydrolysis of CMC was further investigated under supercritical CO_2 at different pressures, temperatures, and reaction times in a batch mode. The temperature and pressure showed substantial influence on the enzyme activity. The optimum temperature remains the same as the atmospheric condition (48 °C) (Figure 5-6a). The $scCO_2$ pressure of 10.0-16.0 MPa was optimum, and a further increase in pressure reduced the enzyme activity (Figure 5-6b). The cocktail aerogel under $scCO_2$ (without mixing) showed an increased TRS yield of 27.3±2.2 wt.% at 48.0 °C and 10.0 MPa as compared to atmospheric pressure yield of 21.4±0.2 wt.% in 4.0 h reaction time (Figure 5-6c).

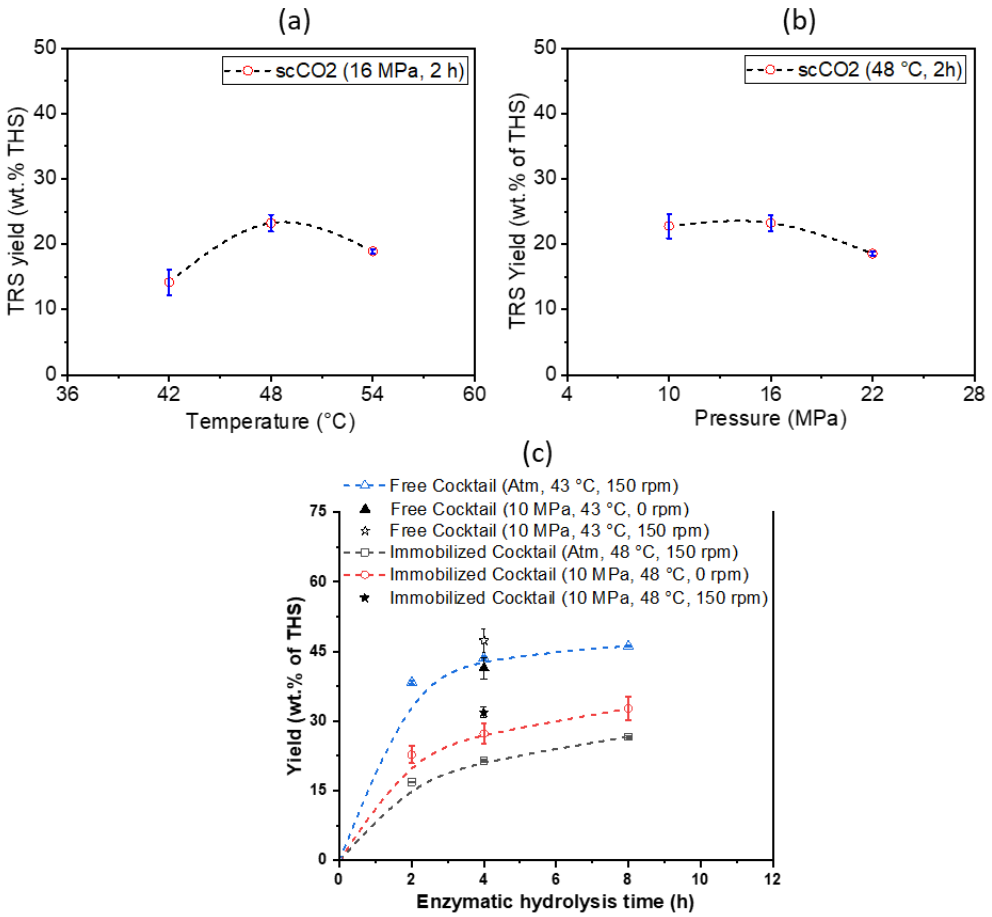

Figure 5-6. Enzymatic hydrolysis of carboxymethyl cellulose (22.5 g/L) using free enzyme cocktail (4.1 g/L) and cocktail aerogel (15.0 g/L) under $scCO_2$ where (a) effect of temperature, (b) effect of pressure and (c) hydrolysis reaction time on TRS yield in comparison with atmospheric reaction (n=2).

Additionally, the effect of mixing under the $scCO_2$ reactor was investigated in the supercritical reactor with an overhead stirrer with a six-bladed turbine impeller at 150.0 rpm at 10.0 MPa, 48.0 °C. Conducting the reaction under continuous mixing led to a higher TRS yield 32.1±1.1 wt.% compared to yield achieved under $scCO_2$ without mixing (27.3±2.2 wt.%) and atmospheric pressure reaction (21.4±0.2 wt.%) (Table 5-3). However, the BCA protein assay of the hydrolysate showed that the enzyme cocktail (27.0±3.0 % of initial enzyme in aerogel) leached out of the aerogel to the hydrolysate and it may have worked as a free enzyme (Table S9-6). The leached free enzyme cocktail led to increased yield compared

to cocktail aerogel under atmospheric condition. Additionally, there was no substantial effect on TRS yield by free enzyme cocktail under $scCO_2$ (10.0 MPa, 43.0 °C, 4.0 h) with or without mixing (Figure 5-6c and Table 5-3).

Table 5-3. Comparison of total reducing sugars (TRS) yield under different conditions of enzyme and reaction environment: free enzyme cocktail (4.1 g/L) or aerogel cocktail (15.0 g/L), carboxymethyl cellulose 22.5 g/L, 4.0 h (n=2).

Reaction condition	**Atmospheric condition**	**$scCO_2$ condition**
Free enzyme (pH 3.3, 43 °C)	43.1±0.4% (150 rpm)	41.4±2.3% (0 rpm)
Immobilized enzyme (pH 4.0, 48 °C)	23.3±0.2% (150 rpm)	27.3±2.2% (0 rpm)
Free enzyme (pH 3.3, 43 °C)	44.3±0.2% (150 rpm)	47.1±2.4% (150 rpm)
Immobilized enzyme (pH 4.0, 48 °C)	21.4±0.2% (150 rpm)	32.1±1.1% (150 rpm)

5.6.6. Reusability of immobilized enzyme aerogel

The reusability of the cocktail aerogel was investigated at an enzyme aerogel concentration of 14.8 g/L with three different loads of enzyme cocktail in the aerogel: 36.0-144 mg enzyme per g aerogel enzyme under atmospheric conditions. The reaction was conducted using CMC (15.0 g/L) at pH 4.0, 48.0 °C, and 150.0 rpm agitation speed for 72.0 h per cycle under atmospheric pressure. The TRS yield decreased from 29.3 to 10.1 wt.% after the reuse cycle of the immobilized enzyme (144 mg per g aerogel) (Figure 5-7). Cocktail aerogel retained 53.0 % residual yield after the fourth cycle and decreased below 50.0 % in the fifth cycle. The aerogel with lower enzyme concentrations (36.0 mg and 72.0 mg/g aerogel) showed a sharp decrease in the TRS yield over three cycles of reuse, and the residual yield reached <50.0 %. A similar residual yield of below 50.0 % was observed for silica aerogel entrapped cellulase, where the reaction time was 24.0 h per cycle [343]. Retention of residual yield around 50.0 % after 4 cycles is still

beneficial over the other immobilization support matrices such as polyvinyl alcohol nanofibers, which showed residual activity below 40.0 % after the fourth cycle of reuse with 0.5 h reaction time, and sodium alginate immobilized cellulase from *Bacillus subtilis* TD6, which retained 45.0 % residual yield after third cycles with reaction time 0.5 h [469-470]. The decreased residual activity could be due to several reasons, including enzyme leaching, porosity, surface area reduction, and stability over time [356, 471].

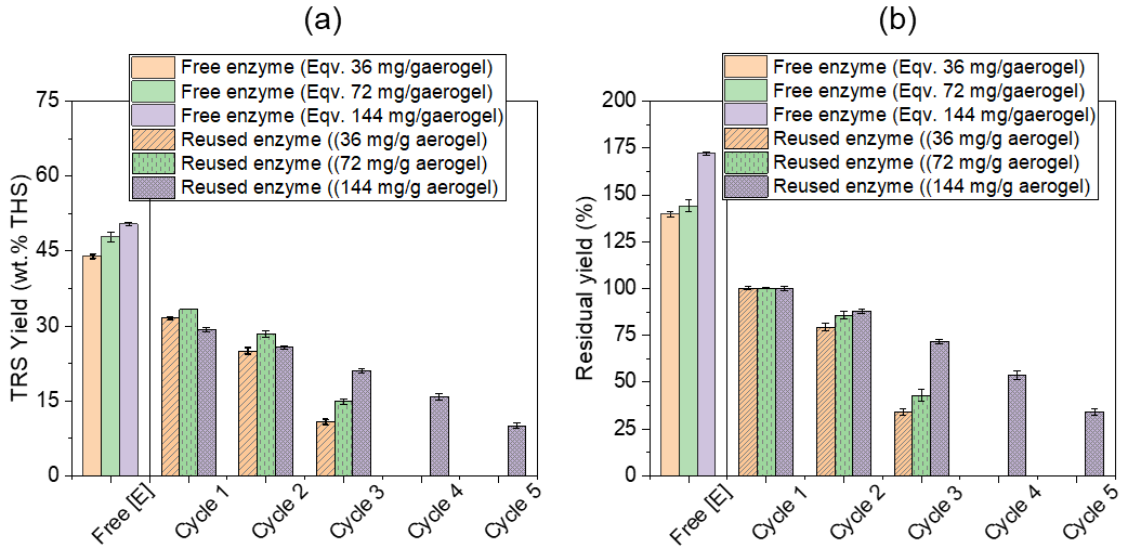

Figure 5-7. Reusability test of cocktail aerogel with carboxymethyl cellulose (15.0 g/L) for a reaction time of 72 h per cycle: (a) absolute total reducing sugars (TRS) yield and (b) residual TRS yield relative to the cycle 1 where corresponding TRS yield from free enzyme is presented in first bars.

Herein, the enzyme leaching from the aerogel could be attributed to impurities (specifically sugars) in the enzyme cocktail, which may cause improper entrapment of enzyme molecules in the aerogels. For comparison, the pure cellulase enzyme was immobilized under the same procedure at an enzyme concentration of 111.0 mg cellulase per g aerogel (Figure S9-4). The immobilized cellulase retained 64.6 % residual yield after the fifth reuse cycle compared to the first cycle. It was

consistently stable at 64.6-65.4 % residual yield in the subsequent three cycles, as shown in Figure S9-4. Although the aerogels are mesoporous, the entrapment of enzyme molecules may need further optimization for different enzymes to achieve the proper entrapment and retain the enzymes and reaction yield to facilitate the reusability of immobilized enzymes. On the other hand, reusing the cocktail aerogel under $scCO_2$ condition was not feasible under the investigated condition due to the substantial enzyme leaching. In contrast, Paljevac et al. (2007) used the aerogel-immobilized cellulase enzyme under the $scCO_2$ (10.0 MPa, 40.0 °C, 5.0 h) condition to hydrolyze the carboxymethyl cellulose (CMC) substrate. The aerogel-immobilized cellulase was used for 20.0 reuse cycles without loss of enzyme activity [115]. Compared to immobilized cellulase under atmospheric pressure (40.0 °C, 5.0 h), the reaction under $scCO_2$ (10.0 MPa, 40 °C, 5.0 h) did not significantly improve the TRS yield in the first cycle. However, over the 15.0 cycles of enzyme reuse for 5.0 h per cycle, the relative yield gradually increased to ~150.0 % [115]. However, the authors did not report the morphological characterization of the enzyme aerogels over the reuse cycles, which could have been beneficial to understanding the effects of recovery and reuse. On the other hand, there are a few studies with co-valent bonded, cross-linking methods of enzyme immobilization which have shown up to 99.0-167.0 % relative activity after with pretreatment under $scCO_2$ compared untreated immobilized enzymes including cellulase, lipase, amylase from different microorganisms [408]. Therefore, the co-valent bonding method of enzyme immobilization may be beneficial for the enzymatic reaction under high pressures including $scCO_2$ [283, 300].

5.6.7. Aerogel immobilized enzyme morphology characterization

The cocktail aerogel at different concentrations were further analyzed with SEM before and after reusing in three cycles. The aerogel surface morphology appeared more well-packed than the unused aerogels (Figure S9-5). However, visual differences among the aerogel surfaces of different enzyme concentrations were undistinguishable for significant differences. The aerogels were further analyzed with a BET/BJH instrument to measure surface area and porous volume. a-g shows that the isotherms of aerogel samples are type IV hysteresis, which is attributed to the mesoporous internal structure of the solids [472]. As enzyme concentrations were increased (0.0, 36.0, 72.0, and 144.0 mg/g aerogel), the amount of adsorbed and desorbed nitrogen gas decreased, reflected in the surface area and porous volumes in Figure 5-8h. The control aerogel with no enzyme showed the highest surface area and porous volume (Figure 5-8a). Also, the surface area and porous volume were decreased after recovering and reusing the aerogels for three cycles (Figure 5-8b-g). The leaching of enzyme molecules from the aerogel and the reduction in the porous volume and surface area caused the reduced TRS yield after the subsequent reuse of immobilized enzymes.

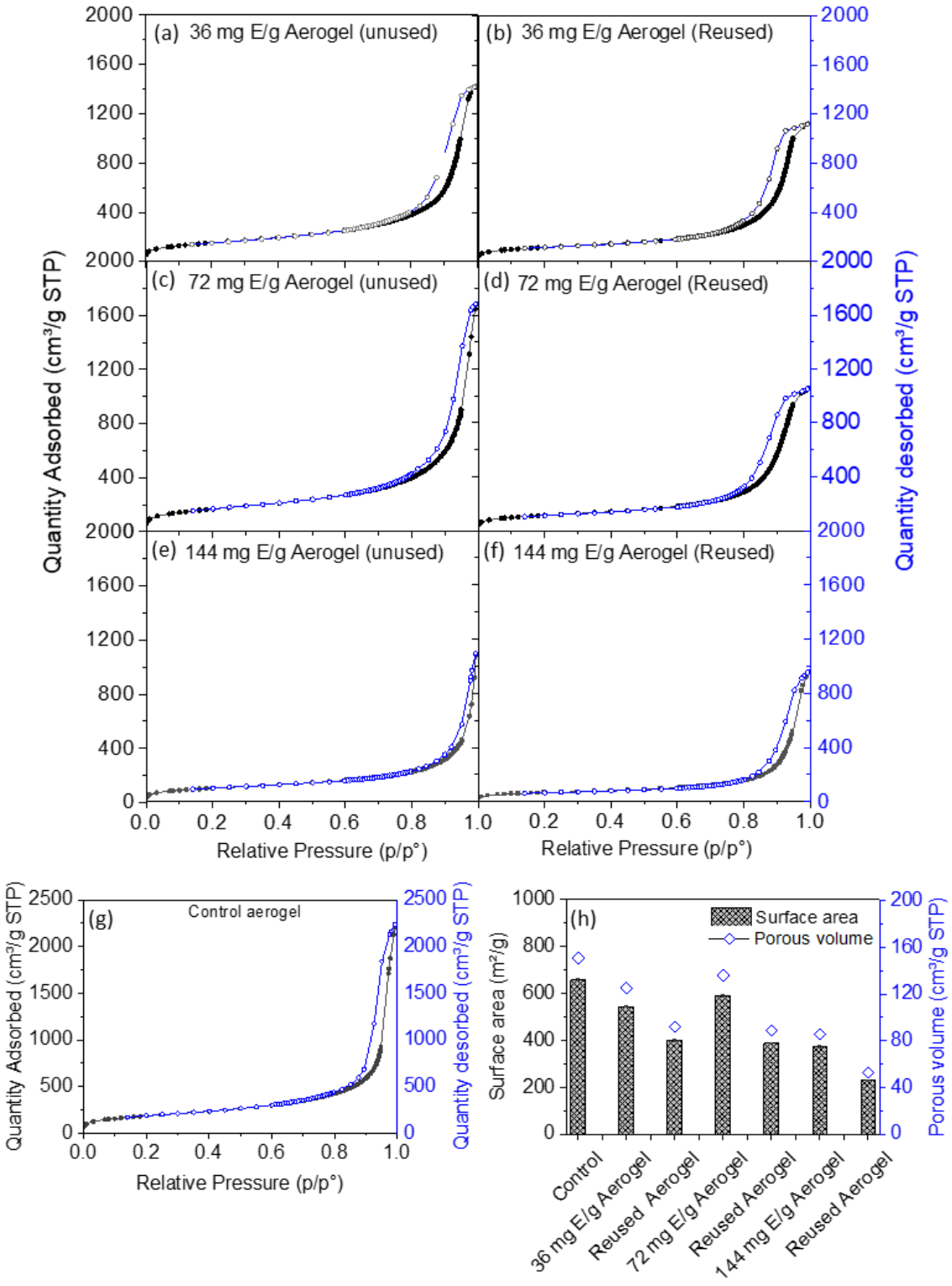

Figure 5-8. BET isotherms of enzyme cocktail aerogels unused (a, c, e) and after three reused cycles (b, d, f) and corresponding surface area and porous volume of unused and reused aerogel samples (g) and BET isotherm of control aerogel with no enzyme (h).

5.8. Conclusion

Enzyme immobilization into the aerogel support materials offers better internal mass transfer for the soluble substrates due to its high surface area and mesoporous structures. However, the soluble substrate has better reach to the active sites of the entrapped enzyme into the aerogel as it was observed in this study with carboxymethyl cellulose (CMC) which had TRS yield of 36.0±3.8 wt.% of total hydrolysable sugars (THS) with cocktail aerogel whereas water insoluble bleached wood pulp substrate had only 14.8±0.1 wt.% TRS yield of in 72.0 h under atmospheric condition. The morphological characterization of the cocktail aerogel showed that increase in enzyme concentrations reduced the porous volume and surface area of aerogel. The reuse of enzyme with enzyme concentrations 36.0-144.0 mg enzyme/g aerogel showed retention of >50.0 % residual activity after fourth cycles by 144.0 mg/g aerogel whereas lower enzyme concentrations had residual activity <50.0 % under the atmospheric pressure reactions. On the other hand, the cocktail aerogel showed significant enzyme leaching under $scCO_2$ in the first cycles and lost more than 90.0 % of the activity that implies to unsuitable conditions for aerogel entrapped enzyme under $scCO_2$ for its reusability. Furthermore, the morphological analysis of unused and reused cocktail aerogel after three cycles showed that the surface area and porous volume were decreased which may also be attributed to reduction in residual activity of enzyme over reuse cycles under atmospheric pressure. Therefore, the aerogel immobilized enzyme cocktail under investigated conditions did not result the desired outcome. The method aerogel entrapment could be further extended to optimization of

immobilization process to achieve the retention of enzyme in aerogel over the recycle process. Additionally, it is recommended to explore different methods of enzyme immobilization including co-valent bonding and cross-linking of enzyme on immobilization matrices. Additionally, use of enzymes from different sources and their characterization after treatment under pressure and $scCO_2$ would benefit future research.

5.9. Acknowledgement

The research was financially supported by an NSERC-Strategic grant [506346-2017-STPGP] and Nova Scotia Innovation Hub awarded to Dr. Satinder Kaur Brar and Dr. Azadeh Kermanshahi-pour. Pawan Kumar acknowledges scholarship support from NSERC-CREATE-ASPIRE. Support provided by Grace O'Conner, Lauren MacEachern, and Dr. Mahmoud Mirmehrabi of Solid-State Pharma Inc. to access $scCO_2$ equipment equipped with mixer is acknowledged. The BET/BJH nitrogen adsorption-desorption apparatus (Micromeritics 3FLEX, GA, USA) instrumental support from Sarah Martell and Dr. Mita Dosag at Department of chemistry, Dalhousie university is acknowledged.

CHAPTER 6 CONCLUSION

6.1. Conceptual highlights

- The cellulose pulp extracted from the acetosolv pulping-alkaline peroxide bleaching process has a threshold requirement of the acid concentration under certain temperature and treatment duration in order penetrate into the cellulose chains and hydrolyze the amorphous region. However, there should be a certain amount of sulfate group on CNCs in order to get better dispersion without having an adverse effect on their thermal stability because sulfate group catalyze the thermal degradation of CNCs.
- Ultrasonic dispersion of acid hydrolyzed cellulose pulp to individual nanocrystals depends on the extent of sulfate groups attached to the surface of CNCs. Therefore, the time and amplitude of ultrasonic treatments are critical to disperse CNCs without damaging their rod-shape morphology.
- The longer hydrolysis reaction time may reduce the product yield by individual enzyme due to several reasons such as loss of activity over time. Use of combination of enzyme with different hydrolytic action on the same substrate enhances the overall rate of reaction due to synergistic activity of enzyme.
- Deconstruction of lignin-hemicellulose network requires a certain amount of water molecules and chemical catalysts under mild to moderate reaction conditions such boiling point temperature of reaction solvent. In other case, using degradation temperature (>200 °C) of hemicellulose during pretreatment could hydrolyze the hemicellulose in presence water molecules.

Removing the lignin and hemicellulose exposes the cellulose chains to the enzyme and therefore, the enzymatic digestibility of pretreated biomass gets enhanced.

- The enzymes are biological molecules and their molecular structure vary based on the sources. Upon exposure to high pressure or supercritical CO_2, the structural rearrangement in secondary and tertiary structure affects the enzyme activity. Additionally, investigation of such changes in enzyme structure requires to analyze the individual peptide of the enzymes present in the enzyme solution.
- The presence of sugars and other components of microbial growth media interferes with the silica precursor (i.e., tetramethoxysilane) and reduces the aerogel structural stability. As a consequence, the entrapped enzyme leaches out under harsh reaction condition.

6.2. Research conclusion

The study focused on using wood biomass to produce cellulose nanocrystals (CNCs) and fermentable reducing sugars using greener and reusable chemical and biochemical methods to fill the knowledge gap and respective research questions observed in the literature review. The study's primary objective was to understand the influence of process parameters on the yield and characteristics of the targeted bioproducts. Therefore, the research objectives were divided into the following three phases. (1) Cellulose nanocrystals production, (2) pretreatment of wood and enzyme cocktail for fermentable sugar production, and (3) enzyme

cocktail immobilization into silica oxide aerogel for fermentable sugar production under atmospheric and supercritical CO_2 ($scCO_2$) conditions.

The acetosolv pulping followed by alkaline-hydrogen peroxide pretreatment of spruce wood resulted in cellulose-rich pulp with lignin content <0.7 wt.% of dry weight of the pulp. Further hydrolyzing the bleached wood pulp with sulfuric acid concentration (62-65 wt.%) produced well-individualized cellulose nanocrystals with high cellulose content and crystallinity index. The ultrasonic treatment of acid-hydrolyzed pulp released rod-like cellulose nanocrystals at high ultrasonic amplitude for a short duration (80%, 5 min) without a significant impact on the crystallinity index, whereas the lower amplitude was not enough for individualizing CNCs. Longer ultrasonic treatment led to the destruction of the rod-shaped morphology of CNCs. The physicochemical characteristics (i.e., yield, crystallinity index, purity, surface area) of CNCs produced in this study were comparable to commercial CNCs.

On the other hand, the spruce wood was pretreated with three different methods that, include acetosolv pulping-alkaline peroxide bleaching treatment, alkali-assisted ultrasonic treatment, and $scCO_2$ pretreatment for fermentable reducing sugars production by enzymatic hydrolysis of pretreated wood by a cellulolytic enzyme cocktail. The cellulolytic enzyme cocktail was developed by optimizing the enzyme concentrations and temperature and showed a synergism of 1.34 among the enzymes present in the cocktail. The ultrasound-assisted-alkali pretreatment and $scCO_2$ pretreatment had the least effect on the spruce wood. They showed a slight improvement in the total reducing sugar (TRS) yield with a

maximum of 19.5±1.0 wt.% of THS at 72.0 h for a water solid ratio of 10 (g/g) for $scCO_2$ (20 MPa, 180 °C, 1 h) and 20.0±2.8 wt.% of THS for ultrasound-assisted alkali pretreatments. In contrast, the acetosolv pulping-alkaline hydrogen peroxide pretreatment showed a TRS yield of ~95.0 wt.% in 144.0 h due to the removal of the non-cellulosic component during pretreatment. Furthermore, the $scCO_2$ pretreatment of the enzyme for a short time of 0.5-1 h did not substantially influence the enzymatic hydrolysis yield of BWP. However, the more prolonged pretreatment of the enzyme for 24 h showed a substantial reduction in the TRS yield of 6.3±1.1 wt.% THS in 24 h.

Further, the enzyme cocktail was immobilized in the silica oxide aerogel prepared by sol-gel entrapment method using $scCO_2$ drying (10 MPa, 40 C, 5 h). Three enzyme concentrations were immobilized into the aerogel (36-144 mg enzyme/g aerogel) to understand its effect on enzymatic hydrolysis reaction and aerogel morphology. Further, the aerogel was used under atmospheric and $scCO_2$ conditions to hydrolyze the water-soluble substrate carboxy methyl cellulose (CMC) and the reusability of cocktail aerogel. The results showed that the higher enzyme concentration in aerogel retained >50 % of the residual yield of the first cycle of the immobilized enzyme. In contrast, the lower enzyme concentrations in the aerogel retained <50 % residual yield after four reuse cycles. BET/BJH analysis of unused and used aerogel showed reduced surface area and porous volume after the recovery and reuse of the cocktail aerogel after three cycles under atmospheric pressure. On the other hand, the cocktail aerogel showed significant enzyme leaching under $scCO_2$ in the first cycles and lost more than 90 % of the

activity, which implies unsuitable conditions for aerogel-entrapped enzyme under $scCO_2$ for its reusability. The protein assay of the hydrolysates showed that 27 % of the initial enzyme amount in aerogel was leached out to the hydrolysate, leading to <10 % residual activity retention in the second cycle under $scCO_2$. Therefore, the aerogel entrapment method of enzyme immobilization may not be suitable for enzymatic reaction under $scCO_2$.

6.3. Future recommendations

The study showed promising results for the sustainable process development to move to large-scale production of CNCs from spruce wood under the corresponding optimization at different levels of CNCs production. The scope of this study covered only spruce wood, and therefore, there is a broad scope to study other wood biomass with high cellulosic composition. A comparative study of different wood under the developed process may add insights into the impact of the type of feedstock on CNCs yield and its physicochemical properties. The lignin component was removed and recovered up to 91 % of the initial mass in wood, which could be further studied to enhance the circularity of the biomass components under a biomass circular economy. Additionally, life cycle assessment and techno-economic analysis may further bring insights to improve CNC production's process cost and environmental sustainability in the non-conventional approach. The acid hydrolysis stage in the developed process of CNCs production could be substituted by developing an enzymatic hydrolysis process that will further improve the environmental sustainability of the process.

Using an enzyme cocktail is a synergistic approach to reduce the cost of the enzyme and improve the product yield. In this study, Cellulase from *Trichoderma reesei* ATCC 26921 and cellulolytic enzyme complex Viscozyme L (solution containing xylanases, pectinases, β-glucanase enzymes along with high concentration glucose and xylose sugars) from *Aspergillus aculeatus* were investigated. Several other commercial enzymes could also be investigated to minimize the enzyme dose per g of cellulosic substrate. The emerging study of enzyme pretreatment under high pressure and $scCO_2$ has shown varying influences on different enzymes from different microbial sources. Therefore, applying $scCO_2$ pretreatment on different enzymes will be beneficial to understanding the impact of enzyme source and structure on the outcome of $scCO_2$ pretreatment.

Further, the immobilization of enzymes is a broad area with various support matrices that could be investigated. Herein, the results showed that the aerogel-entrapped enzyme cocktail has better reusability under atmospheric pressure than the $scCO_2$ reaction condition. However, only a few enzymes (cellulase, lipase, and amylase) have been explored under $scCO_2$ reaction conditions in free state or immobilized on/in limited immobilization matrices. Therefore, there is a huge opportunity to explore the area using different immobilization support materials under high pressure and $scCO_2$ conditions with different enzymes from various sources.

Bibliography

[1] I. E. Agency, 18 August 2022 ed., **2022**.

[2] I. E. Agency, *Can be found under https://www.capp.ca/energy/world-energy-needs/#:~:text=Energy%20Consumption%20by%20the%20Numbers&text=In%20its%202019%20report%2C%20the%20IEA%20projects%20that%20by%202040,is%20forecast%20to%20increase%2024%25.* **2019**.

[3] IEA, *Retrieved on 11th May 2020 from <https://www.iea.org/data-and-statistics/?country=WORLD&fuel=Energy%20consumption&indicator=Total%20final%20consumption%20(TFC)%20by%20source>* **2019**.

[4] T. J. D. Wang, **2019**.

[5] I. R. Forecast, *retrieved in September 2019 from https://inkwoodresearch.com/reports/bio-based-chemicals-market/* **2018**.

[6] W. S. Shan Gao, and Mingxin Guo, *Industrial Biotechnology* **2020**, *16*, 13-25.

[7] J. Castilla-Archilla, V. O'Flaherty, P. N. Lens, Biorefineries: Industrial Innovation and Tendencies in *Biorefinery*, Springer, **2019**, pp. 3-35.

[8] H. A. Ruiz, R. M. Rodríguez-Jasso, B. D. Fernandes, A. A. Vicente, J. A. Teixeira, *Renewable and Sustainable Energy Reviews* **2013**, *21*, 35-51.

[9] J. Zhang, D. Cai, Y. Qin, D. Liu, X. Zhao, *Biofuels, Bioprod. Biorefin.* **2020**, *14*, 371-401.

[10] C. Park, J. Lee, *Green Chem* **2020**, *22*, 2628-2642.

[11] M. Balakrishnan, E. R. Sacia, A. T. Bell, *Green Chem* **2012**, *14*, 1626-1634.

[12] T. F. Lopes, R. Bogel-Lukasik, *Acta Innovations* **2020**, *36*, 57-63.

[13] P. Bajpai, Structure of Lignocellulosic Biomass in *Pretreatment of Lignocellulosic Biomass for Biofuel Production*, Springer Singapore, Singapore, **2016**, pp. 7-12.

[14] H. Chen, Chemical composition and structure of natural lignocellulose in *Biotechnology of lignocellulose*, Springer, **2014**, pp. 25-71.

[15] M. j. Zhao, Q.-q. Xu, G.-m. Li, Q.-z. Zhang, D. Zhou, J.-z. Yin, H.-s. Zhan, *J. Energy Chem.* **2019**, *31*, 39-45.

[16] Q. Zhang, P. Zhang, Z. J. Pei, F. Xu, D. Wang, P. Vadlani, *Renewable Energy* **2015**, *76*, 160-166.

[17] A. Toscan, A. R. C. Morais, S. M. Paixao, L. Alves, J. Andreaus, M. Camassola, A. J. P. Dillon, R. M. Lukasik, *Bioresource technology* **2017**, *224*, 639-647.

[18] S. P. Magalhães da Silva, A. R. C. Morais, R. Bogel-Łukasik, *Green Chem.* **2014**, *16*, 238-246.

[19] D. A. Cantero, C. Martínez, M. Bermejo, M. Cocero, *Green Chem.* **2015**, *17*, 610-618.

[20] J. S. Luterbacher, J. W. Tester, L. P. Walker, *Biotechnol. Bioeng.* **2010**, *107*, 451-460.

[21] T. Yewale, S. Panchwagh, S. Rajagopalan, P. B. Dhamole, R. Jain, *3 Biotech* **2016**, *6*, 75.

[22] D. H. Fockink, A. R. C. Morais, L. P. Ramos, R. M. Łukasik, *Energy* **2018**, *151*, 536-544.

[23] J. S. Luterbacher, J. W. Tester, L. P. Walker, *Biotechnol. Bioeng.* **2012**, *109*, 1499-1507.

[24] H. Zhang, S. Wu, **2015**, *90*, 1640-1645.

[25] Y. Kim, T. Kreke, N. S. Mosier, M. R. Ladisch, *Biotechnol. Bioeng.* **2014**, *111*, 254-263.

[26] Z. Wang, S. Winestrand, T. Gillgren, L. J. Jönsson, *Biomass Bioenergy* **2018**, *109*, 125-134.

[27] H. Jeong, Y.-C. Park, Y.-J. Seong, S. M. Lee, *Bioresour. Technol.* **2017**, *245*, 351-357.

[28] C. Sievers, M. B. Valenzuela-Olarte, T. Marzialetti, D. Musin, P. K. Agrawal, C. W. Jones, *Ind. Eng. Chem. Res.* **2009**, *48*, 1277-1286.

[29] M. Yang, M. Xu, Y. Nan, S. Kuittinen, M. K. Hassan, J. Vepsäläinen, D. Xin, J. Zhang, A. J. B. t. Pappinen, **2018**, *257*, 113-120.

[30] Y. Ma, Q. Xia, Y. Liu, W. Chen, S. Liu, Q. Wang, Y. Liu, J. Li, H. Yu, *ACS Omega* **2019**, *4*, 8539-8547.

[31] J. A. Melero, J. Iglesias, A. Garcia, *Energy & environmental science* **2012**, *5*, 7393-7420.

[32] J. Zakzeski, P. C. A. Bruijnincx, A. L. Jongerius, B. M. Weckhuysen, *Chemical reviews* **2010**, *110*, 3552-3599.

[33] F. Cherubini, *Energy conversion and management* **2010**, *51*, 1412-1421.

[34] J. Baruah, B. K. Nath, R. Sharma, S. Kumar, R. C. Deka, D. C. Baruah, E. Kalita, *Frontiers in Energy Research* **2018**, *6*.

[35] FAOSTAT, *Retrieved on 23rd Sept 2019 from <http://www.fao.org/faostat/en/#data/QC/visualize>* **2016**.

[36] S. Yu, J. Sun, Y. Shi, Q. Wang, J. Wu, J. Liu, *Environmental Science and Ecotechnology* **2021**, *5*, 100077.

[37] W. B. Data, *Retrieved on 23rd Sept 2019 from <https://data.worldbank.org/indicator/AG.LND.FRST.K2?end=2016&locations=FM&most_recent_value_desc=true&start=1990&type=shaded&view=chart>* **2016**.

[38] M. J. Cocero, A. Cabeza, N. Abad, T. Adamovic, L. Vaquerizo, C. M. Martinez, M. V. Pazo-Cepeda, *J. Supercrit. Fluids* **2018**, *133*, 550-565.

[39] Ž. Knez, M. K. Hrnčič, M. Čolnik, M. Škerget, *J. Supercrit. Fluids* **2018**, *133*, 591-602.

[40] P. K. Sarangi, S. Nanda, P. Mohanty, *Recent Advancements in Biofuels and Bioenergy Utilization, Vol. 232*, Springer, **2018**.

[41] S. K. Bhatia, S. S. Jagtap, A. A. Bedekar, R. K. Bhatia, A. K. Patel, D. Pant, J. Rajesh Banu, C. V. Rao, Y.-G. Kim, Y.-H. Yang, *Bioresour. Technol.* **2020**, *300*, 122724.

[42] H. Li, H. Wu, Z. Yu, H. Zhang, S. Yang, *ChemSusChem* **2020**, *13*, 3565-3582.

[43] R. Roy, M. S. Rahman, D. E. Raynie, *Current Research in Green and Sustainable Chemistry* **2020**, *3*, 100035.

[44] P. Kumar, A. Kermanshahi-pour, S. K. Brar, M. S.-L. Brooks, *Advanced Sustainable Systems* **2021**, *5*, 2000275.

[45] J. Tang, J. Sisler, N. Grishkewich, K. C. Tam, *Journal of Colloid and Interface Science* **2017**, *494*, 397-409.

[46] Q. Xu, Y. Gao, M. Qin, K. Wu, Y. Fu, J. Zhao, *Int. J. Biol. Macromol.* **2013**, *60*, 241-247.

[47] L. Rueda, B. Fernández d'Arlas, Q. Zhou, L. A. Berglund, M. A. Corcuera, I. Mondragon, A. Eceiza, *Composites Science and Technology* **2011**, *71*, 1953-1960.

[48] J. K. Jackson, K. Letchford, B. Z. Wasserman, L. Ye, W. Y. Hamad, H. M. Burt, *Int J Nanomedicine* **2011**, *6*, 321-330.

[49] H. Dong, Q. Ding, Y. Jiang, X. Li, W. Han, *Carbohydr. Polym.* **2021**, *265*, 118101.

[50] L. Li, J. Zhuang, H. Zou, J. Pang, S. Yu, *Carbohydr. Polym.* **2020**, *229*, 115533.

[51] Z. Karim, S. Afrin, Q. Husain, R. J. C. r. i. b. Danish, **2017**, *37*, 355-370.

[52] M. Rajinipriya, M. Nagalakshmaiah, M. Robert, S. Elkoun, *ACS Sustainable Chemistry & Engineering* **2018**, *6*, 2807-2828.

[53] D. M. Nascimento, J. S. Almeida, A. F. Dias, M. C. B. Figueirêdo, J. P. S. Morais, J. P. A. Feitosa, M. d. F. Rosa, *Carbohydr. Polym.* **2014**, *110*, 456-463.

[54] H. Wang, H. Xie, H. Du, X. Wang, W. Liu, Y. Duan, X. Zhang, L. Sun, X. Zhang, C. Si, *Carbohydr. Polym.* **2020**, *239*, 116233.

[55] Z. Wang, Z. Yao, J. Zhou, Y. Zhang, *Carbohydr. Polym.* **2017**, *157*, 945-952.

[56] Z. Liu, X. Li, W. Xie, H. Deng, *Carbohydr. Polym.* **2017**, *173*, 353-359.

[57] F. I. Ditzel, E. Prestes, B. M. Carvalho, I. M. Demiate, L. A. Pinheiro, *Carbohydr. Polym.* **2017**, *157*, 1577-1585.

[58] S. Dong, M. J. Bortner, M. Roman, *Ind. Crops Prod.* **2016**, *93*, 76-87.

[59] D. V. Savant, R. Abdul-Rahman, D. R. Ranade, *Bioresour. Technol.* **2006**, *97*, 1092-1104.

[60] S. Agnihotri, I. A. Johnsen, M. S. Bøe, K. Øyaas, S. Moe, *Wood Science and Technology* **2015**, *49*, 881-896.

[61] A. Johansson, O. Aaltonen, P. Ylinen, *Biomass* **1987**, *13*, 45-65.

[62] T. Shui, S. Feng, Z. Yuan, T. Kuboki, C. Xu, *Bioresour. Technol.* **2016**, *218*, 953-961.

[63] J. Zhang, D. Cai, Y. Qin, D. Liu, X. Zhao, **2020**, *14*, 371-401.

[64] T. Saito, S. Kimura, Y. Nishiyama, A. Isogai, *Biomacromolecules* **2007**, *8*, 2485-2491.

[65] A. Serra, I. González, H. Oliver-Ortega, Q. Tarrès, M. Delgado-Aguilar, P. Mutjé, *Polymers* **2017**, *9*, 557.

[66] S. Elazzouzi-Hafraoui, Y. Nishiyama, J.-L. Putaux, L. Heux, F. Dubreuil, C. Rochas, *Biomacromolecules* **2008**, *9*, 57-65.

[67] M. A. Gallardo-Sánchez, T. Diaz-Vidal, A. B. Navarro-Hermosillo, E. B. Figueroa-Ochoa, R. Ramirez Casillas, J. Anzaldo Hernández, L. C. Rosales-Rivera, J. F. A. Soltero Martínez, S. García Enríquez, E. R. Macías-Balleza, *Nanomaterials* **2021**, *11*, 520.

[68] Y. Guo, Y. Zhang, D. Zheng, M. Li, J. Yue, *Int. J. Biol. Macromol.* **2020**, *163*, 927-933.

[69] R. Berry, A. Granger.(Celluforce Inc., Montreal (CA)).**2014**

[70] K. Rajan, A. Djioleu, G. Kandhola, N. Labbé, J. Sakon, D. J. Carrier, J.-W. Kim, *Cellulose* **2020**, *27*, 3693-3706.

[71] L. P. Novo, J. Bras, A. García, N. Belgacem, A. A. d. S. Curvelo, *Ind. Crops Prod.* **2016**, *93*, 88-95.

[72] L. P. Novo, J. Bras, A. García, N. Belgacem, A. A. S. Curvelo, *ACS Sustainable Chem. Eng.* **2015**, *3*, 2839-2846.

[73] A. Romaní, G. Garrote, J. L. Alonso, J. C. Parajó, *Bioresour. Technol.* **2010**, *101*, 8706-8712.

[74] A. Singh, R. M. Rodríguez Jasso, K. D. Gonzalez-Gloria, M. Rosales, R. Belmares Cerda, C. N. Aguilar, R. R. Singhania, H. A. Ruiz, *Bioresource Technology Reports* **2019**, *7*, 100257.

[75] F. Regis, A. H. A. Monteverde, D. Fino, *Energy* **2023**, *274*, 127318.

[76] P. Alvira, E. Tomás-Pejó, M. Ballesteros, M. Negro, *Bioresour. Technol.* **2010**, *101*, 4851-4861.

[77] E. Smullen, J. Finnan, D. Dowling, P. Mulcahy, *Renewable Energy* **2019**, *142*, 527-534.

[78] S. Sun, S. Sun, X. Cao, R. J. B. t. Sun, **2016**, *199*, 49-58.

[79] B. Kumar, N. Bhardwaj, K. Agrawal, V. Chaturvedi, P. Verma, *Fuel Processing Technology* **2020**, *199*, 106244.

[80] J. Singh, M. Suhag, A. Dhaka, *Carbohydr. Polym.* **2015**, *117*, 624-631.

[81] S. G. Allen, D. Schulman, J. Lichwa, M. J. Antal, E. Jennings, R. Elander, *Ind. Eng. Chem. Res.* **2001**, *40*, 2352-2361.

[82] S. J. Horn, V. G. Eijsink, *Bioscience, biotechnology, and biochemistry* **2010**, *74*, 1157-1163.

[83] N. Jacquet, N. Quievy, C. Vanderghem, S. Janas, C. Blecker, B. Wathelet, J. Devaux, M. Paquot, *Polymer Degradation and Stability* **2011**, *96*, 1582-1588.

[84] R. Martín-Sampedro, M. Eugenio, J. García, F. Lopez, J. Villar, M. Diaz, *Biomass Bioenergy* **2012**, *42*, 97-106.

[85] A. Goshadrou, K. Karimi, M. J. Taherzadeh, in *WREC11 World Renewable Energy Conference 2011, Linköping, Sweden*, Linköping University Electronic Press, **2011**, pp. 1-7.

[86] T. Marzialetti, M. B. Valenzuela Olarte, C. Sievers, T. J. Hoskins, P. K. Agrawal, C. W. Jones, *Ind. Eng. Chem. Res.* **2008**, *47*, 7131-7140.

[87] D. Salvi, G. Aita, D. Robert, V. Bazan, *Journal of Industrial Microbiology and Biotechnology* **2010**, *37*, 27.

[88] X. b. Zhao, L. Wang, D. h. Liu, *Journal of Chemical Technology & Biotechnology: International Research in Process, Environmental & Clean Technology* **2007**, *82*, 1115-1121.

[89] T. Fernandes, G. K. Bos, G. Zeeman, J. Sanders, J. Van Lier, *Bioresour. Technol.* **2009**, *100*, 2575-2579.

[90] L. J. Jönsson, C. Martín, *Bioresour. Technol.* **2016**, *199*, 103-112.

[91] S. Ethaib, R. Omar, S. M. Kamal, D. A. Biak, *Journal of Engineering Science and Technology* **2015**, *2*, 97-109.

[92] N. Narayana Swamy, *Master Thesis*, Ohio University **2010**.

[93] L. D. Serna, C. O. Alzate, C. C. Alzate, *Bioresour. Technol.* **2016**, *199*, 113-120.

[94] A. R. Morais, A. M. da Costa Lopes, R. Bogel-Łukasik, *Chemical reviews* **2014**, *115*, 3-27.

[95] T. Gu, Pretreatment of lignocellulosic biomass using supercritical carbon dioxide as a green solvent in *Green Biomass Pretreatment for Biofuels Production*, Springer, **2013**, pp. 107-125.

[96] J. Zheng, L. Rehmann, *Int. J. Mol. Sci.* **2014**, *15*, 18967-18984.

[97] M. Beroual, L. Boumaza, O. Mehelli, D. Trache, A. F. Tarchoun, K. Khimeche, *Journal of Polymers and the Environment* **2021**, *29*, 130-142.

[98] F. Jiang, Y.-L. Hsieh, *Carbohydr. Polym.* **2015**, *122*, 60-68.

[99] S. V. Vassilev, D. Baxter, L. K. Andersen, C. G. Vassileva, *Fuel* **2013**, *105*, 40-76.

[100] M. Rosa, E. Medeiros, J. Malmonge, K. Gregorski, D. Wood, L. Mattoso, G. Glenn, W. Orts, S. Imam, *Carbohydr. Polym.* **2010**, *81*, 83-92.

[101] D. Tian, N. Zhong, J. Leung, F. Shen, J. Hu, J. N. Saddler, *ACS Applied Bio Materials* **2020**, *3*, 2201-2208.

[102] A. Bhatnagar, M. Sain, *Journal of Reinforced Plastics and Composites* **2005**, *24*, 1259-1268.

[103] P. Lu, Y.-L. Hsieh, *Carbohydr. Polym.* **2012**, *87*, 564-573.

[104] Y. Li, Y. Liu, W. Chen, Q. Wang, Y. Liu, J. Li, H. J. G. C. Yu, **2016**, *18*, 1010-1018.

[105] M. Hingsamer, G. Jungmeier, Biorefineries in *The role of bioenergy in the bioeconomy*, Elsevier, **2019**, pp. 179-222.

[106] H. Zhang, S. Wu, *J. Chem. Technol. Biotechnol.* **2015**, *90*, 1640-1645.

[107] F. M. Relvas, A. R. C. Morais, R. Bogel-Lukasik, *J. Supercrit. Fluids* **2015**, *99*, 95-102.

[108] H. Zhang, S. Wu, *Bioresour. Technol.* **2013**, *149*, 546-550.

[109] M. Gao, F. Xu, S. Li, X. Ji, S. Chen, D. Zhang, *Biosystems Engineering* **2010**, *106*, 470-475.

[110] R. Alinia, S. Zabihi, F. Esmaeilzadeh, J. F. Kalajahi, *Biosystems Engineering* **2010**, *107*, 61-66.

[111] D. T. Phan, C.-S. Tan, *Bioresour. Technol.* **2014**, *167*, 192-197.

[112] K. H. Kim, J. Hong, *Bioresour. Technol.* **2001**, *77*, 139-144.

[113] M. J. Eisenmenger, J. I. Reyes-De-Corcuera, *Enzyme Microb. Technol.* **2009**, *45*, 331-347.

[114] M. Paljevac, M. Primožič, M. Habulin, Z. Novak, Ž. Knez, *J. Supercrit. Fluids* **2007**, *43*, 74-80.

[115] M. Paljevac, M. Primožič, M. Habulin, Z. Novak, Ž. Knez, *The Journal of Supercritical Fluids* **2007**, *43*, 74-80.

[116] A. K. Kumar, S. Sharma, *Bioresources and bioprocessing* **2017**, *4*, 7.

[117] H. K. Sharma, C. Xu, W. Qin, *Waste Biomass Valorization* **2019**, *10*, 235-251.

[118] A. W. Bhutto, K. Qureshi, K. Harijan, R. Abro, T. Abbas, A. A. Bazmi, S. Karim, G. Yu, *Energy* **2017**, *122*, 724-745.

[119] J. D. McMillan, in *National Renewable Energy Lab., Golden*, National Renewable Energy Lab., Golden, CO, United States, **1992**, p. 48.

[120] I. J. Kim, H. J. Lee, I.-G. Choi, K. H. Kim, *Applied Microbiology and Biotechnology* **2014**, *98*, 8469-8480.

[121] M. G. Resch, B. S. Donohoe, J. O. Baker, S. R. Decker, E. A. Bayer, G. T. Beckham, M. E. Himmel, *Energy & Environmental Science* **2013**, *6*, 1858-1867.

[122] P. Phanthong, P. Reubroycharoen, X. Hao, G. Xu, A. Abudula, G. Guan, *Carbon Resources Conversion* **2018**, *1*, 32-43.

[123] F. Hemmati, S. M. Jafari, R. A. Taheri, *Int. J. Biol. Macromol.* **2019**, *137*, 374-381.

[124] T. Yang, Y. Guo, N. Gao, X. Li, J. Zhao, *Carbohydr. Polym.* **2020**, *234*, 115862.

[125] S. Zhang, F. Zhang, L. Jin, B. Liu, Y. Mao, Y. Liu, J. Huang, *Cellulose* **2019**, *26*, 5177-5185.

[126] M. Shoda, Y. Sugano, *Biotechnology and bioprocess engineering* **2005**, *10*, 1-8.

[127] M. Martínez-Sanz, P. Lopez-Sanchez, M. J. Gidley, E. P. Gilbert, *Cellulose* **2015**, *22*, 1541-1563.

[128] H. Ullah, H. A. Santos, T. Khan, *Cellulose* **2016**, *23*, 2291-2314.

[129] D. Trache, A. F. Tarchoun, M. Derradji, T. S. Hamidon, N. Masruchin, N. Brosse, M. H. Hussin, *Frontiers in Chemistry* **2020**, *8*, 392.

[130] Y. Chu, Y. Sun, W. Wu, H. Xiao, *Carbohydr. Polym.* **2020**, *250*, 116892.

[131] A. Dufresne, *Materials today* **2013**, *16*, 220-227.

[132] C. P. Staff*, Vol. 2023*, **2010**.

[133] P. a. P. C. Staff, in *Pulp and Paper canada*, Annex Business Media, **2012**.

[134] F. Markets, **2019**.

[135] A. Bhattacharya, (Ed.: A. Bhattacharya), IMARC Services Pvt Ltd., India, **2023**.

[136] S. K. Maity, *Renewable Sustainable Energy Rev.* **2015**, *43*, 1427-1445.

[137] V. P. Soudham, D. Rodriguez, G. J. M. Rocha, M. J. Taherzadeh, C. Martin, *Forestry studies in China* **2011**, *13*, 64-70.

[138] R. O. Almeida, A. Moreira, D. Moreira, M. E. Pina, M. G. Carvalho, M. G. Rasteiro, J. A. Gamelas, *RSC Adv.* **2022**, *12*, 3979-3989.

[139] M. A. Alio, O.-C. Tugui, C. Vial, A. Pons, *Bioresour. Technol.* **2019**, *276*, 170-176.

[140] P. Heidarian, T. Behzad, M. J. C. Sadeghi, **2017**, *24*, 3323-3339.

[141] W. Chen, H. Yu, Y. Liu, P. Chen, M. Zhang, Y. Hai, *Carbohydr. Polym.* **2011**, *83*, 1804-1811.

[142] K. Abe, S. Iwamoto, H. J. B. Yano, **2007**, *8*, 3276-3278.

[143] T. Yang, X. Li, Y. Guo, J. Zhao, Y. Qu, *Carbohydr. Polym.* **2023**, *301*, 120291.

[144] G. A. Siqueira, I. K. R. Dias, V. Arantes, *Int. J. Biol. Macromol.* **2019**, *133*, 1249-1259.

[145] Z. Shang, X. An, F. T. Seta, M. Ma, M. Shen, L. Dai, H. Liu, Y. Ni, *Carbohydr. Polym.* **2019**, *222*, 115037.

[146] Z. Li, D. Xie, W. Zhu, H. Wang, T. Ouyang, J. Sun, Y. Wu, F. Cheng, *iScience* **2023**, *26*, 105771.

[147] Y. Habibi, L. A. Lucia, O. J. J. C. r. Rojas, **2010**, *110*, 3479-3500.

[148] H. Sadeghifar, I. Filpponen, S. P. Clarke, D. F. Brougham, D. S. Argyropoulos, *Journal of materials science* **2011**, *46*, 7344-7355.

[149] H. Yu, Z. Qin, B. Liang, N. Liu, Z. Zhou, L. Chen, *Journal of Materials Chemistry A* **2013**, *1*, 3938-3944.

[150] S. Camarero Espinosa, T. Kuhnt, E. J. Foster, C. Weder, *Biomacromolecules* **2013**, *14*, 1223-1230.

[151] T. Gabriel, A. Belete, F. Syrowatka, R. H. H. Neubert, T. Gebre-Mariam, *Int. J. Biol. Macromol.* **2020**, *158*, 1248-1258.

[152] C. Wu, D. J. McClements, M. He, L. Zheng, T. Tian, F. Teng, Y. Li, *Carbohydr. Polym.* **2021**, *255*, 117364.

[153] L. Segal, J. J. Creely, A. E. Martin, C. M. Conrad, *Textile Research Journal* **1959**, *29*, 786-794.

[154] A. Thygesen, J. Oddershede, H. Lilholt, A. B. Thomsen, K. Ståhl, *Cellulose* **2005**, *12*, 563.

[155] S. Rashid, H. Dutta, *Ind. Crops Prod.* **2020**, *154*, 112627.

[156] A. Mandal, D. Chakrabarty, *Carbohydr. Polym.* **2011**, *86*, 1291-1299.

[157] R. Hernández Pérez, R. Salgado Delgado, A. Olarte Paredes, A. Salgado Delgado, E. García Hernández, A. Medrano Valis, F. Martínez Candia, *Journal of Nanotechnology* **2022**, *2022*, 5882113.

[158] V. A. Barbash, O. V. Yaschenko, O. M. Shniruk, *Nanoscale Research Letters* **2017**, *12*, 241.

[159] E. F. Sucinda, M. S. Abdul Majid, M. J. M. Ridzuan, M. T. H. Sultan, A. G. Gibson, *Int. J. Biol. Macromol.* **2020**, *155*, 241-248.

[160] A. L. M. P. Leite, C. D. Zanon, F. C. Menegalli, *Carbohydr. Polym.* **2017**, *157*, 962-970.

[161] N. B. Machado, J. P. Miguez, I. C. A. Bolina, A. B. Salviano, R. A. B. Gomes, O. L. Tavano, J. H. H. Luiz, P. W. Tardioli, É. C. Cren, A. A. Mendes, *Enzyme Microb. Technol.* **2019**, *128*, 9-21.

[162] Y. Xu, A. Atrens, J. R. Stokes, *Advances in Colloid and Interface Science* **2020**, *275*, 102076.

[163] E. C. Lengowski, E. A. Bonfatti Júnior, M. M. N. Kumode, M. E. Carneiro, K. G. Satyanarayana, Nanocellulose-Reinforced Adhesives for Wood-Based Panels in *Sustainable Polymer Composites and Nanocomposites* (Eds.: Inamuddin, S. Thomas, R. Kumar Mishra, A. M. Asiri), Springer International Publishing, Cham, **2019**, pp. 1001-1025.

[164] B. Li, C. Wu, Y. Zhang, X. Cao, Z. Luo, *Journal of Macromolecular Science, Part B* **2020**, *59*, 223-234.

[165] Y. Li, L. Cao, L. Li, C. Yang, *Journal of Hazardous Materials* **2015**, *289*, 140-148.

[166] J. Li, R. Cha, K. Mou, X. Zhao, K. Long, H. Luo, F. Zhou, X. Jiang, *Advanced Healthcare Materials* **2018**, *7*, 1800334.

[167] H. Zhang, Y. She, S. Song, Q. Lang, J. Pu, *Journal of Adhesion Science and Technology* **2013**, *27*, 1023-1031.

[168] B. Thomas, M. C. Raj, A. K. B, R. M. H, J. Joy, A. Moores, G. L. Drisko, C. Sanchez, *Chemical reviews* **2018**, *118*, 11575-11625.

[169] A. L. Menas, N. Yanamala, M. T. Farcas, M. Russo, S. Friend, P. M. Fournier, A. Star, I. Iavicoli, G. V. Shurin, U. B. Vogel, *Chemosphere* **2017**, *171*, 671-680.

[170] L. Bacakova, J. Pajorova, M. Bacakova, A. Skogberg, P. Kallio, K. Kolarova, V. Svorcik, in *Nanomaterials, Vol. 9*, **2019**.

[171] G. M. A. Ndong Ntoutoume, R. Granet, J. P. Mbakidi, F. Brégier, D. Y. Léger, C. Fidanzi-Dugas, V. Lequart, N. Joly, B. Liagre, V. Chaleix, V. Sol, *Bioorganic & Medicinal Chemistry Letters* **2016**, *26*, 941-945.

[172] W. Zhu, M. Han, D. Kim, J. Park, H. Choi, G. Kwon, J. You, S. Li, T. Park, J. Kim, *Journal of Water Process Engineering* **2023**, *53*, 103620.

[173] A. Zaman, J. T. Orasugh, P. Banerjee, S. Dutta, M. S. Ali, D. Das, A. Bhattacharya, D. Chattopadhyay, *Carbohydr. Polym.* **2020**, *246*, 116661.

[174] P. Manzanares, *Acta Innovations* **2020**, *37*, 47-56.

[175] P. Cheali, J. A. Posada, K. V. Gernaey, G. Sin, *Biomass Bioenergy* **2015**, *75*, 282-300.

[176] M. Li, X. Yang, T. Lu, L. Zhou, *J. Chem. Technol. Biotechnol.* **2020**, *95*, 2237-2242.

[177] D. V. Kazachkin, M. Colakyan, F. J. Moesler.(Renmatix, Inc.).US.8,999,065, **2015**

[178] FAOSTAT, in *Can be found under* http://www.fao.org/faostat/en/#data/QC/visualize, FAOSTAT, **2016**.

[179] H. Xu, J. Peng, Y. Kong, Y. Liu, Z. Su, B. Li, X. Song, S. Liu, W. Tian, *Bioresour. Technol.* **2020**, *310*, 123416.

[180] A. M. da Costa Lopes, R. M. G. Lins, R. A. Rebelo, R. M. Łukasik, *Green Chem.* **2018**, *20*, 4043-4057.

[181] T. Gu, M. A. Held, A. Faik, *Environ. Technol.* **2013**, *34*, 1735-1749.

[182] G. Zang, A. Shah, C. Wan, *Biofuels, Bioproducts and Biorefining* **2020**, *14*, 326-343.

[183] C. Florindo, F. Lima, B. D. Ribeiro, I. M. Marrucho, *Current Opinion in Green and Sustainable Chemistry* **2019**, *18*, 31-36.

[184] J. T. Gorke, F. Srienc, R. J. Kazlauskas, *Chemical Communications* **2008**, 1235-1237.

[185] X. Hou, Z. Wang, J. Sun, M. Li, S. Wang, K. Chen, Z. Gao, *Bioresour. Technol.* **2019**, *272*, 99-104.

[186] X.-J. Shen, J.-L. Wen, Q.-Q. Mei, X. Chen, D. Sun, T.-Q. Yuan, R.-C. Sun, *Green Chem.* **2019**, *21*, 275-283.

[187] P. Weerachanchai, J.-M. Lee, *Journal of Industrial and Engineering Chemistry* **2017**, *49*, 122-132.

[188] T. Reyes, S. Bandyopadhyay, B. McCoy, *J. Supercrit. Fluids* **1989**, *2*, 80-84.

[189] J. Bludworth, F. C. Knopf, *J. Supercrit. Fluids* **1993**, *6*, 249-254.

[190] T. Wu, B. Han, Supercritical carbon dioxide (CO_2) as green solvent in *Innovations in Green Chemistry and Green Engineering*, Springer, **2013**, pp. 297-326.

[191] S. Kilambi, K. L. Kadam.(Renmatix Inc.).US.10,053,745, **2015**

[192] Ž. Knez, E. Markočič, M. Leitgeb, M. Primožič, M. K. Hrnčič, M. Škerget, *Energy* **2014**, *77*, 235-243.

[193] A. Baiker, *Chemical reviews* **1999**, *99*, 453-474.

[194] P. E. Savage, S. Gopalan, T. I. Mizan, C. J. Martino, E. E. Brock, *AIChE J.* **1995**, *41*, 1723-1778.

[195] E. J. Beckman, *J. Supercrit. Fluids* **2004**, *28*, 121-191.

[196] Y. Medina-Gonzalez, S. Camy, J.-S. Condoret, *International Journal of Sustainable Engineering* **2012**, *5*, 47-65.

[197] L. Motamedi, *RIZA Werkdocument No. 96.072X retrieved on 22 April 2020 from <https://www.rijkswaterstaat.nl/rws/riza/spaportaal/Documenten/Droge_productie/drogechemie_verkenning.pdf>* **1996**.

[198] A. Kruse, H. Vogel, *Chemical Engineering & Technology: Industrial Chemistry-Plant Equipment-Process Engineering-Biotechnology* **2008**, *31*, 23-32.

[199] A. Kruse, H. Vogel, *Chemical Engineering & Technology: Industrial Chemistry-Plant Equipment-Process Engineering-Biotechnology* **2008**, *31*, 1391-1395.

[200] G. Brunner, *Annu. Rev. Chem. Biomol. Eng.* **2010**, *1*, 321-342.

[201] W. E. Rudzinski, T. M. Aminabhavi, *Energy Fuels* **2000**, *14*, 464-475.

[202] D. Wen, H. Jiang, K. Zhang, *Prog. Nat. Sci.* **2009**, *19*, 273-284.

[203] F. Temelli, O. N. Ciftci, *J. Supercrit. Fluids* **2015**, *96*, 77-85.

[204] M. K. Akalın, K. Tekin, S. Karagöz, *Environmental Chemistry Letters* **2017**, *15*, 29-41.

[205] Y. Liu, Y. Nie, X. Lu, X. Zhang, H. He, F. Pan, L. Zhou, X. Liu, X. Ji, S. Zhang, *Green Chem.* **2019**, *21*, 3499-3535.

[206] R. Gallego, M. Bueno, M. Herrero, *TrAC Trends in Analytical Chemistry* **2019**, *116*, 198-213.

[207] K. Zhang, Z. Pei, D. J. B. t. Wang, *Bioresour. Technol.* **2016**, *199*, 21-33.

[208] W.-C. Tu, J. P. Hallett, *Current Opinion in Green and Sustainable Chemistry* **2019**, *20*, 11-17.

[209] J. C. Solarte-Toro, J. M. Romero-García, J. C. Martínez-Patiño, E. Ruiz-Ramos, E. Castro-Galiano, C. A. J. R. Cardona-Alzate, S. E. Reviews, *Renewable Sustainable Energy Rev.* **2019**, *107*, 587-601.

[210] S. Wang, L. Copeland, *Crit. Rev. Food Sci. Nutr.* **2015**, *55*, 1081-1097.

[211] S. Parekh, C. P. Felice.(Sweetwater Energy Inc.).US.8,563,277 B1, **2015**

[212] A. Shahbazi, B. Zhang, Dilute and concentrated acid hydrolysis of lignocellulosic biomass in *Bioalcohol Production*, Elsevier, **2010**, pp. 143-158.

[213] A. R. Morais, A. C. Mata, R. Bogel-Lukasik, *Green Chem.* **2014**, *16*, 4312-4322.

[214] N. Narayanaswamy, A. Faik, D. J. Goetz, T. Gu, *Bioresour. Technol.* **2011**, *102*, 6995-7000.

[215] Y.-S. Choi, S. Nešić, C. J, in *Corrosion 2009 conference & expo*, NACE International, USA, **2009**.

[216] A. Toscan, A. R. C. Morais, S. M. Paixão, L. Alves, J. Andreaus, M. Camassola, A. J. P. Dillon, R. M. Lukasik, *Bioresour. Technol.* **2017**, *224*, 639-647.

[217] M. Chuang, M. Johannsen, in *9th international symposium on supercritical fluids (ISSF 2009), Arcachon, France*, **2009**.

[218] J. W. King, K. Srinivas, O. Guevara, Y.-W. Lu, D. Zhang, Y.-J. Wang, *J. Supercrit. Fluids* **2012**, *66*, 221-231.

[219] H. L. Chum, D. K. Johnson, S. K. Black, R. P. J. A. b. Overend, biotechnology, *Appl. Biochem. Biotechnol.* **1990**, *24*, 1.

[220] G. P. Van Walsum, in *Twenty-Second Symposium on Biotechnology for Fuels and Chemicals, Vol. 91 - 93* (Ed.: J. M. a. M. F. Brian H. Davison), Springer Science+ Business Media, LLC **2001**, pp. 317-329.

[221] J. Yin, L. Hao, W. Yu, E. Wang, M. Zhao, Q. Xu, Y. Liu, *Chin. J. Catal.* **2014**, *35*, 763-769.

[222] N. Srinivasan, L.-K. Ju, *Biomass Bioenergy* **2012**, *47*, 451-458.

[223] N. Srinivasan, L.-K. Ju, *Bioresour. Technol.* **2010**, *101*, 9785-9791.

[224] H. Zhang, S. Wu, *Bioresour. Technol.* **2014**, *158*, 161-165.

[225] Y. M. Questell-Santiago, M. V. Galkin, K. Barta, J. S. Luterbacher, *Nat. Rev. Chem.* **2020**, *4*, 311-330.

[226] M. Sasaki, K. Goto, K. Tajima, T. Adschiri, K. J. G. C. Arai, *Green Chem.* **2002**, *4*, 285-287.

[227] D. A. Cantero, M. D. Bermejo, M. J. Cocero, *ChemSusChem* **2015**, *8*, 1026-1033.

[228] M. Mohan, T. Banerjee, V. V. Goud, *Bioresour. Technol.* **2015**, *191*, 244-252.

[229] S. M. Islam, J. R. Elliott, L.-K. Ju, *Bioresour. Technol.* **2018**, *251*, 84-92.

[230] A. Barakat, X. Rouau, *Biotechnol. Biofuels* **2014**, *7*, 138.

[231] N. Bhati, Shreya, A. K. Sharma, *J. Food Process Eng.* **2020**, *n/a*, e13623.

[232] A. Taheri-Kafrani, S. Kharazmi, M. Nasrollahzadeh, A. Soozanipour, F. Ejeian, P. Etedali, H.-A. Mansouri-Tehrani, A. Razmjou, S. M.-G. Yek, R. S. Varma, *Crit. Rev. Food Sci. Nutr.* **2020**, 1-37.

[233] A. Mena-García, A. I. Ruiz-Matute, A. C. Soria, M. L. Sanz, *TrAC Trends in Analytical Chemistry* **2019**, *119*, 115612.

[234] S. Kilambi, K. L. Kadam.(Renmatix Inc.).US.8,282,738, **2012**

[235] Q. Zhang, M. Zhao, Q. Xu, H. Ren, J. Yin, *Appl. Biochem. Biotechnol.* **2019**, *188*, 101-111.

[236] X. Hu, L. Cheng, Z. Gu, Y. Hong, Z. Li, C. Li, *Ind. Crops Prod.* **2018**, *122*, 142-147.

[237] T. Benazzi, S. Calgaroto, C. Dalla Rosa, J. Vladimir Oliveira, M. A. Mazutti, *J. Chem. Technol. Biotechnol.* **2013**, *88*, 1766-1768.

[238] M. Sasaki, Z. Fang, Y. Fukushima, T. Adschiri, K. Arai, *Ind. Eng. Chem. Res.* **2000**, *39*, 2883-2890.

[239] C. M. Martínez, D. A. Cantero, M. Cocero, *J. Cleaner Prod.* **2018**, *204*, 888-895.

[240] P. A. Marrone, *J. Supercrit. Fluids* **2013**, *79*, 283-288.

[241] C. Czeslik, T. Q. Luong, R. Winter, *MRS Bull.* **2017**, *42*, 738-742.

[242] V. Schuabb, C. J. L. Czeslik, *Langmuir* **2014**, *30*, 15496-15503.

[243] P. C. Michels, D. S. Clark, Pressure dependence of enzyme catalysis in *Biocatalysis at Extreme Temperatures, Vol. 498*, American Chemical Society, **1992**, pp. 108-121.

[244] T. Q. Luong, S. Kapoor, R. Winter, *ChemPhysChem* **2015**, *16*, 3555-3571.

[245] H. Eyring, J. L. Magee, *J. Cell. Comp. Physiol.* **1942**, *20*, 169-177.

[246] V. V. Mozhaev, N. Bec, C. Balny, *Biochem. Mol. Biol. Int.* **1994**, *34*, 191-199.

[247] G. Jenner, Effect of Pressure on Reaction Kinetics. The Components of the Activation Volume Revisited in *High Pressure Molecular Science*, Springer, **1999**, pp. 291-311.

[248] B. B. Boonyaratanakornkit, C. B. Park, D. S. Clark, *Biochimica et Biophysica Acta (BBA) - Protein Structure and Molecular Enzymology* **2002**, *1595*, 235-249.

[249] R. Melgosa, M. T. Sanz, Á. G. Solaesa, S. L. Bucio, S. Beltrán, *J. Supercrit. Fluids* **2015**, *97*, 51-62.

[250] V. V. Mozhaev, R. Lange, E. V. Kudryashova, C. Balny, *Biotechnol. Bioeng.* **1996**, *52*, 320-331.

[251] H. H. Sunwoo, N. Gujral, A. C. Huebl, C.-T. Kim, *Food Bioprocess Technol.* **2014**, *7*, 1246-1254.

[252] V. Schuabb, S. Cinar, C. Czeslik, *Colloids Surf., B* **2016**, *140*, 497-504.

[253] L. A. S. Gorman, J. S. Dordick, *Biotechnol. Bioeng.* **1992**, *39*, 392-397.

[254] M. Z. Kamal, P. Yedavalli, M. V. Deshmukh, N. M. Rao, *Protein Sci.* **2013**, *22*, 904-915.

[255] X.-Q. Xu, Y. Shi, X.-B. Wu, X.-L. Zhan, H.-T. Zhou, Q.-X. Chen, *Int. J. Biol. Macromol.* **2015**, *81*, 1012-1018.

[256] R. Ahmad, S. K. J. B. t. Khare, *Bioresour. Technol.* **2018**, *252*, 72-75.

[257] A. Gießauf, W. Magor, D. J. Steinberger, R. J. E. Marr, m. technology, *Enzyme Microb. Technol.* **1999**, *24*, 577-583.

[258] Y. Liu, D. Chen, L. Xu, Y. Yan, *Enzyme Microb. Technol.* **2012**, *51*, 354-358.

[259] R. Brunecky, B. S. Donohoe, J. M. Yarbrough, A. Mittal, B. R. Scott, H. Ding, L. E. Taylor Ii, J. F. Russell, D. Chung, J. Westpheling, S. A. Teter, M. E. Himmel, Y. J. Bomble, *Sci Rep* **2017**, *7*, 9622.

[260] B. M. Brena, F. Batista-Viera, Immobilization of Enzymes in *Immobilization of Enzymes and Cells* (Ed.: J. M. Guisan), Humana Press, Totowa, NJ, **2006**, pp. 15-30.

[261] C. Altinkaynak, S. Tavlasoglu, N. ÿzdemir, I. Ocsoy, *Enzyme Microb. Technol.* **2016**, *93-94*, 105-112.

[262] N. R. Mohamad, N. H. C. Marzuki, N. A. Buang, F. Huyop, R. A. Wahab, *Biotechnol. Biotechnol. Equip.* **2015**, *29*, 205-220.

[263] P. Gallezot, *Chem. Soc. Rev.* **2012**, *41*, 1538-1558.

[264] A. Bayu, A. Yoshida, S. Karnjanakom, K. Kusakabe, X. Hao, T. Prakoso, A. Abudula, G. Guan, *Green Chem.* **2018**, *20*, 4112-4119.

[265] Y. Román-Leshkov, C. J. Barrett, Z. Y. Liu, J. A. Dumesic, *Nature* **2007**, *447*, 982-985.

[266] J. Tian, J. Wang, S. Zhao, C. Jiang, X. Zhang, X. Wang, *Cellulose* **2010**, *17*, 587-594.

[267] R. Galaverna, M. r. C. Breitkreitz, J. C. Pastre, *ACS Sustainable Chem. Eng.* **2018**, *6*, 4220-4230.

[268] W. Niu, H. Willett, J. Mueller, X. He, L. Kramer, B. Ma, J. Guo, *Metab. Eng.* **2020**, *59*, 151-161.

[269] J. P. Buyondo, S. Liu, *J. Sci. Technol. For. Prod. Processes* **2011**, *1*, 38.

[270] C. Asada, C. Sasaki, Y. Nakamura, *Waste Biomass Valorization* **2019**, *10*, 433-439.

[271] P. o. Lisa Zyga *can be found under https://phys.org/news/2011-10-supercritical-biomass-to-fuel-conversion-large-scale.html* **2011**.

[272] O. Gerald, in *Chemical Engineering, Vol. 118*, Access Intelligence, LLC, **2011**.

[273] I. Renmatix, *Can be found under https://renmatix.com/products/products-list/industrial* **2020**.

[274] Farm-energy, *Can be found under https://farm-energy.extension.org/renmatix-turns-biomass-into-sugars-for-industrial-use/* **2019**.

[275] Renmatix, *can be found under https://renmatix.com/1-million.html* **2016**.

[276] R. Melgosa, M. T. Sanz, Á. G. Solaesa, E. de Paz, S. Beltrán, D. L. Lamas, *Journal of CO2 Utilization* **2017**, *17*, 170-179.

[277] V. C. Badgujar, K. C. Badgujar, P. M. Yeole, B. M. Bhanage, *Bioprocess and Biosystems Engineering* **2019**, *42*, 47-61.

[278] P. dos Santos, C. A. Rezende, J. Martínez, *The Journal of Supercritical Fluids* **2016**, *107*, 170-178.

[279] Y. Ikushima, N. Saito, M. Arai, H. W. Blanch, *The Journal of Physical Chemistry* **1995**, *99*, 8941-8944.

[280] G. Hojnik Podrepšek, Ž. Knez, M. Leitgeb, *The Journal of Supercritical Fluids* **2019**, *154*, 104629.

[281] M. Leitgeb, M. Čolnik, M. Primožič, P. Zalar, N. G. Cimerman, Ž. Knez, *The Journal of Supercritical Fluids* **2013**, *78*, 143-148.

[282] Y. Zheng, G. T. Tsao, *Biotechnology Letters* **1996**, *18*, 451-454.

[283] D. Senyay-Oncel, O. Yesil-Celiktas, *Cellulose* **2015**, *22*, 3619-3631.

[284] P. Bridgman, The coagulation of albumen by pressure in *Volume II Collected Experimental Papers, Volume II*, Harvard University Press, **2013**, pp. 735-736.

[285] L. Heremans, K. Heremans, *Biochimica et Biophysica Acta (BBA) - Protein Structure and Molecular Enzymology* **1989**, *999*, 192-197.

[286] V. Kasche, R. Schlothauer, G. Brunner, *Biotechnology Letters* **1988**, *10*, 569-574.

[287] S. Kamat, J. Barrera, J. Beckman, A. J. Russell, *Biotechnol. Bioeng.* **1992**, *40*, 158-166.

[288] S. Kunugi, *Annals of the New York Academy of Sciences* **1992**, *672*, 293-304.

[289] V. V. Mozhaev, R. Lange, E. V. Kudryashova, C. Balny, *Biotechnol. Bioeng.* **1996**, *52*, 320-331.

[290] P. C. Michels, D. S. Clark, *Applied and environmental microbiology* **1997**, *63*, 3985-3991.

[291] K. J. Frye, C. A. Royer, *Protein Sci.* **1998**, *7*, 2217-2222.

[292] S. J. Park, J. I. Lee, J. Park, *Journal of Food Science* **2002**, *67*, 1827-1834.

[293] E. J. Beckman, *The Journal of Supercritical Fluids* **2004**, *28*, 121-191.

[294] C. Laane, S. Boeren, K. Vos, C. Veeger, *Biotechnol. Bioeng.* **1987**, *30*, 81-87.

[295] N. Doukyu, H. Ogino, *Biochemical Engineering Journal* **2010**, *48*, 270-282.

[296] N. Mase, T. Sako, Y. Horikawa, K. Takabe, *Tetrahedron Letters* **2003**, *44*, 5175-5178.

[297] H. R. Hobbs, N. R. Thomas, *Chemical reviews* **2007**, *107*, 2786-2820.

[298] D. Senyay-Oncel, O. Yesil-Celiktas, *Journal of Bioscience and Bioengineering* **2011**, *112*, 435-440.

[299] D. Senyay-Oncel, O. Yesil-Celiktas, *Journal of Molecular Catalysis B: Enzymatic* **2013**, *91*, 72-76.

[300] K. C. Badgujar, B. M. Bhanage, *Process Biochemistry* **2015**, *50*, 1224-1236.

[301] A. A. Homaei, R. Sariri, F. Vianello, R. Stevanato, *Journal of Chemical Biology* **2013**, *6*, 185-205.

[302] J. Eriksson, M. Malmsten, F. Tiberg, T. H. Callisen, T. Damhus, K. S. Johansen, *Journal of Colloid and Interface Science* **2005**, *285*, 94-99.

[303] M. K. Bhat, *Biotechnology Advances* **2000**, *18*, 355-383.

[304] A. Gomaa, *J. Nutr. Food Sci. Forecast* **2018**, *1*.

[305] B. A. Law, Enzymes in Dairy Product Manufacture in *Enzymes in Food Technology*, **2009**, pp. 88-102.

[306] Y. Bai, H. Huang, K. Meng, P. Shi, P. Yang, H. Luo, C. Luo, Y. Feng, W. Zhang, B. Yao, *Food Chemistry* **2012**, *131*, 1473-1478.

[307] B. Ismail, S. S. Nielsen, *Journal of Dairy Science* **2010**, *93*, 4999-5009.

[308] K. Marszałek, P. Doesburg, S. Starzonek, J. Szczepańska, Ł. Woźniak, J. M. Lorenzo, S. Skąpska, S. Rzoska, F. J. Barba, *Journal of CO_2 Utilization* **2019**, *29*, 46-56.

[309] Â. C. Salvador, M. d. C. Santos, J. A. Saraiva, *Green Chem.* **2010**, *12*, 632-635.

[310] T. Q. Luong, R. Winter, *Physical Chemistry Chemical Physics* **2015**, *17*, 23273-23278.

[311] M. de Souza Melchiors, J. G. Veneral, A. Furigo Junior, J. V. de Oliveira, M. Di Luccio, L. T. Prando, H. Terenzi, D. de Oliveira, *The Journal of Supercritical Fluids* **2017**, *130*, 125-132.

[312] Y. Liu, D. Chen, S. Wang, **2013**, *88*, 1750-1756.

[313] C. Albrecht, *Principles of fluorescence spectroscopy*, Springer, **2008**.

[314] N. M. Micaêlo, C. M. Soares, *The FEBS Journal* **2007**, *274*, 2424-2436.

[315] P.-Y. Stergiou, A. Foukis, M. Filippou, M. Koukouritaki, M. Parapouli, L. G. Theodorou, E. Hatziloukas, A. Afendra, A. Pandey, E. M. Papamichael, *Biotechnology Advances* **2013**, *31*, 1846-1859.

[316] G. E. Jeromin, A. Zoor, *Biotechnology letters* **2008**, *30*, 925-928.

[317] R. L. Silveira, J. Martínez, M. S. Skaf, L. Martínez, *The Journal of Physical Chemistry B* **2012**, *116*, 5671-5678.

[318] I. Aavatsmark, R. Kaufmann, *International Journal of Greenhouse Gas Control* **2015**, *32*, 47-55.

[319] Z. Wang, Q. Zhou, H. Guo, P. Yang, W. Lu, *Fluid Phase Equilibria* **2018**, *476*, 170-178.

[320] X. Li, H.-Y. Yu, *Journal of Industrial Microbiology and Biotechnology* **2013**, *40*, 1357-1365.

[321] R. Gaur, S. Tiwari, *BMC Biotechnology* **2015**, *15*, 19.

[322] G. P. Van Walsum, *Appl. Biochem. Biotechnol.* **2001**, *91*, 317-329.

[323] Y. Choi, S. Nesic, *NACE international, Georgia, USA* **2009**, 09256.

[324] H. Monhemi, M. R. Housaindokht, *The Journal of Supercritical Fluids* **2016**, *117*, 147-163.

[325] S. Takenouchi, G. C. Kennedy, *American Journal of Science* **1964**, *262*, 1055.

[326] G. Muratov, K.-W. Seo, C. Kim, *Journal of Industrial and Engineering Chemistry* **2005**, *11*, 42-46.

[327] Ž. Knez, *The Journal of Supercritical Fluids* **2018**, *134*, 133-140.

[328] T. Dumont, D. Barth, C. Corbier, G. Branlant, M. Perrut, *Biotechnol. Bioeng.* **1992**, *40*, 329-333.

[329] M. G. Aucoin, R. L. Legge, *Biotechnology Letters* **2001**, *23*, 1863-1870.

[330] C. Y. Park, Y. W. Ryu, C. Kim, *Korean Journal of Chemical Engineering* **2001**, *18*, 475-478.

[331] S. Urresti, A. Cartmell, F. Liu, P. H. Walton, G. J. Davies, *Acta Crystallographica Section F* **2018**, *74*, 496-505.

[332] T. M. Alvarez, J. H. Paiva, D. M. Ruiz, J. P. L. F. Cairo, I. O. Pereira, D. A. A. Paixão, R. F. de Almeida, C. C. C. Tonoli, R. Ruller, C. R. Santos, F. M. Squina, M. T. Murakami, *PLOS ONE* **2013**, *8*, e83635.

[333] G. Parsiegla, A. Belaïch, J. P. Belaïch, R. Haser, *Biochemistry* **2002**, *41*, 11134-11142.

[334] S. Khademi, D. Zhang, S. M. Swanson, A. Wartenberg, K. Witte, E. F. Meyer, *Acta Crystallographica Section D* **2002**, *58*, 660-667.

[335] M. P. Williamson, R. Kitahara, *Biochimica et Biophysica Acta (BBA) - Proteins and Proteomics* **2019**, *1867*, 350-358.

[336] G. Pintér, K. F. Hohmann, J. T. Grün, J. Wirmer-Bartoschek, C. Glaubitz, B. Fürtig, H. Schwalbe, *Magn. Reson.* **2021**, *2*, 291-320.

[337] R. W. Peterson, N. V. Nucci, A. J. Wand, *Journal of Magnetic Resonance* **2011**, *212*, 229-233.

[338] R. Kitahara, S. Sareth, H. Yamada, E. Ohmae, K. Gekko, K. Akasaka, *Biochemistry* **2000**, *39*, 12789-12795.

[339] R. A. Sheldon, *Advanced Synthesis & Catalysis* **2007**, *349*, 1289-1307.

[340] S. S. Betigeri, S. H. Neau, *Biomaterials* **2002**, *23*, 3627-3636.

[341] M. D. Trevan, Enzyme Immobilization by Entrapment in *New Protein Techniques* (Ed.: J. M. Walker), Humana Press, Totowa, NJ, **1988**, pp. 491-494.

[342] Q. Shen, R. Yang, X. Hua, F. Ye, W. Zhang, W. Zhao, *Process Biochemistry* **2011**, *46*, 1565-1571.

[343] M. Ungurean, C. Paul, F. Peter, *Bioprocess and Biosystems Engineering* **2013**, *36*, 1327-1338.

[344] C. Vasilescu, S. Marc, I. Hulka, C. Paul, *Gels* **2022**, *8*, 626.

[345] M. Khoobi, S. F. Motevalizadeh, Z. Asadgol, H. Forootanfar, A. Shafiee, M. A. Faramarzi, *Biochemical Engineering Journal* **2014**, *88*, 131-141.

[346] M. P. Santos, M. J. Brito, E. C. Junior, R. C. Bonomo, C. M. Veloso, *J. Chem. Technol. Biotechnol.* **2019**, *94*, 1982-1990.

[347] S. L. Hirsh, M. M. M. Bilek, N. J. Nosworthy, A. Kondyurin, C. G. dos Remedios, D. R. McKenzie, *Langmuir* **2010**, *26*, 14380-14388.

[348] J. Mehta, N. Bhardwaj, S. K. Bhardwaj, K.-H. Kim, A. Deep, *Coordination Chemistry Reviews* **2016**, *322*, 30-40.

[349] M. Zhou, X. Ju, Z. Zhou, L. Yan, J. Chen, X. Yao, X. Xu, L.-Z. Li, *ACS Sustainable Chem. Eng.* **2019**, *7*, 19185-19193.

[350] A. Perzon, C. Dicko, Ö. Çobanoğlu, O. Yükselen, J. Eryilmaz, E. S. Dey, *J. Chem. Technol. Biotechnol.* **2017**, *92*, 1645-1649.

[351] J. Zdarta, A. S. Meyer, T. Jesionowski, M. Pinelo, *Catalysts* **2018**, *8*, 92.

[352] R. Fernandez-Lafuente, *Enzyme Microb. Technol.* **2009**, *45*, 405-418.

[353] J. Alftrén, T. J. Hobley, *Biomass Bioenergy* **2014**, *65*, 72-78.

[354] X.-S. Li, G.-T. Zhu, Y.-B. Luo, B.-F. Yuan, Y.-Q. Feng, *TrAC Trends in Analytical Chemistry* **2013**, *45*, 233-247.

[355] B. Qi, J. Luo, Y. Wan, *Bioresour. Technol.* **2018**, *268*, 577-582.

[356] S. Talekar, A. Joshi, G. Joshi, P. Kamat, R. Haripurkar, S. Kambale, *RSC Adv.* **2013**, *3*, 12485-12511.

[357] K. Khoshnevisan, F. Vakhshiteh, M. Barkhi, H. Baharifar, E. Poor-Akbar, N. Zari, H. Stamatis, A.-K. Bordbar, *Molecular Catalysis* **2017**, *442*, 66-73.

[358] A. Samaratunga, O. Kudina, N. Nahar, A. Zakharchenko, S. Minko, A. Voronov, S. W. Pryor, *Appl. Biochem. Biotechnol.* **2015**, *175*, 2872-2882.

[359] R. E. Abraham, M. L. Verma, C. J. Barrow, M. Puri, *Biotechnol. Biofuels* **2014**, *7*, 90.

[360] M. A. Yassin, A. A. M. Gad, A. F. Ghanem, M. H. Abdel Rehim, *Carbohydrate Polymers* **2019**, *205*, 255-260.

[361] H.-C. Roth, S. Schwaminger, F. Peng, S. Berensmeier, *ChemistryOpen* **2016**, *5*, 183 - 187.

[362] F. B.-O. Daoud, S. Kaddour, T. Sadoun, *Colloids Surf., B* **2010**, *75*, 93-99.

[363] K. A. Araus, V. Casado, J. M. del Valle, P. S. Robert, J. C. de la Fuente, *The Journal of Supercritical Fluids* **2019**, *143*, 205-210.

[364] Ž. Knez, S. Kavčič, L. Gubicza, K. Bélafi-Bakó, G. Németh, M. Primožič, M. Habulin, *The Journal of Supercritical Fluids* **2012**, *66*, 192-197.

[365] S.-H. Yoon, H. Nakaya, O. Ito, O. Miyawaki, K.-H. Park, K. Nakamura, *Bioscience, Biotechnology, and Biochemistry* **1998**, *62*, 170-172.

[366] N. L. D. Nyari, G. L. Zabot, R. Zamadei, A. R. Paluzzi, M. V. Tres, J. Zeni, L. D. Venquiaruto, R. M. Dallago, *J. Chem. Technol. Biotechnol.* **2018**, *93*, 897-908.

[367] M. Leitgeb, M. Primožič, Ž. Knez, *Acta chimica slovenica* **2007**, *54*, 667-677.

[368] D. Oliveira, A. Feihrmann, A. Rubira, M. Kunita, C. Dariva, J. V. Oliveira, *The Journal of Supercritical Fluids* **2006**, *38*, 373-382.

[369] A. Chakrabarty, Y. Teramoto, *Polymers* **2018**, *10*, 517.

[370] B. Zhang, C. Huang, H. Zhao, J. Wang, C. Yin, L. Zhang, Y. Zhao, *Polymers* **2019**, *11*, 2063.

[371] Reshmy, D. Thomas, E. Philip, S. A. Paul, A. Madhavan, R. Sindhu, P. Binod, A. Pugazhendhi, R. Sirohi, A. Tarafdar, A. Pandey, *Chemosphere* **2021**, *281*, 130738.

[372] B. Li, Y. Zhang, C. Wu, B. Guo, Z. Luo, *Carbohydr. Polym.* **2018**, *198*, 1-8.

[373] M. Li, Y. Pu, V. M. Thomas, C. G. Yoo, S. Ozcan, Y. Deng, K. Nelson, A. J. Ragauskas, *Composites Part B: Engineering* **2020**, *200*, 108254.

[374] A. Kausar, Chapter 17 - Nanocellulose in polymer nanocomposite in *Sustainable Nanocellulose and Nanohydrogels from Natural Sources* (Eds.: F. Mohammad, H. A. Al-Lohedan, M. Jawaid), Elsevier, **2020**, pp. 357-366.

[375] H. Voisin, L. Bergström, P. Liu, A. P. Mathew, *Nanomaterials* **2017**, *7*, 57.

[376] R. Zhang, Y. Liu, *Sci Rep* **2018**, *8*, 16505.

[377] W. Y. Hamad, T. Q. Hu, *The Canadian Journal of Chemical Engineering* **2010**, *88*, 392-402.

[378] X. Fu, H. Ji, B. Wang, W. Zhu, Z. Pang, C. Dong, *Cellulose* **2020**, *27*, 1289-1299.

[379] G. Duarte Urueña, K. C. Ribeiro, E. Prestes, L. A. Pinheiro, B. M. Carvalho, *Waste Biomass Valorization* **2021**.

[380] M. Mahardika, H. Abral, A. Kasim, S. Arief, M. Asrofi, *Fibers* **2018**, *6*, 28.

[381] J. Buffiere, Z. Balogh-Michels, M. Borrega, T. Geiger, T. Zimmermann, H. Sixta, *Carbohydr. Polym.* **2017**, *178*, 48-56.

[382] N. A. Mohd Ishak, I. Khalil, F. Z. Abdullah, N. Muhd Julkapli, *Carbohydr. Polym.* **2020**, *246*, 116553.

[383] Z. Lu, L. Fan, H. Zheng, Q. Lu, Y. Liao, B. Huang, *Bioresour. Technol.* **2013**, *146*, 82-88.

[384] A. Sluiter, B. Hames, R. Ruiz, C. Scarlata, J. Sluiter, D. Templeton, D. Crocker, *Laboratory analytical procedure* **2008**, *1617*, 1-16.

[385] N. Amiralian, P. K. Annamalai, C. J. Garvey, E. Jiang, P. Memmott, D. J. Martin, *Cellulose* **2017**, *24*, 3753-3766.

[386] G. Zhao, J. Du, W. Chen, M. Pan, D. Chen, *Cellulose* **2019**, *26*, 8625-8643.

[387] Y. Yue, C. Zhou, A. D. French, G. Xia, G. Han, Q. Wang, Q. Wu, *Cellulose* **2012**, *19*, 1173-1187.

[388] J.-W. Rhim, J. P. Reddy, X. Luo, *Cellulose* **2015**, *22*, 407-420.

[389] Y. Yin, L. Berglund, L. Salmén, *Biomacromolecules* **2011**, *12*, 194-202.

[390] R. M. Sheltami, I. Abdullah, I. Ahmad, A. Dufresne, H. Kargarzadeh, *Carbohydr. Polym.* **2012**, *88*, 772-779.

[391] Y. Peng, D. J. Gardner, Y. Han, A. Kiziltas, Z. Cai, M. A. Tshabalala, *Cellulose* **2013**, *20*, 2379-2392.

[392] X. Y. Tan, S. B. Abd Hamid, C. W. Lai, *Biomass Bioenergy* **2015**, *81*, 584-591.

[393] J. Han, C. Zhou, A. D. French, G. Han, Q. Wu, *Carbohydr. Polym.* **2013**, *94*, 773-781.

[394] N. Wang, E. Ding, R. Cheng, *Polymer* **2007**, *48*, 3486-3493.

[395] M. I. Voronova, O. V. Surov, A. G. Zakharov, *Carbohydr. Polym.* **2013**, *98*, 465-469.

[396] P. Tomme, R. A. J. Warren, N. R. Gilkes, Cellulose Hydrolysis by Bacteria and Fungi in *Advances in Microbial Physiology, Vol. 37* (Ed.: R. K. Poole), Academic Press, **1995**, pp. 1-81.

[397] M. Suhr, G. Klein, I. Kourti, M. R. Gonzalo, G. G. Santonja, S. Roudier, L. D. Sancho, *Eur. Comm* **2015**, *906*.

[398] K. Statistics, *CESI report* **2007**.

[399] M. J. Quina, C. T. Pinheiro, *Applied Sciences* **2020**, *10*, 2317.

[400] M. Golmaei, T. Kinnarinen, E. Jernström, A. Häkkinen, *J. Cleaner Prod.* **2018**, *183*, 162-171.

[401] S. Rebello, A. N. Anoopkumar, E. M. Aneesh, R. Sindhu, P. Binod, A. Pandey, *Bioresour. Technol.* **2020**, *301*, 122678.

[402] S. Chuetor, V. Champreda, N. Laosiripojana, *Bioresour. Technol.* **2019**, *292*, 121966.

[403] P. Kumar, K. Miller, A. Kermanshahi-Pour, S. K. Brar, R. F. Beims, C. C. Xu, *Int. J. Biol. Macromol.* **2022**.

[404] H. Chen, J. Zhao, T. Hu, X. Zhao, D. Liu, *Applied Energy* **2015**, *150*, 224-232.

[405] D. Chuanyun, W. Bochu, Z. Huan, H. Conglin, D. Chuanren, L. Wangqian, Y. Toyama, A. Sakanishi, *Colloids Surf., B* **2004**, *34*, 7-11.

[406] M. Yaldagard, S. Mortazavi, F. Tabatabaie, *Korean Journal of Chemical Engineering* **2008**, *25*, 517-523.

[407] G. González, J. López-Santín, G. Caminal, C. Sola, *Biotechnol. Bioeng.* **1986**, *28*, 288-293.

[408] P. Kumar, A. Kermanshahi-Pour, S. K. Brar, Q. S. He, J. K. Rainey, *Biotechnology Advances* **2023**, *68*, 108219.

[409] M. Tobiszewski, A. Mechlińska, J. Namieśnik, *Chem. Soc. Rev.* **2010**, *39*, 2869-2878.

[410] P. T. Anastas, J. C. Warner, *Frontiers* **1998**, *640*, 1998.

[411] T. Ghose, *Pure and applied Chemistry* **1987**, *59*, 257-268.

[412] M. G. Resch, J. Baker, S. Decker, *Low Solids Enzymatic Saccharification of Lignocellulosic Biomass*, National Renewable Energy Laboratory Golden, CO, **2015**.

[413] P. K. Smith, R. I. Krohn, G. T. Hermanson, A. K. Mallia, F. H. Gartner, M. D. Provenzano, E. K. Fujimoto, N. M. Goeke, B. J. Olson, D. C. Klenk, *Analytical Biochemistry* **1985**, *150*, 76-85.

[414] A. O. Converse, J. D. Optekar, *Biotechnol. Bioeng.* **1993**, *42*, 145-148.

[415] T. Jeoh, D. B. Wilson, L. P. Walker, *Biotechnology Progress* **2006**, *22*, 270-277.

[416] D. M. Byler, H. Susi, *Biopolymers* **1986**, *25*, 469-487.

[417] A. Pandey, M. Sarker, X. Q. Liu, J. K. Rainey, *Biochem Cell Biol* **2014**, *92*, 269-278.

[418] M. F. Demirbas, *Energy Sources, Part A* **2010**, *32*, 909-916.

[419] P. Nargotra, V. Sharma, S. Sharma, R. Bangotra, B. K. Bajaj, *Environmental Sustainability* **2022**, *5*, 313-323.

[420] A. O. Sulyman, A. Igunnu, S. O. Malomo, *Heliyon* **2020**, *6*, e05668.

[421] M. Maleki, M. F. Shahraki, K. Kavousi, S. Ariaeenejad, G. Hosseini Salekdeh, *Int. J. Biol. Macromol.* **2020**, *154*, 349-360.

[422] J. d. J. Montoya-Rosales, D. K. Olmos-Hernández, R. Palomo-Briones, V. Montiel-Corona, A. G. Mari, E. Razo-Flores, *Bioresour. Technol.* **2019**, *283*, 251-260.

[423] H. R. Sørensen, A. S. Meyer, S. Pedersen, *Biotechnol. Bioeng.* **2003**, *81*, 726-731.

[424] J. Moore, Z. Cheng, L. Su, L. Yu, *Journal of Agricultural and Food Chemistry* **2006**, *54*, 9032-9045.

[425] H. Liu, J. Sun, S.-Y. Leu, S. Chen, *Biofuels, Bioproducts and Biorefining* **2016**, *10*, 648-663.

[426] C. G. Yoo, X. Meng, Y. Pu, A. J. Ragauskas, *Bioresour. Technol.* **2020**, *301*, 122784.

[427] K. Mirahmadi, M. M. Kabir, A. Jeihanipour, K. Karimi, M. Taherzadeh, *BioResources* **2010**, *5*, 928-938.

[428] B. Wang, X.-J. Shen, J.-L. Wen, L. Xiao, R.-C. Sun, *Int. J. Biol. Macromol.* **2017**, *97*, 447-459.

[429] M.-Q. Zhu, J.-L. Wen, Y.-Q. Su, Q. Wei, R.-C. Sun, *Bioresour. Technol.* **2015**, *185*, 378-385.

[430] C. Huang, X. Jiang, X. Shen, J. Hu, W. Tang, X. Wu, A. Ragauskas, H. Jameel, X. Meng, Q. Yong, *Renewable Sustainable Energy Rev.* **2022**, *154*, 111822.

[431] H. Liu, J. Sun, S. Y. Leu, S. Chen, *Biofuels, Bioproducts and Biorefining* **2016**, *10*, 648-663.

[432] S. Hou, B. Shen, D. Zhang, R. Li, X. Xu, K. Wang, C. Lai, Q. Yong, *Bioresour. Technol.* **2022**, *362*, 127825.

[433] X. Luo, J. Liu, P. Zheng, M. Li, Y. Zhou, L. Huang, L. Chen, L. Shuai, *Biotechnol. Biofuels* **2019**, *12*, 51.

[434] P. Wang, Q. Wang, T. Liu, J. Guo, Y. Jin, H. Xiao, J. Song, *Arabian Journal of Chemistry* **2022**, *15*, 103910.

[435] S. Brahms, J. Brahms, *Journal of Molecular Biology* **1980**, *138*, 149-178.

[436] X. Yao, L. Xiao, H. Liu, M. Zhou, Z. Zhou, X. Ju, L. Li, *Biomass Conversion and Biorefinery* **2022**, *12*, 5011-5018.

[437] P. B. Subhedar, P. R. Gogate, *Journal of Molecular Catalysis B: Enzymatic* **2014**, *101*, 108-114.

[438] N. Adlakha, R. Rajagopal, S. Kumar, V. S. Reddy, S. S. Yazdani, *Applied and Environmental Microbiology* **2011**, *77*, 4859-4866.

[439] G. P. Furtado, L. F. Ribeiro, C. R. Santos, C. C. Tonoli, A. R. de Souza, R. R. Oliveira, M. T. Murakami, R. J. Ward, *Process Biochemistry* **2011**, *46*, 1202-1206.

[440] P. Kumar, K. Miller, A. Kermanshahi-pour, S. K. Brar, R. F. Beims, C. C. Xu, *Int. J. Biol. Macromol.* **2022**, *221*, 426-434.

[441] Q.-Q. Xu, M.-J. Zhao, Z.-Z. Yu, J.-Z. Yin, G.-M. Li, M.-Y. Zhen, Q.-Z. Zhang, *Ind. Crops Prod.* **2017**, *109*, 220-226.

[442] L. Shuai, Q. Yang, J. Y. Zhu, F. C. Lu, P. J. Weimer, J. Ralph, X. J. Pan, *Bioresour. Technol.* **2010**, *101*, 3106-3114.

[443] A. Bala, B. Singh, *Renewable Energy* **2019**, *136*, 1231-1244.

[444] Y. H. Percival Zhang, M. E. Himmel, J. R. Mielenz, *Biotechnology Advances* **2006**, *24*, 452-481.

[445] A. A. Klyosov, *Biochemistry* **1990**, *29*, 10577-10585.

[446] M. Valdivia, J. L. Galan, J. Laffarga, J. L. Ramos, *Microbial biotechnology* **2016**, *9*, 585-594.

[447] A. Karim, Z. Bibi, M. A. Nawaz, A. Aman, S. A. U. Qader, *Bioprocess and Biosystems Engineering* **2021**, *44*, 2417-2427.

[448] V. Stepankova, S. Bidmanova, T. Koudelakova, Z. Prokop, R. Chaloupkova, J. Damborsky, *ACS Catalysis* **2013**, *3*, 2823-2836.

[449] A. C. Pierre, *Journal of Sol-Gel Science and Technology* **2019**, *90*, 172-186.

[450] I. Smirnova, P. Gurikov, *The Journal of Supercritical Fluids* **2018**, *134*, 228-233.

[451] K. Han, Z. Wu, J. Lee, I.-S. Ahn, J. W. Park, B. R. Min, K. Lee, *Biochemical Engineering Journal* **2005**, *22*, 161-166.

[452] A. A. N. Saqib, P. J. Whitney, *Biomass Bioenergy* **2011**, *35*, 4748-4750.

[453] G. L. Miller, *Analytical chemistry* **1959**, *31*, 426-428.

[454] H. R. Luckarift, J. C. Spain, R. R. Naik, M. O. Stone, *Nature biotechnology* **2004**, *22*, 211-213.

[455] I. Gill, A. Ballesteros, *Journal of the American Chemical Society* **1998**, *120*, 8587-8598.

[456] J. Fu, S. Wang, C. He, Z. Lu, J. Huang, Z. Chen, *Carbohydr. Polym.* **2016**, *147*, 89-96.

[457] L. Sutarlie, K.-L. Yang, *Journal of Colloid and Interface Science* **2013**, *411*, 76-81.

[458] R. Darias, R. Villalonga, *J. Chem. Technol. Biotechnol.* **2001**, *76*, 489-493.

[459] M. Holtzapple, M. Cognata, Y. Shu, C. Hendrickson, *Biotechnol. Bioeng.* **1990**, *36*, 275-287.

[460] S. Al-Zuhair, *Bioresour. Technol.* **2008**, *99*, 4078-4085.

[461] D. Sillu, S. Agnihotri, *ACS Sustainable Chem. Eng.* **2020**, *8*, 900-913.

[462] P. A. Limadinata, A. Li, Z. Li, *Green Chem.* **2015**, *17*, 1194-1203.

[463] S. Zhang, D. E. Wolfgang, D. B. Wilson, *Biotechnol. Bioeng.* **1999**, *66*, 35-41.

[464] V.-H. Sotaniemi, S. Taskila, H. Ojamo, J. Tanskanen, *Biomass Bioenergy* **2016**, *91*, 271-277.

[465] Y. E. C. Sugiharto, A. Harimawan, M. T. A. P. Kresnowati, R. Purwadi, R. Mariyana, H. N. Fitriana, H. F. Hosen, *Bioresour. Technol.* **2016**, *207*, 175-179.

[466] J. Du, Y. Cao, G. Liu, J. Zhao, X. Li, Y. Qu, *Bioresour. Technol.* **2017**, *229*, 88-95.

[467] C. M. Roche, C. J. Dibble, J. S. Knutsen, J. J. Stickel, M. W. Liberatore, *Biotechnol. Bioeng.* **2009**, *104*, 290-300.

[468] J. J. Stickel, J. S. Knutsen, M. W. Liberatore, W. Luu, D. W. Bousfield, D. J. Klingenberg, C. T. Scott, T. W. Root, M. R. Ehrhardt, T. O. Monz, *Rheologica Acta* **2009**, *48*, 1005-1015.

[469] L. Wu, X. Yuan, J. Sheng, *Journal of Membrane Science* **2005**, *250*, 167-173.

[470] D. Andriani, C. Sunwoo, H.-W. Ryu, B. Prasetya, D.-H. Park, *Bioprocess and Biosystems Engineering* **2012**, *35*, 29-33.

[471] J. Cui, Y. Feng, S. Yue, Y. Zhao, L. Li, R. Liu, T. Lin, *J. Chem. Technol. Biotechnol.* **2016**, *91*, 1905-1913.

[472] S. Lowell, J. E. Shields, M. A. Thomas, M. Thommes, *Characterization of porous solids and powders: surface area, pore size and density, Vol. 16*, Springer Science & Business Media, **2006**.

[473] J. Wang, J. Xu, S. Zhu, Q. Wu, J. Li, Y. Gao, B. Wang, J. Li, W. Gao, J. Zeng, K. Chen, *Carbohydr. Polym.* **2021**, *251*, 117094.

[474] E. d. M. Teixeira, T. J. Bondancia, K. B. R. Teodoro, A. C. Corrêa, J. M. Marconcini, L. H. C. Mattoso, *Ind. Crops Prod.* **2011**, *33*, 63-66.

[475] K. K. Pandey, *Journal of Applied Polymer Science* **1999**, *71*, 1969-1975.

[476] X.-J. Pan, Y. Sano, **1999**, *53*, 511-518.

[477] D. Watkins, M. Nuruddin, M. Hosur, A. Tcherbi-Narteh, S. Jeelani, *Journal of Materials Research and Technology* **2015**, *4*, 26-32.

[478] N. Mahmood, Z. Yuan, J. Schmidt, C. Xu, *Bioresour. Technol.* **2013**, *139*, 13-20.

APPENDIX A: CHAPTER 3 SUPPLEMENTARY INFORMATION

1.1 HPLC method used for sugar estimation in acid hydrolysates

The hydrolysate from the acid hydrolysis was neutralized with calcium hydroxide and analyzed by high-performance liquid chromatography (HPLC) installed with a refractive index detector (RID). Agilent Hi-plex H (6.5 x 300 mm, particles size 8 µm) column was used to analyze the released sugars (glucose, cellobiose, xylose, mannose, and arabinose). Water was used as the mobile phase at a 0.6 mL/min flow rate. Column and RID temperature were set at 65 °C and 55 °C, respectively. The pH was neutralized (5-6) hydrolysate with calcium hydroxide. It was injected (10 µL volume) by an autosampler and analyzed using a 20 min isocratic method. The samples were filtered using a syringe filter (0.22 µm) before injecting them into the HPLC.

1.2. Chemical composition analysis of processed materials

The chemical composition analysis was performed as per the NREL method as described in the manuscript. The determined compositions of the wood, pulps, and CNC samples are listed in Table S7-1.

Table S7-1. The Chemical composition of the initial feedstock material, pulp, and CNC samples, where the numbers are reported as the mean ± standard deviation of triplicate samples (g/100 g wood).

Sample name	Cellulose	Hemicellulose	Lignin
Wood	47.06±2.21	20.10±0.75	29.35±0.22
Acetosolv pulp	78.19±2.46	4.73±0.52	5.02±0.54
Bleached pulp	88.5±0.71	6.20±0.70	<0.66
CNC59	88.97±0.98	3.26±0.59	<0.66
CNC62	89.88±1.12	2.57±0.08	<0.66

CNC65	93.26±0.54	1.96±0.26	<0.66

1.3. Yield calculation

The yield of the acetosolv pulp obtained in acetosolv pulping reaction is calculated using Equation S3-1.

$$Acetsolv\ pulp\ yield\ (per\ 100\ g\ wood) = \frac{Weight\ of\ oven\ dry\ acetosolv\ pulp\ obtained\ (g)}{Weight\ of\ \ wood\ used\ (g)} \times 100 \qquad \text{(S3-1)}$$

The yield of bleached pulp obtained from alkaline hydrogen peroxide bleaching reaction is calculated using Equation S3-2.

$$Bleached\ pulp\ yield = \frac{Weight\ of\ oven\ dry\ bleached\ pulp\ obtained\ (g)}{Weight\ of\ oven\ dry\ acetosolv\ pulp\ used\ (g)} \times 100 \qquad \text{(S3-2)}$$

The overall yield of bleached pulp (microcrystalline cellulose) from the wood was calculated using Equation S3-3.

$$Bleached\ pulp\ yield = \frac{Weight\ of\ ovent\ dry\ pulp\ (g)}{Weight\ of\ extractive\ and\ moisture\ free\ wood\ (g)} \times 100 \qquad \text{(S3-3)}$$

The solid recovered from the sulfuric acid hydrolysis reaction was used for the mechanical treatment where the microparticles transformed into nanoparticles, and therefore, the nanocellulose yield was calculated as the weight of solid obtained after acid hydrolysis using equation 4:

$$Nanocellulose\ yield\ (wt.\%\ of\ Bleached\ pulp) = \frac{dry\ weight\ of\ acid\ hydrolyzed\ solid\ (g)}{dry\ weight\ of\ bleached\ pulp\ used\ (g)} \times 100 \qquad \text{(S3-5)}$$

Or $$Nanocellulose\ yield\ (wt.\%\ of\ dry\ wood) = \frac{dry\ weight\ of\ acid\ hydrolyzed\ solid\ (g)}{dry\ weight\ of\ bleached\ pulp\ used\ (g)} \times 100 \qquad \text{(S3-4)}$$

The yield of the CNCs produced at different concentrations of sulfuric acid are as mentioned in Table S7-2

Table S7-2. Triplicate analysis of the acid hydrolysis reaction at three different sulfuric acid concentrations (g/100 g of bleached pulp).

Sulfuric Acid concentration. (% w/w)	CNC yield (n=3)			Mean±Sd
59	97.59	96.53	97.33	97.2±0.6
62	60.09	59.44	62.85	60.8±1.8
65	28.38	15.87	14.33	19.5±7.7

1.4. Mass balance of acid hydrolysis reaction

The mass balance of the acid hydrolysis reaction at three concentrations of sulfuric acid was analyzed. The 65 wt.% sulfuric acids hydrolyzed more of the pulp and some of the sugars were lost during the washing and dialysis of the cellulose nanocrystals after the acid hydrolysis. The mass balance analysis was performed in duplicates as shown in Figure S7-1 and Table S7-3.

Table S7-3. Mass balance of acid hydrolysis reaction (g/100 g bleached pulp)

Acid Concentration	Total wt. of pulp solid (A), (g)	Anhydrous sugars in hydrolysate (B), (g)	Solid in washing effluent (C), g	Sum (A+B+C), (g)	Mass loss*, %
59 wt.%_1	97.590	3.151	-	100.741	
59 wt.%_2	96.330	3.117	-	99.447	
		Mean ± SD of (A+B+C)		100.1±0.91	0
62 wt.%_1	60.090	13.151	5.933	79.174	
62 wt.%_2	59.440	11.204	5.120	75.764	
		Mean ± SD of (A+B+C)		77.47±2.41	22.53
65 wt.%_1	14.330	36.220	11.060	61.610	
65 wt.%_2	15.870	35.501	12.200	63.571	
		Mean ± SD of (A+B+C)		62.59±1.39	37.41

*The loss of mass during acid hydrolysis at 59 wt.%, 62 wt.%, and 65 wt.% sulfuric acid concentrations could be assumed to be sugars that were released lost during the washing and dialysis stage.

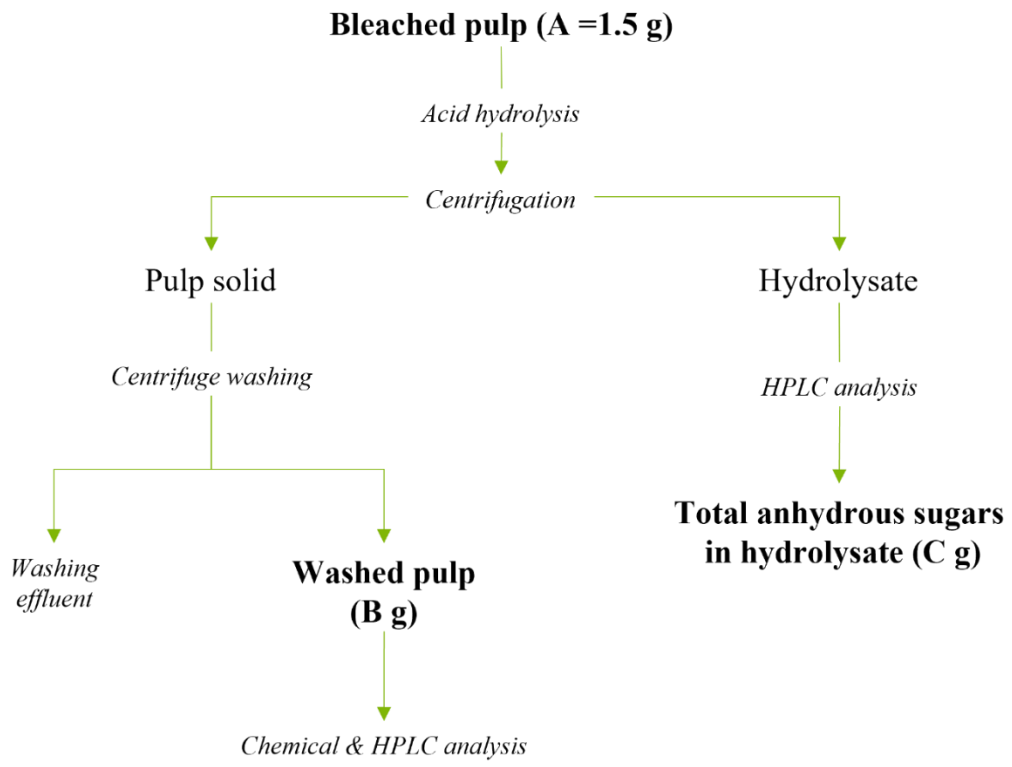

Figure S7-1. Mass flow of acid hydrolysis reaction and analysis for mass balance.

1.5. SEM sample preparation:

The samples for SEM were prepared by diluting the suspension sample to a concentration of 0.005 wt.% in water. The 40-50 µL samples were placed on double-sided adhesive carbon tape, supported on aluminum stab, and kept at room temperature for 24 h to evaporate the water. The samples were then placed in an oven at 55 °C under an active vacuum for 24 h to remove excess moisture from the sample. The dried samples were sputter-coated with gold to a thickness of 5 nm prior to characterization using a scanning electron microscope (FE-SEM, Mira3 LMU, Tescan, Czech Republic).

1.6. TEM sample preparation:

Samples prepared using an ultrasonic probe were analyzed using a transmission electron microscope (JEOL 1230 TEM) at 80 kV accelerating voltage. Samples

were prepared at a concentration of 0.005 wt.% and a drop of the suspension was placed on a formvar-coated 200 mesh copper grid, stained with uranyl acetate (1 wt.%), and left to dry in ventilated place for 24 h prior to analysis by TEM.

1.7. Statistical analysis of crystallinity index for ultrasonic treatment

The optimization of the ultrasonic treatment was performed at different intensities where amplitude varied from 30-80% and treatment time from 5-15 min. A total of 7 runs was performed using four corner points and three center points as shown in Figure S7-2.

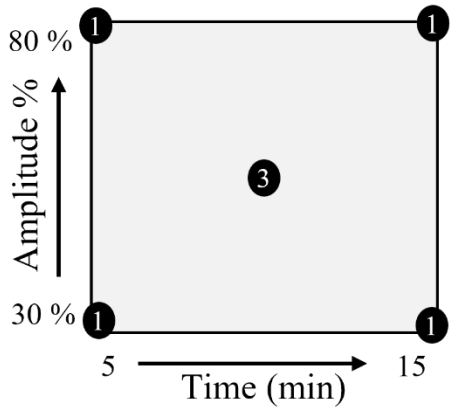

Figure S7-2. Ultrasonic intensity optimization model (4 corner points and 3 center points) for crystallinity index in response to amplitude and time as input factors

The ultrasonically treated samples were analyzed by TEM for particle length and diameter. Further, the samples were freeze-dried for 3-4 days and analyzed for crystallinity index. The crystallinity index was measured based on area as well as the Seagal intensity ratio. The results of the particle size, crystallinity index, and the spent energy in corresponding runs were mentioned in Table S7-4. The ANOVA response (Table S7-5) of the ultrasonic treatment for crystallinity index showed a high p-value of 0.19 for the model which means an insignificant change in the crystallinity index of CNC prepared at a varying range of amplitude and time.

Table S7-4. Design of experiments (two factors two levels with three center points) for ultrasonic treatment optimization of amplitude and time parameters as input for crystallinity index as the response, particle size, and spent energy.

Run Order	Amplitude (%)	Time (min)	Crystallinity index (CrI %)* area ratio based	Crystallinity index (CrI %)* intensity ratio based	Particle length (nm)	Particle diameter (nm)	Energy spent (J)
Control	-	-	70.8±1.6	83.5±2.1	18540±13050	3920±2650	-
1	30	15	66.1±0.8	76.1±1.1	BDL	BDL	14658
2 Ct Pt	55	10	66.4±0.6	76.2±3.5	BDL	BDL	16054
3 Ct Pt	55	10	61.7±0.9	74.7±2.3	BDL	BDL	14517
4	30	5	68.6±1.2	78.3±2.7	215.4±80	12±3	5275
5	80	15	62.7±0.8	75.6±2.2	BDL	BDL	34163
6 Ct Pt	55	10	64.5±1.9	76.7±1.3	BDL	BDL	17223
7	80	5	63.2±0.2	74.3±1.2	225.37±64.54	19.63±4.88	18553

Values with standard deviation are from three runs on the same sample. BDL- below detection limit.

Table S7-5. ANOVA response of ultrasonic optimization model for crystallinity index % in response to amplitude % and time (min) as input factors.

Source	**Sum of squares**	**df**	**Mean square**	**F-value**	**p-value**	**Result**
Model	6.06	2	3.03	2.58	**0.1910**	**not significant**
Amplitude	6.00	1	6.00	5.10	0.0869	
Time	0.0625	1	0.0625	0.0531	0.8291	
Residual	4.71	4	1.18			
Lack of fit	2.60	2	1.30	1.24	0.4473	not significant
Pure error	2.11	2	1.05			
Cor total	10.77	6				

1.8. TEM analysis of CNC released after acid hydrolysis and without/with ultrasonic treatment

The acid hydrolysis released some of the small cellulose chains which were observed under TEM microgrid at 20000X resolution while the 2000X magnification showed that the acid hydrolyzed (at 62 wt.% sulfuric acid concentration) samples and microparticles of CNC (Figure S7-3).

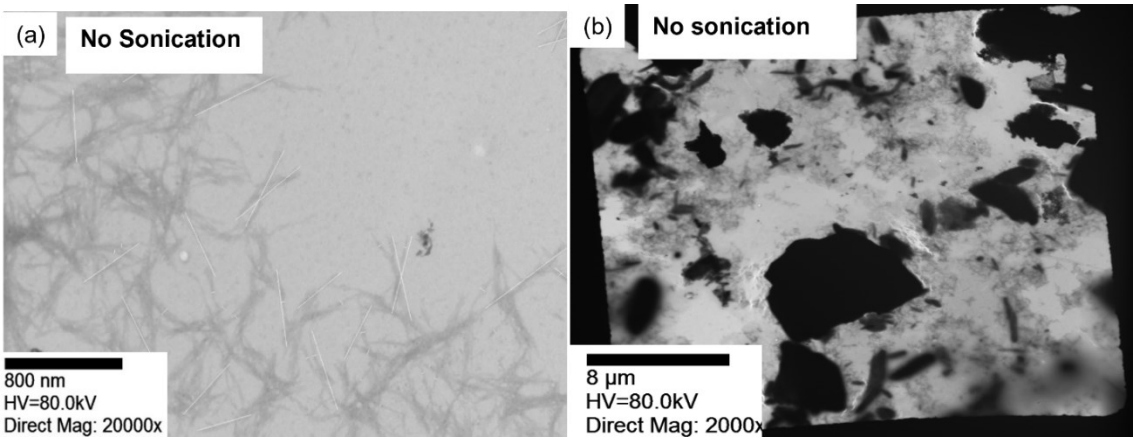

Figure S7-3. CNC from the suspension released during acid hydrolysis (at 62 wt.% sulfuric acid concentration) was stirred at 500 rpm without ultrasonic treatment (a) at 800 nm scale bar and (b) at 8 µm scale bar of TEM analysis of the same sample.

Further, the ultrasonically treated samples were observed under TEM which showed the cellulose nanocrystals were formed when it was treated for 5 min at 30 % and 80 % amplitudes. The samples treated for more than 5 min showed no whisker like CNC morphology (Figure S7-4).

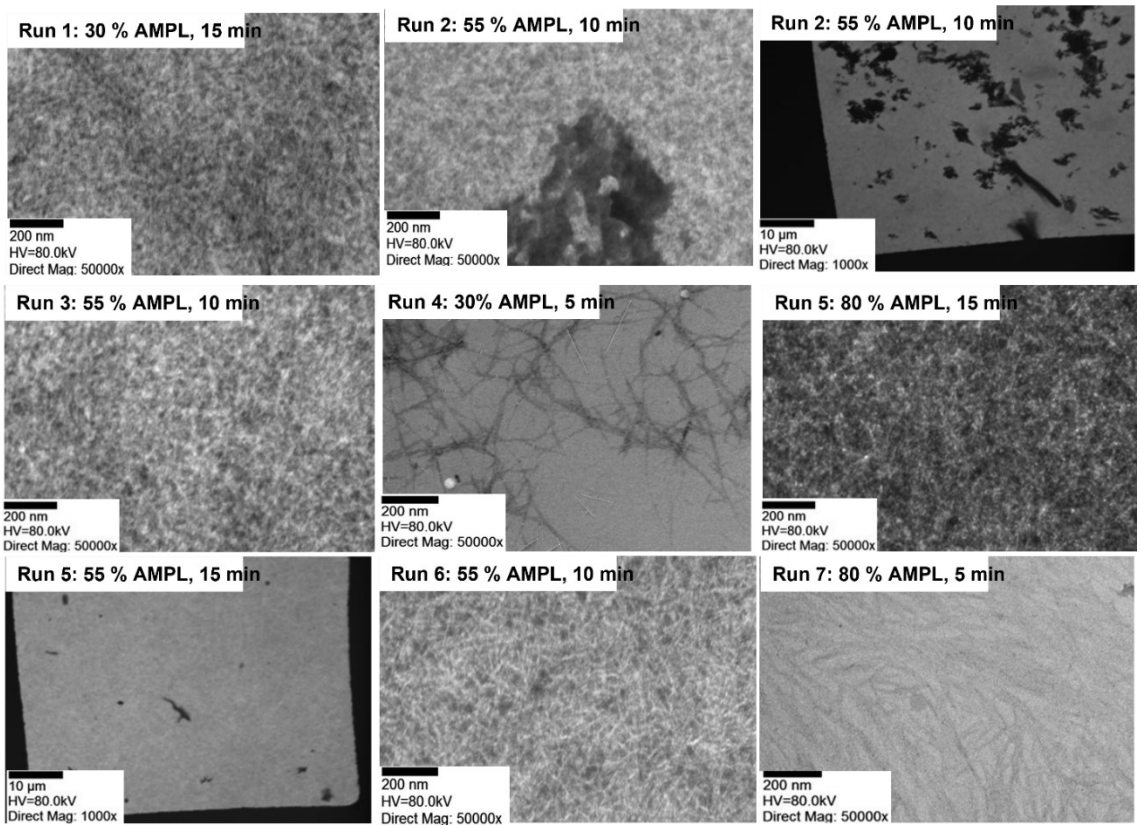

Figure S7-4. TEM images of CNCs from different ultrasonic treatments for optimization of amplitude and time.

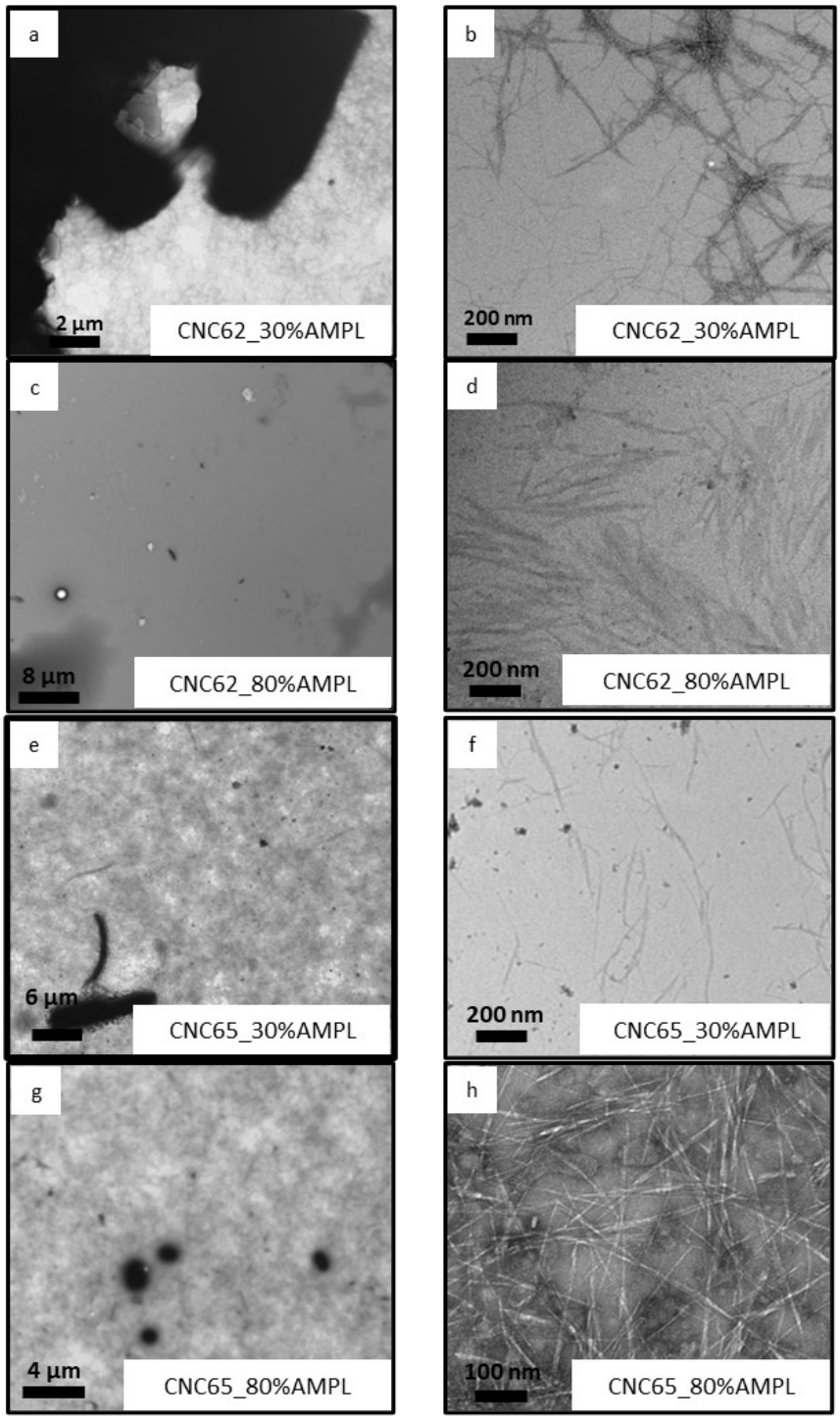

Figure S7-5. TEM images of CNCs from different micron and nano scales show the homogeneity of dispersed nanocrystals.

1.9. Comparison of the characteristics of cellulose nanocrystals (CNCs)

Table S7-6. Comparison of the characteristics of cellulose nanocrystals from different biomass and methods of cellulose extractions

Initial material	Methods	Pulp purity	CNC yield (g/100 g of bleached pulp)	Nanocellulose dimensions (L, D nm); CrI	Characterization	Ref
Beached eucalyptus kraft pulp	58 wt.% sulfuric acid hydrolysis at 56 °C for 3 h	Glucan 88.5±0.3%,Xylan 11.0±0.5%, Lignin <0.1%	68 %	216 ± 34, 10 ± 2; 76.2%	Treated by ultrasonic cleaner (45 kHz, 180 W) for 10 min before imaging.	[54]
	0.5:8.5:1 (sulfuric acid, acetic acid & water mass ratio) at 80 °C for 3 h		81 %	264 ± 114, 16 ± 3; 79.9 %		
Pine wood	62 wt.% sulfuric acid hydrolysis at 44 °C for 1.5 h	NA	2.3 %	220.2 (mean spherical diameter), -; 67.8 %	Homogenized at 1000 rpm for 5 min	[57]
Microcrystalline cellulose			25.5 % of MCC	28.2 nm (mean spherical diameter), -; 79.3 %		
Corn cob			6.0 %	30.0-70.0 nm (mean spherical diameter), -; 70.9 %		
Bleached softwood kraft pulp	0.3 wt.% sulfuric acid hydrolysis 160 °C for 2 h	Cellulose 87.9 ± 0.5 %, Hemicellulose 0.2 ± 1.1 %, Lignin 0.25 ± 0.01 %	15.78 % CNC along with 69 % CNF	150 ~500 nm, 10~40 nm; 77.35 % to 79.32 %	Ultrasound treatment by probe for 5 min for CNC, Microfluidizer 25,000 psi	[473]
Bleached sugarcane bagasse	46.8 wt.% sulfuric acid hydrolysis at 45 °C for 30 min	Only lignin content analyzed, 5.8 %	58 %	255±55 nm, 4±2 nm; 87 %	Suspension ultrasonicated for 5 min	[474]
Bleached pulp from spruce	62 wt.% sulfuric acid, 44 °C for 90 min, 650 rpm	Cellulose 91.05±0.6%, Hemicellulose 5.3 ±0.2%, Lignin <0.66 %	60.8±1.8 %	225.4±64.5 nm, 19.6±4.9 nm; 79.8±2.6 %	Ultrasonic probe treatment for 5 min	This study

1.10. FT-IR characteristic bands for bonds qualitative observation of functional groups in wood, pulps, and lignin

Various bonds and functional groups present in the wood, acetosolv pulp, bleached pulp, lignin, and CNC were identified by their presence or absence in the IR spectra of the corresponding samples. The characteristic absorption bands are listed in Table S7-7 and Table S7-8. The IR spectra of the recovered lignin has been shown in Figure S7-6.

Table S7-7. Characteristic bands identified in lignocellulose biomass and pulps by infrared spectroscopy (IR) [155, 160, 387-390]

Biomass component	Wavenumber (cm^{-1})	Characteristic bonds	Corresponding functional group or compound
Cellulose	3500–3000	H---OH	Intermolecular H-bonds
	2890	H-C-H	alkyl
	1640	Fiber---OH	Absorbed water
	1170-1082	C-O-C	Pyranose ring skeletal
	1108	C-OH	Acid, methanol
	897	C-O-C	β-glycosidic linkages
Hemicellulose	2890	H-C-H	Alkyl, aliphatic
	1765-1715	C=O	Ketone, carbonyl, O=C-OH group of the glucuronic acid in hemicellulose
	1108	OH	Acid, methanol
Lignin	2890	H-C-H	Alkyl, aliphatic
	1730–1700	Aromatic ring	Aromatic ring
	1632	C=C	Benzene ring stretching
	1613–1450	C=C	Aromatic skeletal
	1430	O-CH3	Methoxy group
	1270–1232	C-O-C	Aryl-alkyl ether
	1215	C-O	Phenol

	1108	OH	C-OH
	700–900	C-H	Aromatic hydrogen

The KBr pellet method was used with a Perkin-Elmer Frontier FTIR spectrometer in the range of 600-4000 cm^{-1}. About 10 mg of lignin were mixed with 200 mg of fine potassium bromide (KBr) powder and pressed into a 13 mm diameter pellet.

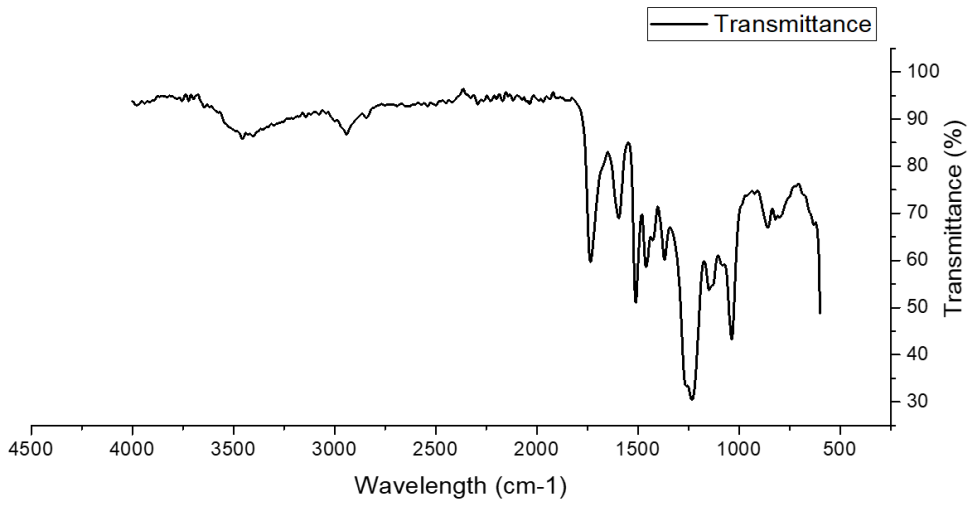

Figure S7-6. FT-IR spectrum of the recovered lignin from acetosolv pulping

Table S7-8. FT-IR characterized peaks of major functional groups present in the recovered lignin [475-477]

Peaks (cm^{-1})	**Corresponding functional groups/bonds of lignin**
3340	of O-H in aliphatic/phenolic structure
2930	aromatic ring vibrations
1600	-OH, phenolic groups
1515	C=C aromatic skeletal vibrations
1365	syringyl ring
1270	guaiacyl ring

1.11. Gel Permeation Chromatography analysis of lignin:

Gel Permeation Chromatography (GPC) analysis was carried out using a Waters Breeze GPC-HPLC instrument (1525 binary pump, UV detector set at 270 nm, Waters Styryl gel HR 1 column at a column temperature of 40 °C). Tetrahydrofuran

(THF) was used as the eluant at a 1.0 mL/min flow rate, and linear polystyrene standards were used for the molecular weight calibration curve. The recovered lignin was acetylated before GPC to improve its solubility in THF, following the method described by Mahmood et al. (2013) [478]. The acetylation was carried out as follows: 1 g of oven-dried lignin was dissolved in a 1:1 (v/v) mixture of pyridine (5 mL) and acetic anhydride (5 mL) in a vial followed by stirring for 48 h. The acetylated lignin was then precipitated in 100 mL of ice-cooled 1 wt.% HCl solution, followed by washing with distilled water until the filtrate reached pH 7. The acetylated lignin was dried at 105 °C for 24 h to remove residual water before use.

From the GPC analysis, it was found that the average molecular weight (Mw) was 10,282 g/mol and number average molecular weight (Mn) 1,565 g/mol. Therefore, the polydispersity index (PDI) was determined as 6.57.

1.12. Lignin purity analysis

The purity of the obtained crude lignin was determined using the acid hydrolysis method as described by Shui et al. (2016) [62]. Approximately 0.3 g of lignin was loaded into a glass tube with 4.92 g of 72 wt.% solution H_2SO_4 and stirred for 2 h in a shaker bath (~30 °C). After 2 h, the mixture was transferred to a 100 mL glass pressure reactor and diluted with 84 g of water. The mixture was heated at 121 °C for 60 min. After the time elapsed, the reactor was cooled down to room temperature, followed by filtration and washing with distilled water until the filtrate was pH ~7. The obtained solid was then dried in an oven at 105 °C under an active vacuum for 24 h.

$$Lignin\ purity = \frac{\text{final mass } (m_f)}{\text{initial mass } (m_i)} \times 100$$

Table S7-9. Lignin purity analysis by acid digestion of crude lignin.

Test	**m_i (g)**	**m_f (g)**	**Purity (%)**
01	0.2967	0.2534	85.41
02	0.3027	0.2509	82.89
03	0.2902	0.2355	81.15
		Average:	83.15
		St. dev.:	2.14

APPENDIX B: CHAPTER 4 SUPPLEMENTARY INFORMATION

2.1. Enzyme activity

The enzyme activity was analyzed using 2 % (w/v) microcrystalline cellulose, MCC (also known as cotton linters) substrate and enzyme concentration 0.050 mg/mL in 2 mL reaction volume. The reaction temperature was 55 °C, pH of 5.0 of 10 mM sodium citrate buffer at shaking speed of 150 rpm. After enzyme hydrolysis of MCC substrate for 60 min, the enzyme activity was calculated using Equation 13 and Equation 14.

$$\text{Enzyme activity (U/mL)} = \frac{total\ sugar\ released\ (mg) \times \frac{1 \mu mol\ glucose}{0.180\ mg\ glucose}}{Enzyme\ volume\ \ (mL) \times 60\ min} \quad (13)$$

$$\text{Specific activity (U/mg enzyme)} = \frac{Enzyme\ activity\ \frac{U}{mL}}{Enzyme\ protein\ concentration\ (\frac{mg}{mL})} \quad (14)$$

2.2. Enzyme concentration and temperature optimization of individual enzyme

The enzyme concentration and optimum temperature for both enzymes cellulase and Viscozyme L were optimized separately using untreated wood substrate. Cellulase and Viscozyme L have specific enzyme activities of 0.342 U/mg cellulase at pH 5.0, 55 °C, and 0.046 U/mg Viscozyme L at 5.0 and 45 °C. Spruce wood of 0.5-1.0 mm particle size has been used as substrate in both enzymes. The total sugar released in control (without enzyme or without substrate) and in the reaction, was calculated using DNS method. The sugar yield in terms of wt.% of total hydrolyzable sugars (THS) was calculated as below:

$$\text{Sugar yield (wt.\% of THS)} = \frac{total\ sugar\ released\ (mg)}{\frac{cellulose\ in\ feedstock\ (mg)}{0.9} + \frac{hemicellulose\ (mg)}{0.88}} \times 100 \quad (8)$$

Table S8-1. Response surface method (RSM) for optimizing individual enzyme (cellulase and cellulolytic enzyme complex Viscozyme L) concentration and temperature at atmospheric pressure

Factors	Unit	-α	-1	0	+1	+α
Temperature (X_1)	(°C)	36.9	40	47.5	55	58.1
Enzyme concentration (X_2)	(U enzyme/g-wood)	2.04	3.46	6.92	10.39	11.80

Table S8-2. Design of experiment for optimizing cellulase concentration and temperature using for response surface method using 4 factorial, 4 axial, and 4 center points.

Run Order	Pt Type	Temperature (°C)	Enzyme (U/g biomass)	Sugar yield (wt.% of THS)
1	-1	58.1	6.92	1.95
2	1	40.0	3.46	2.74
3	0	47.5	6.92	3.59
4	1	55.0	3.46	2.52
5	-1	47.5	2.04	2.88
6	-1	47.5	11.80	3.49
7	0	47.5	6.92	3.23
8	1	55.0	10.38	2.79
9	0	47.5	6.92	3.49
10	1	40.0	10.38	2.73
11	-1	36.9	6.92	2.93
12	0	47.5	6.92	3.59

Table S8-3. Design of experiment for optimizing individual cellulolytic enzyme complex Viscozyme L concentration and temperature using for response surface method using 4 factorial, 4 axial, and 4 center points.

Run Order	Pt Type	Temperature (°C)	Enzyme (U/g biomass)	Sugar yield (wt.% of THS)
1	-1	58.1	6.92	0.42
2	1	40.0	3.46	3.48
3	0	47.5	6.92	4.33
4	1	55.0	3.46	0.51

5	-1	47.5	2.04	2.22
6	-1	47.5	11.80	9.52
7	0	47.5	6.92	5.71
8	1	55.0	10.38	0.55
9	0	47.5	6.92	3.76
10	1	40.0	10.38	5.95
11	-1	36.9	6.92	5.33
12	0	47.5	6.92	3.62

The enzymatic hydrolysis reaction at atmospheric condition were conducted for 72 h and samples were taken at 0, 2, 4, 8, 16, 24, 48, 72 h. A 300 µL from the reactions was taken at sampling times and diluted three time by adding 600 µL distilled water. The enzymatic reaction was stopped by heating the diluted solution in water bath (100 °C) for 5 min. The hydrolysates were analyzed by HPLC for the sugar released in the hydrolysate.

The RSM analysis showed that the purified cellulase from *Trichoderma reesei* ATCC 26921, has optimum temperature between 45-48 °C at 7-9 activity U of enzyme per g of wood substrate in 10 mM citrate buffer. In the chosen range of temperature and enzyme concentration, Temperature has the major significant effect. The optimized condition of cellulase was 8.31 U/g wood at 46 °C (Figure S8-3). The RSM analysis of Viscozyme L (from *Aspergillus sp.*) showed that the Viscozyme L enzyme has optimum temperature ~37-42 °C at enzyme concentration of above 11 activity U per g of wood substrate in 10 mM citrate buffer solution. The optimum condition of Viscozyme L was above 11.61 U/g wood at 37 5 °C (Figure S8-1).

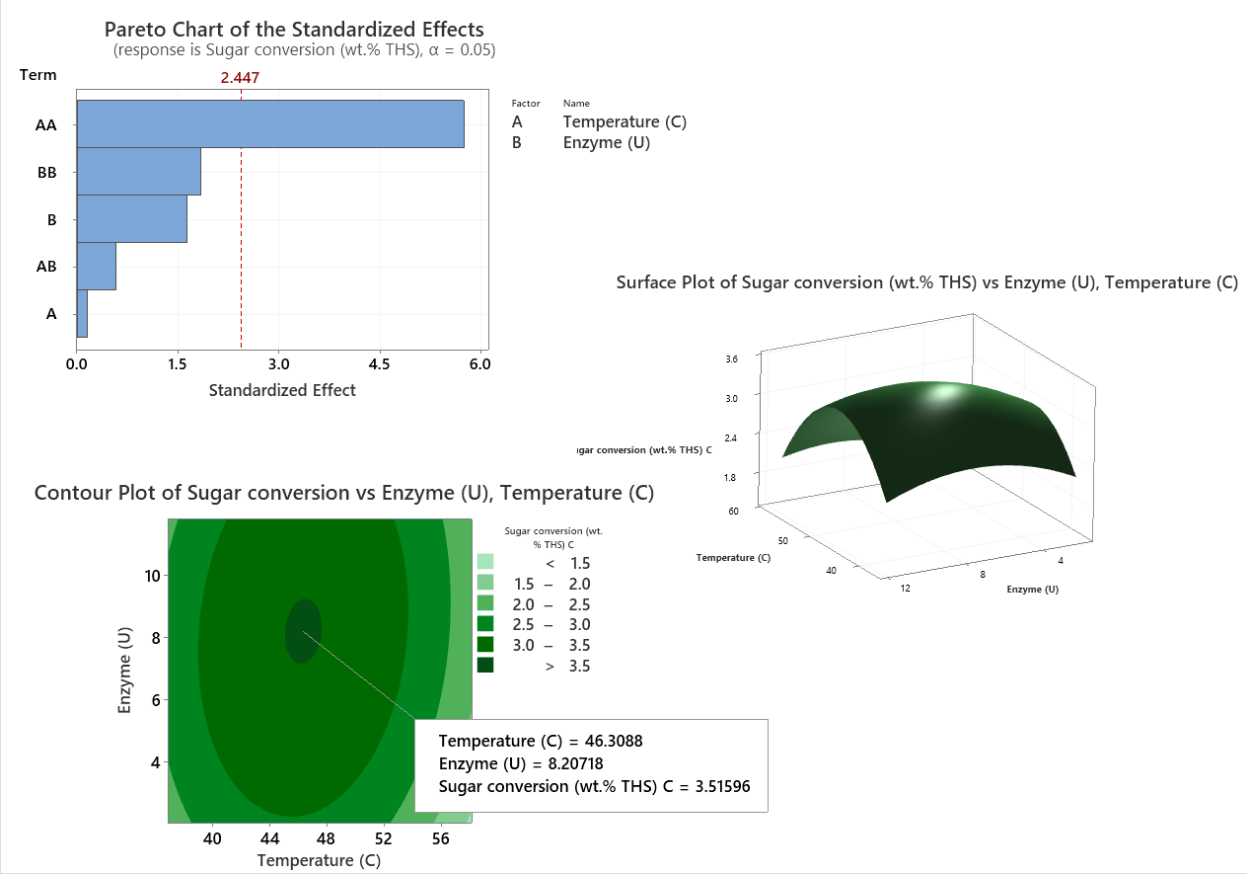

Figure S8-1. Pareto, surface, and contour plot of the response surface method of optimization model for purified cellulase enzyme (n=4 center points)

Table S8-4. Analysis of Variance for the cellulase enzyme.

Source	DF	Adj SS	Adj MS	F-Value	P-Value
Model	5	2.41852	0.48370	8.36	**0.011**
Linear	2	0.15489	0.07744	1.34	0.331
Temperature (°C)	1	0.00138	0.00138	0.02	0.882
Enzyme (U)	1	0.15351	0.15351	2.65	0.154
Square	2	1.94303	0.97152	16.79	0.003
Temperature (°C)*Temperature (°C)	1	1.91400	1.91400	33.08	0.001
Enzyme (U)*Enzyme (U)	1	0.19475	0.19475	3.37	0.116
2-Way Interaction	1	0.01960	0.01960	0.34	0.582
Temperature (°C)*Enzyme (U)	1	0.01960	0.01960	0.34	0.582
Error	6	0.34717	0.05786		

Lack-of-Fit	3	0.26047	0.08682	3.00	0.195
Pure Error	3	0.08670	0.02890		
Total	11	2.76569			

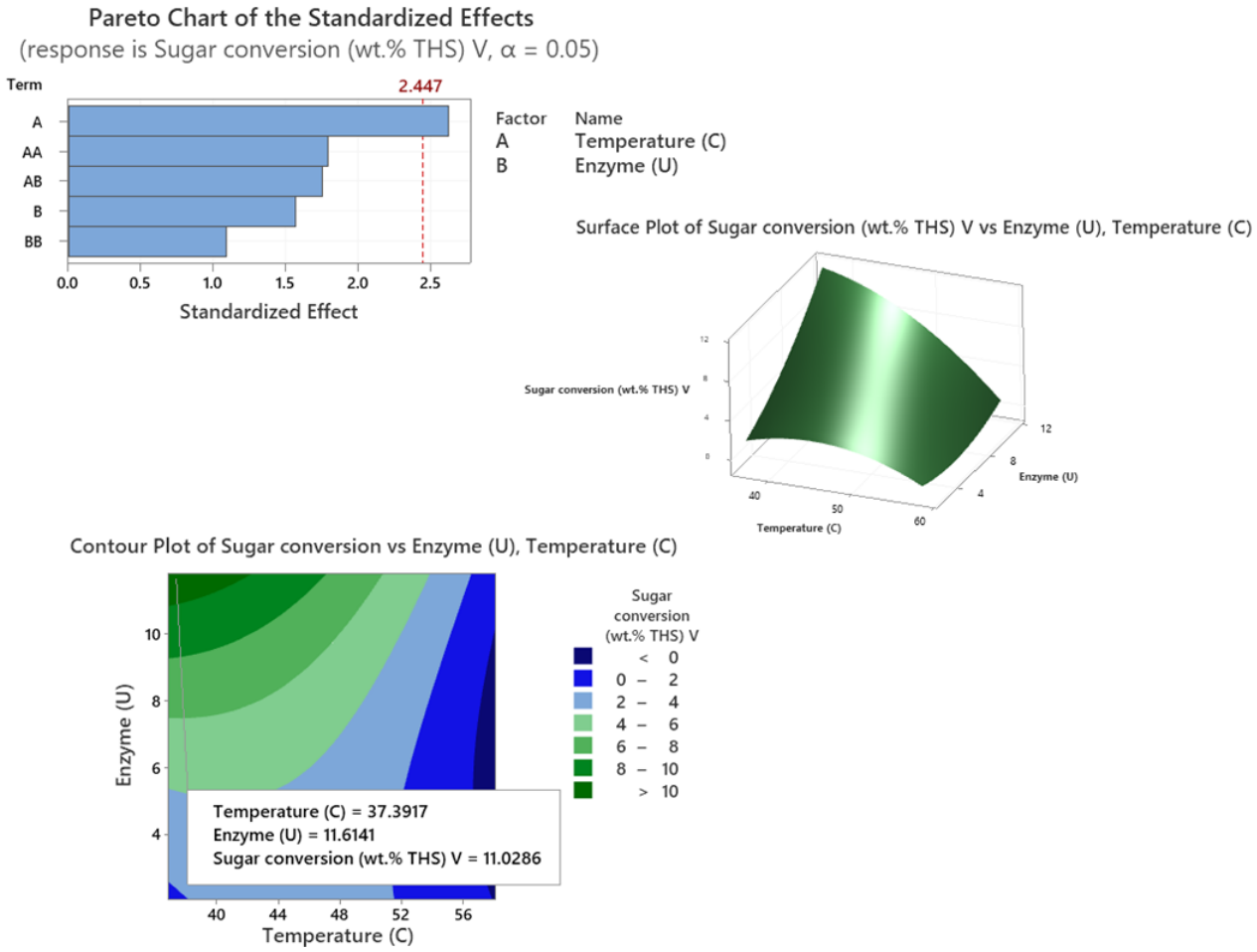

Figure S8-2. Pareto, surface, and contour plot of the response surface method of optimization model for cellulolytic enzyme mixture Viscozyme L (n=4 center points)

Table S8-5. Analysis of Variance of Viscozyme L enzyme.

Analysis of Variance

Source	DF	Adj SS	Adj MS	F-Value	P-Value
Model	5	79.9723	15.9945	9.9	0.007
Linear	2	15.0793	7.5396	4.67	0.06
Temperature (°C)	1	11.1043	11.1043	6.87	0.04
Enzyme (U)	1	3.9749	3.9749	2.46	0.168

Square	2	8.6814	4.3407	2.69	0.147
Temperature (°C)*Temperature (°C)	1	5.1589	5.1589	3.19	0.124
Enzyme (U)*Enzyme (U)	1	1.9278	1.9278	1.19	0.317
2-Way Interaction	1	4.9506	4.9506	3.06	0.131
Temperature (°C)*Enzyme (U)	1	4.9506	4.9506	3.06	0.131
Error	6	9.6963	1.616		
Lack-of-Fit	3	8.8501	2.95	10.46	0.043

2.3 Optimization enzyme concentrations and temperature of cocktail enzyme

Further, the enzyme concentration (cellulase 5-15 U/g wood and Viscozyme L 10-30 U/g wood) and temperature (30-50 °C) were optimized for the mixture of cellulase, and Viscozyme L enzymes based on the optimized condition of cellulase (8.31 U/g wood at 46 °C) and Viscozyme L (11.61 U/g wood at 37 5 °C). The cellulase and Viscozyme L enzymes were mixed to make enzyme cocktail. The concentrations of the two enzymes and the temperature were optimized by RSM where concentration of enzymes and temperature were the factors and total sugar yield (wt.% of THS) was the response as shown in Table S8-6.

Table S8-6. Response surface optimization model for enzyme concentration and temperature of combination of cellulase and Viscozyme L enzymes (n=4)

Cellulase (U/g-wood)	Viscozyme L (U/g-wood)	Temperature (°C)	Sugars (C5+C6) wt.% of THS	Xylose (C6) wt.% of THS	Glucose (C5) wt.% of THS
7.50	17.00	29.89	4.60	2.92	1.68
5.00	10.00	35.00	8.78	6.10	2.68
10.00	10.00	35.00	7.50	5.08	2.42
5.00	24.00	35.00	14.97	9.64	5.33
10.00	24.00	35.00	11.53	7.40	4.13
7.50	17.00	42.50	15.10	9.62	5.48

11.70	17.00	42.50	13.07	9.03	4.05
7.50	28.77	42.50	14.46	9.85	4.62
7.50	17.00	42.50	13.00	8.97	4.03
7.50	17.00	42.50	12.30	8.44	3.83
7.50	5.23	42.50	6.79	4.92	1.86
7.50	17.00	42.50	12.85	7.99	4.86
3.30	17.00	42.50	12.17	7.83	4.34
10.00	10.00	50.00	9.56	6.26	3.30
10.00	24.00	50.00	16.33	10.56	5.76
5.00	24.00	50.00	14.39	9.02	5.36
5.00	10.00	50.00	8.35	5.48	2.87
7.50	17.00	55.11	4.52	2.77	1.75

Based on the above observation of optimum temperature and enzyme concentration, cellulase concentration (Factor A) in rage of 5-10 U/g wood, and Viscozyme L concentration (Factor B) in range of 10-24 U/g, and the temperature (Factor C) in range of 35-50 °C wood will be used for used to determine the optimum condition of enzyme mixture concentration and Temperature for the sugar conversion of biomass.

The enzymatic reaction of mixed enzyme system is completed and analyzed with the Minitab software for analysis of variance (ANOVA) and response optimum conditions to validate the model. Below are the ANOVA and validation conditions in Table S8-7.

Table S8-7. Analysis of Variance for sugar conversion in 72 h of enzymatic digestion of untreated spruce wood powder

Source	DF	Adj SS	Adj MS	F-Value	P-Value
Model	9	198.361	22.0401	6.34	**0.008**

Linear	3	96.917	32.3058	9.30	0.006
Cellulase (U/g-wood)	1	0.000	0.0002	0.00	0.994
Viscozyme L (U/g-wood)	1	94.525	94.5253	27.21	0.001
Temperature (°C)	1	2.392	2.3919	0.69	0.431
Square	3	92.608	30.8692	8.89	0.006
Cellulase (U/g-wood)*Cellulase (U/g-wood)	1	0.960	0.9602	0.28	0.613
Viscozyme L (U/g-wood)*Viscozyme L (U/g-wood)	1	2.337	2.3369	0.67	0.436
Temperature (°C)*Temperature (°C)	1	83.815	83.8150	24.13	0.001
2-Way Interaction	3	8.836	2.9454	0.85	0.506
Cellulase (U/g-wood)*Viscozyme L (U/g-wood)	1	0.256	0.2556	0.07	0.793
Cellulase (U/g-wood)*Temperature (°C)	1	7.742	7.7421	2.23	0.174
Viscozyme L (U/g-wood)*Temperature (°C)	1	0.839	0.8385	0.24	0.636
Error	8	27.792	3.4740		
Lack-of-Fit	5	23.260	4.6520	3.08	0.192
Pure Error	3	4.532	1.5106		
Total	17	226.153			

The ANOVA analysis of the RSM model showed that the model is significant with Viscozyme L as the influencing factor for maximizing the sugar conversion. It could be observed in the contour and surface response plot of Viscozyme L and cellulase enzyme that the increasing concentration of cellulase has no significant effect whereas the increase in the Viscozyme L concentration lead to increase in the sugar conversion (Figure S8-3 and Figure S8-4). Effect of temperature with respect to two enzymes, 36 °C to 48 °C is the most effective range of the temperature for the mixed enzyme system with optimum at 42.5 °C.

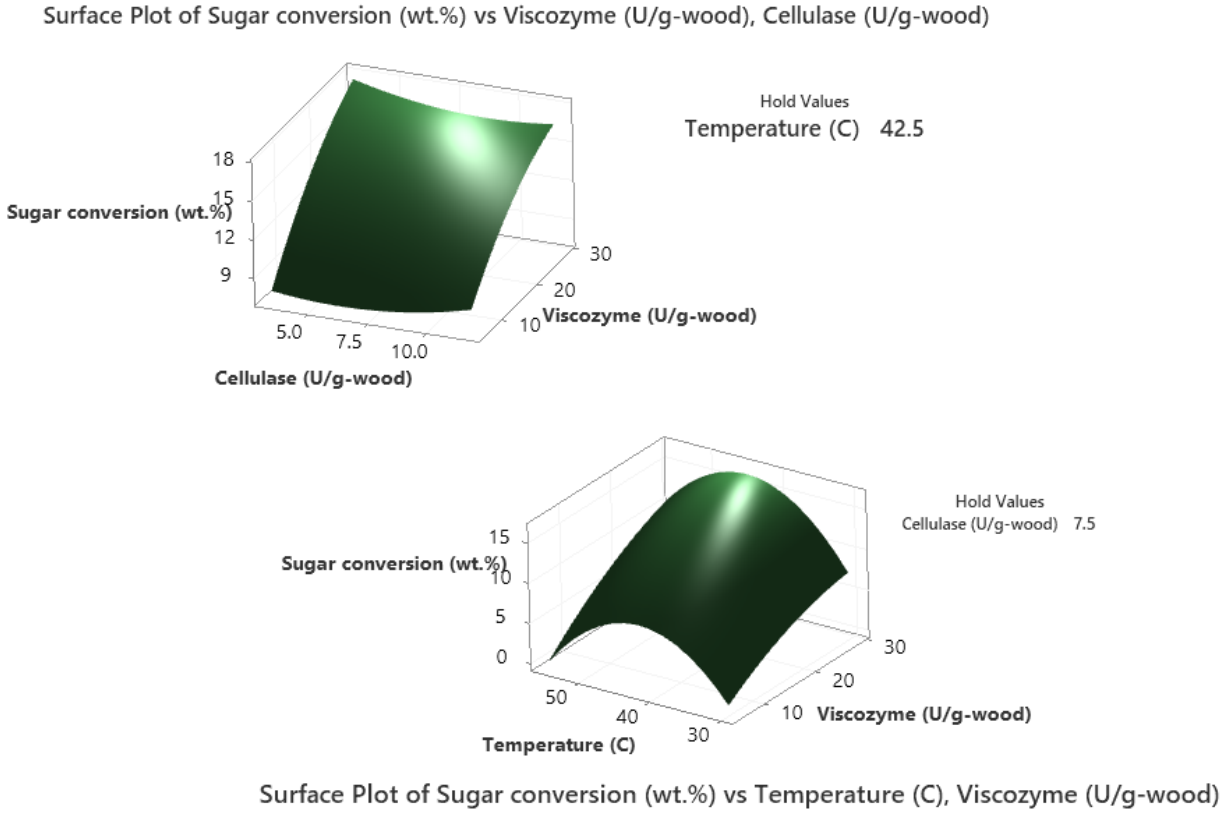

Figure S8-3. Surface response plot of sugar conversion with respect to Viscozyme L, cellulase, and temperature in enzyme cocktail at atmospheric pressure reaction.

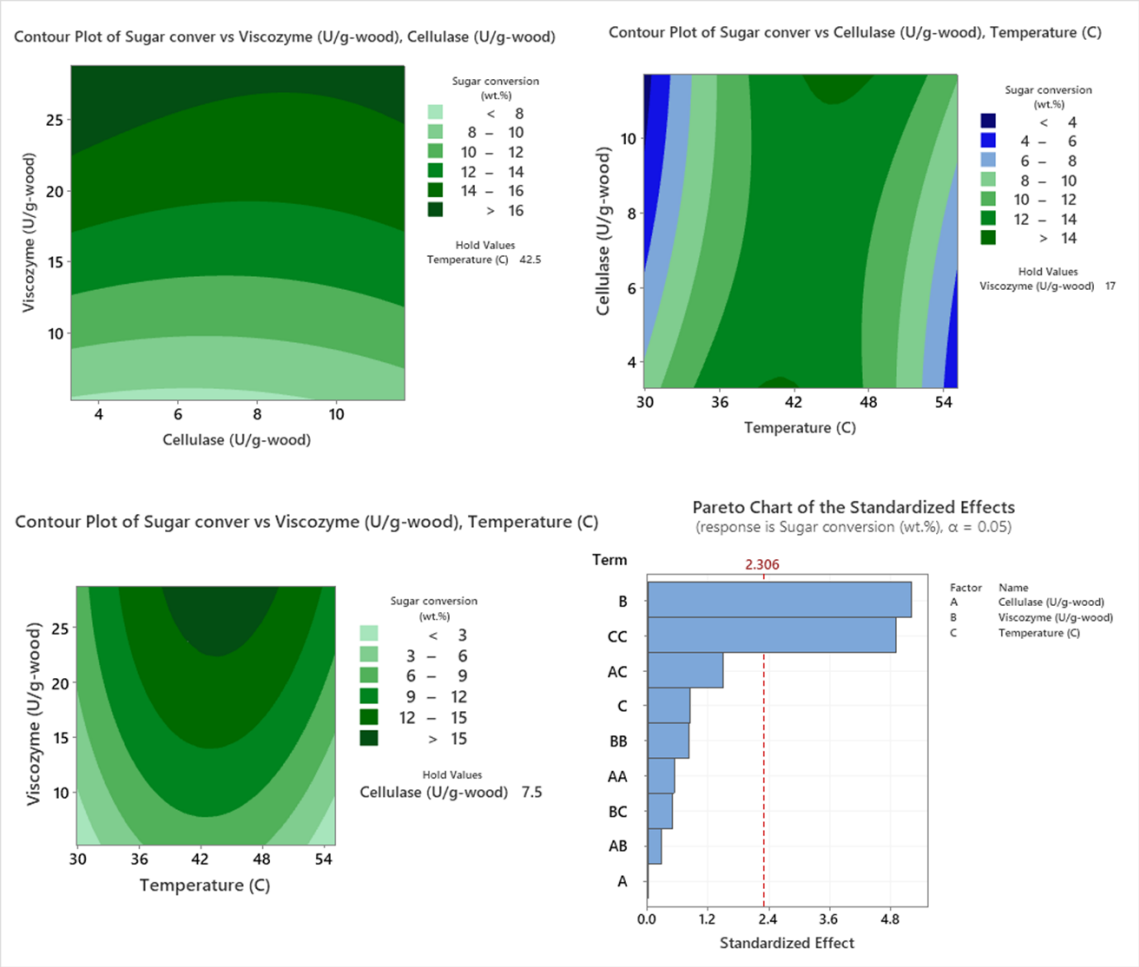

Figure S8-4. Surface response of cellulase, Viscozyme L and temperature variable for sugar conversion

The optimized reaction condition of the mixed enzyme system for untreated spruce wood hydrolysis is listed in the Table S8-8 below:

Table S8-8. Optimized concentration of enzymes in cocktail enzyme for 200 mg substrate in 10 mL citrate buffer

Components (stock concentration)	**Amount (in 10 mL citrate buffer (10 mM, pH 5.0))**
Spruce wood biomass	200.00 mg
Cellulase (14.69 mg/mL)	9.7 mg enzyme/g wood (or 0.132 mL)
Viscozyme L (220 mg/mL)	598.4 mg enzyme/g wood (or 0.544 mL)
Sodium Azide (0.002% w/v)	0.04 mL
Buffer (50 mM)	2 mL
Water	7.284 mL

2.4. Effect of supercritical CO_2 pretreatment of cornstalk

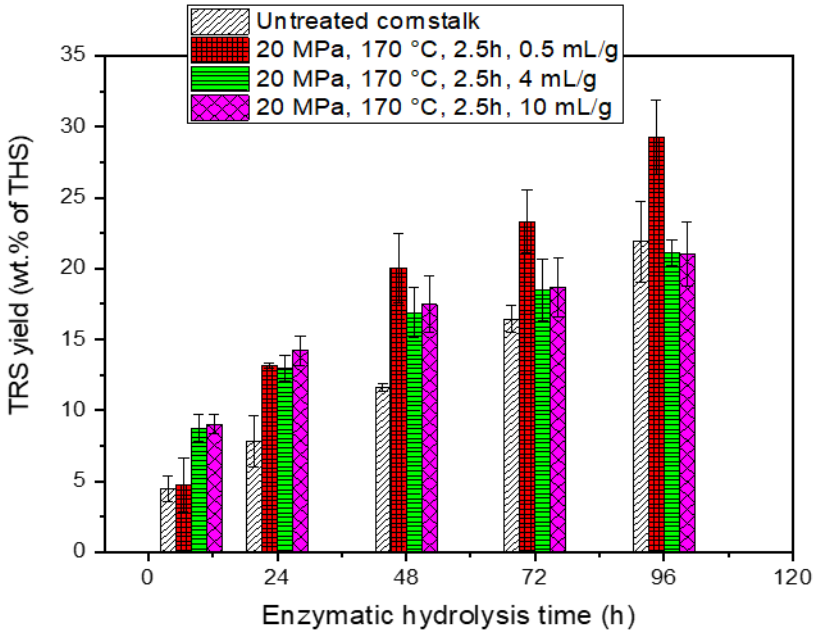

Figure S8-5. Effect of $scCO_2$ on enzymatic digestibility of cornstalk agricultural biomass

2.6. Influence of initial sugar concentration in enzyme cocktail

The presence of sugars in the commercial Viscozyme L enzyme introduces a significant 141.9 mg/L sugar concentration in the enzyme cocktail. However, the effect of sugar removal was investigated to analyze its influence on the enzymatic activity. Therefore, enzyme cocktail was purified using a spin concentrator and used to hydrolyze the cellulosic substrate (bleached wood pulp). Total protein content of enzyme cocktail decreased to 51.75 from 102.92 mg per 10 mL cocktail solution along with 90-95% initial sugar concentration. There was no significant loss in enzyme activity of the enzyme cocktail (Table S8-9 Figure S8-6).

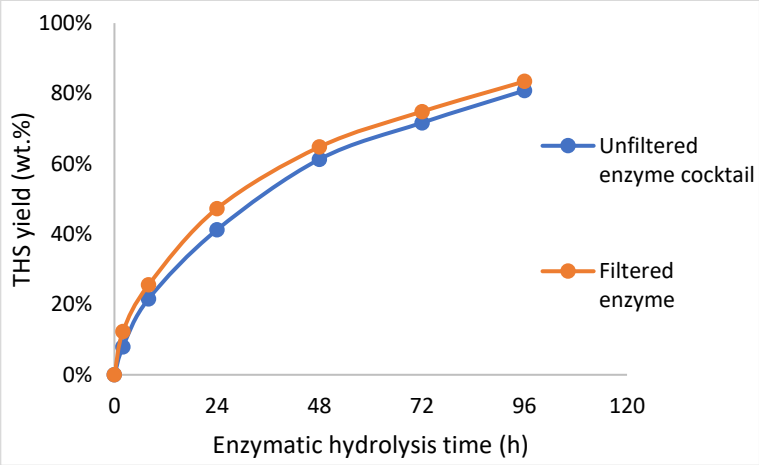

Figure S8-6. Influence of initial sugar concentration on enzyme activity

Table S8-9. Enzyme cocktail purification using spin concentrator to remove sugars

Sample	Protein mass (mg/mL)	Sugar mass (mg/mL)
Enzyme cocktail original	10.3	14.1
Enzyme cocktail purified	5.2	1.0
Filtration waste	5.1	13.8

2.6. Secondary structure analyses

2.6.1. Fourier transform infrared (FTIR) spectra were collected using a liquid nitrogen-cooled Nicolet iZ10 spectrometer (Thermo Fisher Scientific) equipped with a ConcentratorIR2 Multiple Refraction Attenuated Total Reflection (ATR) attachment with a Silicon ATR crystal (Harrick Scientific Products Inc.) (32 scans, 4.000 cm-1 resolution, range of 4000 to 700 cm-1) at room temperature (22.5 +/- 2.5 ˚C). Data collection and analysis were performed using the software Omnic version 9.11.745 (Thermo Fisher Scientific). Following baseline correction, the amide I region (1600 – 1700 cm-1) was deconvoluted to evaluate protein secondary structure.

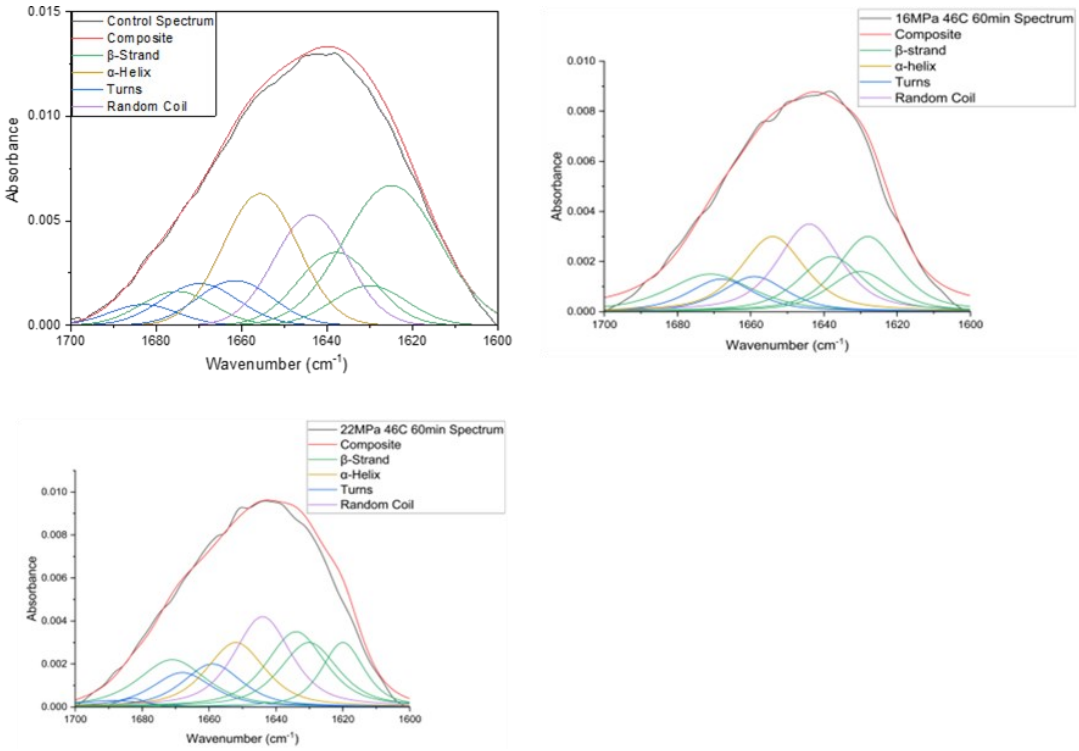

Figure S8-7. FTIR deconvoluted spectra of untreated and $scCO_2$ pretreated enzyme cocktail enzyme

2.6.2. Circular dichroism (CD) spectra were collected on an Olis DSM20 Circular Spectrophotometer (Bogart, GA) with integration time determined as a function of High Volts in Olis SpectralWorks Version 5.888.272. CD spectra were acquired from 270-180 nm with a 1 nm step size using quartz cuvettes of 0.01 mm path length (Hellma Canada Limited; Concord, ON). Spectra were obtained by averaging three individual scans. The spectra of 20 mM sodium citrate blanks were measured before the samples and were subtracted from the 0.1 mg/mL protein sample CD spectra. The spectra were normalized to their respective minima.

APPENDIX C: CHAPTER 5 SUPPLEMENTARY INFORMATION

3.1. Enzyme cocktail optimization

3.1.1. Design of experiment

The optimization of enzymes in cocktail solution and its temperature with wood biomass as substrate has been done in second manuscript work. In the current work, CMC is being used a model substrate (water soluble) and there for another set of experiments are being used to optimize the concentration, pH and temperature of the cocktail enzyme with CMC substrate. The tables listed below are the previous data that are being used to determine the boundary condition of enzymes in new optimization model (Table S9-1 and Table S9-2).

Table S9-1. Optimization of enzyme concentrations, pH, and temperature of the cocktail enzyme solution

Factors	**Unit**	**-α**	**-1**	**0**	**+1**	**+α**
pH (X_1)	-	3.05	3.5	4.25	5.0	5.45
Temperature (X_2)	(°C)	31.8	36.0	43.0	50.0	54.2
Cellulase concentration (X_3)	(mg Enzyme/g-CMC)	5.8	10.0	17.0	24.0	28.8
Viscozyme L concentration (X_4)	(mg Enzyme/g-CMC)	90.0	150	250.0	350.0	410

Viscozyme L enzyme protein concentration: 106.2 mg/mL (after filtration) from 200.8 mg/mL (without filtration).

Table S9-2. Design of experiment for optimizing the pH, Temperature, and enzyme concentrations of cellulase and filtered Viscozyme L (n=6)

Run #	Point Type	pH	Temperature (°C)	Cellulase (mg E/g CMC)	Viscozyme L (mg E/g CMC)	TRS yield (wt.%) at plateau
1	-1	4.25	31.8	17	250	43.12
2	1	3.5	36	24	150	44.93
3	1	5	36	10	150	38.30
4	1	3.5	36	10	150	46.19

5	1	5	36	24	150	39.56
6	1	5	36	10	350	37.31
7	1	5	36	24	350	39.68
8	1	3.5	36	24	350	46.94
9	1	3.5	36	10	350	46.31
10	-1	4.25	43	17	90	48.09
11	0	4.25	43	17	250	47.03
12	0	4.25	43	17	250	48.00
13	0	4.25	43	17	250	48.65
14	0	4.25	43	17	250	48.49
15	-1	3.05	43	17	250	52.08
16	-1	4.25	43	5.8	250	47.51
17	0	4.25	43	17	250	48.33
18	-1	4.25	43	28.2	250	48.33
19	0	4.25	43	17	250	47.19
20	-1	5.45	43	17	250	41.00
21	-1	4.25	43	17	410	45.56
22	1	5	50	24	150	40.98
23	1	3.5	50	24	150	46.82
24	1	3.5	50	10	150	46.04
25	1	5	50	10	150	40.35
26	1	5	50	10	350	41.10
27	1	3.5	50	24	350	47.26
28	1	3.5	50	10	350	45.36
29	1	5	50	24	350	41.26
30	-1	4.25	54.2	17	250	49.14

3.1.2. Optimization result

The analysis of variance results showed that the pH and temperature have significant influence on the TRS yield with p-value <0.05 (Table S9-3). The

interaction of the parameters has been plotted in contour plots that shows the range of optimal parameter conditions (Figure S9-1).

Table S9-3. ANOVA result of the optimization runs

Analysis of Variance (ANOVA)

Source	F-Value	P-Value
Model	15.64	0
Blocks	10.58	0.006
Linear	37.07	0
pH	135.54	0
Temperature	10.9	0.005
Cellulase	1.72	0.211
Viscozyme L	0.11	0.741
Square	11.77	0
pH*pH	12.25	0.004
Temperature*Temperature	15.67	0.001
Cellulase*Cellulase	3.84	0.07
Viscozyme L*Viscozyme L	10.13	0.007
2-Way Interaction	0.51	0.788
pH*Temperature	2.24	0.156
pH*Cellulase	0.21	0.653
pH*Viscozyme L	0.11	0.742
Temperature*Cellulase	0.01	0.929

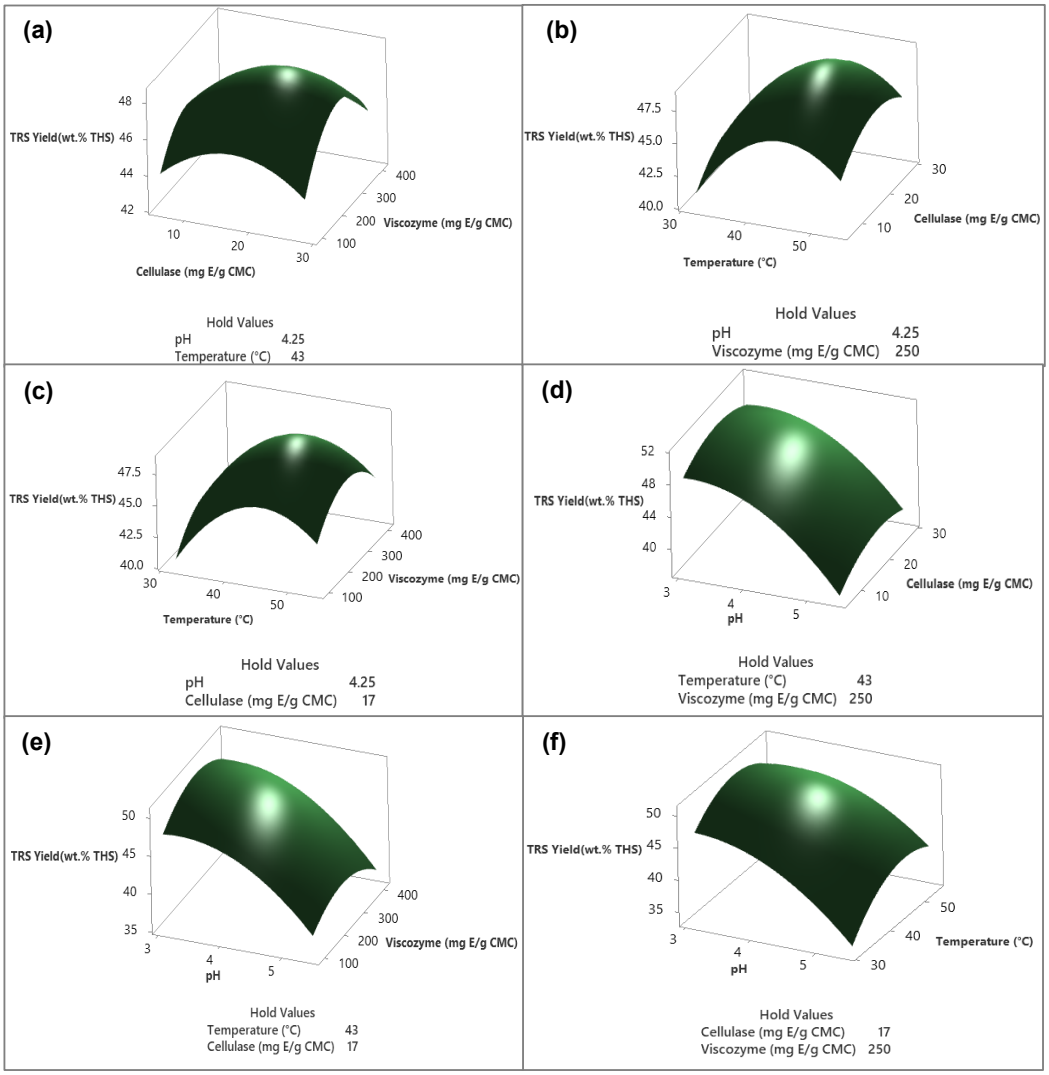

Figure S9-1. Response surface plot of the TRS yield versus two parameters while holding the other two at center point. (A) TRS yield (wt.% THS) versus cellulase and Viscozyme L enzyme concentrations (mg Enzyme/g CMC), (B) TRS yield (wt.% THS) versus cellulase enzyme concentrations (mg Enzyme/g CMC) and temperature (°C), (C) TRS yield (wt.% THS) versus Viscozyme L enzyme concentrations (mg Enzyme/g CMC) and temperature (°C), (D) TRS yield (wt.% THS) versus cellulase enzyme concentrations (mg Enzyme/g CMC) and pH, (D) TRS yield (wt.% THS) versus Viscozyme L enzyme concentrations (mg Enzyme/g CMC) and pH, (E) TRS yield (wt.% THS) versus temperature (°C) and pH.

The optimum condition of the individual parameters has been shown in Figure S9-2. Based on the model, optimized solution and validated result has been shown in Table S9-4.

Table S9-4. Model validation based on predicted optimized condition (1X)

pH	3.3
Temperature (°C)	43.8
Cellulase (mg E/g CMC)	18.1
Viscozyme L (mg E/g CMC)	254.8
Result	
Model prediction (TRS yield, wt.% of THS)	50.63±1.8
Actual response (TRS yield, wt.% of THS)	51.0±0.9

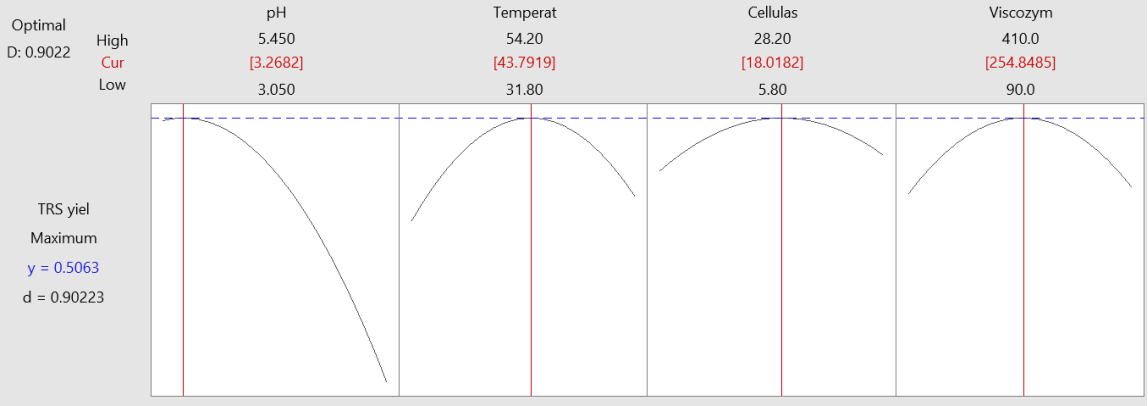

Figure S9-2. The optimum condition of individual parameters

3.1.3. Optimized model validation

To validate the optimized conditions, the enzymatic hydrolysis of CMC was conducted at predicted conditions as mentioned in Table S9-4. The corresponding result showed that the predicted conditions are at optimum points and the actual result was similar to predicted value of TRS yield (Figure S9-3).

The enzyme cocktail load of the optimized concentrations of cellulase and filtered Viscozyme L were used to validate the model and to find the optimum enzyme load. The increase in the enzyme load of cocktail slightly increased the TRS yield. However, the amount of enzyme load increased was three times to get increased yield from 51% to 58.8%.

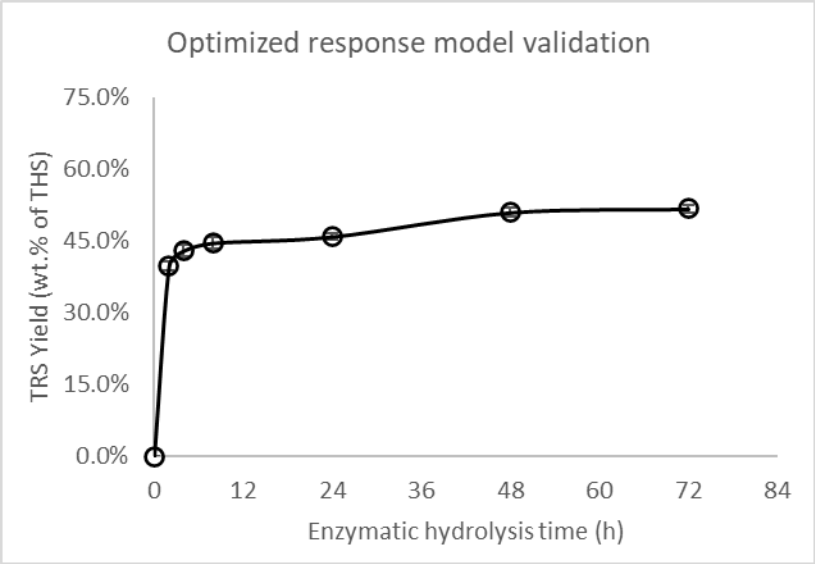

Figure S9-3. Enzymatic hydrolysis of CMC at optimized condition and optimum load of enzyme cocktail (predicted concentration).

3.2. Cocktail immobilization

For the cocktail immobilization, cellulase, filtered Viscozyme L, and the buffer solution mixed in optimized concentrations to prepare the cocktail solution. The immobilization procedure are as follows:

I. Mix 4 g of TMOS to 16 g of anhydrous ethanol for 15 mins using magnetic stirring

II. Add the 4.468 mL of enzyme cocktail solution, keep the solution on magnetic stirring 500 rpm

III. 0.292 mL ammonium hydroxide (56.6 % w/w) solution was added as a catalyst for sol-gel synthesis and stir at 1000 rpm for 2 min. it will form an opaque gel.

IV. The headspace of the gel containing vial was purged with N_2 gas to remove air and stored at ambient temperature for 24 h.

V. The alcogel was moved to refrigerator (4 °C) for next 72 hours for aging of gel.

VI. To dry the alcogel to aerogel, the gel (covered in Kimwipe paper) will be placed in 100 mL SFT vessel. The 45 mL anhydrous ethanol will be added to reactor vessel to submerge the alcogel.

VII. The reactor will be closed and pressurized to tank pressure to test the leak, then after the oven temperature will be raised to 40 C for 15 min to preheat the vessel.

VIII. The alcogel will be dried to aerogel by $scCO_2$ drying at 10 MPa (1450 psi), 40 °C for 4-6 h.

IX. After drying, the reactor will be depressurized slowly in 30-40 min to recover the aerogel.

X. The weight of aerogel will be measured and stored in refrigerator (4 °C) for further analysis

3.3. Reusability of immobilized enzyme acerogel under atmospheric pressure

The immobilized cellulase enzyme in the aerogel by entrapment method has been in investigated for its reusability. The TRS yield obtained by immobilized cellulase was around 70 % of TRS yield obtained by free cellulase (Figure S9-4). The TRS yield remained 65-70 % of the TRS yield obtained in the first cycle of immobilized cellulase and remained consisted after 5^{th} cycles.

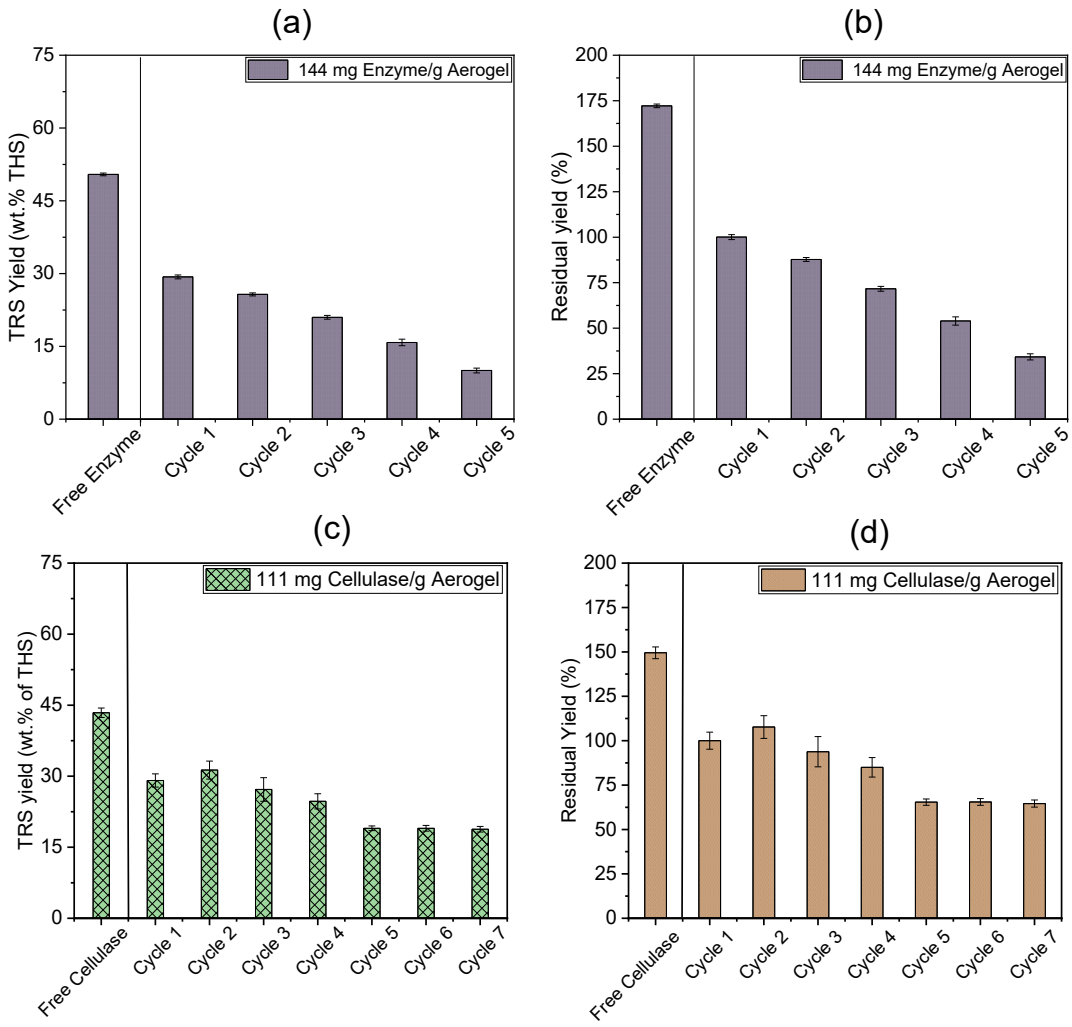

Figure S9-4. Reusability test of immobilized enzyme cocktail aerogel (pH 4.0, temperature 48 C, 14.8 g/L aerogel with 15.0 g/L CMC) for reaction time of 72 h per cycle along with immobilized pure cellulase enzyme with reuse of 7 cycle at 120 h per cycle with CMC substrate under optimized conditions of pH 4.5, temperature 46 C at 22.5 g/L aerogel concentrations with 15.0 g/L CMC substrate concentration

3.4. Aerogel immobilized enzyme morphology characterization

The surface morphology of the aerogel immobilized enzyme with different enzyme concentrations was analyzed with SEM, as shown in Figure S5-5a-c. The SEM images showed that the surfaces of the different aerogels, including the control, had rough mesoporous surfaces. However, visual differences between the aerogel

surfaces of different enzyme concentrations were undistinguishable for significant differences.

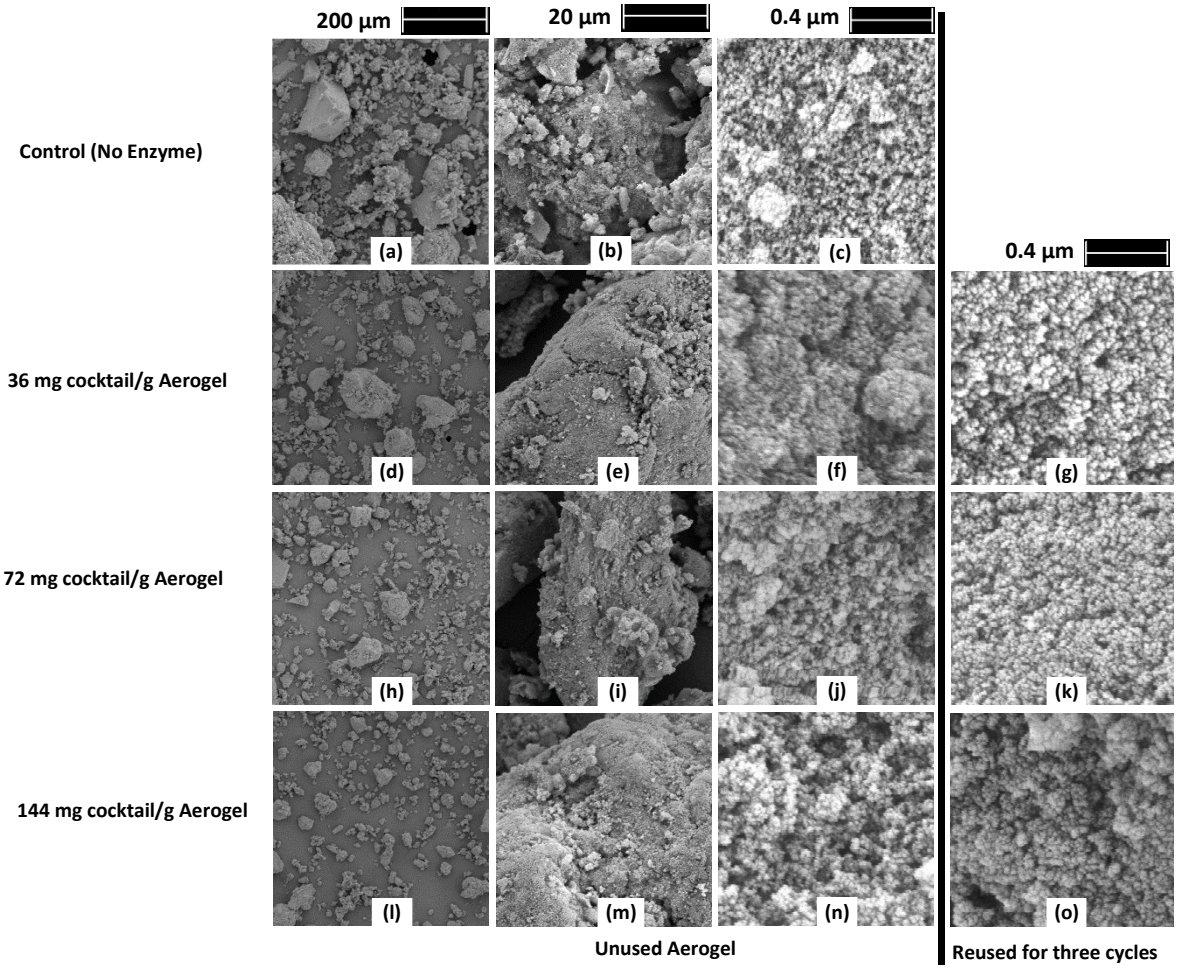

Figure S9-5. Surface morphology of aerogel immobilized enzymes with different enzyme loads (no enzyme as control a-c, 36 mg enzyme/g aerogel d-g, 72 mg enzyme/g aerogel h-k, and 144 mg enzyme/g aerogel l-o), where unused aerogels (d-f, h-j, and l-n) reused aerogel after third cycles (g, k, and o). Scale bar: a, d, h, l at 200 µm, b, e, l, m at 20 µm, and c, f, g, j, k, n, o at 0.4 µm.

3.5. Reusability of enzyme aerogels under $scCO_2$

The enzyme aerogel reusability of was tested under the $scCO_2$ conditions for the cocktail aerogel as well as cellulase aerogel. The TRS yield was significantly higher under $scCO_2$ than the atmospheric conditions for the enzyme aerogels.

3.5.1. Comparison of TRS yield (wt.% of THS) under different conditions of free and immobilized enzyme as well as under atmospheric and $scCO_2$ conditions

Table S9-5. Comparison of TRS yield under different condition of enzyme and reaction environment where the reaction was conducted for 4 h at listed pH and temperature of enzyme.

Reaction condition	Atmospheric condition	$scCO_2$ condition
Cellulase enzyme (0.25g/L cellulase or 11.2 g/L aerogel, 15 g/L CMC)		
Free enzyme (pH 3.5, 46 °C)	45.2±0.1%	41.4±2.3%
Immobilized enzyme (pH 4.5, 46 °C)	26.3±0.1%	21.7±0.4%
Cocktail enzyme (1.1 g/L cocktail or 14.7 g/L aerogel, 22.5 g/L CMC)		
Free enzyme (pH 3.3, 43 °C)	43.1±0.4%	41.4±2.3%
Immobilized enzyme (pH 4.0, 48 °C)	23.3±0.2%	27.3±2.2%
Cocktail enzyme with *mixing effect* (1.1 g/L cocktail or 14.7 g/L aerogel, 22.5 g/L CMC)		
Free enzyme (pH 3.3, 43 °C)	44.3±0.2%	47.1±2.4%
Immobilized enzyme (pH 4.0, 48 °C)	21.4±0.2%	32.1±1.1%

3.5.2. Mass balance of enzyme protein in the reaction for the leaching of enzyme from aerogel under $scCO_2$ condition due to significant loss in the TRS yield after first cycle of reuse

Table S9-6. Verification of enzyme leaching during the reuse of aerogel immobilized enzyme cocktail under $scCO_2$ by mass balance of enzymes in aerogel and hydrolysate.

Total enzyme protein IN immobilized into aerogel	Total protein OUT in the Hydrolysate
For cellulase aerogel	
1.25 mg cellulase in aerogel	0.95±0.36 mg cellulase in 5 mL hydrolysate
Leached out enzyme from aerogel	75.8±28.8 % enzyme mass
Loss in TRS Yield	>90 % (TRS was below detection limit at 4 h)

For cocktail enzyme	
10.63 mg cocktail in aerogel	2.9±0.3 mg cocktail in hydrolysate
Leached out enzyme from aerogel	27.0±3.0 % enzyme mass
Loss in TRS Yield	>90 % (TRS was below detection limit at 4 h)

APPENDIX D: COPYRIGHT AGREEMENTS

Copyright agreement for Chapter 2 section 2.2

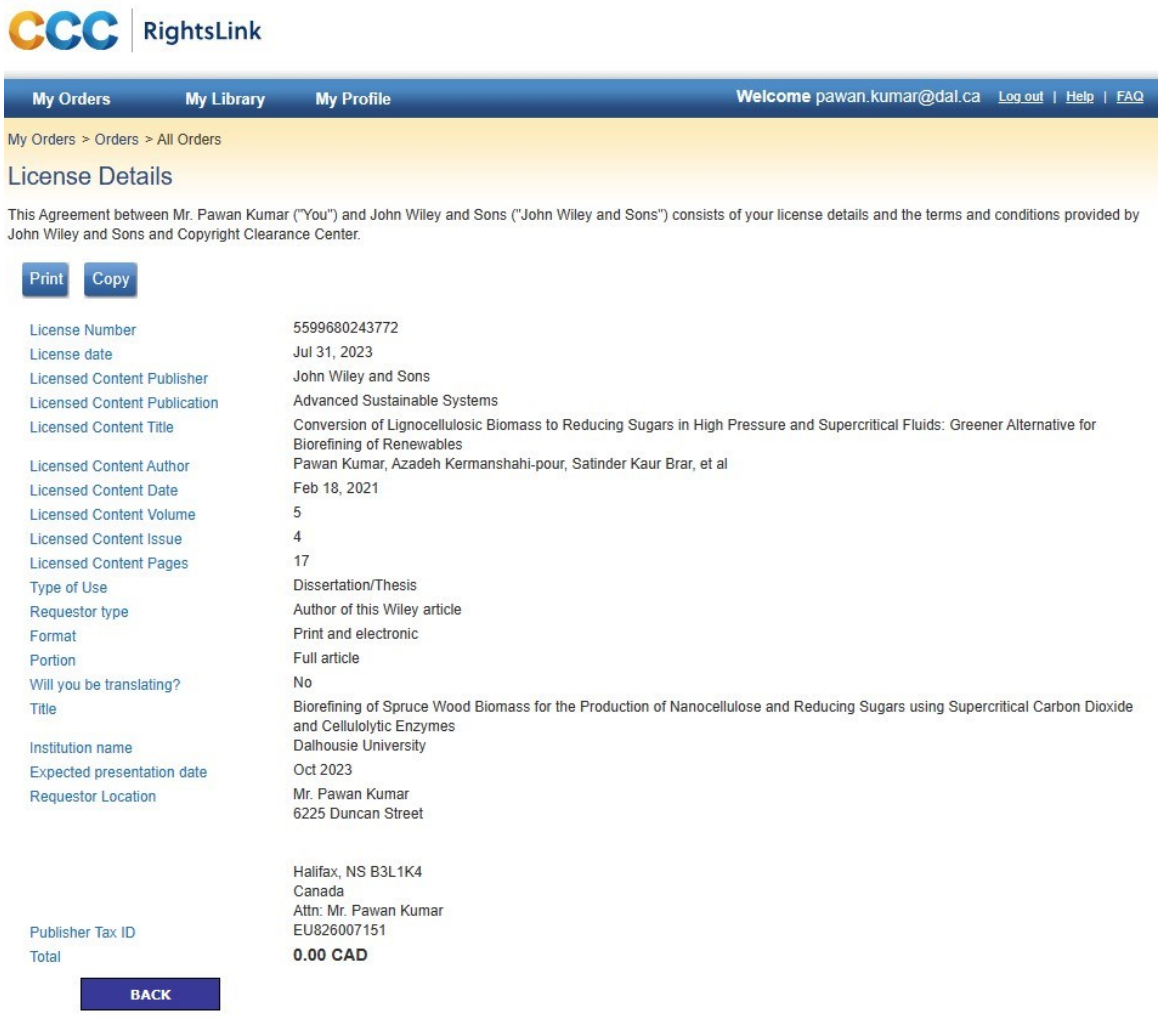

RightsLink

My Orders | My Library | My Profile | Welcome pawan.kumar@dal.ca | Log out | Help | FAQ

My Orders > Orders > All Orders

License Details

This Agreement between Mr. Pawan Kumar ("You") and John Wiley and Sons ("John Wiley and Sons") consists of your license details and the terms and conditions provided by John Wiley and Sons and Copyright Clearance Center.

Print Copy

License Number	5599680243772
License date	Jul 31, 2023
Licensed Content Publisher	John Wiley and Sons
Licensed Content Publication	Advanced Sustainable Systems
Licensed Content Title	Conversion of Lignocellulosic Biomass to Reducing Sugars in High Pressure and Supercritical Fluids: Greener Alternative for Biorefining of Renewables
Licensed Content Author	Pawan Kumar, Azadeh Kermanshahi-pour, Satinder Kaur Brar, et al
Licensed Content Date	Feb 18, 2021
Licensed Content Volume	5
Licensed Content Issue	4
Licensed Content Pages	17
Type of Use	Dissertation/Thesis
Requestor type	Author of this Wiley article
Format	Print and electronic
Portion	Full article
Will you be translating?	No
Title	Biorefining of Spruce Wood Biomass for the Production of Nanocellulose and Reducing Sugars using Supercritical Carbon Dioxide and Cellulolytic Enzymes
Institution name	Dalhousie University
Expected presentation date	Oct 2023
Requestor Location	Mr. Pawan Kumar 6225 Duncan Street Halifax, NS B3L1K4 Canada Attn: Mr. Pawan Kumar
Publisher Tax ID	EU826007151
Total	**0.00 CAD**

BACK

Copyright agreement for Chapter 2 section 2.3

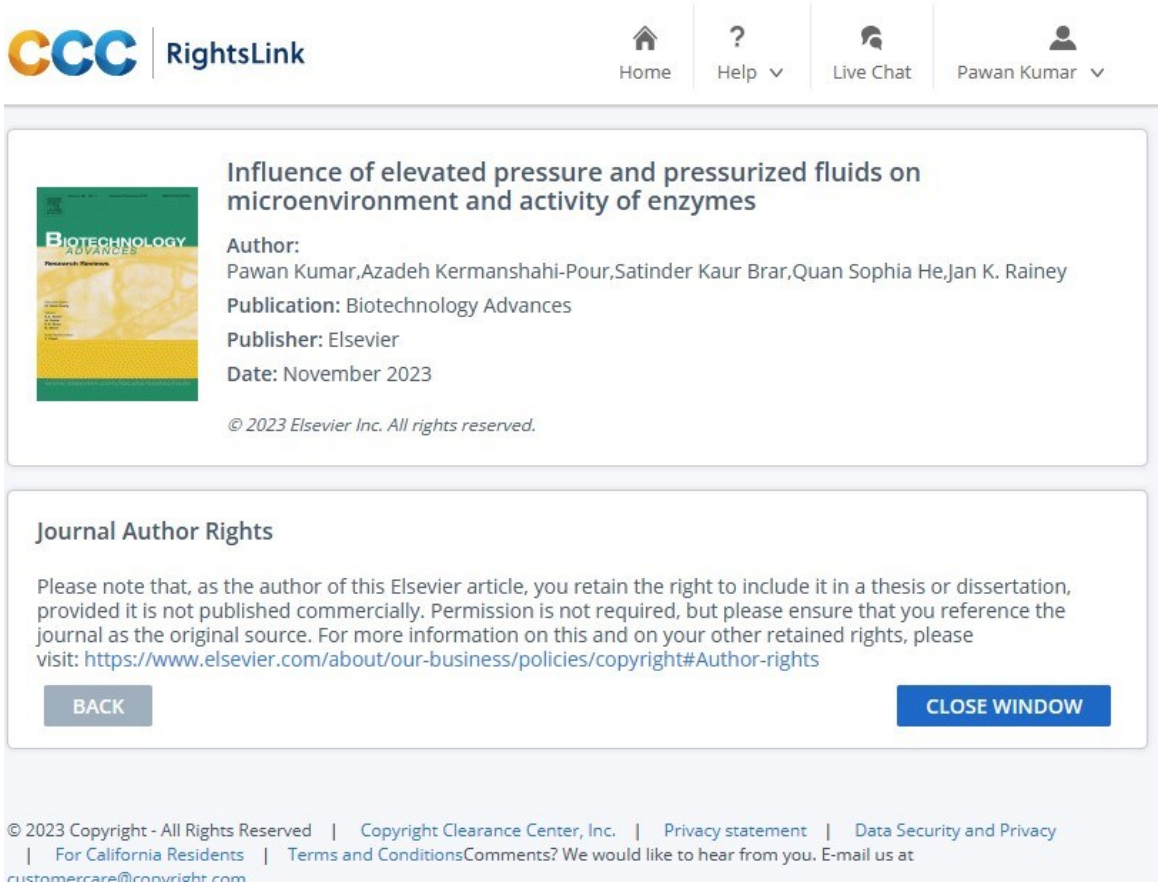

RightsLink

Home | Help | Live Chat | Pawan Kumar

Influence of elevated pressure and pressurized fluids on microenvironment and activity of enzymes

Author:
Pawan Kumar,Azadeh Kermanshahi-Pour,Satinder Kaur Brar,Quan Sophia He,Jan K. Rainey

Publication: Biotechnology Advances

Publisher: Elsevier

Date: November 2023

© 2023 Elsevier Inc. All rights reserved.

Journal Author Rights

Please note that, as the author of this Elsevier article, you retain the right to include it in a thesis or dissertation, provided it is not published commercially. Permission is not required, but please ensure that you reference the journal as the original source. For more information on this and on your other retained rights, please visit: https://www.elsevier.com/about/our-business/policies/copyright#Author-rights

BACK CLOSE WINDOW

© 2023 Copyright - All Rights Reserved | Copyright Clearance Center, Inc. | Privacy statement | Data Security and Privacy | For California Residents | Terms and ConditionsComments? We would like to hear from you. E-mail us at customercare@copyright.com

Copyright agreement for Chapter 3

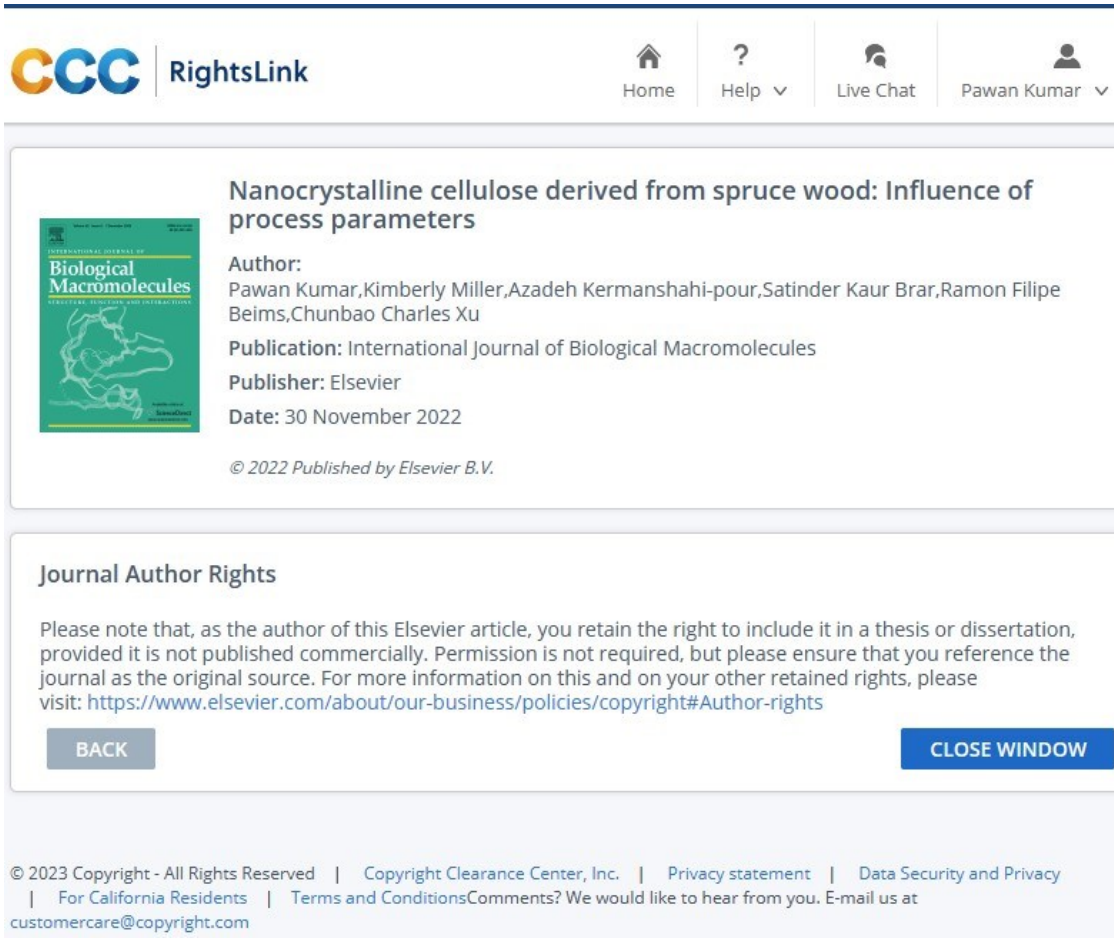

Copyright agreement for Chapter 4

CCC Marketplace

This is a License Agreement between Pawan Kumar / Dalhousie University ("User") and Copyright Clearance Center, Inc. ("CCC") on behalf of the Rightsholder identified in the order details below. The license consists of the order details, the Marketplace Permissions General Terms and Conditions below, and any Rightsholder Terms and Conditions which are included below.

All payments must be made in full to CCC in accordance with the Marketplace Permissions General Terms and Conditions below.

Order Date	12-Dec-2023	Type of Use	Republish in a thesis/dissertation
Order License ID	1426789-1	Publisher	Elsevier
ISSN	2405-8440	Portion	Chapter/article

LICENSED CONTENT

Publication Title	Heliyon	Rightsholder	Elsevier Science & Technology Journals
Article Title	Enzymatic digestibility of lignocellulosic wood biomass: Effect of enzyme treatment in supercritical carbon dioxide and biomass pretreatment	Publication Type	e-Journal
		Start Page	e21811
		Issue	11
Date	01/01/2015	Volume	9
Language	English		
Country	United Kingdom of Great Britain and Northern Ireland		

REQUEST DETAILS

Portion Type	Chapter/article	Rights Requested	Main product
Page Range(s)	21811-21824	Distribution	Worldwide
Total Number of Pages	13	Translation	Original language of publication
Format (select all that apply)	Print, Electronic	Copies for the Disabled?	No
Who Will Republish the Content?	Academic institution	Minor Editing Privileges?	Yes
Duration of Use	Life of current edition	Incidental Promotional Use?	Yes
Lifetime Unit Quantity	Up to 499	Currency	CAD

NEW WORK DETAILS

Title	Biorefining of Spruce Wood for Nanocellulose and Reducing Sugars Production: Exploring Greener Alternatives	Institution Name	Dalhousie University
		Expected Presentation Date	2023-12-12
Instructor Name	Pawan Kumar		

ADDITIONAL DETAILS

Order Reference Number	N/A	The Requesting Person / Organization to Appear on the License	Pawan Kumar / Dalhousie University

REQUESTED CONTENT DETAILS

Title, Description or Numeric Reference of the Portion(s)	Biorefining of Spruce Wood for Nanocellulose and Reducing Sugars Production: Exploring Greener Alternatives	Title of the Article / Chapter the Portion Is From	Enzymatic digestibility of lignocellulosic wood biomass: Effect of enzyme treatment in supercritical carbon dioxide and biomass pretreatment
Editor of Portion(s)	Kumar, Pawan; Kermanshahi-pour, Azadeh; Brar, Satinder Kaur; Xu, Chunbao Charles; He, Quan Sophia; Evans, Sara; Rainey, Jan K.	Author of Portion(s)	Kumar, Pawan; Kermanshahi-pour, Azadeh; Brar, Satinder Kaur; Xu, Chunbao Charles; He, Quan Sophia; Evans, Sara; Rainey, Jan K.
Volume / Edition	9		
Page or Page Range of Portion	e21811	Issue, if Republishing an Article From a Serial	11
		Publication Date of Portion	2023-11-06